UNIVERSITÀ DEGLI STUDI DI MILANO

Doctorate in Pharmaceutical Sciences – XXXVII cycle

DEPARTMENT OF PHARMACEUTICAL SCIENCES

Application of omics approaches in drug discovery and biomarker identification

CHEM-07/A

BEATRICE ZOANNI

R13389

Tutor: Prof.ssa Marina CARINI

Coordinator: Prof. Giulio VISTOLI

Academic year 2023 - 2024

Table of contents

ABSTRACT

Recent advances in omics sciences have represented a revolution in many fields of biological research. Among these, lipidomics and metabolomics are gaining increasing interest due to their close connection with the organism's phenotype. As the main analytical goal of omics approaches is to identify and quantify as many compounds as possible within a studied system, powerful analytical techniques and bioinformatics tools are required. Mass spectrometry (MS) coupled with liquid chromatography (LC) is one of the most powerful analytical platforms for the analysis of the lipidome in complex biological matrices and offers promising new insights in this field. Lipids are a large class of biomolecules involved in many biological processes with signalling, biophysical, and metabolic functions. The lipidome is complex, consisting of many species that share the same elemental composition but have different structural and physicochemical properties. Its comprehensive analysis is, therefore, technically challenging, and advanced LC-MS-based lipidomics workflows aim to better address this complexity. Lipidomics approaches can potentially be applied in all therapeutic areas, including cardiovascular, metabolic and inflammatory diseases. This is because an increasing number of human diseases are associated with significant lipidome remodelling, and changes in lipid profile have been identified as a major risk factor for many of them. With this thesis, we aimed to unravel the complexity of the lipidome and to assemble this knowledge in the description of biological systems to highlight lipid changes in pathology or response to drug treatment. To this end, we have optimized MS-based untargeted analytical workflows for the comprehensive profiling of lipids in different biological matrices and under various experimental conditions (*in vitro* and *in vivo* models) using advanced high-resolution LC-MS approaches.

In **Chapter 2,** we integrated omics approaches into phenotypic screening drug discovery to support the identification of novel bioactive compounds. These studies aimed to apply untargeted multi-omics approaches to infer the mechanism of action of phytocomplex with potential lipid-lowering properties. Once better understood, lipid metabolism can be targeted pharmacologically. Phytochemicals from natural extracts represent an important source of bioactive compounds potentially useful in treating metabolic diseases characterized by major lipidome remodelling. However, the heterogeneity of natural matrices emphasizes the need for advanced analytical workflows to explore their

beneficial effects, elucidating their mechanism of action and potential molecular targets. Using untargeted MS-based measurement of lipids and proteins allows a comprehensive investigation of the molecular mechanism of *Scutellaria baicalensis* (**Study I**) across different cellular states to help define the molecular changes responsible for its beneficial effect against liver disorders. In **Study II,** we established an analytical workflow to identify bioactive compounds in a polyphenolic fraction of bergamot leaves (*Citrus bergamia*). The experimental approach, which included a prefractionation step followed by LC-MS/MS analysis and phenotypic screening, revealed the great potential of leaves, usually considered as only waste products, as a source of polyphenols with positive effects on liver lipid metabolism.

In Chapters 3 and **4,** we applied UHPLC-MS analysis to study lipidome signatures in *in vivo* models focusing on specific key objects. Our primary goal was to determine the applicability of untargeted LC-MS/MS methods for the comprehensive analysis of lipid profiles in complex biological samples and to ensure that the analytical method was effective in capturing lipidome diversity and possible alterations with respect to environmental damage or pathological features. This helped us to derive some knowledge about how such stimuli could affect lipid metabolism. In particular, for both studies, we also investigated whether drug treatment could influence the lipidomic profile of the different biological samples analyzed (skin, liver and plasma).

In Chapter 5, we aimed to accurately annotate oxidized lipid molecular species in complex biological matrices. Technically, the discovery and structural elucidation of oxidized lipids are still lacking, as their identification in biological samples is hampered by their low natural abundance and structural diversity. To deal with this complexity, advanced analytical and computational tools are required. We optimized a workflow combining a rapid untargeted lipidomic analysis with our newly assembled pipeline to support high-throughput detection and annotation of oxidized lipid molecular species in liver and plasma samples. The proposed workflow demonstrates its potential to address changes in oxidized lipidome in an untargeted manner and to guide future research on the role of oxidized lipids in biological systems. I.E. modified lipid species, which are known to be massively involved in the regulation of physiological and pathological conditions.

In Chapter 6, we used the lipidomic dataset generated in Chapter 5 to infer deeper structural information about oxidized lipids putatively annotated. Currently, no single analytical method can fully characterize a lipid, and even in the field of MS-based lipidomics, more than one MS experiment is usually required to obtain deeper structural information. To identify the exact localization of unsaturation and oxidation positions within the acyl chains of oxidized lipids, we applied a different type of fragmentation mechanism, such as electron-activated dissociation (EAD). With EAD, we could generate accurate annotations of all selected oxidized lipids, providing information on chain length, location of oxygen, double bonds, and regioisomerism.

Overall, this thesis highlights the utility of omics studies, particularly lipidomics, to the comprehensive description of biological systems. The project underlines the necessity of including omics analysis in drug discovery screening to explore molecular patterns responsible for observed phenotypic effects and generate hypotheses about the molecular targets. Moreover, our omics datasets helped us uncover molecular patterns defining pathological states and identify lipid species involved in the response of the organism to external stimuli. This also extends to deciphering the regulatory capacity of oxidized lipids. We believe that our efforts in the field of omics sciences have the potential to significantly advance our understanding of biological processes, improve drug discovery and development, and ultimately contribute to better therapeutic strategies.

CHAPTER 1:
GENERAL INTRODUCTION

OMICS SCIENCES

The advent of omics sciences has represented a revolution in many areas of biological research. The term ‘omics’ refers to the comprehensive study of the identity, roles, and actions of different molecular species in biological samples to offer a fine-grained representation of the cellular state which can ultimately reveal networks and interactions.[1]

As omics data help to derive knowledge about biological systems, their application in biomedical research, including biomarker and drug discovery, is indispensable for future progress in these fields. In particular, omics sciences are increasingly being used to diagnose disease, understand disease mechanisms, identify novel drug targets, discover new drugs, and monitor therapeutic outcomes[2]. The increasing accessibility of omics sciences could therefore offer good opportunities for drug discovery campaigns, genome-wide association studies, and personalized medicine, to customize individual’s medical treatment according to specific omics profiles.[3]

To confirm these achievements, proteomics applications have been successfully used to identify biomarkers and signatures for various diseases, including cardiovascular, cancer, and inflammatory diseases[4]. Proteomics follows the exploration of protein complexity and dynamicity and offers a detailed biochemical snapshot of the molecular systems[4]. Although proteomics stands out as the most established and powerful omics approach, other omics applications, such as metabolomics and lipidomics, have recently emerged and gained interest due to their close connection with the organism’s phenotype[5]. Indeed, metabolomics and lipidomic profiling can yield important information about the actual cellular status, thus reporting ‘what is currently happening’ in cells and organisms. This information cannot be fully accessible either with genomic or proteomic data and has already helped to clarify unexpected roles of small molecules in the development of complex diseases, including cardiovascular[6], liver and metabolic disorders[7,8] and cancer[9]. According to data in the Human Metabolome Database (HMDB), more than 400 disease conditions are associated with prognostic or diagnostic metabolite biomarkers[10]. The discovery of novel metabolic connections to diseases is also leading to the identification of new drug targets, opening up new opportunities for drug discovery and development.[10]

Omics sciences have become an integral part of modern targeted and phenotypic drug discovery. In particular, phenotypic screening drug discovery is becoming more popular following advances in the development of cellular assays as surrogate disease models. As this approach is untargeted, it can be successfully applied to derive a solid mechanistic understanding of the molecular mechanism of action of small molecule bioactive compounds and drug-target relationships without prior hypothesis[11]. Interestingly, a recent study has shown that the contribution of phenotypic screening to drug discovery is more successful than target-based approaches in the discovery of new first-in-class small-molecule drugs[12]. While powerful as such, phenotypic screening usually allows for the measurement of a relatively small number of phenotypic features (e.g. apoptosis, redox state, migration, differentiation, senescence[13]) and does not provide direct information on the possible targets of the bioactive compounds screened. Thus, the application of omics approaches, and lipidomics in particular, offers a good opportunity to overcome these limitations. Omics profiles of different analytes have helped to derive a deeper understanding of cell states and changes in response to drug treatment. It can be used as a starting point to generate data and hypotheses that can be used as the basis for a more tailored and targeted analysis. There are many examples of how lipidomics can support drug discovery. For instance, lipidomic analysis recently facilitated the discovery of two new therapeutic strategies for the treatment of liver metabolic diseases.[14,15]

As the main analytical goal of omics approaches is to identify and/or quantify as many compounds as possible within an investigated system, powerful analytical techniques and bioinformatics tools are required[16]. Mass spectrometry (MS) represents one of the most powerful analytical platforms for the analysis of diverse molecular species in complex biological matrices. However, despite the growing importance of lipidomics[17], MS-based lipidomics is still an emerging field and suffers from a lack of standardization of methodological protocols and community consensus, making compound annotation and interpretation of the data difficult[18]. Indeed, while instrumentation has achieved great performance, streamlined data processing remains a challenge, especially for large-scale untargeted omics analyses.

ANALYTICAL APPROACHES IN LIPIDOMICS

Lipidomics is the analysis of lipid species' abundance, biological activities, subcellular localization, and tissue distribution[19]. Lipids are involved in many complex biological

processes with signalling, biophysical, and metabolic functions[20,21]. Lipid composition is highly characteristic and tightly regulated, and the accurate characterization of diverse lipid molecules is critical to understanding their roles in biochemical pathways (Figure 1).

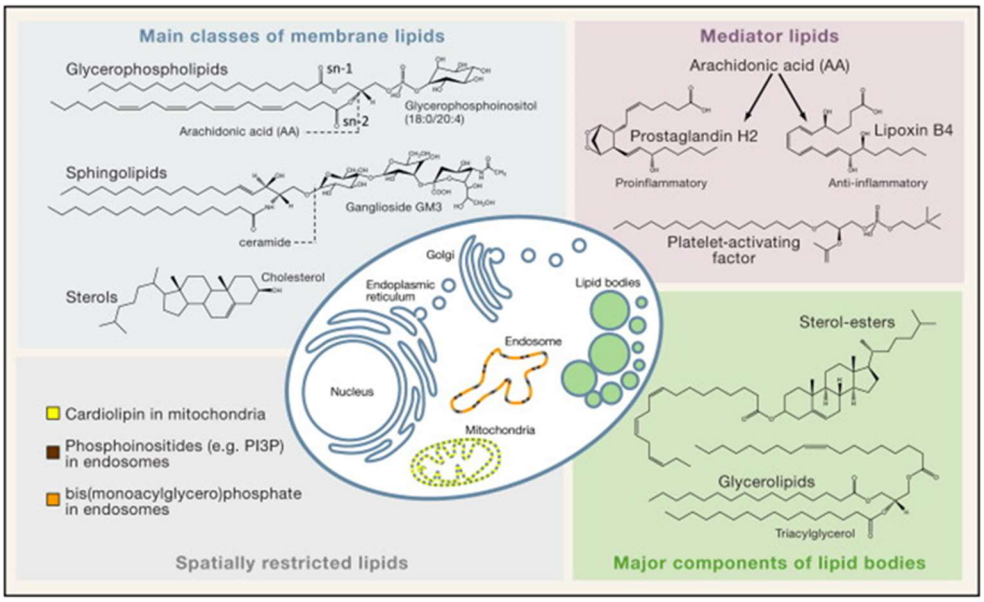

Figure 1: The Cellular Compartments of Common Biological Lipids. Adapted from Wenk *et al*. [21]

According to the LIPID MAPS consortium, lipids are defined as *"hydrophobic or amphipathic small molecules that originate entirely or in part by carbanion-based condensations of thioesters and/or by carbocation-based condensations of isoprene units"*[22]. Lipids can be divided into eight main categories: fatty acyls (FA), glycerolipids (GL), glycerophospholipids (GP), sphingolipids (SP), sterols (ST), prenol lipids (PR), saccharolipids (SL), and polyketides (PK). Each category is subdivided into lipid classes and subclasses, which add further chemical variation. Although lipids fall into defined classes that share similar chemical properties, their diversity is enormous. To date, based on this classification scheme, the LIPID MAPS Structure Database contains 46843 lipid structures, either experimentally proven and curated or generated in silico[23,24]. However, the number of possible molecular species is even higher if we provide more detail and consider all the possible combinations of double bond positions on the carbon chain, backbone substitutions, and stereochemistry[25].

The lipidome is complex and consists of many species that share the same elemental composition but have different structural and physicochemical properties. Lipids have different solubilities, from amphipathic to hydrophobic, and consist of many isomeric

(same elemental composition) and isobaric (same nominal mass) chemical entities, which require high-resolution approaches for their analysis. Comprehensive analysis of lipidomes is therefore technically challenging and advanced analytical lipidomic workflows aim to better address this[19].

Sample selection and preparation

When lipidomic analysis is performed on biological matrices like plasma, serum, or cells, proper sampling, sample storage, and adequate sample preparation are necessary, followed by the most suitable analyses and data processing. Sample preparation can be adjusted according to the type of biological matrix to be analyzed. In principle, lipid extraction from biological matrices is performed by liquid-liquid extraction (two-phase extraction methods such as the classical Bligh and Dyer[26] or Folch extraction[27]), or on protein precipitation (one-phase extraction) using a mixture of organic solvents with different polarities, such as Methyl Tert-Butyl Ether (MTBE), chloroform, methanol, isopropanol, and water. Besides the proper sample preparation method, the selection of appropriate samples to address biological questions is the most critical step and varies across biological and clinical research. In biological research, cellular models offer easily controlled experimental variables and good reproducibility and are, therefore, widely used to infer lipid metabolism and interactions. Mammalian cells represent a good target for lipidomic studies as they provide relevant physiological contexts that closely mimic *in vivo* systems[28]. *In vitro* models can be easily used to study the effects on lipid profiles of different stimuli, including drugs. However, only animal models can describe lipidome profiles in a more complex and dynamic environment. In clinical lipidomic research, tissue or biofluid samples are used due to their ease of collection and biological relevance[29]. Biofluids such as blood and urine are particularly advantageous as they can be obtained through minimally invasive procedures and can serve as potential biomarkers for diagnosis, prognosis, and therapeutic monitoring. Tissue samples, on the other hand, offer detailed insights into localized lipid changes within specific organs or pathological sites, contributing to a deeper understanding of disease mechanisms at the molecular level.

Mass-spectrometry methods to study the lipidome

As the main analytical goal in lipidomics is to identify and/or quantify as many compounds as possible in a biological system under investigation, powerful analytical

techniques are required. MS plays a key role in lipidomics thanks to its sensitivity and enhanced resolution. MS is capable of profiling hundreds of lipids in a high throughput manner, covering a wide dynamic range of concentrations and chemical classes of lipids [30,31]. An advantage of MS is that it can be combined with different separation techniques (e.g. liquid, gas and supercritical gas chromatography), which improves lipid detection and sensitivity and reduces ion suppression and matrix effects[32,33]. The choice of the LC-MS analytical approach determines the depth of lipid profiling. Lipidomics measurements are generally divided into targeted and untargeted approaches. Targeted lipidomics focuses on analyzing a selected panel of analytes and determining their quantities by comparing them with the response of analytical standards. Such an approach is often applied to routine analysis and to test hypotheses [34,35]. Targeted methods are generally performed on triple quadrupole MS with selective scanning modes (e.g. multiple reaction monitoring MRM), which greatly increases the detection sensitivity and is suitable for absolute quantification of the targeted lipids, with advantages in terms of good linearity, repeatability, and ability to detect low abundant species[36]. However, despite the development of pseudo-targeted methods aimed at covering a broader range of lipid species[37], this approach is limited to known compounds. Therefore, for screening purposes, untargeted approaches are still the best method of choice.

Untargeted lipidomics aims to determine the global lipid profile in a biological sample[38] . This approach is typically performed using fast MS detectors with high mass accuracy and resolving power, enabling them to detect all ionizable compounds. In the identification step, this helps to reduce ambiguity in lipid annotation, thus improving the biological interpretation of the data[36]. Now, thousands of lipids can be detected in a single run thanks to the high scanning speed of MS detectors such as Quadrupole Time-of-Flight (Q-ToF) and Orbitrap, resulting in sufficient data points for each lipid peak, allowing linearity, repeatability, and comparisons[39]. Furthermore, the possibility to perform MS/MS events (either in data-dependent (DDA) or data independent (DIA) acquisition mode) leads to the collection of fragmentation patterns that support identification and increase its accuracy[39]. Nevertheless, even if untargeted approaches aim to detect “all” ion features in biological samples, some of them may be missed due to ionization efficiency in specific polarity mode or ionization method, low abundance, and coelution, making the identification of lipid features challenging[40].

Therefore, the use of a single analytical method to cover the entire lipid biochemical space is not possible, and a comprehensive lipidomic analysis requires a combination of analytical tools. Specifically, for untargeted lipidomics, the application of multiple chromatographic methods like Normal Phase (NP), HILIC, Reverse Phase (RP) and Supercritical Fluid Chromatography (SFC) to the same analysis can greatly improve sample profiling[36,41]. Additionally, the choice of suitable modifier (e.g. ammonium acetate), type of ion source (Electrospray ionization or ESI; Atmospheric Pressure Chemical Ionization or APCI), and fragmentation mode (CID Collision-Induced Dissociation; EAD Electron-Activated Dissociation) further improves the breadth of lipidomic analysis[42,43].

Bioinformatics for Lipidome Data Processing

The large amount of data generated by untargeted profiling requires an advanced computational workflow to be processed. Key steps include peak picking, alignment based on retention time, deconvolution, annotation, normalization, and (relative) quantification. These steps are now implemented in software such as MS-DIAL[44], XCMS[45], LipoStar[46] , MZmine [47]and SLAW[48]. In particular, MS-DIAL represents a largely validated software for MS-based untargeted lipidomics that supports data analysis in all the steps, from data processing to statistical analysis, with a very intuitive interface. LipoStar is a license-based software for high-throughput lipid identification, quantification, and visualization, and in its latest version, it can be interfaced with other software for high-throughput identification of oxidized lipids[49]. Moreover, SLAW (Statistical Lipidomics Analysis Workflow) is a complete and scalable tool for processing untargeted LC-MS lipidomics data that efficiently analyzes datasets that differ in size, MS technology, and gradient length[48]. All the software mentioned was applied throughout this PhD project.

Data analysis

Independent of the software chosen for data processing, automated peak picking may still include low reproducible signals that need to be removed before statistical analysis. The data-cleaning step is crucial to obtaining good and reliable results and, therefore, needs to be carefully evaluated.

A key aspect of this process is filtering out features in QC samples that exhibit high variability, typically by retaining only those with a coefficient of variance (CV%) below a

predefined threshold, often between 15% and 30%. Additionally, subtracting blanks helps to remove background noise and contaminants, preserving only lipid features relevant to the analysis. Moreover, the wide dynamic range inherent in untargeted analysis can result in low-intensity, potentially biologically significant species being masked by highly intense signals, thereby influencing the outcomes of multivariate analysis. This issue can be partially addressed through data preprocessing techniques such as centering (subtracting the mean), scaling (normalizing by the standard deviation or using Pareto scaling), or transforming the dataset, often by applying a $\log_{10}$ transformation. Using a log transformation, such as $\log_{10}$, to normalize lipidomics data is a widely recognized practice for managing data with large variations in intensity and right-skewed distributions. This approach is particularly useful because it compresses the scale of high-intensity values, reducing their disproportionate influence and making patterns in the data easier to detect. It also helps stabilize variance across the dataset, which is essential for reliable statistical comparisons, particularly when combining datasets with differing magnitudes of intensities[50]. For these reasons, this type of transformation was frequently employed during the analysis of lipidomics datasets throughout this thesis.

Studies in metabolomics and lipidomics often employ log transformations to prepare data for downstream analyses, including principal component analysis (PCA) and t-tests, which assume approximately normal distributions. This transformation improves the interpretability of fold changes by converting them into a logarithmic scale, enabling more accurate comparisons between experimental groups.

Another critical step is to choose the right method to normalize the data. In principle, several normalization methods can be applied to the dataset to correct for systematic variation. The samples can be normalized by total protein content, number of cells, and weight of tissues. Normalization can also be done by total ion chromatogram (TIC), median fold changes or reference compounds, such as internal or external standards, which can be added at the beginning of sample preparation and allow correction for possible variations in sample processing. However, if the analytical system is performing well, normalization is not indispensable for tissue and plasma samples if proper sample preparation is carried out and if steps are taken during sampling to minimize variability.

One of the ultimate goals of lipidomics data analysis is to identify any significant features whose changes in concentration or profile are associated with the experimental condition

of interest. This is the first step in understanding the biological processes involved in the condition under study. A variety of approaches have been developed for these tasks. Univariate methods (t-tests and ANOVA) are widely used in lipidomics studies to select important features from lipidomic datasets. However, univariate approaches are often considered not optimal, as they ignore correlations that are known to be present among variables. Multivariate methods, which simultaneously consider all variables, are generally considered more suitable for the analysis of high-dimensional “omics” data. PCA is the most widely used exploratory and unbiased multivariate method. It reduces the number of dimensions by projecting samples onto new dimensions. This approach visualizes and discriminates samples in a new space defined by few principal components in an unsupervised manner. Partial least squares discriminant analysis (PLS-DA) and random forest are supervised multivariate methods used to search for lipids with discriminatory power to separate the experimental groups. Given the high dimensionality and complex nature of lipidomics data, PLS-DA ability to reduce noise, focus on discriminant variables, and build predictive models made it appropriate for identifying lipid biomarkers and understanding biological differences between experimental groups.

LIPIDOMICS CHALLENGES

Lipid annotations

Lipid annotation is an important task in untargeted analysis but also represents one of the major bottlenecks. Identification of lipids requires the integration of multiple parameters, such as accurate m/z, fragmentation pattern, and retention time matching with reference standards for the highest confidence[51]. However, several issues can limit the accuracy of annotations (e.g. isobaric and isomeric species, species abundance, and adducts formation), and further inspection is indispensable to reduce the number of false positives. This is true, especially for automated annotation of lipid species where spectra are matched to lipids by software tools. The collaborative efforts of the lipidomic community, and in particular of the International Lipidomics Society (ILS) and the LIPID MAPS consortium, have led to the development of guidelines for the correct annotation of lipidomic data[52,53], which contributes to strongly improving the biological relevance of the lipidomic results.

In principle, different levels of structural information have been defined for accurate lipid annotation: only structural information derived from experimental data should be considered and included in the final dataset with appropriate nomenclature (Figure 2). For instance, for lipids where specific information on the individual fatty acyl chains is unknown, the nomenclature consists of the lipid class abbreviation followed by the total number of carbon and double bond of all chains (e.g. PC 34:1). In contrast, if the different fatty acid compositions are known, an underscore separator is used between the carbon and double bond composition of each chain (PC 16:0_18:1). All double bond positions are enumerated according to the Δ-nomenclature and indicated within parentheses, e.g. PC 16:0_18:1(9).

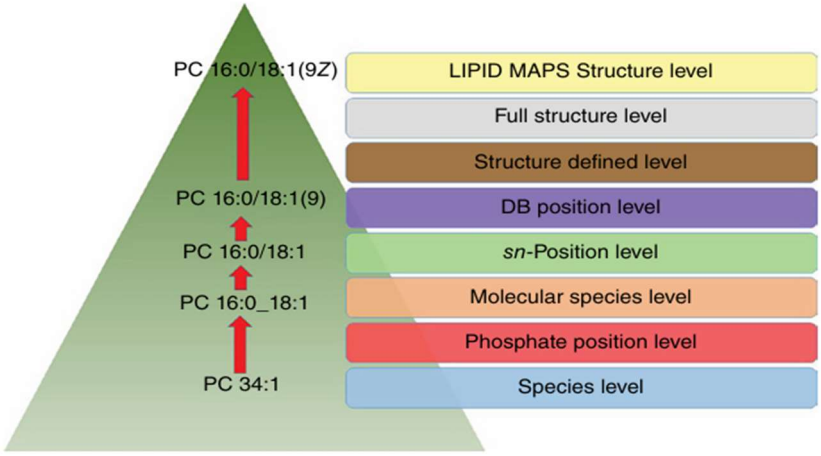

Figure 2: Hierarchical lipid annotation is based on distinct and specialized levels of structural information. Image adapted from the book "Mass Spectrometry for Lipidomics"[54].

Most lipid identifications stop at the molecular species level, leaving chemical information such as sn position, double bond location, and configuration unresolved. The depth of structural identification depends on the analytical technique used, and advanced MS/MS methods are required to reach higher levels of the pyramid. In particular, one of those MS approaches was used during my thesis.

Lipid Structural Characterization

The structural diversity of lipids yielding from the different combinations of backbone, polar head group, and acyl chain length, saturation, and double bond position add a substantial layer of variability that can ultimately have implications for health and disease [55–57]. For instance, a potential biomarker for breast cancer could be a single shift in double bond from delta 7 to delta 9 in phospholipid, and a change in the sn1 and sn2

positions of an acyl chain in phosphatidylinositols has the potential to be a marker for prostate cancer[58]. Currently, no single analytical method can fully characterize a lipid, and even in MS-based lipidomics, more than one MS experiment is usually required to obtain complete structural information.

Using conventional tandem MS methods, such as collisional-induced dissociation (CID), lipid species produce informative fragments that allow unequivocal lipid class assignment[57]. However, such fragmentation methods can often leave gaps in the structural elucidation of lipids as they are often limited to the characterization of the head group, the lengths of chains, and the numbers of double bonds on the acyl chains. To elucidate the in-depth structure, newly developed dissociation techniques can be applied, such as ozone-induced dissociation (OzID)[59], UV-induced Paternò-Büchi reaction[60], and UV photodissociation (UVPD)[61], as well as complex chromatographic strategies (Figure 3). As an alternative for the in-depth characterization of lipids, electron-based fragmentation mechanisms such as electron-activated dissociation (EAD) have been recently used[62]. This fragmentation method results in a high abundance of product ions, generating more diagnostic fragments that can be used to pinpoint double bond positions. In short, EAD can fragment virtually any C-C bond in the acyl chain and, depending on the mass shift of the individual fragments, determine whether the two carbons are bound by single or double bonds. Interestingly, the integration of EAD fragmentation into the commercially available mass spectrometer has enabled the acquisition of EAD-based spectra on a fast LC-MS timescale. As a main advantage, EAD combined with DDA enables a significant increase in compound characterization through extended fragmentation and in the number of compounds with confident identification.

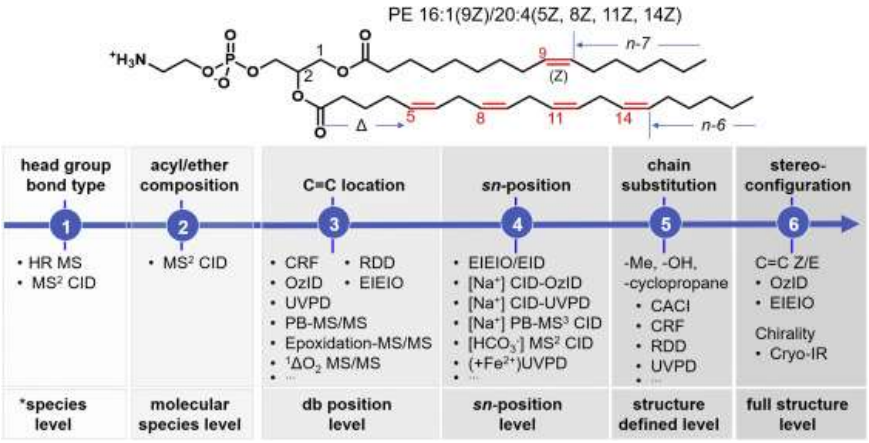

Figure 3: Image adapted from[63] . Advanced MS approaches can be used for fine-grained structural elucidation of lipid molecular species. The identified structural levels are named according to Liebisch *et al*. [64]

Study of modified lipids: epilipidomics

The lipidome is also subjected to various modifications through the introduction of small chemical groups via enzymatic and non-enzymatic reactions, which ultimately affect their structure, function, and reactivity[65]. These modifications, which include nitration, sulfation, halogenation, and oxidation, are collectively referred to as the epilipidome and play crucial roles in regulating several biological functions, including the dynamic properties of cellular membranes.[66]

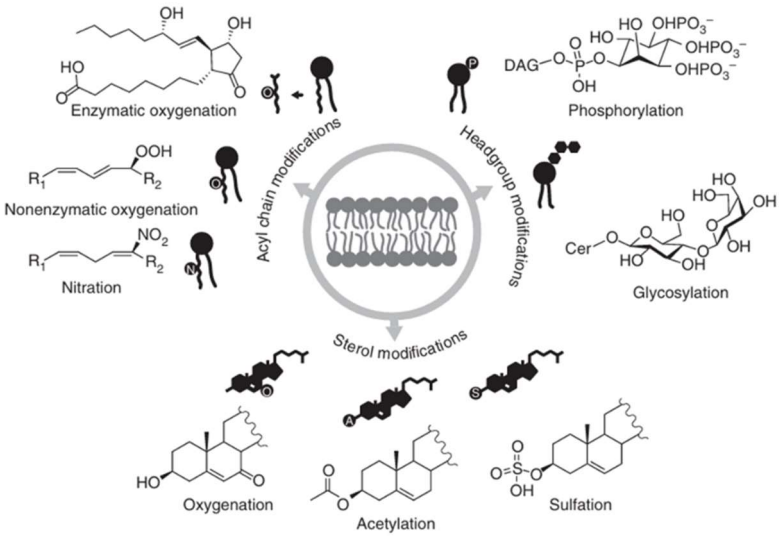

Figure 4: Lipids can undergo various chemical modifications by adding small functional groups, which can occur via enzymatic reactions or non-enzymatic processes. These modifications alter their structure and, consequently, their biological roles, influencing properties such as reactivity, functionality, and interactions within cellular systems. Figure adapted from[67]

Among these, the oxidation of lipids occurs in many pathological conditions often associated with oxidative stress, such as cardiovascular and metabolic disorders[67]. Oxidized lipids are well recognized as markers of biological oxidative stress and bioactive molecules with pro-inflammatory effects. Polyunsaturated fatty acids (PUFAs) are among the primary targets for oxidative modification in their free form or esterified complex lipids such as triglycerides and phospholipids. For example, studies on oxidized phospholipids have recognized their central role in ferroptotic cell death and in the regulation of the innate immune response. Moreover, peroxidized and hydroxylated lipids found at the skin molecular level induced the production of inflammatory mediators[68] and modulated skin responses to environmental stimuli[69]. Despite these relevant roles, the discovery and structural elucidation of oxidized lipids are still lacking,

as their identification in biological samples is hampered by their low natural abundance and structural diversity. To overcome these analytical limitations, oxidized species are often analyzed by targeted LC-MS/MS, but this does not capture the complexity of the epilipidome and prevents the discovery of new species. For more comprehensive profiling, the epilipidomic analysis can be performed by untargeted approaches, which require advanced bioinformatic tools to be processed and can potentially expand the knowledge of the functions of oxidative modifications.

Lipid Ontology, Pathways and Multi-Omics Analysis

As the detail and dimension of lipidomic datasets continue to grow, the interpretation of complex changes in lipidome (and epilipidome) profiles is becoming increasingly challenging.

Collectively, lipids can be organized and visualized in different ways to derive biological information from lipidomic datasets. However, unlike genes, proteins, or even metabolites, the classification of lipids according to their function is still challenging because relevant perturbations usually do not happen at the level of a single molecular species but involve entire lipid subclasses[70]. Moreover, the available bioinformatic tools for lipid pathway analysis are still limited and generally rely on public databases (HMDB, KEGG) that struggle to interpret lipidomic ontology.

Recently, new tools have been developed to help researchers try to extract biological knowledge from lipidome data. One such tool is LipidOntology (LION), which associates lipid species with chemical, biophysical, and biological terms[71,72]. The enrichment of LION terms can be obtained either by comparing subsets of lipids to background lipidomes (e.g., to evaluate the enrichment of LION terms in significantly altered lipids) or by analyzing the distribution of LION terms across a ranked list of lipids (such as when comparing condition A to condition B). Another tool is BioPAN, a web-based tool on the LIPID MAPS platform designed to analyze lipidomic data by integrating them into metabolic pathways, facilitating the understanding of lipid dynamics in biological systems [73]. Since this tool has been widely used in this thesis, a short description of the principles behind it is worth to be introduced. BioPAN relies on Z-scores derived from t-tests to identify significant changes in lipid metabolic pathways by comparing two different conditions. A positive z-score suggests activation, while negative scores indicate suppression, highlighting metabolic shifts under different biological states. Reactions are

visually represented with arrows, showing substrate-to-product transformations and directionality. By quantitatively analyzing lipid levels, BioPAN calculates activity scores to identify which pathways are activated or suppressed. These insights enhance understanding of metabolic processes, driving into disease mechanisms, therapeutic targets, and biomarker discovery while supporting hypothesis generation in lipidomics.

In addition to the lipidomic ontology and pathway analysis, a more comprehensive understanding of lipidome functions can be achieved by integrating multiple molecular layers of information[70]. Developing these techniques now offers the opportunity to characterise the whole phenotype and to elucidate the functional roles of lipids in complex biomolecular network interactions. Several studies have integrated lipidomics with other omics layers better to interpret altered lipid metabolism under disease state conditions[74–76]. In principle, there are two main strategies to analyze multi-omics datasets: knowledge-based approaches, which align multi-omics patterns with established networks to develop mechanistic hypotheses, and data-driven approaches, which rely on minimal prior knowledge and employ statistical techniques or neural networks for prediction and hypothesis formulation[77]. Knowledge-based methods have more statistical power but can be challenging when combining data from different datasets. Yet, the selection of the analysis method depends on the biological question and factors such as the type of analytical platform and quality of the data.

To date, selecting the most appropriate approach for specific lipidomic applications has largely depended on ad hoc testing, which is not trivial. In response, the LIPID MAPS consortium is making great efforts and recently introduced a “Lipidomic Tools Guide” to support scientists in constructing a comprehensive data analysis workflow and choosing the most suitable tools for processing lipidome datasets[78]. The tools address key areas of data processing, including “lipid-focused databases, mass spectrometry repositories, analysis of targeted lipidomics datasets, lipid identification and quantification in untargeted datasets, statistical analysis, data visualization, and integration solutions”[78] (Figure 5).

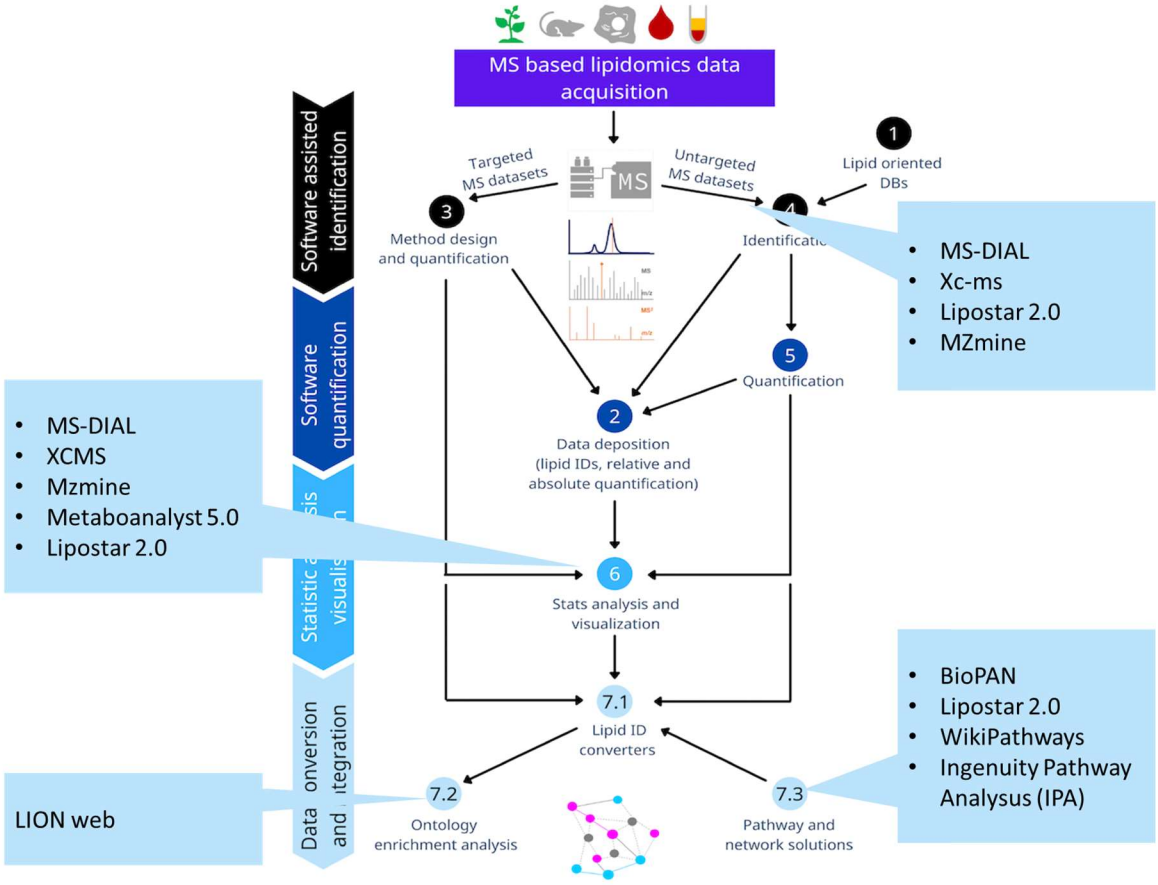

Figure 5: Workflow chart of Lipidomics Tools Guide. Image adapted from[78].

REFERENCES

(1) Joyce, A. R.; Palsson, B. Ø. The Model Organism as a System: Integrating "omics" Data Sets. *Nat Rev Mol Cell Biol* **2006**, *7* (3), 198–210. https://doi.org/10.1038/nrm1857.

(2) Wishart, D. S. Emerging Applications of Metabolomics in Drug Discovery and Precision Medicine. *Nat Rev Drug Discov* **2016**, *15* (7), 473–484. https://doi.org/10.1038/nrd.2016.32.

(3) Olivier, M.; Asmis, R.; Hawkins, G. A.; Howard, T. D.; Cox, L. A. The Need for Multi-Omics Biomarker Signatures in Precision Medicine. *Int J Mol Sci* **2019**, *20* (19), 4781. https://doi.org/10.3390/ijms20194781.

(4) Aslam, B.; Basit, M.; Nisar, M. A.; Khurshid, M.; Rasool, M. H. Proteomics: Technologies and Their Applications. *J Chromatogr Sci* **2017**, *55* (2), 182–196. https://doi.org/10.1093/chromsci/bmw167.

(5) Patti, G. J.; Yanes, O.; Siuzdak, G. Metabolomics: The Apogee of the Omics Trilogy. *Nat Rev Mol Cell Biol* **2012**, *13* (4), 263–269. https://doi.org/10.1038/nrm3314.

(6) Talayero, B. G.; Sacks, F. M. The Role of Triglycerides in Atherosclerosis. *Curr Cardiol Rep* **2011**, *13* (6), 544–552. https://doi.org/10.1007/s11886-011-0220-3.

(7) Lydic, T. A.; Goo, Y. Lipidomics Unveils the Complexity of the Lipidome in Metabolic Diseases. *Clin Transl Med* **2018**, *7* (1). https://doi.org/10.1186/s40169-018-0182-9.

(8) Chiappini, F.; Coilly, A.; Kadar, H.; Gual, P.; Tran, A.; Desterke, C.; Samuel, D.; Duclos-Vallée, J.-C.; Touboul, D.; Bertrand-Michel, J.; Brunelle, A.; Guettier, C.; Le Naour, F. Metabolism Dysregulation Induces a Specific Lipid Signature of Nonalcoholic Steatohepatitis in Patients. *Sci Rep* **2017**, *7* (1), 46658. https://doi.org/10.1038/srep46658.

(9) Kelley, N. S.; Hubbard, N. E.; Erickson, K. L. Conjugated Linoleic Acid Isomers and Cancer ,. *J Nutr* **2007**, *137* (12), 2599–2607. https://doi.org/10.1093/jn/137.12.2599.

(10) Wishart, D. S. Applications of Metabolomics in Drug Discovery and Development. *Drugs in R & D* **2008**, *9* (5), 307–322. https://doi.org/10.2165/00126839-200809050-00002.

(11) Holbrook-Smith, D.; Durot, S.; Sauer, U. High-throughput Metabolomics Predicts Drug–Target Relationships for Eukaryotic Proteins. *Mol Syst Biol* **2022**, *18* (2). https://doi.org/10.15252/msb.202110767.

(12) Swinney, D. C. Phenotypic vs. Target-Based Drug Discovery for First-in-Class Medicines. *Clin Pharmacol Ther* **2013**, *93* (4), 299–301. https://doi.org/10.1038/clpt.2012.236.

(13) Michelini, E.; Cevenini, L.; Mezzanotte, L.; Coppa, A.; Roda, A. Cell-Based Assays: Fuelling Drug Discovery. *Anal Bioanal Chem* **2010**, *398* (1), 227–238. https://doi.org/10.1007/s00216-010-3933-z.

(14) Zhang, X.-J.; She, Z.-G.; Wang, J.; Sun, D.; Shen, L.-J.; Xiang, H.; Cheng, X.; Ji, Y.-X.; Huang, Y.-P.; Li, P.-L. Multiple Omics Study Identifies an Interspecies Conserved Driver for Nonalcoholic Steatohepatitis. *Sci Transl Med* **2021**, *13* (624), eabg8117.

(15) Calle, R. A.; Amin, N. B.; Carvajal-Gonzalez, S.; Ross, T. T.; Bergman, A.; Aggarwal, S.; Crowley, C.; Rinaldi, A.; Mancuso, J.; Aggarwal, N.; Somayaji, V.; Inglot, M.; Tuthill, T. A.; Kou, K.; Boucher, M.; Tesz, G.; Dullea, R.; Bence, K. K.; Kim, A. M.; Pfefferkorn, J. A.; Esler, W. P. ACC Inhibitor Alone or Co-Administered with a DGAT2 Inhibitor in Patients with Non-Alcoholic Fatty Liver Disease: Two Parallel, Placebo-Controlled, Randomized Phase 2a Trials. *Nat Med* **2021**, *27* (10), 1836–1848. https://doi.org/10.1038/s41591-021-01489-1.

(16) Yang, L.; Li, M.; Shan, Y.; Shen, S.; Bai, Y.; Liu, H. Recent Advances in Lipidomics for Disease Research. *J Sep Sci* **2016**, *39* (1), 38–50. https://doi.org/10.1002/jssc.201500899.

(17) Sethi, S.; Brietzke, E. Recent Advances in Lipidomics: Analytical and Clinical Perspectives. *Prostaglandins Other Lipid Mediat* **2017**, *128–129*, 8–16. https://doi.org/10.1016/j.prostaglandins.2016.12.002.

(18) Liebisch, G.; Ahrends, R.; Arita, M.; Arita, M.; Bowden, J. A.; Ejsing, C. S.; Griffiths, W. J.; Holčapek, M.; Köfeler, H.; Mitchell, T. W.; Wenk, M. R.; Ekroos, K. Lipidomics Needs More Standardization. *Nat Metab* **2019**, *1* (8), 745–747. https://doi.org/10.1038/s42255-019-0094-z.

(19) Li, M.; Yang, L.; Bai, Y.; Liu, H. Analytical Methods in Lipidomics and Their Applications. *Anal Chem* **2014**, *86* (1), 161–175. https://doi.org/10.1021/ac403554h.

(20) Shevchenko, A.; Simons, K. Lipidomics: Coming to Grips with Lipid Diversity. *Nat Rev Mol Cell Biol* **2010**, *11* (8), 593–598. https://doi.org/10.1038/nrm2934.

(21) Wenk, M. R. Lipidomics: New Tools and Applications. *Cell* **2010**, *143* (6), 888–895. https://doi.org/10.1016/j.cell.2010.11.033.

(22) Fahy, E.; Subramaniam, S.; Brown, H. A.; Glass, C. K.; Merrill, A. H.; Murphy, R. C.; Raetz, C. R. H.; Russell, D. W.; Seyama, Y.; Shaw, W.; Shimizu, T.; Spener, F.; van Meer, G.; VanNieuwenhze, M. S.; White, S. H.; Witztum, J. L.; Dennis, E. A. A Comprehensive Classification System for Lipids. *J Lipid Res* **2005**, *46* (5), 839–861. https://doi.org/10.1194/jlr.E400004-JLR200.

(23) *https://www.lipidmaps.org/data/structure*.

(24) O'Donnell, V. B.; Dennis, E. A.; Wakelam, M. J. O.; Subramaniam, S. LIPID MAPS: Serving the next Generation of Lipid Researchers with Tools, Resources, Data, and Training. *Sci Signal* **2019**, *12* (563). https://doi.org/10.1126/scisignal.aaw2964.

(25) Yetukuri, L.; Ekroos, K.; Vidal-Puig, A.; Orešič, M. Informatics and Computational Strategies for the Study of Lipids. *Mol. BioSyst.* **2008**, *4* (2), 121–127. https://doi.org/10.1039/B715468B.

(26) Bligh, E. G.; Dyer, W. J. A RAPID METHOD OF TOTAL LIPID EXTRACTION AND PURIFICATION. *Can J Biochem Physiol* **1959**, *37* (8), 911–917. https://doi.org/10.1139/o59-099.

(27) Folch, J.; Lees, M.; Stanley, G. H. S. A SIMPLE METHOD FOR THE ISOLATION AND PURIFICATION OF TOTAL LIPIDES FROM ANIMAL TISSUES. *Journal of Biological Chemistry* **1957**, *226* (1), 497–509. https://doi.org/10.1016/S0021-9258(18)64849-5.

(28) Han, X.; Gross, R. W. Shotgun Lipidomics: Multidimensional MS Analysis of Cellular Lipidomes. *Expert Rev Proteomics* **2005**, *2* (2), 253–264. https://doi.org/10.1586/14789450.2.2.253.

(29) Dunn, W. B.; Broadhurst, D.; Begley, P.; Zelena, E.; Francis-McIntyre, S.; Anderson, N.; Brown, M.; Knowles, J. D.; Halsall, A.; Haselden, J. N.; Nicholls, A. W.; Wilson, I. D.; Kell, D. B.; Goodacre, R. Procedures for Large-Scale Metabolic Profiling of Serum and Plasma Using Gas Chromatography and Liquid Chromatography Coupled to Mass Spectrometry. *Nat Protoc* **2011**, *6* (7), 1060–1083. https://doi.org/10.1038/nprot.2011.335.

(30) Wenk, M. R. The Emerging Field of Lipidomics. *Nat Rev Drug Discov* **2005**, *4* (7), 594–610. https://doi.org/10.1038/nrd1776.

(31) Han, X.; Gross, R. W. Global Analyses of Cellular Lipidomes Directly from Crude Extracts of Biological Samples by ESI Mass Spectrometry: A Bridge to Lipidomics. *J Lipid Res* **2003**, *44* (6), 1071–1079. https://doi.org/10.1194/jlr.R300004-JLR200.

(32) Hu, C.; van der Heijden, R.; Wang, M.; van der Greef, J.; Hankemeier, T.; Xu, G. Analytical Strategies in Lipidomics and Applications in Disease Biomarker Discovery. *Journal of Chromatography B* **2009**, *877* (26), 2836–2846. https://doi.org/10.1016/j.jchromb.2009.01.038.

(33) Cajka, T.; Fiehn, O. Comprehensive Analysis of Lipids in Biological Systems by Liquid Chromatography-Mass Spectrometry. *TrAC Trends in Analytical Chemistry* **2014**, *61*, 192–206. https://doi.org/10.1016/j.trac.2014.04.017.

(34) Zhao, Y.-Y.; Cheng, X.-L.; Lin, R.-C.; Wei, F. Lipidomics Applications for Disease Biomarker Discovery in Mammal Models. *Biomark Med* **2015**, *9* (2), 153–168. https://doi.org/10.2217/bmm.14.81.

(35) Quehenberger, O.; Armando, A. M.; Brown, A. H.; Milne, S. B.; Myers, D. S.; Merrill, A. H.; Bandyopadhyay, S.; Jones, K. N.; Kelly, S.; Shaner, R. L.; Sullards, C. M.; Wang, E.; Murphy, R. C.; Barkley, R. M.; Leiker, T. J.; Raetz, C. R. H.; Guan, Z.; Laird, G. M.; Six, D. A.; Russell, D. W.; McDonald, J. G.; Subramaniam, S.; Fahy, E.; Dennis, E. A.

Lipidomics Reveals a Remarkable Diversity of Lipids in Human Plasma. *J Lipid Res* **2010**, *51* (11), 3299–3305. https://doi.org/10.1194/jlr.M009449.

(36) Avela, H. F.; Sirén, H. Advances in Lipidomics. *Clinica Chimica Acta* **2020**, *510*, 123–141. https://doi.org/10.1016/j.cca.2020.06.049.

(37) Xuan, Q.; Hu, C.; Yu, D.; Wang, L.; Zhou, Y.; Zhao, X.; Li, Q.; Hou, X.; Xu, G. Development of a High Coverage Pseudotargeted Lipidomics Method Based on Ultra-High Performance Liquid Chromatography–Mass Spectrometry. *Anal Chem* **2018**, *90* (12), 7608–7616. https://doi.org/10.1021/acs.analchem.8b01331.

(38) Patti, G. J.; Yanes, O.; Siuzdak, G. Metabolomics: The Apogee of the Omics Trilogy. *Nat Rev Mol Cell Biol* **2012**, *13* (4), 263–269. https://doi.org/10.1038/nrm3314.

(39) Cajka, T.; Fiehn, O. Toward Merging Untargeted and Targeted Methods in Mass Spectrometry-Based Metabolomics and Lipidomics. *Anal Chem* **2016**, *88* (1), 524–545. https://doi.org/10.1021/acs.analchem.5b04491.

(40) Köfeler, H. C.; Eichmann, T. O.; Ahrends, R.; Bowden, J. A.; Danne-Rasche, N.; Dennis, E. A.; Fedorova, M.; Griffiths, W. J.; Han, X.; Hartler, J.; Holčapek, M.; Jirásko, R.; Koelmel, J. P.; Ejsing, C. S.; Liebisch, G.; Ni, Z.; O'Donnell, V. B.; Quehenberger, O.; Schwudke, D.; Shevchenko, A.; Wakelam, M. J. O.; Wenk, M. R.; Wolrab, D.; Ekroos, K. Quality Control Requirements for the Correct Annotation of Lipidomics Data. *Nat Commun* **2021**, *12* (1), 4771. https://doi.org/10.1038/s41467-021-24984-y.

(41) Chollet, C.; Boutet-Mercey, S.; Laboureur, L.; Rincon, C.; Méjean, M.; Jouhet, J.; Fenaille, F.; Colsch, B.; Touboul, D. Supercritical Fluid Chromatography Coupled to Mass Spectrometry for Lipidomics. *Journal of Mass Spectrometry* **2019**, *54* (10), 791–801. https://doi.org/10.1002/jms.4445.

(42) Rustam, Y. H.; Reid, G. E. Analytical Challenges and Recent Advances in Mass Spectrometry Based Lipidomics. *Anal Chem* **2018**, *90* (1), 374–397. https://doi.org/10.1021/acs.analchem.7b04836.

(43) Baba, T.; Campbell, J. L.; Le Blanc, J. C. Y.; Baker, PaulR. S.; Ikeda, K. Quantitative Structural Multiclass Lipidomics Using Differential Mobility: Electron Impact Excitation of Ions from Organics (EIEIO) Mass Spectrometry. *J Lipid Res* **2018**, *59* (5), 910–919. https://doi.org/10.1194/jlr.D083261.

(44) Tsugawa, H.; Cajka, T.; Kind, T.; Ma, Y.; Higgins, B.; Ikeda, K.; Kanazawa, M.; VanderGheynst, J.; Fiehn, O.; Arita, M. MS-DIAL: Data-Independent MS/MS Deconvolution for Comprehensive Metabolome Analysis. *Nat Methods* **2015**, *12* (6), 523–526. https://doi.org/10.1038/nmeth.3393.

(45) Smith, C. A.; Want, E. J.; O'Maille, G.; Abagyan, R.; Siuzdak, G. XCMS: Processing Mass Spectrometry Data for Metabolite Profiling Using Nonlinear Peak Alignment, Matching, and Identification. *Anal Chem* **2006**, *78* (3), 779–787. https://doi.org/10.1021/ac051437y.

(46) Goracci, L.; Tortorella, S.; Tiberi, P.; Pellegrino, R. M.; Di Veroli, A.; Valeri, A.; Cruciani, G. Lipostar, a Comprehensive Platform-Neutral Cheminformatics Tool for Lipidomics. *Anal Chem* **2017**, *89* (11), 6257–6264. https://doi.org/10.1021/acs.analchem.7b01259.

(47) Pluskal, T.; Castillo, S.; Villar-Briones, A.; Orešič, M. MZmine 2: Modular Framework for Processing, Visualizing, and Analyzing Mass Spectrometry-Based Molecular Profile Data. *BMC Bioinformatics* **2010**, *11* (1), 395. https://doi.org/10.1186/1471-2105-11-395.

(48) Delabriere, A.; Warmer, P.; Brennsteiner, V.; Zamboni, N. SLAW: A Scalable and Self-Optimizing Processing Workflow for Untargeted LC-MS. *Anal Chem* **2021**, *93* (45), 15024–15032. https://doi.org/10.1021/acs.analchem.1c02687.

(49) Ni, Z.; Angelidou, G.; Hoffmann, R.; Fedorova, M. LPPtiger Software for Lipidome-Specific Prediction and Identification of Oxidized Phospholipids from LC-MS Datasets. *Sci Rep* **2017**, *7* (1), 15138. https://doi.org/10.1038/s41598-017-15363-z.

(50) Wanichthanarak, K.; In-on, A.; Fan, S.; Fiehn, O.; Wangwiwatsin, A.; Khoomrung, S. Data Processing Solutions to Render Metabolomics More Quantitative: Case Studies in Food and Clinical Metabolomics Using Metabox 2.0. *Gigascience* **2024**, *13*. https://doi.org/10.1093/gigascience/giae005.

(51) Köfeler, H. C.; Eichmann, T. O.; Ahrends, R.; Bowden, J. A.; Danne-Rasche, N.; Dennis, E. A.; Fedorova, M.; Griffiths, W. J.; Han, X.; Hartler, J.; Holčapek, M.; Jirásko, R.; Koelmel, J. P.; Ejsing, C. S.; Liebisch, G.; Ni, Z.; O'Donnell, V. B.; Quehenberger, O.; Schwudke, D.; Shevchenko, A.; Wakelam, M. J. O.; Wenk, M. R.; Wolrab, D.; Ekroos, K. Quality Control Requirements for the Correct Annotation of Lipidomics Data. *Nat Commun* **2021**, *12* (1), 4771. https://doi.org/10.1038/s41467-021-24984-y.

(52) Liebisch, G.; Vizcaíno, J. A.; Köfeler, H.; Trötzmüller, M.; Griffiths, W. J.; Schmitz, G.; Spener, F.; Wakelam, M. J. O. Shorthand Notation for Lipid Structures Derived from Mass Spectrometry. *J Lipid Res* **2013**, *54* (6), 1523–1530. https://doi.org/10.1194/jlr.M033506.

(53) Liebisch, G.; Fahy, E.; Aoki, J.; Dennis, E. A.; Durand, T.; Ejsing, C. S.; Fedorova, M.; Feussner, I.; Griffiths, W. J.; Köfeler, H.; Merrill, A. H.; Murphy, R. C.; O'Donnell, V. B.; Oskolkova, O.; Subramaniam, S.; Wakelam, M. J. O.; Spener, F. Update on LIPID MAPS Classification, Nomenclature, and Shorthand Notation for MS-Derived Lipid Structures. *J Lipid Res* **2020**, *61* (12), 1539–1555. https://doi.org/10.1194/jlr.S120001025.

(54) *Mass Spectrometry for Lipidomics*; Holčapek, M., Ekroos, K., Eds.; Wiley, 2023. https://doi.org/10.1002/9783527836512.

(55) Perrotti, F.; Rosa, C.; Cicalini, I.; Sacchetta, P.; Del Boccio, P.; Genovesi, D.; Pieragostino, D. Advances in Lipidomics for Cancer Biomarkers Discovery. *Int J Mol Sci* **2016**, *17* (12), 1992. https://doi.org/10.3390/ijms17121992.

(56) Ma, X.; Chong, L.; Tian, R.; Shi, R.; Hu, T. Y.; Ouyang, Z.; Xia, Y. Identification and Quantitation of Lipid C=C Location Isomers: A Shotgun Lipidomics Approach Enabled by Photochemical Reaction. *Proceedings of the National Academy of Sciences* **2016**, *113* (10), 2573–2578. https://doi.org/10.1073/pnas.1523356113.

(57) Han, X. *Lipidomics: Comprehensive Mass Spectrometry of Lipids*; 2016.

(58) Ma, X.; Chong, L.; Tian, R.; Shi, R.; Hu, T. Y.; Ouyang, Z.; Xia, Y. Identification and Quantitation of Lipid C=C Location Isomers: A Shotgun Lipidomics Approach Enabled by Photochemical Reaction. *Proceedings of the National Academy of Sciences* **2016**, *113* (10), 2573–2578. https://doi.org/10.1073/pnas.1523356113.

(59) Pham, H. T.; Maccarone, A. T.; Thomas, M. C.; Campbell, J. L.; Mitchell, T. W.; Blanksby, S. J. Structural Characterization of Glycerophospholipids by Combinations of Ozone- and Collision-Induced Dissociation Mass Spectrometry: The next Step towards "Top-down" Lipidomics. *Analyst* **2014**, *139* (1), 204–214. https://doi.org/10.1039/C3AN01712E.

(60) Ma, X.; Xia, Y. Pinpointing Double Bonds in Lipids by Paternò-Büchi Reactions and Mass Spectrometry. *Angewandte Chemie International Edition* **2014**, *53* (10), 2592–2596. https://doi.org/10.1002/anie.201310699.

(61) Williams, P. E.; Klein, D. R.; Greer, S. M.; Brodbelt, J. S. Pinpointing Double Bond and *Sn* -Positions in Glycerophospholipids via Hybrid 193 Nm Ultraviolet Photodissociation (UVPD) Mass Spectrometry. *J Am Chem Soc* **2017**, *139* (44), 15681–15690. https://doi.org/10.1021/jacs.7b06416.

(62) Campbell, J. L.; Baba, T. Near-Complete Structural Characterization of Phosphatidylcholines Using Electron Impact Excitation of Ions from Organics. *Anal Chem* **2015**, *87* (11), 5837–5845. https://doi.org/10.1021/acs.analchem.5b01460.

(63) Zhang, W.; Jian, R.; Zhao, J.; Liu, Y.; Xia, Y. Deep-Lipidotyping by Mass Spectrometry: Recent Technical Advances and Applications. *J Lipid Res* **2022**, *63* (7), 100219. https://doi.org/10.1016/j.jlr.2022.100219.

(64) Liebisch, G.; Fahy, E.; Aoki, J.; Dennis, E. A.; Durand, T.; Ejsing, C. S.; Fedorova, M.; Feussner, I.; Griffiths, W. J.; Köfeler, H.; Merrill, A. H.; Murphy, R. C.; O'Donnell, V. B.; Oskolkova, O.; Subramaniam, S.; Wakelam, M. J. O.; Spener, F. Update on LIPID MAPS Classification, Nomenclature, and Shorthand Notation for MS-Derived Lipid Structures. *J Lipid Res* **2020**, *61* (12), 1539–1555. https://doi.org/10.1194/jlr.S120001025.

(65) Criscuolo, A.; Nepachalovich, P.; Garcia-del Rio, D. F.; Lange, M.; Ni, Z.; Baroni, M.; Cruciani, G.; Goracci, L.; Blüher, M.; Fedorova, M. Analytical and Computational Workflow for In-Depth Analysis of Oxidized Complex Lipids in Blood Plasma. *Nat Commun* **2022**, *13* (1), 6547. https://doi.org/10.1038/s41467-022-33225-9.

(66) Ni, Z.; Goracci, L.; Cruciani, G.; Fedorova, M. Computational Solutions in Redox Lipidomics – Current Strategies and Future Perspectives. *Free Radic Biol Med* **2019**, *144*, 110–123. https://doi.org/10.1016/j.freeradbiomed.2019.04.027.

(67) Penkov, S.; Fedorova, M. Membrane Epilipidome—Lipid Modifications, Their Dynamics, and Functional Significance. *Cold Spring Harb Perspect Biol* **2024**, *16* (7), a041417. https://doi.org/10.1101/cshperspect.a041417.

(68) Niki, E. Lipid Oxidation in the Skin. *Free Radic Res* **2015**, *49* (7), 827–834. https://doi.org/10.3109/10715762.2014.976213.

(69) Ottaviani, M.; Alestas, T.; Flori, E.; Mastrofrancesco, A.; Zouboulis, C. C.; Picardo, M. Peroxidated Squalene Induces the Production of Inflammatory Mediators in HaCaT Keratinocytes: A Possible Role in Acne Vulgaris. *Journal of Investigative Dermatology* **2006**, *126* (11), 2430–2437. https://doi.org/10.1038/sj.jid.5700434.

(70) Checa, A.; Bedia, C.; Jaumot, J. Lipidomic Data Analysis: Tutorial, Practical Guidelines and Applications. *Anal Chim Acta* **2015**, *885*, 1–16. https://doi.org/10.1016/j.aca.2015.02.068.

(71) Molenaar, M. R.; Haaker, M. W.; Vaandrager, A. B.; Houweling, M.; Helms, J. B. Lipidomic Profiling of Rat Hepatic Stellate Cells during Activation Reveals a Two-Stage Process Accompanied by Increased Levels of Lysosomal Lipids. *Journal of Biological Chemistry* **2023**, *299* (4), 103042. https://doi.org/10.1016/j.jbc.2023.103042.

(72) Molenaar, M. R.; Jeucken, A.; Wassenaar, T. A.; van de Lest, C. H. A.; Brouwers, J. F.; Helms, J. B. LION/Web: A Web-Based Ontology Enrichment Tool for Lipidomic Data Analysis. *Gigascience* **2019**, *8* (6). https://doi.org/10.1093/gigascience/giz061.

(73) Gaud, C.; C. Sousa, B.; Nguyen, A.; Fedorova, M.; Ni, Z.; O'Donnell, V. B.; Wakelam, M. J. O.; Andrews, S.; Lopez-Clavijo, A. F. BioPAN: A Web-Based Tool to Explore Mammalian Lipidome Metabolic Pathways on LIPID MAPS. *F1000Res* **2021**, *10*, 4. https://doi.org/10.12688/f1000research.28022.1.

(74) Muqaku, B.; Eisinger, M.; Meier, S. M.; Tahir, A.; Pukrop, T.; Haferkamp, S.; Slany, A.; Reichle, A.; Gerner, C. Multi-Omics Analysis of Serum Samples Demonstrates Reprogramming of Organ Functions Via Systemic Calcium Mobilization and Platelet Activation in Metastatic Melanoma. *Molecular & Cellular Proteomics* **2017**, *16* (1), 86–99. https://doi.org/10.1074/mcp.M116.063313.

(75) Braun, F.; Rinschen, M. M.; Bartels, V.; Frommolt, P.; Habermann, B.; Hoeijmakers, J. H. J.; Schumacher, B.; Dollé, M. E. T.; Müller, R.-U.; Benzing, T.; Schermer, B.; Kurschat, C. E. Altered Lipid Metabolism in the Aging Kidney Identified by Three Layered Omic Analysis. *Aging* **2016**, *8* (3), 441–454. https://doi.org/10.18632/aging.100900.

(76) Kamoun, A.; Idbaih, A.; Villa, C. Integrated Multi-Omics Analysis of Oligodendroglial Tumours Identifies Three Subgroups of 1p/19q Co-Deleted Gliomas. *Nat Commun* **2016**, *7* (1), 11263. https://doi.org/10.1038/ncomms11263.

(77) Graw, S.; Chappell, K.; Washam, C. L.; Gies, A.; Bird, J.; Robeson, M. S.; Byrum, S. D. Multi-Omics Data Integration Considerations and Study Design for Biological Systems and Disease. *Mol Omics* **2021**, *17* (2), 170–185. https://doi.org/10.1039/D0MO00041H.

(78) Ni, Z.; Wölk, M.; Jukes, G.; Mendivelso Espinosa, K.; Ahrends, R.; Aimo, L.; Alvarez-Jarreta, J.; Andrews, S.; Andrews, R.; Bridge, A.; Clair, G. C.; Conroy, M. J.; Fahy, E.; Gaud, C.; Goracci, L.; Hartler, J.; Hoffmann, N.; Kopczyinki, D.; Korf, A.; Lopez-Clavijo, A. F.; Malik, A.; Ackerman, J. M.; Molenaar, M. R.; O'Donovan, C.; Pluskal, T.; Shevchenko, A.; Slenter, D.; Siuzdak, G.; Kutmon, M.; Tsugawa, H.; Willighagen, E. L.; Xia, J.; O'Donnell, V. B.; Fedorova, M. Guiding the Choice of Informatics Software and Tools for Lipidomics Research Applications. *Nat Methods* **2023**, *20* (2), 193–204. https://doi.org/10.1038/s41592-022-01710-0.

AIMS OF THE THESIS

Recent advances in omics sciences have highlighted the importance of lipidomics in biomedical research. Despite the advances in analytical techniques, the study of the lipidome remains hindered by the lack of fully validated pipelines and standardized methodologies to guide researchers through the analysis of complex datasets. This gap, compared to other omics fields like proteomics, is due to the relatively recent emergence of lipidomics and the inherent analytical challenges associated with characterizing a wide variety of lipids on a large scale. Perturbations in lipid metabolism can contribute to the development of diseases such as inflammation, cancer, and metabolic disorders, and in many cases, alterations in lipid profiles serve as key risk factors. By analyzing lipidome profiles, we can potentially understand how lipid signalling pathways respond to diseases or specific biological triggers. This approach can be used for diagnostic purposes, disease profiling, and studying drug metabolism.

As the main analytical goal of lipidomics is to identify and/or quantify as many compounds as possible, powerful analytical techniques and bioinformatics tools are required. Mass spectrometry is one of the most widely used analytical platforms to analyze the lipidome in complex biological matrices and offers promising new insights in this field.

With this thesis, we aim to study lipidome complexity by establishing an analytical workflow based on advanced mass spectrometry techniques that can be applied to different biological matrices under various experimental conditions (*in vitro* and *in vivo* models). We expect that a comprehensive analytical description of lipidomes could help to add new layers of information about biological systems and, in combination with other omics sciences, support the identification of new biomarkers or the discovery of new drugs.

In Chapter 2, our goal was to describe the molecular patterns that define the lipid-lowering activity of phytochemical compounds through an untargeted lipidomic approach. To that end, I first developed an *in vitro* model for the phenotypic screening of bioactive compounds. I grew HepG2 cells in a medium supplemented with oleic acid to promote lipid droplet formation, a common feature of the NAFLD phenotype, and challenged them with the compounds of interest. Next, with the same experimental

setup, I performed untargeted measurements of lipids. In both studies presented in this chapter, the analysis of lipidomic patterns revealed significant changes in cellular states and proved valuable in understanding the molecular mechanisms driving the lipid-lowering effects.

In Chapters 3 and **4,** I defined lipid patterns in animal models working with different biological matrices. The goal was to establish an analytical pipeline for fast and reliable analysis of lipid profiles for screening to identify biologically relevant features that define pathological states or responses to different stimuli, including those induced by drugs. In addition to the ongoing development of new workflows, our broader goal is to explore how available MS-based analytical techniques can be used to study the effects of different stimuli on multiple biological matrices. This approach represents a significant step forward as it enhances our ability to study complex biological systems (i.e. animal models) and better understand lipid dynamics under different conditions.

In Chapter 5, I took advantage of a lipidomic dataset from Chapter 4 to establish a workflow based on advanced LC-MS/MS approaches for the comprehensive profiling of oxidized lipids. The method combined a 2.4-minute untargeted lipidomic analysis with our newly assembled pipeline for unmodified and modified lipid (epilipid) annotation, enabling high-throughput detection of oxidized molecular species.

Finally, **in Chapter 6**, I applied Electron-Activated Dissociation (EAD) fragmentation to structurally characterize oxidized lipids identified in Chapter 5. This advanced MS approach allows for a fine-grained elucidation of these species beyond their molecular level.

CHAPTER 2:
PHENOTYPIC SCREENING DRUG DISCOVERY FOR THE IDENTIFICATION OF NOVEL BIOACTIVE COMPOUNDS IN *IN VITRO* CELL MODELS

STUDY I: MULTI-OMICS ANALYSIS TO ELUCIDATE MOLECULAR MECHANISMS RESPONSIBLE FOR *IN VITRO* LIPID-LOWERING PROPERTIES OF *SCUTELLARIA BAICALENSIS*

Summary

Phytochemicals from natural extracts represent an important source of bioactive compounds potentially useful in treating metabolic diseases characterized by major lipidome reconfiguration. Among them, non-alcoholic fatty liver disease (NAFLD) is a metabolic disorder caused by the accumulation of lipids in the liver as a result of an imbalance between lipid synthesis, uptake, and export. Treatment options are scarce partly due to a lack of reliable human *in vitro* disease models. *Scutellaira baicalensis*, a plant used in Chinese officinal medicine for its hypolipidemic properties, has shown several beneficial activities associated with lipid, cholesterol-lowering and anti-inflammatory effects, mainly due to its principal constituent, baicalin. However, the mechanism of action responsible for these effects is not completely understood. In this study, the *in vitro* lipid-lowering effect of *S. baicalensis* was evaluated in HepG2 cells by multi-omics studies. Oleic acid (OA) was used to promote intracellular lipid accumulation and steatosis. Using untargeted lipidomics and proteomics approaches, we investigated the changes in lipid and protein profiles associated with the lipid-lowering process. Our findings highlight the potential of *S.baicalensis* in modulating key pathways involved in lipid metabolism, transport, and accumulation, offering new insights into its therapeutic potential and highlights the importance of integrating omics studies into phenotypic screening to elucidate the molecular effects of phytocompounds.

Background

Non-alcoholic fatty liver disease (NAFLD) encompasses a range of liver disorders, including hepatic steatosis and non-alcoholic steatohepatitis (NASH), which can progress to more severe conditions such as fibrosis, cirrhosis, and hepatocellular carcinoma[1]. The excessive accumulation of lipids in the liver is a primary factor driving these diseases' onset and progression, leading to structural and functional disruptions in liver architecture[2]. The imbalance between lipid synthesis, uptake, and export in the liver causes the formation of intracellular lipid droplets, which in turn contribute to inflammation and liver damage, ultimately leading to NASH[3]. Although the precise

molecular mechanisms driving NAFLD progression remain under investigation, lipid droplets are increasingly recognized as promising therapeutic targets in the early and advanced stages of the disease. Reducing steatosis is often essential for resolving steatohepatitis, highlighting the critical role that lipids play in the development and progression of NAFLD.[4]

Despite its prevalence, NAFLD still lacks approved therapies[5], with current treatments focusing on diet and lifestyle interventions. This underscores the ongoing search for pharmacological solutions that address the disease's core mechanisms. Progress in this area has been limited, however, by the lack of reliable and translational preclinical models. In recent years, various *in vitro* models of fatty liver disease have been developed to better capture the different mechanistic aspects of the disease. These models, which include both scaffold-containing and scaffold-free systems, aim to replicate the complex pathophysiology of fatty liver disease.[6]

In this study, we developed a model of human steatosis using Human hepatocellular carcinoma cells (HepG2) under both physiological and pathophysiological conditions. Our findings show that HepG2 cells accumulate lipid droplets when exposed to excess free fatty acids, particularly oleic acid, a monounsaturated fatty acid, omega-9 (C18:1)[7]. In this culture system, hepatocytes maintain their viability, phenotype, and metabolic activity. Moreover, this system replicates in *vivo* phenomena such as the formation of lipid droplets (LD), the reversibility of steatosis, and successful treatment with various drugs. Collectively, this *in vitro* system offers mechanistic insights into the pathogenesis of steatosis, providing new perspectives on potential pharmaceutical targets.

Phytochemicals, which are plant secondary metabolites found in fruits and vegetables, have shown protective effects against metabolic diseases, particularly NAFLD, and are now becoming a valuable source of bioactive compounds[8–10]. Special attention has been dedicated to the study of medicinal plants used in traditional Chinese medicine, as they comprise a multitude of bioactive compounds to be used as therapeutic alternatives to prevent and treat steatosis with minimal adverse effects. Among them, *Scutellaria baicalensis* has emerged as a promising candidate due to its lipid-lowering effects already observed either *in vitro* or *in vivo*.[11–14]

The LC-MS/MS analytical profile of *S. baicalensis* extract has recently been obtained in our laboratory[15]. In total, 12 different flavonoids were identified, including baicalin. Baicalin is the most abundant component of the extract and accounts for 30% of the total polyphenolic content of *S.baicalensis*. It presents anti-cancer and anti-inflammatory properties, with a well-documented beneficial effect on metabolic and liver disease.[16]

Besides the beneficial effect on liver disease, the mechanism of action as well as the molecular targets responsible for this effect are not clear[17]. A chemoproteomic study suggested baicalin activates carnitine palmitoyltransferase I (CPT1), the enzyme responsible for the transport of long-chain fatty acids into mitochondria, thereby improving fatty acid metabolism[18]. More recently, Glyceraldehyde-3-Phosphate Dehydrogenase (GAPDH) was identified as one of the potential target proteins of baicalin[19]. However, no systematic studies on whole natural extracts have been conducted so far.

This study aims to investigate the lipid-lowering properties of *S. baicalensis* and to elucidate the molecular mechanisms responsible for such effects using multi-omics analysis. This approach aims to clarify the lipid and protein profile changes driving the lipid-lowering properties and to identify potential therapeutic targets for NAFLD.

Materials and Methods

Cell Culture

Human hepatocellular carcinoma cells HepG2 were cultured in T-75 cell culture flasks in minimal essential medium (MEM, EuroClone™) supplemented with 10% (v/v) fetal bovine serum (FBS), 5% penicillin/streptomycin, 5% Sodium Pyruvate and 2 mM L-glutamine. Cells were kept at 37°C with 21% O_2 and 5% CO_2. Cell culture media was replaced on alternate days, and cells were passaged once a week when confluency reached approximately 80%.

Preparation of oleic acid and steatosis induction

The preparation protocol was adapted from[20,21]. In brief, the oleic acid (OA) stock solution (0.6 M in ethanol, O1008, Sigma-Aldrich) was diluted 1:1000 (0.6 mM) in MEM

medium containing fatty acid-free BSA (molar ratio 5:1) to facilitate free fatty acid uptake to hepatocytes for 30 minutes at 37°C. HepG2 cells were exposed to this medium supplemented with OA for up to 24 hours. The control conditions were maintained in a complete medium without the OA: BSA complex.

Quantification of steatosis: AdipoRed ™ Assay

AdipoRed™ (Lonza, Switzerland) assay enables the relative quantification of intracellular lipid droplets. The reagent is a solution of Hydrophilic Stain Nile Red, which becomes fluorescent when partitioned into a hydrophobic environment, such as intracellular lipid droplets. Here, lipid accumulation was measured according to the manufacturer's instructions and optimized for solvent, concentration, and use in a 96-well-based assay.

For phenotypic screening, 1.8 x 10^4 HepG2 cells (four biological replicates for each condition tested) were plated in the 96-well plates for 24 hours in MEM complete medium. The medium was then supplemented with OA for 24 hours. Six hours after OA supplementation, compounds to be tested were added to the same medium for 18 hours. For prevention experiments, a fresh medium containing drugs was added to the cells for 18 hours and then replaced with MEM supplemented with oleic acid. At the end of the experiment, the medium was removed, and cells were carefully washed with 200 µL of phosphate-buffered saline (PBS 1X). Each well was then filled with 200 µL of prewarmed PBS, and 5 µL of AdipoRed™ Reagent was added. After 10 minutes, the fluorescence was measured with excitation at 485 nm and emission at 535 nm, with readings taken every second. Statistical analysis was done on GraphPad Prism version 8 (GraphPad Software Inc. La Jolla, CA, USA). Significance was calculated using One-way ANOVA (Adj P-value < 0.05). Data are expressed as % relative lipid content, where 100% represents results obtained with OA-treated HepG2 cells.

For validation with fenofibrate, I tested concentrations of the inhibitor previously used for HepG2 and other cell lines. The drug dissolved in Dimethyl Sulfoxide (DMSO) was added to the medium at the indicated concentration. A control condition medium containing the same concentration of DMSO was prepared.

MTT Assay

For cell viability assays, *S. baicalensis* was tested at the same concentrations used in the AdipoRed™ assay. 20.000 cells were seeded in 96-well plates and treated with different extract concentrations for 24 h in a complete medium (MEM 10% FBS, 1% penicillin/streptomycin). The medium was then removed, and cells were washed with 100 µL PBS. Then, 100 µL of MEM, not supplemented with FBS and penicillin/streptomycin, was added to each well, and the four-hour incubation was started after the addition of 11 µL MTT reagent 5 mg/mL (3-(4,5-Dimethylthiazol-2-yl)-2,5-Diphenyltetrazolium Bromide). After medium removal, cells were lysed with 100 µL of a solution consisting of DMSO, 8 mM HCl and 5% TWEEN20. The 96-well plate was shaken in the dark on a plate shaker for 15 min, and the absorbance was measured at 575 nm and 630 nm using a plate reader (BioTek's PowerWave HT, Winooski, VT, USA). Cells incubated with DMSO (0.1%) were used as a control for 100% cell proliferation.

Lipidomics

For the lipidomic experiment, cells were seeded in T-25 cell culture flasks at a final concentration of 800.000 cells/mL. After 24 hours, *Scutellaria baicalensis* was added to the medium at 150 µg/mL. The medium was then removed and replaced with MEM supplemented with OA 0.6mM (Sigma-Aldrich™) and bovine serum albumin 0.12mM (BSA, Sigma-Aldrich™ cat no. A8806) for 18 hours. Cells were washed with prewarmed PBS twice, detached with trypsin and centrifuged for 10 minutes at 15.000 rpm. Lipids were extracted with ice-cold extraction buffer, with MTBE/methanol/water (10:3:2.5, v/v/v) for 1 hour at 4°C. All solvents contained butylated hydroxytoluene (BHT) (0.1%) w/v. After centrifugation, the supernatants (lipids extract) were dried and stored at -80°C until measurement. Untargeted lipidomics of lipid extracts was performed on a TripleTOF 6600 (SCIEX) coupled to an HPLC Dionex Ultimate 3000 (Thermo Scientific) equipped with an Accucore C18 column (150 × 2.1 mm; 2.6 µm. 150 Å; Thermo Scientific, Bremen, Germany). During separation, the column temperature was maintained at 45°C, and the flow rate was set to 0.3 mL/min. Lipid classes were separated by 30-minute gradient elution using the following mobile phases: A) acetonitrile: water (6:4 v/v) with 10mM ammonium acetate and 0.1% formic acid, B) isopropanol: acetonitrile (9:1 v/v) with 10mM ammonium acetate and 0.1% formic acid. The following gradient was applied:

Time (min)	*A(%)*	*B(%)*
0	55	45
25	3	97
30	3	97
35	55	45

Table 1: LC conditions

Measurement was performed in either positive or negative ionization mode, and spectra were detected from an m/z of 50 to 1500 and MS/MS acquired in data-dependent acquisition (DDA), top 5 mode. MS parameters used are the following:

Source Parameters	***Value***
Ion Source Gas 1 (psi)	55
Ions source Gas 2 (psi)	65
Curtain Gas	35
Temperature (°C)	550
Stray Voltage	4500
MS Parameters	**Value**
Scan Type	TOF MS
Accumulation time (ms)	250
Declustering Potential (V)	80
Collision Energy (V)	10
Collision Energy Spread (V)	0
Range	50-1500 m/z
MS/MS Parameters	**Value**
Scan Type	TOF MS/MS
Maximum Candidate Ions	5
Intensity Threshold (counts/s)	100
Mass Tolerance (mDa)	50
Accumulation Time (ms)	100
Declustering Potential	50
CES	15
CE	35

Table 2: TOF MS and TOF MS/MS parameters

Features were annotated based on results from MS-Dial (ver.4.9.221218)[22] with a tolerance of 0.01 Da for MS1 and 0.025 Da for MS2. Data analysis was performed using

Metaboanalyst v5.0 online software. Data were subjected to normalization by internal standards mix (Splash Lipidomix - Avanti® Polar Lipids) added at the beginning of sample preparation and by protein concentration. Signals found in blank samples were discarded from the dataset. For multivariate analysis, data were log_{10} transformed and autoscaled. Lipidomic pathway analysis was performed using BioPAN. In pathway mapping, altered reactions are identified as either activated or suppressed based on a Z-score, which indicates whether a specific reaction has significantly changed between control and treated conditions. Reactions are then ranked by their Z-scores to reflect the extent of alteration. For enrichment analysis, LION-web was used. The enrichment of LION terms is determined by assessing their distribution across a ranked list of lipids and comparing the two experimental conditions.

Proteomics

For the proteomic experiment, 300.000 cells were seeded in 2 mL MEM medium in a 6-well plate and treated with *Scutellaria baicalensis* at 150 µg/mL for 24 hours. The medium was changed and replaced with MEM supplemented with oleic acid 0.6mM (Sigma-Aldrich™) and bovine serum albumin 0.12mM (BSA, Sigma-Aldrich™) for 18 hours. After removal of medium and washing of cells with PBS, cells were detached with trypsin, pelleted, and lysed with lysis buffer (SDS 5% (sodium dodecyl sulfate), TEAB 50 mM (triethylammonium bicarbonate buffer), $MgCl_2$ 2 mM (magnesium chloride), one cOmplete EDTA-free protease inhibitor cocktail tablet and 100 Unit of benzonase) (Sigma-Aldrich, Milan, Italy). The lysates were completely solubilized and centrifuged at 10,000× g for 15 min at 4 °C. Protein concentration was determined by BCA assay (Thermo Scientific, USA), and 30 µg of protein extract was processed through tryptic digestion using the S-Trap spin-columns (Protifi, Huntington, New York, USA). Protein lysates were reduced with tris(2-carboxyethyl)phosphine (TCEP) 5mM in 50 mM AMBIC (ammonium bicarbonate) for 10 min at 95 °C and alkylated with 20 mM IAA (iodoacetamide) in 50 mM AMBIC for 45 min at room temperature in the dark. Proteins were further denatured by acidification with 12% phosphoric acid solution in water (1:10 relative to sample volume), and 25 µL loaded onto S-trap columns with 165 µL of the binding buffer (90% methanol, 10% TEAB 1 M), then centrifuged at a speed of 4000× g for 1 min at 15 °C; this step was repeated until the protein sample was fully loaded onto the columns. After that, three washing steps by adding 150 µL of binding buffer, followed

by centrifugation (1 min, 4000× g, 15 °C), were performed to remove all the excess of unbound samples. Trypsin (sequencing-grade trypsin, Roche) was added to the samples to achieve a 20:1 sample trypsin (w/w) ratio, and the mix was incubated for 1.5 h at 47 °C under slow stirring (400 rpm). The peptide mixture was recovered by loading two different solutions; 40 µL of elution buffer 1 (10% H_2O, 90% ACN, 0.2% FA) and 35 µL of elution buffer 2 (60% H_2O, 40% ACN, 0.2% FA) onto the columns (elution and 1′ centrifugation, 4000× g, 15 °C). The collected peptide mixtures were dried in the SpeedVac at 37 °C and stored at −80 °C until analysis. Before MS measurements, samples were purified and concentrated using ZipTip C18 resin (Millipore Sigma, cat. no. ZTC18S).

Peptides were analyzed using a Dionex Ultimate 3000 nano-LC chromatography system (Thermo Scientific, Sunnyvale) with a heated column compartment set at 35 °C. Peptide mixtures were pre-concentrated onto an Acclaim PepMap 100 - 100 µm × 2 cm C18 and separated on EASY-Spray column, 15 cm × 75 µm ID packed with Thermo Scientific Acclaim PepMap RSLC C18, 3 µm, 100 Å keeping a constant flow rate of 0.3 µl/min. Mobile phases were the following: 0.1% FA in water (solvent A) and 0.1% FA in water/acetonitrile with 2/8 ratio (solvent B). The elution gradient was from 96% A to 40% B for 140 min. Peptides from each sample were analysed on an Orbitrap Fusion Tribrid Mass Spectrometer (Thermo Scientific, Bremen, Germany) in DDA mode. DDA mode was set to acquire full MS spectra in “profile” mode over a scan range of 375-1500 m/z, using a resolution setting of 120,000, an automatic gain control (AGC) target of 1 x 10^6 and a cycle time of 3 seconds. Higher-energy collision dissociation (HCD) was performed with collision energy set at 35 eV in positive polarity. Each sample was analyzed in three technical replicates.

All the RAW files were then analyzed using MaxQuant v.1.6.0 (Max Plank Institute of Biochemistry, Germany) and setting the Homo sapiens proteome database (Taxonomy ID: 9606). Only unique and razor peptides were considered for quantification, employing the MaxLFQ algorithm (version 1.6.2.3, Max Planck Institute of Biochemistry, Martinsried, Germany). Data was searched with trypsin as the protease allowing for 2 missed cleavages. A tolerance limit of 5 ppm was set for the identification of precursor ions, consistent with the performance of high-resolution instruments. Finally, chemical modifications of some amino acid residues were included in the input:

carbamidomethylation of cysteines, oxidation of methionine, and acetylation at the N-terminus of the protein.

Statistical analysis

Perseus software was used (version 1.6.1.43; Max Planck Institute of Biochemistry, Martinsried, Germany). Label-free quantification (LFQ) intensity values were first converted to a base-two logarithmic scale and then filtered for significance (Benjamini - Hochberg corrected two-sample t-test with a threshold value of 0.05 False Discovery Rate - FDR). Three comparison matrices were then constructed to calculate log2 Fold-Change values (or difference or ratio). The information on significantly up- and down-regulated proteins was then used to study the modulated pathways in the different experimental groups; a functional investigation was then conducted using Ingenuity Pathway Analysis (IPA).

IPA is a bioinformatics tool designed for the functional interpretation of quantitative omics data. It uses the Gene Ontology (GO) knowledge base to predict how up- and down-regulated proteins interact and affect specific cellular pathways. Predictions are quantified using Z-score values, where a Z-score ≥ 2.00 indicates pathway activation and ≤ -2.00 indicates inhibition. Results are visually represented with colour codes: up-regulated genes (red) suggest pathway activation (red-orange), while down-regulated genes (green) suggest inhibition (blue). Users input a matrix with log2 Fold-Change values of significantly regulated proteins and their p-values. IPA provides a more realistic view of phenotypic patterns by considering the magnitude and direction of protein expression changes.

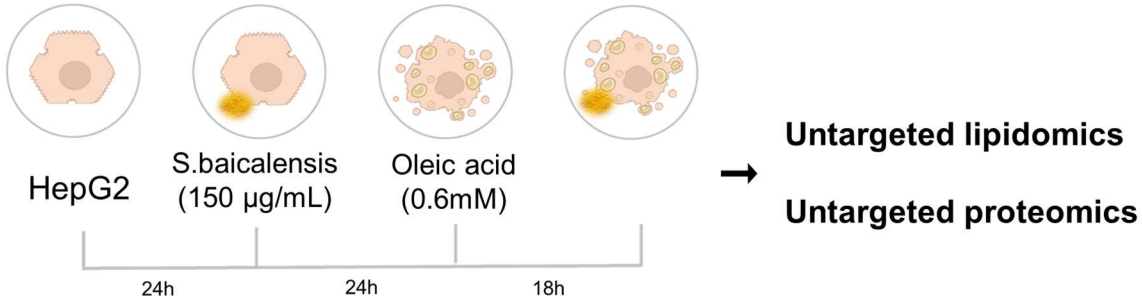

Experimental workflow for omics studies

Results

Treatment with free fatty acids promotes lipid accumulation in hepatocytes in a dose-dependent and time-dependent manner

We aimed to develop a workflow for screening bioactive compounds to evaluate their lipid-lowering effects. For this purpose, we selected a hepatocellular carcinoma cell line (HepG2) to infer the cellular state under both physiological conditions and conditions characterized by altered lipid metabolism. The initial aim was to establish conditions to induce a steatotic-like phenotype in HepG2 cells. Steatosis can be induced *in vitro* by growing cells in a medium enriched with high concentrations of free fatty acids (FFAs), in line with *in vivo* human NAFLD data[21]. For this purpose, I tested the supplementation with oleic acid (OA), a monounsaturated fatty acid, in the growing medium. The culture medium used was minimal essential medium (MEM) supplemented with 10% fetal bovine serum (FBS), which is found to be suitable for HepG2 cell growth, with 80% confluence achieved within 7 days (Figure1A). To determine the effect of OA supplementation, I initially investigated the optimal conditions and timeframe for the induction of steatosis in the *in vitro* cellular system. Cells were seeded at 20.000 cells/mL and exposed to different concentrations of OA complexed with bovine serum albumin (BSA) for up to 24 hours (Figure 1B). The concentrations tested ranged from 0.1 mM to 1.2 mM. The presence of OA in the medium promoted intracellular lipid accumulation in a dose- and time-dependent manner. The increase is observable already after 6 hours compared to the control but is accentuated after 18 and 24 hours (Figure 1D). The cells remained viable during the treatment, as determined by the MTT assay (Figure 1C). A clear dose-dependency of induction of steatosis was also observed. (Figure 1E)

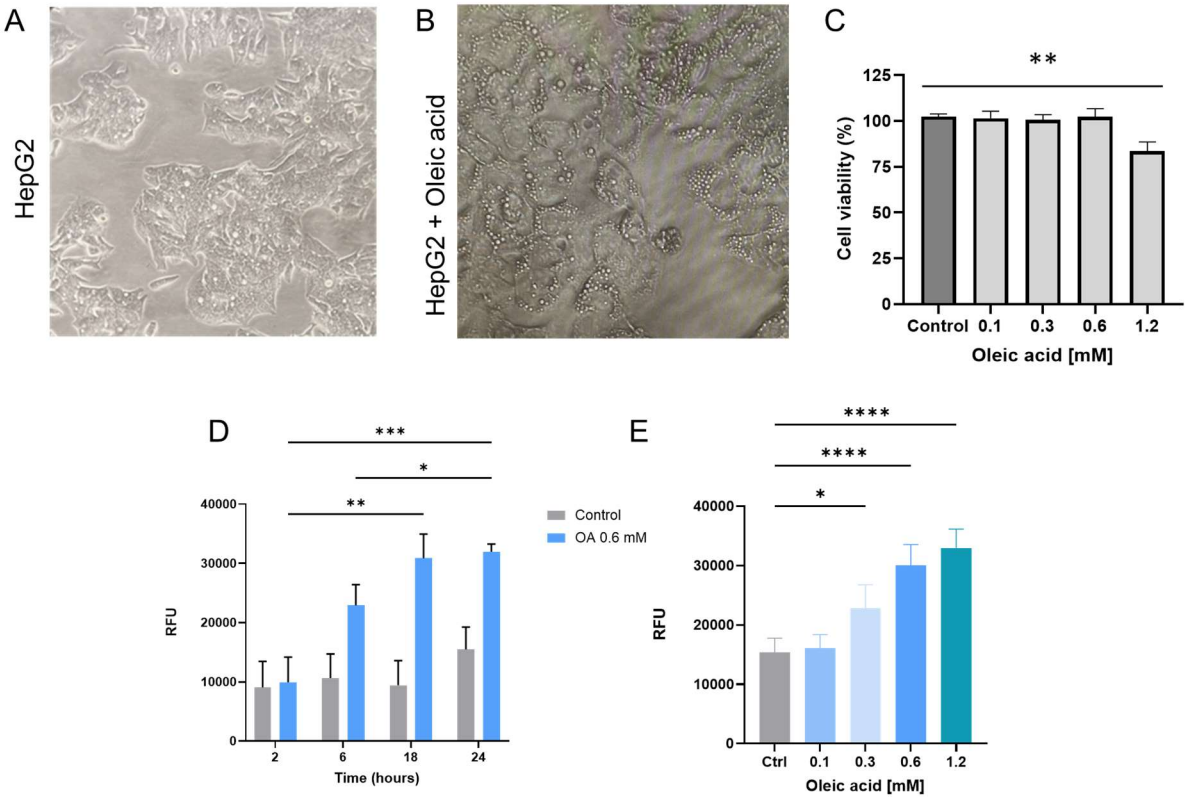

Figure 1: HepG2 as an *in vitro* model for steatosis: A) HepG2 cells at 80% confluency B) HepG2 cells treated with oleic acid (0.6mM) for 18h C) Cell viability MTT assay D) Time-dependence lipid accumulation in HepG2 E) Dose-dependent lipid accumulation in HepG2.

Steatotic phenotype is reversible in HepG2, and the system responds to drug treatment

I next investigated whether the steatotic phenotype in HepG2 cells could be reversed by treatment with drugs with known lipid-lowering properties, such as fenofibrate. Fenofibrate is a proliferator-activated receptor alpha (PPARα) agonist already used in *vivo* for the treatment of NAFLD due to its hypolipidaemic effects[23]. The drug was evaluated for its preventive effect on lipid accumulation or for the treatment of steatosis. The maximum dose of fenofibrate tested was 200 μM, as concentrations above this dose reduced cell viability. I found that fenofibrate reduced the development of fatty liver disease in a dose-dependent manner after incubation with a medium containing OA (Figure 2B). Specifically, fenofibrate significantly reduced intracellular lipid content by at least 20% compared to the untreated control, even at lower concentrations (50 μM) after 18 hours. In contrast, the prevention of steatosis is significantly relevant only at higher concentrations (Figure 2A).

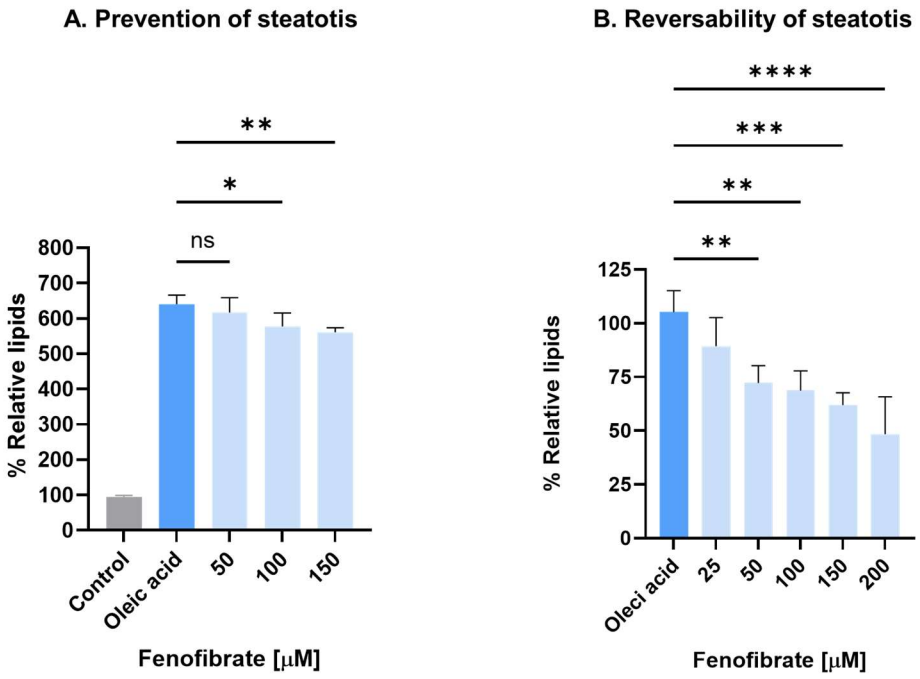

Figure 2: Fenofibrate reduced in a dose-dependent manner the development of fatty liver disease following incubation with a medium containing OA. A) Pre-treatment with fenofibrate B) Treatment with fenofibrate.

Scutellaria baicalensis reduces lipid content in OA-treated HepG2 cells

Given the positive effect of *S. baicalensis* on liver diseases, I performed the same phenotypic assay on this natural extract. Interestingly, *S. baicalensis* dose-dependently reduced intracellular lipid accumulation in a concentration range of 50 to 200 µg/mL after 24 hours of incubation without affecting cell viability. The results are summarized in Figure 3 and are expressed as a relative percentage of lipid content, where 100% represents results obtained with OA-treated HepG2 cells. The high sensitivity of HepG2 to drug treatment can be reached when cells are pretreated with the natural extract and then exposed to OA.

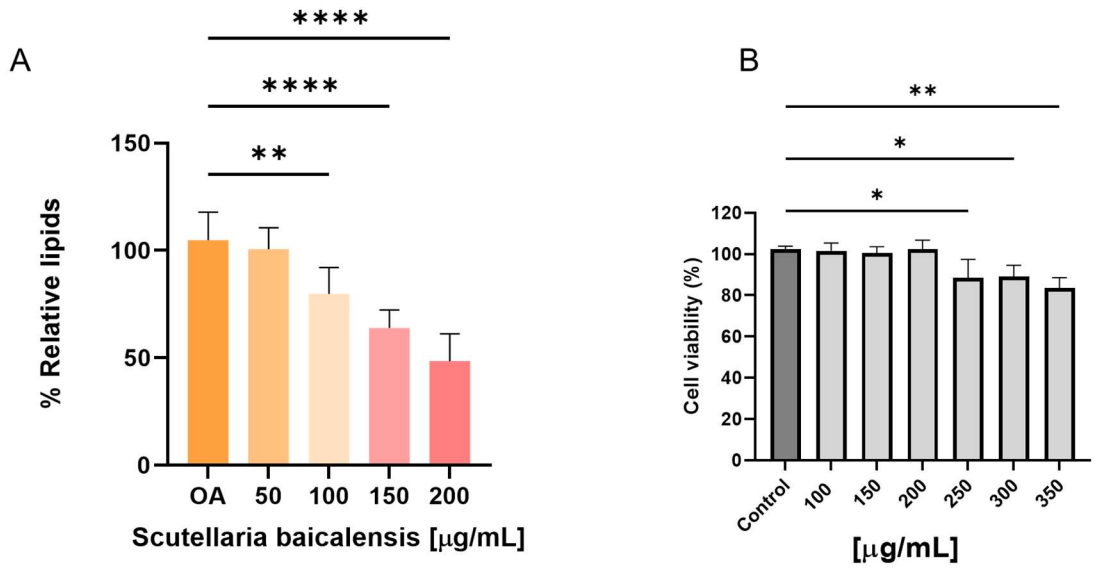

Figure 3: A) *Scutellaria baicalensis* reduced lipid content in OA-treated HepG2Dose-dependent lipid-lowering effect of *S.baicalensis* B) Cell viability MTT assay. Data are expressed as % relative lipid content, where 100% represents results obtained with OA-treated HepG2 cells.

To infer the molecular patterns that define the observed phenotypic effect, I applied MS-based omics studies. The experimental groups were as follows: untreated hepatocyte group (control cells), HepG2 treated with *Scutellaria baicalensis* (control + Sb), oleic acid-stimulated HepG2 group (OA group), and OA-stimulated HepG2 with *Scutellaria baicalensis* treatment (OA+ Sb group).

Distinct lipidomic signatures underlie steatosis induction in HepG2 cells

On top of the general lipid accumulation, comprehensive lipidomic profiling can help to understand better the response of *S. baicalensis* to steatosis in cellular systems. Firstly, I analyzed lipidome to deepen our understanding of which lipid features support the transition into the steatotic phenotype of HepG2. Therefore, I performed MS-based untargeted lipidomics of lipid species that were extracted after 18 hours of treatment with OA. Normalization of extraction efficiency was done by adding a mix of deuterated internal standards before lipid extraction. In total, I measured and annotated 463 lipids detected in both positive and negative ion modes covering 21 lipid classes. Principal Component Analysis (PCA) showed a clear separation between the control and OA experimental groups (Figure 4A). Among the lipid species explaining this separation are triacylglycerides (TG). TG-species were significantly up-regulated after the treatment with OA, following the formation of lipid droplets (LD) within hepatocytes (Figure 4B).

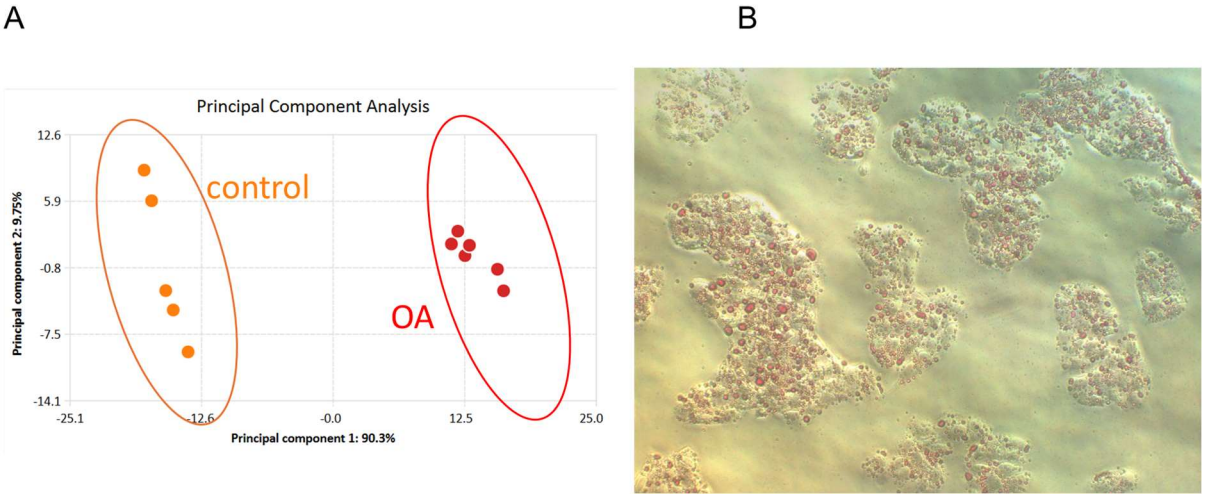

Figure 4: Distinct lipidomic signatures underlie steatosis induction in HepG2 cells A) Multivariate statistical analysis representing the lipidomic data. PCA score plot clearly shows differences between the control and cells treated with oleic acid. B) Representative image of induction of hepatic steatosis. Oil Red O staining is used to observe intracellular lipid droplet accumulation.

The steatotic phenotype was also characterized by decreased phosphatidylcholines (PC) and phosphatidylethanolamines (PE) lipid species. This decrease was accompanied by reduced levels of diacylglycerols (DG) with saturated and monounsaturated fatty acids (DG (16:0_16:1), DG (16:1_16:1) and DG (16:1_18:1)). In contrast, DG (16:0_20:4), and DG (18:1_22:6) were found to be increased (Figure 5).

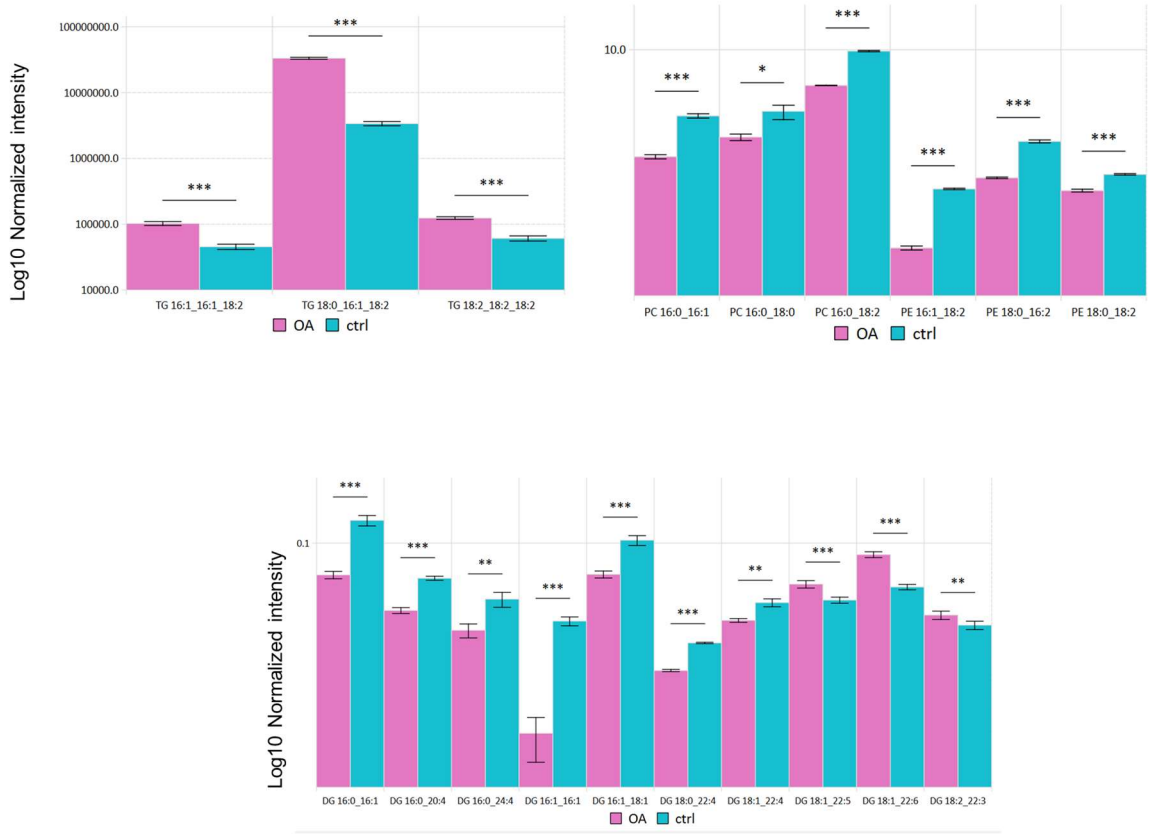

Figure 5: The steatotic phenotype was characterized by changes in the lipidome profile, mainly in TG, DG and PL lipid classes.

To visualize the most characteristic signatures and give more biological meaning to the lipidomic dataset, I performed an enrichment analysis using Lipid Ontology (LION), which associates lipid species with their chemical, biophysical, and biological information. In line with the statistical analysis, LION-terms of interest enriched in the analysis are associated with lipid droplet formation, lipid storage, and glycerolipids. As expected, this increase is mainly driven by lipids associated with “18 carbons” and monounsaturated fatty acids. Inspection of the lipid terms significantly enriched revealed a remarkable decrease in the LION signatures glycerophosphate (Figure 6).

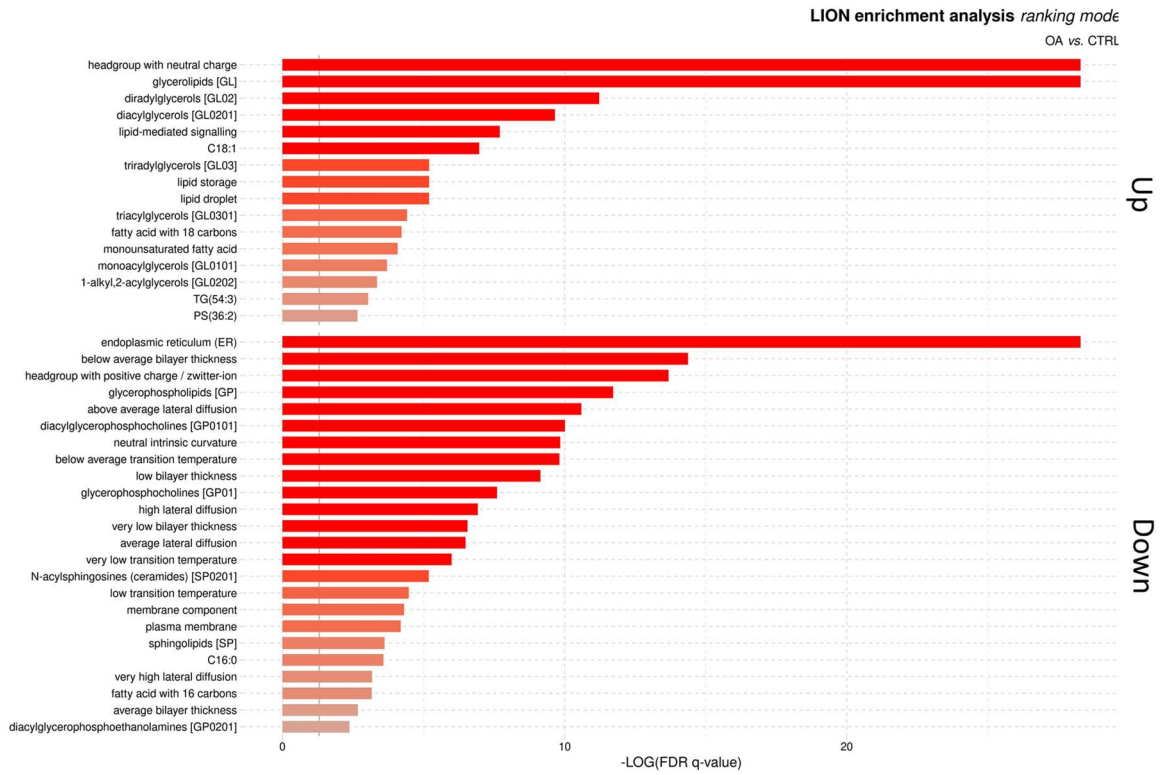

Figure 6: LION enrichment analysis of the OA group versus the control group was conducted using the "ranking mode." Significant enrichments (q < 0.05) are marked by grey vertical lines on the graph. The bars are color-coded to reflect the enrichment scores, scaled as −log(q-values), where darker colors represent higher enrichment levels.

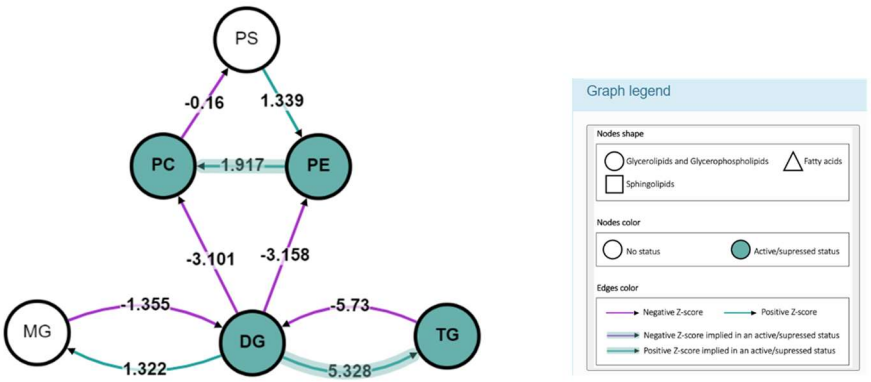

lipid subclass most active pathway (OA. vs CTRL.)			
Pathways	**Classification(s) of the pathways**	**Z-score**	**Predicted genes**
DG→TG	Triglycerol biosynthesis (Triglycerol metabolism)	5.328	*DGAT2*
PE→PC	Biosynthesis of PC (Glycerolipids and Glycerophospholipids)	1.917	*PEMT*

lipid subclass suppressed pathway (OA. vs CTRL.)			
Pathways	**Classification(s) of the pathways**	**Z-score**	**Predicted genes**
dhCer→Cer→SM	Biosynthesis of Sphingomyelin (Sphingolipids)	4.769	*DEGS1*, *DEGS2*, *SGMS1*, *SGMS2*, *CERT1*
DG→PE	Biosynthesis of PC (Glycerolipids and Glycerophospholipids), Biosynthesis of PE (Glycerolipids and Glycerophospholipids)	3.158	*CEPT1*
TG→DG→MG	Triglycerol catabolism (Triglycerol metabolism)	3.117	*PNPLA4*, *PNPLA5*, *PNPLA2*, *PNPLA3*

Figure 7: BioPAN lipid network: Green nodes correspond to active lipids, and green shaded arrows to active pathways. Reactions with a positive Z score have green arrows, while negative Z scores are purple. The table contains the active and suppressed reaction chains found by BioPAN according to the Z-score values. Pathway options: OA condition of interest, ctrl control condition, lipid type, active and suppressed status, subclass level, reaction subset of lipid data, p-value 0.05, no paired data. Pathway Analysis also indicates the regulation of specific enzymes Involved in lipid metabolism.

I then investigated systematic changes in lipid pathways using the BioPAN tool[24]. I compared the lipid profile of the OA and the control group. Pathways were scored and visualized in the network as colour-coded nodes and edges. Pathways scores revealed a prominent lipidome shift towards activation of TG synthesis and suppression of TG catabolism. Besides neutral lipids, biosynthesis of PC and PE lipid species from DG and Sphingomyelins (SM) from Ceramides was suppressed (Figure 7).

Treatment with *Scutellaria baicalensis* identifies specific lipidomic patterns underlying its mechanism of action

Next, we aimed to define the effect of *S.baicalensis* on the lipidome profile. Therefore, I pretreated OA-stimulated HepG2 cells with *S.baicalensis* extract for 24h and then performed untargeted lipidomics analysis. PCA indicated significant differences in lipid profiles between OA+Sb and OA groups, suggesting that the extract could modulate the lipid profile of OA-treated HepG2 cells (Figure 8). In total, *S.baicalensis* significantly decreased 89 lipids (fold change > 2, adj p-val< 0.05) when the OA+Sb group was compared with the OA-treated group, and these lipid species mainly belong to the TG class. Meanwhile, the treatment increased the levels of 71 species, principally belonging to the saturated and monounsaturated PC and PE classes.

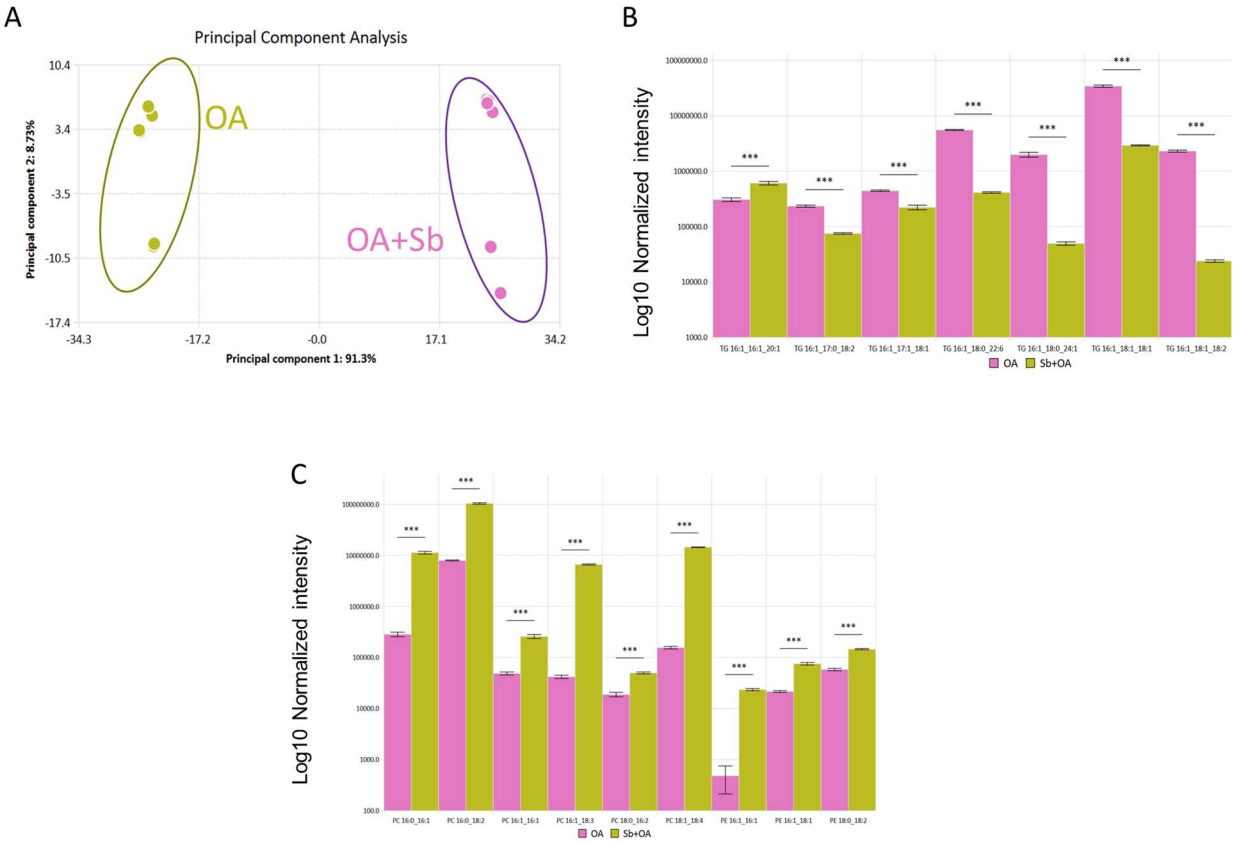

Figure 8: Treatment with *Scutellaria baicalensis* identifies specific lipidomic patterns. A) Principal component analysis B) The triacylglyceride levels are decreased C) *S.baicalensis* increased the levels of phosphatidylcholine and phosphatidylethanolamine classes.

Again, I used Lipid Ontology to enrich for significant lipidome changes across the experimental groups. A downregulation of terms such as lipid droplet and storage was observed and found to follow the decreased levels of neutral TG lipids measured by untargeted lipidomics. By pathway analysis, I identified systematic changes in lipid pathways at the lipid subclass level. The analysis showed an increase in PC and PE biosynthesis. The most significant conversions are Cer> SM, DG>PC, and TG> DG (Figure 10).

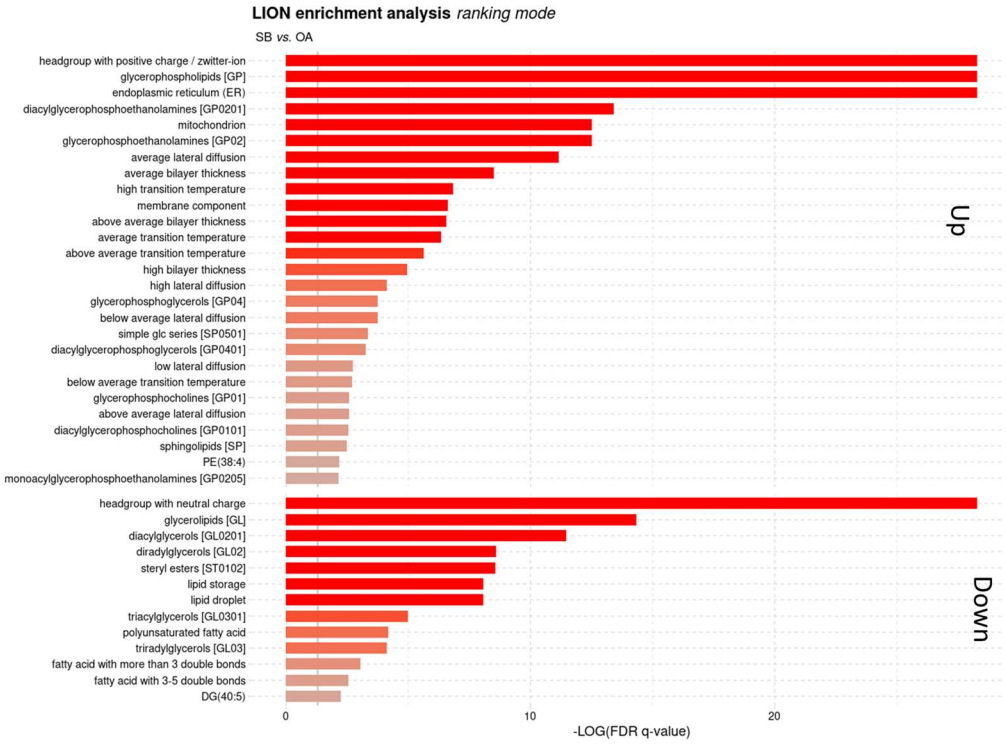

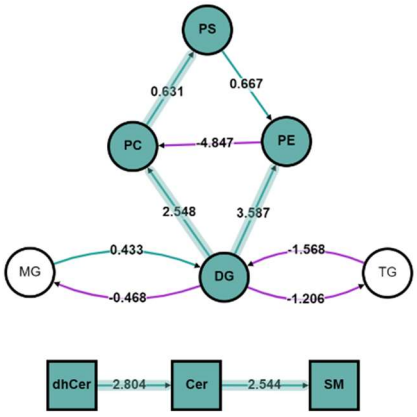

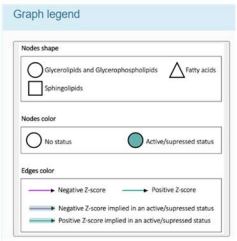

lipid subclass active pathway (SB. vs OA.)

Pathways	Classification(s) of the pathways	Z-score	Predicted genes
dhCer→Cer→SM	Biosynthesis of Sphingomyelin (Sphingolipids)	3.782	*DEGS1*, *DEGS2*, *SGMS1*, *SGMS2*, *CERT1*
DG→PE	Biosynthesis of PC (Glycerolipids and Glycerophospholipids), Biosynthesis of PE (Glycerolipids and Glycerophospholipids)	3.587	*CEPT1*
Cer→SM	Biosynthesis of Sphingomyelin (Sphingolipids)	2.544	*SGMS1*, *SGMS2*, *CERT1*
DG→PC→PS	Biosynthesis of PS (Glycerolipids and Glycerophospholipids), Biosynthesis of PE (Glycerolipids and Glycerophospholipids)	2.248	*CHPT1*, *PTDSS1*

Figure 9: LION enrichment of Sb+OA group vs OA in the “ranking mode”. Bar colours are scaled with the enrichment (−log q-values).

Figure 10: BioPAN lipid network: Green nodes correspond to active lipids, and green shaded arrows to active pathways. Reactions with a positive Z score have green arrows, while negative Z scores are purple. The table contains the active and suppressed reaction chains found by BioPAN according to the Z-score values. Pathway options: Sb+OA condition of interest, OA control condition, lipid type, active and suppressed status, subclass level, reaction subset of lipid data, p-value 0.05, no paired data.

Label-free quantitative proteomics workflow to study protein expression patterns in steatotic cells

Label-free quantitative proteomics allowed us to study the proteomic patterns that define cell state in all the experimental groups. To do this, I seeded the cells at a concentration of 300.000 cells/mL in 6 wells, treated with *S.baicalensis* 150 µg/mL and OA for 18 hours, lysed them in lysis buffer (SDS 5%, TEAB 50 mM, $MgCl_2$ 2 mM), reduced, alkylated the proteins and trypsinized to obtain peptide samples. I normalized for protein concentrations before trypsinization to improve reproducibility between biological replicates.

The peptides were measured by LC-MS/MS where the peptides were separated by a 140-minute gradient on a C18 column and subsequently analyzed using a data-dependent (DDA) approach. The resulting raw files were further processed with MaxQuant, which enabled the identification and label-free quantification of proteins in our samples. The final dataset contained 3500 protein groups identified across all experimental conditions.

First, I compared the quantitative protein profiles of OA-treated and control groups. Significantly modulated proteins (log2FC >0.57 and log2FC < - 0.57) were taken for further functional enrichment analysis and pathway analysis (Table 1).

	N° of identified proteins	*N° of proteins with log2 ratio > 0,57 (sign upreg)*	*N° of proteins with log2 ratio < -0,57 (sign downreg)*
OA vs control	3501	250	94
OA+Sb vs OA	3497	20	76
control+Sb vs control	3497	98	160

Table 1: number of proteins significantly regulated

Pathway analysis confirmed that the biological processes predicted to be activated after the incubation with OA were those involved in lipid metabolism, in particular, 'lipid concentration' with a Z-score=2.466 (Figure 11). Among the proteins involved in the activation of this biological process, perilipin2 (PLIN2) and lipid droplet-associated hydrolase (LDAH) were consistently upregulated. PLIN2 belongs to the class I proteins

associated with lipid droplets and is one of the principal structural proteins of lipid droplets. LDAH enables lipase activity and is involved in lipid storage.

Diseases or Functions Annotation	p-value	Predicted Activation State	Activation z -score
Concentration of lipid	4.06E-04	Increased	2.466
Autophagy	1.03E-07	Increased	2.235
Secretion of molecule	5.03E-04	Increased	2.069
Biosynthesis of hydrogen peroxide	1.01E-03		1.939
Organization of organelle	2.44E-03		1.913
Transport of molecule	1.41E-07		1.765
Conversion of fatty acid	3.92E-03		1.732
Infection of kidney cell lines	1.03E-04		1.704
Vaso-occlusion	2.06E-04		1.667
Occlusion of blood vessel	3.56E-04		1.667
Occlusion of artery	5.10E-04		1.667
Atherosclerosis	8.07E-04		1.667
Secretion of protein	4.68E-04		1.664
Fatty acid metabolism	1.22E-06		1.63
Biosynthesis of reactive oxygen species	1.19E-03		1.606
Synthesis of ATP	2.79E-04		1.414
Dysfunction of mitochondria	1.60E-04		-1.942
Growth of organism	4.97E-06	Decreased	-2.043
Depolarization of mitochondrial membrane	1.86E-03	Decreased	-2.219
Organization of cytoplasm	1.79E-03	Decreased	-2.85

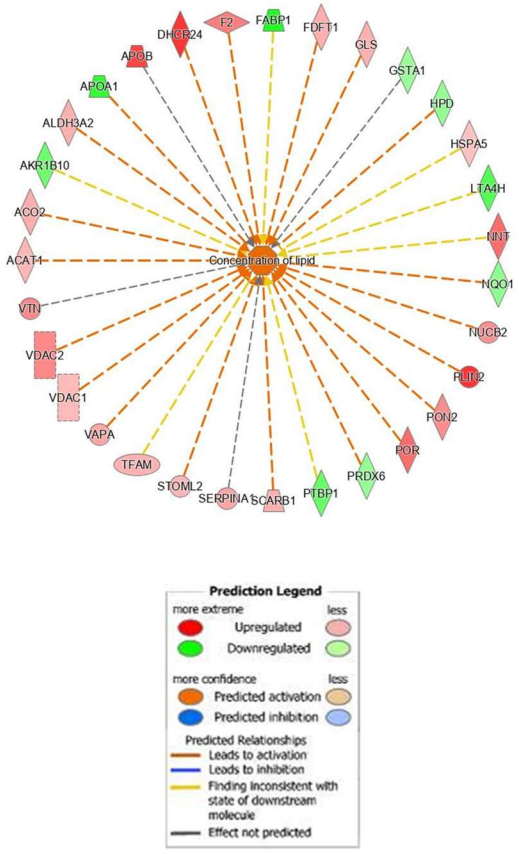

Figure 11: Graphical representation of the 'Concentrations of lipids' pathway for which IPA predicts significant activation with a Z-SCORE value of 2.466. The set of up (red) and down (green) regulated genes supporting the generated hypothesis are shown at the ends of the wheel graph. The prediction legend is essential for understanding networks.

Moreover, other specific marker proteins involved in LD homeostasis showed an increased expression pattern. Acetyl-CoA acetyltransferase (ACAT1) enables the re-esterification of cholesterol and further storage in lipid droplets. Fatty acid CoA ligase (ACSL3) promotes free fatty acids activation, while Sterol-4-alpha-carboxylate 3-dehydrogenase (NSDHL) and NADH-cytochrome b5 reductase 3 (CYB5R3) are involved in cholesterol biosynthesis, and desaturation and elongation of fatty acids respectively. Moreover, apolipoprotein B (APOB) and apolipoprotein O (APOOL) are associated with the trafficking of Very Low-Density Lipoproteins (VLDL).

I found that biosynthesis of hydrogen peroxide, oxidative phosphorylation (synthesis of ATP), and autophagy are three other pathways predicted to be activated. Those pathways have a known role in lipid metabolism. Elevated levels of fatty acids within

hepatocytes promote the activation of oxidative phosphorylation and subsequent formation of reactive oxygen species (ROS), which require a robust antioxidant response to regulate redox signalling. Saccharopine dehydrogenase (SCCPDH), located in the lipid droplets and upregulated in the OA-group, is predicted to enable oxidoreductase activity and to be involved in the glycolipid biosynthetic process.

The treatment with *S. baicalensis* defined distinct proteomic signatures in HepG2 cells

Next, I compared the protein profile of Sb+OA and OA groups. I identified the downregulation of protein markers that regulate lipid concentration, metabolism, and transport in HepG2 pretreated with *S. baicalensis*, which further supports previous results obtained by the phenotypic screening and lipidomics analysis (Figure 12). Of note is the significant reduction of PLIN2, which improved the phenotype of the hepatocytes in physiological conditions. Moreover, proteins such as APOB and Scavenger receptor class B member 1 (SCARB1), up-regulated in the OA-group, are down-regulated in the Sb+OA group. In contrast, the Fatty acid-binding protein (FABP1), which plays a key role in intracellular lipid transport, is found to be up-regulated by *S.baicalensis*. In addition to these proteins, there is a down-regulation of both the enzyme ACSL3 and the microsomal triglyceride transfer protein (MTTP). ACSL3, as anticipated, activates long-chain fatty acids for cellular lipid synthesis, whereas MTTP is required for the assembly and secretion of plasma lipoproteins. The reduction in their expression levels is consistent with decreased intracellular lipid concentration. Reduction in expression levels of proteins in mitochondrial oxidative phosphorylation, such as complex I, II, III and IV proteins (NDUF, SDHA, UQCR, COX, and ATP5F1) are linked to improved mitochondrial activity compared to the OA group and might lead to a higher tolerance of HepG2 cells to oxidative stress. Compared to the OA group, cells treated with *S.baicalensis* have a reduced expression of Ras proteins such as RAB10 and RAB14. This small GTPase controls vesicle traffic from the endoplasmic reticulum to the Golgi apparatus and is, therefore, involved in LD formation.

Diseases or Functions Annotation	p-value	Predicted Activation State	Activation z-score
Secretion of molecule	2.84E-03	Decreased	-2.595
Conversion of lipid	4.29E-03	Decreased	-2.425
Transport of molecule	1.39E-08	Decreased	-2.279
Migration of granulocytes	5.24E-03	Decreased	-2.219
Cell spreading	4.65E-04	Decreased	-2.1
Endocytosis	4.27E-04	Decreased	-2.052
Concentration of ATP	4.28E-03		-1.982
Fatty acid metabolism	3.81E-08		-1.923
Transport of lipid	7.94E-07		-1.729
Synthesis of nitric oxide	2.89E-03		-1.709
Receptor-mediated endocytosis	6.28E-03		-1.698
Transport of steroid	2.82E-05		-1.675
Concentration of lipid	1.85E-05		-1.512
Cholesterol transport	4.72E-05		-1.41
Efflux of cholesterol	7.69E-04		-1.41
Synthesis of lipid	8.49E-06		-1.331
Cell viability of embryonic cell lines	9.03E-03	Increased	2.213

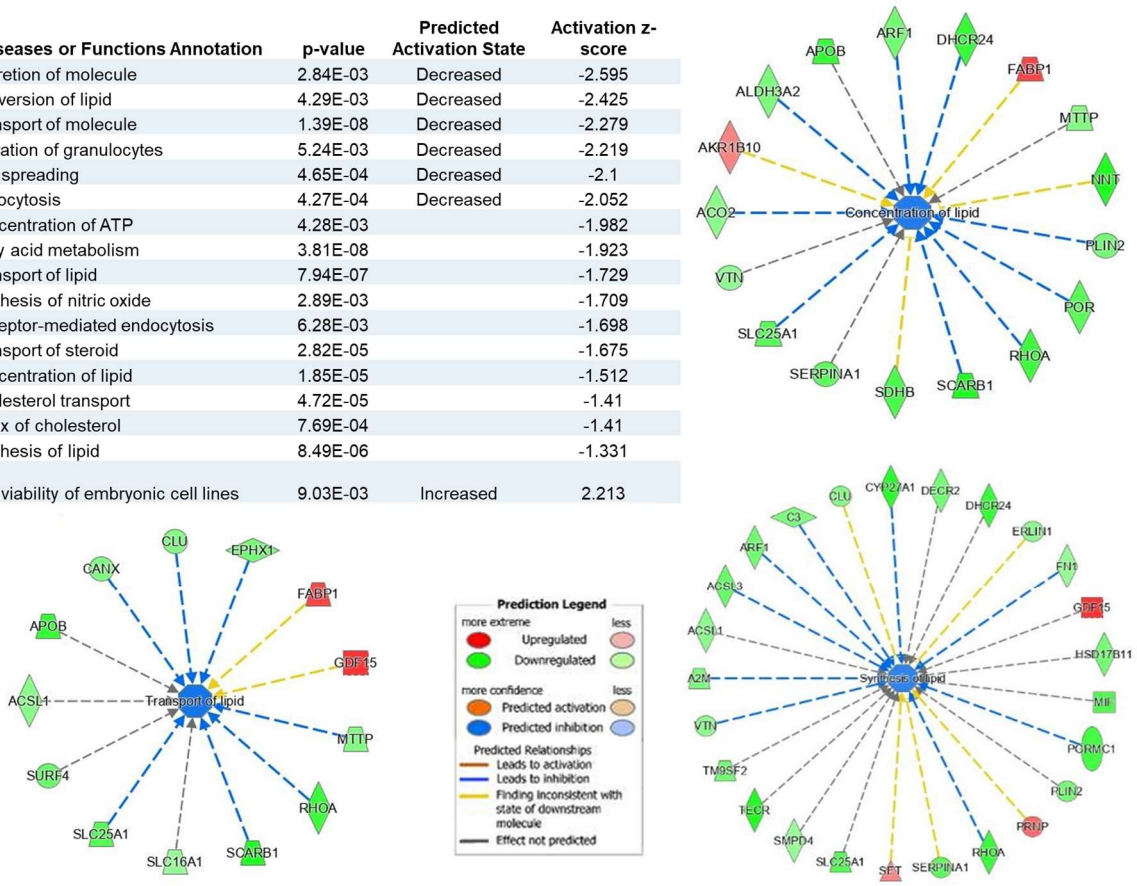

Figure 12: Graphical representation of the 'Concentrations of lipids' and 'Biosynthesis of lipids' and 'transport of lipids' pathway for which IPA predicts significant inhibition with a Z-SCORE value of -1.512, -1.331 and -1.729, respectively. The set of up (red) and down (green) regulated genes supporting the generated hypothesis are shown at the ends of the wheel graph. The prediction legend is essential for understanding networks.

Interestingly, the beneficial effect of *S.baicalensis* on HepG2 can also be observed in physiological conditions. The functional analysis predicts the inhibition of several biological processes after treatment with *S. baicalensis* (Sb group) compared to the control group. Among them, the cellular lipid concentration was significantly modulated (Figure 13). SCARB1 protein was down-regulated after treatment with the extract. There was also an up-regulation of apolipoprotein E (APOE), which mediates the binding, internalization and catabolism of lipoprotein particles, and a down-regulation of Aldehyde dehydrogenase (ALDH3A2), which catalyses the oxidation of aliphatic aldehydes to fatty acids.

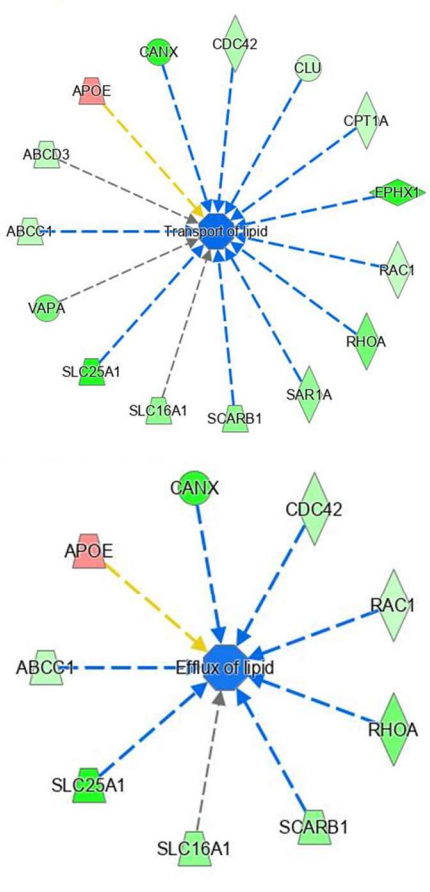

Diseases or Functions Annotation	p-value	Predicted Activation State	Activation z-score
Transport of molecule	6.02E-08	Decreased	-3.273
Reorganization of cytoskeleton	1.12E-04	Decreased	-2.737
Concentration of lipid	2.88E-04	Decreased	-2.675
Export of molecule	2.67E-05	Decreased	-2.277
Organization of cytoplasm	1.55E-04	Decreased	-2.208
Transport of carboxylic acid	1.73E-05	Decreased	-2.147
Cell proliferation of tumor cell lines	9.65E-04	Decreased	-2.082
Synthesis of purine nucleotide	2.83E-03	Decreased	-2.043
Flux of amino acids	3.41E-04		-1.969
Translocation of amino acids	6.89E-04		-1.969
Fatty acid metabolism	1.47E-03		-1.878
Export of lipid	4.21E-04		-1.874
Transport of steroid	4.98E-04		-1.843
Organization of organelle	1.12E-07		-1.841
Catabolism of protein	6.83E-03		-1.799
Cellular homeostasis	2.65E-05		-1.754
Metabolism of membrane lipid derivative	7.33E-03		-1.687
Efflux of lipid	1.13E-03		-1.669
Cholesterol transport	6.17E-03		-1.411
Transport of sterol	2.35E-03		-1.408
Stress response of cells	3.46E-04	Increased	2.008

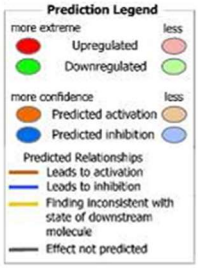

Figure 13: Graphical representation of the 'efflux of lipids' and 'transport of lipids' pathway for which IPA predicts significant inhibition with a Z-SCORE value of -1.874, -1.331 and -1.729, respectively. The set of up (red) and down (green) regulated genes supporting the generated hypothesis are shown at the ends of the wheel graph.

Discussion

The aim of this work was to provide a comprehensive description of the molecular patterns that underlie the lipid-lowering activity of *Scutellaria baicalensis* in an *in vitro* cellular model of steatosis. We found the treatment of HepG2 in a medium with a high concentration of free fatty acid promotes lipid accumulation in a dose-dependent and time-dependent manner without affecting cell viability.

Next, we assessed the diversity of lipid species profiles among different experimental conditions. Untargeted lipidomics highlighted a specific lipidome composition of HepG2 cells after incubating with OA for 18h. Elevated levels of TG with two or more palmitic acid (16:0), palmitoleic (16:1), linoleic acid (18:2), and stearic acid (18:0) substituents were detected in the lipid profiles of OA-treated HepG2. These fatty acids are preferred substrates for storage in TG[25]. However, I observed the concomitant increase of TGs

with PUFA, which may result in less dense packing of the neutral core and more dynamic lipid remodelling processes within hepatocytes.

Modulation of DG and PC levels is a crucial aspect of the study. Most of the identified lipid molecular species belonging to these subclasses were found to be lowered in OA-treated cells. PC are the major constituents of membrane lipids and are required for lipid droplet formation, VLDL production, and intercellular signalling[26]. The observed decrease in these lipid species may be linked to an elevated metabolic interconversion and hepatocyte VLDL secretion, underlined by the upregulation of APOB and APOOL protein. Hepatic synthesis of PC and PE is mainly via the Kennedy pathway from DG lipids, which are found to decrease after the treatment with OA in favour of TG production and storage. Another possible explanation for their reduced levels in the OA group is attributable to the sustained hydrolysis of PC by membrane phospholipases to lysophosphatidylcholines (LPC). Indeed, those species were found to increase by OA stimulation. The decrease in DG levels may also highlight the role of lipid droplets in sequestering lipotoxic species, thereby preventing cellular toxicity.

The pretreatment with the extract of *Scutellaria baicalensis* could, in part, regulate the altered lipid profile found in OA-treated HepG2, suggesting a positive effect on lipid metabolism. I observed a decrease in TG levels, particularly those with monounsaturated fatty acids (MUFA) substituents, the principal components of the neutral core of LD. Moreover, the level of Ceramides was also regulated, which suggested its role as a mediator of lipotoxicity[27]. Besides, the extracts increased the levels of phospholipids, particularly PC and PE subclasses suggesting that *S. baicalensis* can modulate the enzyme(s) involved in their biosynthetic pathway. Interestingly, changes in the phospholipid profile also revealed the potential antioxidant properties of the extract. Indeed, phospholipids esterified with arachidonic acid (20:4) are significantly downregulated in Sb+OA group compared to OA, whereas the levels of LPC and LPE are increased, particularly those containing an unsaturated fatty acyl group that has already showed anti-inflammatory activity both in *in vivo* and *in vitro* models[28].

Next, using the same experimental setup, I assessed the protein profile to derive more knowledge about the mechanism of action of the natural extract at the protein level. Untargeted proteomics confirmed the steatosis phenotype of OA-treated HepG2.

Indeed, I observed the presence of several proteins known to be associated with LD formation and metabolism, such as PLIN proteins. Furthermore, ASCL3 is found to be upregulated after the treatment with OA. ASCL3 plays a key role in lipid biosynthesis and fatty acid metabolism by converting free long-chain fatty acids into fatty acyl-CoA esters. Moreover, the upregulation of SCCPDH is intimately involved in the redox state of hepatocytes.

I found that oxidative phosphorylation and autophagy are top enriched pathways using the list of proteins significantly modulated in the experimental conditions. Both pathways have a known role in lipid metabolism. Hepatic autophagy was enhanced in the early stages of NAFLD development, both *in vivo* and *in vitro* [29,30]. However, the exact role of autophagy in the development of steatosis remains unclear. Specifically, it is necessary to regulate basic metabolism in hepatocytes, such as glycogenolysis and gluconeogenesis, in response to insulin and glucagon signalling. Additionally, the knockout of proteins related to autophagy suggested a critical connection between autophagy and hepatic lipid metabolism, although some results are still ambiguous[31]. While autophagy may seem necessary to support lipid beta-oxidation in some contexts, other evidence suggests that it may also contribute to lipid accumulation.

The activation of oxidative phosphorylation in the presence of a high concentration of fatty acid may have multiple explanations. Recent studies showed that mitochondria that associate with lipid droplets have more respiratory capacity and promote lipid droplet expansion as well as TG synthesis[32]. Furthermore, activation of this process indicates that the cell is actively responding to a stress condition by activating a series of metabolic pathways that require a considerable amount of energy in the form of ATP. However, sustained oxidative phosphorylation produces ROS: the electron transport chain is responsible for most of the radical oxygen species produced in a cell. When ROS levels exceed the ability of basal antioxidant systems to neutralise them, the excess reactive species damage respiratory complexes, which can lead to mitochondrial damage and hepatocyte dysfunction. However, no evidence of organelle dysfunction or reduced cell viability is observed in this study.

The proteomic pattern also underlies changes upon treatment with *S.baicalensis*. We found an almost complete inversion of the molecular pattern described in the

pathological condition (OA). Of particular relevance is the modulation of gene products mainly involved in lipid metabolism, a tangible fact that would explain the decrease in cytoplasmic lipid concentrations and their transport, in contrast to what was observed in the OA condition. Among the genes showing an opposite trend, we mention PLIN2. PLIN family proteins with a monolayer of phospholipids are coated to their surface, which also helps regulate their metabolism through basal and hormonal lipolysis. Under physiological conditions, PLIN protects the LD from the cytosolic lipases promoting the TG storage. PLIN2 deletion significantly reduced hepatic triglycerides and cholesterol levels as well as obesity and insulin sensitivity in Western diet-fed mice compared to unmodified ones[33]. Significant downregulation suggests a faster lipid metabolism, as confirmed by the conversion of lipid classes.

The predicted inactivation of pathways like ‘concentration of lipids’ and ‘’transport of lipids’, indicates extensive molecular adaptation that follows or drives improvement of the HepG2 phenotype. Overall, the dataset of significantly modulated proteins represents a vast resource for further investigations on the role of *S.baicalensis* in LD formation and maintenance and can help to infer possible molecular targets of the extract.

From the results obtained, it is likely that *S.baicalensis* can prevent the formation of LD, and therefore its target(s) should be sought before the formation of lipid droplets. Furthermore, considering its antioxidant and anti-inflammatory effects, the extract may be able to protect the cell from metabolic changes caused by excessive fatty acid intake, thus limiting stress, mitochondrial dysfunction, and other cellular damage that worsens the pathological phenotype *in vivo*. The choice of pre-treating HepG2 is supported by the fact that NAFLD in *vivo* may be reverted at this early stage. The effects of treatment with *Scutellaria baicalensis* under physiological conditions partially overlap with those observed on the pathological phenotype. Taken together, these results suggest that *Scutellaria baicalensis* treatment can improve cellular functions, and the beneficial effect relies on lipid metabolism.

Conclusion

In summary, I developed an experimental workflow in which untargeted multi-omics measurements allow us to study the molecular pattern that can help to inspect the

molecular effects of bioactive compounds from natural matrices with potential lipid-lowering activity and infer their biological targets. The advantage of applying such an innovative platform to drug discovery is that it allows us to extract distinct molecular features at the lipid or protein level and thus assess more knowledge about the biological systems to be studied.

Supplementary Tables

Supplementary Tables with all the identifications, mz, RT, intensity and MS2 can be requested from Beatrice Zoanni at beatrice.zoanni@unimi.it.

References

(1) Tilg, H.; Moschen, A. R. Evolution of Inflammation in Nonalcoholic Fatty Liver Disease: The Multiple Parallel Hits Hypothesis. *Hepatology* **2010**, *52* (5), 1836–1846. https://doi.org/10.1002/hep.24001.

(2) Estes, C.; Razavi, H.; Loomba, R.; Younossi, Z.; Sanyal, A. J. Modeling the Epidemic of Nonalcoholic Fatty Liver Disease Demonstrates an Exponential Increase in Burden of Disease. *Hepatology* **2018**, *67 (*1), 123–133. https://doi.org/10.1002/hep.29466.

(3) Bessone, F.; Razori, M. V.; Roma, M. G. Molecular Pathways of Nonalcoholic Fatty Liver Disease Development and Progression. *Cellular and Molecular Life Sciences* **2019**, *76* (1), 99–128. https://doi.org/10.1007/s00018-018-2947-0.

(4) Lee, S.; Usman, T. O.; Yamauchi, J.; Chhetri, G.; Wang, X.; Coudriet, G. M.; Zhu, C.; Gao, J.; McConnell, R.; Krantz, K.; Rajasundaram, D.; Singh, S.; Piganelli, J.; Ostrowska, A.; Soto-Gutierrez, A.; Monga, S. P.; Singhi, A. D.; Muzumdar, R.; Tsung, A.; Dong, H. H. Myeloid FoxO1 Depletion Attenuates Hepatic Inflammation and Prevents Nonalcoholic Steatohepatitis. *Journal of Clinical Investigation* **2022**, *132* (14). https://doi.org/10.1172/JCI154333.

(5) Friedman, S. L.; Neuschwander-Tetri, B. A.; Rinella, M.; Sanyal, A. J. Mechanisms of NAFLD Development and Therapeutic Strategies. *Nat Med* **2018***, 24* (7), 908–922. https://doi.org/10.1038/s41591-018-0104-9.

(6) Oseini, A. M.; Cole, B. K.; Issa, D.; Feaver, R. E.; Sanyal, A. J. Translating Scientific Discovery: The Need for Preclinical Models of Nonalcoholic Steatohepatitis. *Hepatol Int* **2018**, *12 (*1), 6–16. https://doi.org/10.1007/s12072-017-9838-6.

(7) Altomare, A. A.; Aiello, G.; Garcia, J. L.; Garrone, G.; Zoanni, B.; Carini, M.; Aldini, G.; D'Amato, A. Protein Profiling of a Cellular Model of NAFLD by Advanced Bioanalytical Approaches. *Int J Mol Sci* **2022**, *23* (16), 9025. https://doi.org/10.3390/ijms23169025.

(8) Han, X. Lipidomics for Studying Metabolism. *Nat Rev Endocrinol* **2016**, *12* (11), 668–679. https://doi.org/10.1038/nrendo.2016.98.

(9) Atanasov, A. G.; Waltenberger, B.; Pferschy-Wenzig, E.-M.; Linder, T.; Wawrosch, C.; Uhrin, P.; Temml, V.; Wang, L.; Schwaiger, S.; Heiss, E. H.; Rollinger, J. M.; Schuster, D.; Breuss, J. M.; Bochkov, V.; Mihovilovic, M. D.; Kopp, B.; Bauer, R.; Dirsch, V. M.; Stuppner, H. Discovery and Resupply of Pharmacologically Active Plant-Derived Natural Products: A Review. *Biotechnol Adv* **2015**, *33* (8), 1582–1614. https://doi.org/10.1016/j.biotechadv.2015.08.001.

(10) Li, S.; Xu, Y.; Guo, W.; Chen, F.; Zhang, C.; Tan, H. Y.; Wang, N.; Feng, Y. The Impacts of Herbal Medicines and Natural Products on Regulating the Hepatic Lipid Metabolism. *Front Pharmacol* **2020***, 11*. https://doi.org/10.3389/fphar.2020.00351.

(11) Zhao, T.; Tang, H.; Xie, L.; Zheng, Y.; Ma, Z.; Sun, Q.; Li, X. Scutellaria Baicalensis Georgi. (Lamiaceae): A Review of Its Traditional Uses, Botany, Phytochemistry, Pharmacology and Toxicology. *Journal of Pharmacy and Pharmacology* **2019**, *71* (9), 1353–1369. https://doi.org/10.1111/jphp.13129.

(12) Munjal, K.; Goel, Y.; Gauttam, V. K.; Chopra, H.; Singla, M.; Smriti; Gupta, S.; Sharma, R. Molecular Targets and Therapeutic Potential of Baicalein: A Review. *Drug Target Insights* **2024***, 18* (1), 30–46. https://doi.org/10.33393/dti.2024.2707.

(13) Yang, J.-M.; Sun, Y.; Wang, M.; Zhang, X.-L.; Zhang, S.-J.; Gao, Y.-S.; Chen, L.; Wu, M.-Y.; Zhou, L.; Zhou, Y.-M.; Wang, Y.; Zheng, F.-J.; Li, Y.-H. Regulatory Effect of a Chinese Herbal Medicine Formula on Non-Alcoholic Fatty Liver Disease. *World J Gastroenterol* **2019***, 25* (34), 5105–5119. https://doi.org/10.3748/wjg.v25.i34.5105.

(14) Chen, Q.; Liu, M.; Yu, H.; Li, J.; Wang, S.; Zhang, Y.; Qiu, F.; Wang, T. Scutellaria Baicalensis Regulates FFA Metabolism to Ameliorate NAFLD through the AMPK-Mediated SREBP Signaling Pathway. *J Nat Med* **2018**, *72* (3), 655–666. https://doi.org/10.1007/s11418-018-1199-5.

(15) Baron, G.; Borella, S.; della Vedova, L.; Vittorio, S.; Vistoli, G.; Carini, M.; Aldini, G.; Altomare, A. An Integrated Metabolomic and Proteomic Approach for the Identification of Covalent Inhibitors of the Main Protease (Mpro) of SARS-COV-2 from Crude Natural Extracts. *Talanta* **2023**, *252*, 123824. https://doi.org/10.1016/j.talanta.2022.123824.

(16) Yang, J.; Li, M.; Zhang, C.; Liu, D. Pharmacological Properties of Baicalin on Liver Diseases: A Narrative Review. *Pharmacological Reports* **2021**, *73* (5), 1230–1239. https://doi.org/10.1007/s43440-021-00227-1.

(17) Munjal, K.; Goel, Y.; Gauttam, V. K.; Chopra, H.; Singla, M.; Smriti; Gupta, S.; Sharma, R. Molecular Targets and Therapeutic Potential of Baicalein: A Review. *Drug Target Insights* **2024**, *18* (1), 30–46. https://doi.org/10.33393/dti.2024.2707.

(18) Dai, J.; Liang, K.; Zhao, S.; Jia, W.; Liu, Y.; Wu, H.; Lv, J.; Cao, C.; Chen, T.; Zhuang, S.; Hou, X.; Zhou, S.; Zhang, X.; Chen, X.-W.; Huang, Y.; Xiao, R.-P.; Wang, Y.-L.; Luo, T.;

Xiao, J.; Wang, C. Chemoproteomics Reveals Baicalin Activates Hepatic CPT1 to Ameliorate Diet-Induced Obesity and Hepatic Steatosis. *Proceedings of the National Academy of Sciences* **2018**, *115* (26). https://doi.org/10.1073/pnas.1801745115.

(19) Kusakabe, Y.; Moriya, S.-S.; Sugiyama, T.; Miyata, Y. Isolation and Identification of the New Baicalin Target Protein to Develop Flavonoid Structure-Based Therapeutic Agents. *Bioorg Med Chem* **2023**, *90,* 117362. https://doi.org/10.1016/j.bmc.2023.117362.

(20) Yan, D.; Dou, Q. L.; Wang, Z.; Wei, Y. Y. Establishment of a Hepatocyte Steatosis Model Using Chang Liver Cells. *Genetics and Molecular Research* **2015**, *14* (4), 15224–15232. https://doi.org/10.4238/2015.November.25.10.

(21) Altomare, A. A.; Aiello, G.; Garcia, J. L.; Garrone, G.; Zoanni, B.; Carini, M.; Aldini, G.; D'Amato, A. Protein Profiling of a Cellular Model of NAFLD by Advanced Bioanalytical Approaches. *Int J Mol Sci* **2022**, *23* (16), 9025. https://doi.org/10.3390/ijms23169025.

(22) Tsugawa, H.; Cajka, T.; Kind, T.; Ma, Y.; Higgins, B.; Ikeda, K.; Kanazawa, M.; VanderGheynst, J.; Fiehn, O.; Arita, M. MS-DIAL: Data-Independent MS/MS Deconvolution for Comprehensive Metabolome Analysis. *Nat Methods* **2015***, 12* (6), 523–526. https://doi.org/10.1038/nmeth.3393.

(23) Katsarou, A.; Tsioulos, G.; Kassi, E.; Chatzigeorgiou, A. Current and Experimental Pharmacotherapy for the Management of Non-Alcoholic Fatty Liver Disease. *Hormones* **2024**. https://doi.org/10.1007/s42000-024-00588-1.

(24) Gaud, C.; C. Sousa, B.; Nguyen, A.; Fedorova, M.; Ni, Z.; O'Donnell, V. B.; Wakelam, M. J. O.; Andrews, S.; Lopez-Clavijo, A. F. BioPAN: A Web-Based Tool to Explore Mammalian Lipidome Metabolic Pathways on LIPID MAPS. *F1000Res* **2021***, 10*, 4. https://doi.org/10.12688/f1000research.28022.1.

(25) Ameer, F.; Scandiuzzi, L.; Hasnain, S.; Kalbacher, H.; Zaidi, N. De Novo Lipogenesis in Health and Disease. *Metabolism* **2014**, *63* (7), 895–902. https://doi.org/10.1016/j.metabol.2014.04.003.

(26) Thiam, A. R.; Ikonen, E. Lipid Droplet Nucleation. *Trends Cell Biol* **2021**, *31* (2), 108–118. https://doi.org/10.1016/j.tcb.2020.11.006.

(27) Tanase, D. M.; Gosav, E. M.; Petrov, D.; Jucan, A. E.; Lacatusu, C. M.; Floria, M.; Tarniceriu, C. C.; Costea, C. F.; Ciocoiu, M.; Rezus, C. Involvement of Ceramides in Non-Alcoholic Fatty Liver Disease (NAFLD) Atherosclerosis (ATS) Development: Mechanisms and Therapeutic Targets. *Diagnostics* **2021**, *11* (11), 2053. https://doi.org/10.3390/diagnostics11112053.

(28) Gräler, M. Lysophospholipids and Their G Protein-Coupled Receptors in Inflammation and Immunity. Biochimica et Biophysica Acta (BBA) - *Molecular and Cell Biology of Lipids* **2002**, *1582* (1–3), 168–174. https://doi.org/10.1016/S1388-1981(02)00152-X.

(29) González-Rodríguez, Á.; Mayoral, R.; Agra, N.; Valdecantos, M. P.; Pardo, V.; Miquilena-Colina, M. E.; Vargas-Castrillón, J.; Lo Iacono, O.; Corazzari, M.; Fimia, G. M.; Piacentini, M.; Muntané, J.; Boscá, L.; García-Monzón, C.; Martín-Sanz, P.; Valverde, Á. M. Impaired Autophagic Flux Is Associated with Increased Endoplasmic Reticulum Stress during the Development of NAFLD. *Cell Death Dis* **2014**, *5* (4), e1179–e1179. https://doi.org/10.1038/cddis.2014.162.

(30) Singh, R.; Kaushik, S.; Wang, Y.; Xiang, Y.; Novak, I.; Komatsu, M.; Tanaka, K.; Cuervo, A. M.; Czaja, M. J. Autophagy Regulates Lipid Metabolism. *Nature* **2009**, *458* (7242), 1131–1135. https://doi.org/10.1038/nature07976.

(31) Raza, S.; Rajak, S.; Yen, P. M.; Sinha, R. A. Autophagy and Hepatic Lipid Metabolism: Mechanistic Insight and Therapeutic Potential for MASLD. npj *Metabolic Health and Disease* **2024***, 2* (1), 19. https://doi.org/10.1038/s44324-024-00022-5.

(32) Benador, I. Y.; Veliova, M.; Mahdaviani, K.; Petcherski, A.; Wikstrom, J. D.; Assali, E. A.; Acín-Pérez, R.; Shum, M.; Oliveira, M. F.; Cinti, S.; Sztalryd, C.; Barshop, W. D.; Wohlschlegel, J. A.; Corkey, B. E.; Liesa, M.; Shirihai, O. S. Mitochondria Bound to Lipid Droplets Have Unique Bioenergetics, Composition, and Dynamics That Support Lipid Droplet Expansion. *Cell Metab* **2018**, *27* (4), 869-885.e6. https://doi.org/10.1016/j.cmet.2018.03.003.

(33) Libby, A. E.; Bales, E.; Orlicky, D. J.; McManaman, J. L. Perilipin-2 Deletion Impairs Hepatic Lipid Accumulation by Interfering with Sterol Regulatory Element-Binding Protein (SREBP) Activation and Altering the Hepatic Lipidome. *Journal of Biological Chemistry* **2016**, *291* (46), 24231–24246. https://doi.org/10.1074/jbc.M116.759795.

STUDY II: ANALYTICAL AND OMICS STUDIES FOR THE IDENTIFICATION OF LIPID-LOWERING BIOACTIVE COMPOUNDS FROM *CITRUS BERGAMIA*

Summary

The comprehensive identification of phytochemicals represents a fundamental step in the evaluation of the biological properties of natural matrices. Due to the complexity of plant secondary metabolism, the detailed characterization of phytochemicals is an analytical challenge and requires sensitive and accurate techniques. A pre-fractionation step can be included in the analytical workflow and combined with LC-MS/MS analysis to facilitate the process of identification of bioactive phytochemicals in complex samples, following a relatively simple sample preparation step. The combination of these techniques efficiently covered different classes of secondary metabolites, including those of low abundance but of biological relevance. Of particular interest are the polyphenols derived from bergamot, which exhibited a variety of beneficial functions, including lipid-lowering properties. However, little is known about the bioactive compounds and the molecular mechanism underlying this effect. Omics approaches could better illustrate the biological effects of the extract and identify the most relevant phytochemical compounds. In this study, we propose a workflow integrating analytical and omics approaches for the comprehensive study of bergamot bioactivity in HepG2 cells.

Background

The growing interest in phytochemicals as sources of bioactive compounds has encouraged the development of an analytical pipeline for comprehensive phytochemical characterization to support the discovery of novel bioactive compounds with potential therapeutic properties[1,2]. The search for pharmacologically active molecules from natural sources requires efficient analytical methodologies capable of analyzing the diverse metabolic profiles of plants, which include a wide range of chemical constituents with very diverse physicochemical properties[3].

Bioactive phytochemicals, such as polyphenols, are particularly noteworthy for their beneficial properties, mainly attributed to their antioxidant effects[4]. Among these,

bergamot-enriched polyphenolic fractions (BPF) obtained from the peeled fruit of bergamot have been claimed for their lipid-lowering and anti-inflammatory effects, significantly reducing cardiovascular damage and metabolic disorders[5]. Bergamot (*Citrus bergamia*) is an ancient fruit-bearing tree grown in southern Italy that has numerous beneficial effects on human health. Oral administration of BPF to patients with hyperlipidemia has been shown to reduce triglycerides, total cholesterol, LDL, and blood glucose while increasing HDL levels[6]. Moreover, BPF has also been shown to reduce histological damage by reducing the NF-kB signalling pathway, inflammatory cytokine production, and oxidative stress[7]. In a similar study, the anti-inflammatory activity of bergamot was highlighted in mice with colitis: a reduction in IL-1β and TNF-α levels and a decrease in NF-kB nuclear translocation were observed following consumption of 20mg/kg/day of bergamot juice extract. Plasma levels of oxidized LDL, a biomarker associated with lipid peroxidation, were also lower in BPF-treated mice. Based on growing scientific evidence of the positive effects of the polyphenol-rich fraction of bergamot on human health, demand for BPF is expected to increase in the coming years.

To date, the beneficial effects of bergamot have mainly been studied in the fruit, which is of limited availability due to its seasonal harvest. Interestingly, the phytochemical composition of the leaf shows an overlapping qualitative profile with the fruit, with 100 out of 108 compounds found in both matrices[8]. Moreover, semiquantitative analysis has shown that the leaf contains more polyphenols than the fruit, suggesting that leaves are an attractive, more environmentally sustainable source of polyphenols with potential nutraceutical applications.

These encouraging results have stimulated further investigation into the potential beneficial effects of bergamot leaf polyphenolic extract in the treatment and prevention of metabolic disorders, where altered lipid profiles often accompany disease progression[9]. However, the bioactive compounds responsible for the beneficial effects are unknown. The cholesterol-lowering activity has been attributed to flavonoids bearing the hydroxymethylglutaryl (HMG) moiety, which could inhibit cholesterol synthesis due to structural similarity with endogenous ligands and statins. Recently, it was demonstrated that BPF and its main constituents do not directly inhibit 3-Hydroxy-3-Methylglutaryl-CoA Reductase activity (HMGCR) but instead downregulate the expression of HMGCR in HepG2 cells[10]. This observation is consistent with clinical

findings on the cholesterol-lowering effects of bergamot, suggesting that the cholesterol-lowering activity of bergamot is distinct from that of statins. While this partly explains the cholesterol-lowering mechanisms, the hypolipidemic effect likely results from interactions between bergamot compounds and other biological targets.

In this context, advanced omics studies are invaluable tools for better understanding potential targets and the overall lipid-lowering mechanism of bergamot. Here, we develop a pipeline for the comprehensive description of the phytochemical profile of enriched polyphenolic fractions of bergamot leaves by combining analytical and advanced omics approaches. A pre-fractionation step is included in the analytical workflow, and its combination with LC-MS/MS allowed for a detailed characterization of the polyphenolic profile. A semi-quantitative analysis was carried out to evaluate the relative abundance of identified compounds. Finally, the lipid-lowering activity of each isolated fraction was inferred by cell-based assays, and untargeted lipidomic analysis was conducted to describe changes in the lipid profiles of HepG2 cells upon treatment with bioactive fractions. This work could help promote the use of bergamot leaves as a valuable source of polyphenols for incorporation into health products aimed at preventing or treating liver metabolic disorders.

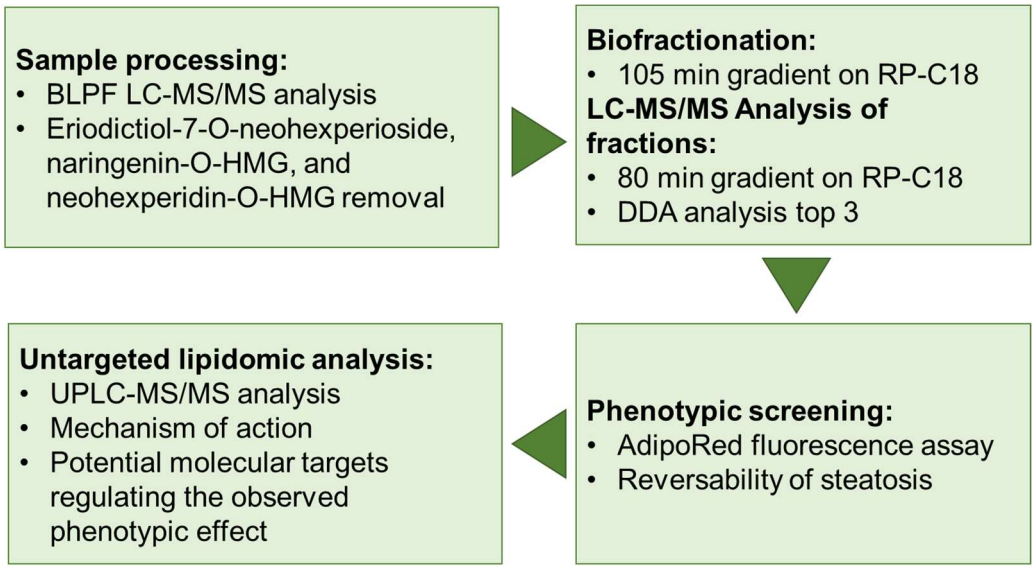

Figure 1: Workflow to study lipid-lowering bioactive compounds from Bergamot BLPF.

Materials and Methods

BLPF Preparation

The leaf polyphenol fraction (BLPF) extract was prepared as described elsewhere[11]. Briefly, the bergamot leaves are harvested and subsequently minced, and a water/ethanol (30/70, %v/v) solution is added to the polyphenols extract. The ethanol is then distilled, and the clarified water solution is passed through a polystyrene absorbing resin bed with pores of 100–150 Å. The entrapped polyphenols are then eluted with pure ethanol. The obtained ethanolic solution is distilled at temperatures of up to 40 °C to obtain a concentrated solution containing residual water with polyphenols, which is then dried in a spray drying system to obtain a powder with less than 4.0% humidity.

Preparative HPLC

BLPF was prepared for fractionation at a concentration of 60 mg/mL in H_2O/ACN, 80/20 % v/v. An aliquot of 500 µL was then injected manually into the LC system. The chromatographic separation was performed on a Synergi^{TM} Fusion-RP 80 Å-C18 column (250 × 10 mm, i.d. 4 µm, Phenomenex, Milan, Italy) through a preparative chromatography system (LC-20AP) equipped with an SPD-40V UV detector, an FRC-10A fraction collector and a CBM-40 system controller (Shimadzu, Milan, Italy) with a multi-step gradient program (105 min) (Table 1) of mobile phase A (H_2O/HCOOH 0.1, % v/v) and B (ACN/HCOOH 0.1, % v/v) (Table 1 left). The fraction collector was set for either the isolation of melitidine and brutieridine or the fractionation step, as shown in Table 1 (right).

Time (min)	*% A*	*% B*	*Time [min]*	*Action*	*Value*
0	90	10	0.33	Valve	Open
66	80	20	0.34	Lock	Unlock
85	40	60	0.35	Level	10000
95	40	60	104.5	Level	10000
95.1	90	10	104.7	Lock	Lock
105	90	10	104.9	Valve	Close

Table 1: Preparative HPLC gradient (left) and fraction collector actions (right).

LC-MS Analysis of Isolated Fractions

The isolated fractions were analyzed by LC-MS/MS and subjected to database searching by matching MS1 and MS2 fragments with an in-house database. Samples

were prepared as stock solutions (10 mg/mL) by dissolving the powder in methanol and then diluted 1:4 in H_2O/HCOOH 0.1, % v/v (mobile phase A). Each sample (20 µL) was analyzed in triplicate by LC-HRMS as described by Baron *et al*[8]. The chromatographic separation was performed using an RP Agilent Zorbax SB-C18 column (150 × 2.1 mm i.d., 3.5 µm, CPS analitica, Milan, Italy) by an UltiMate 3000 system (Dionex) with a multistep gradient program (80 min) of mobile phase A (H_2O/HCOOH 0.1, % v/v) and B (ACN/HCOOH 0.1, % v/v). A high-resolution mass spectrometer with a hybrid Fourier transform ion trap and orbital analyzer (LTQ-Orbitrap XL, Thermo Fisher Scientific, USA) was set to acquire in negative ion mode and using the following source (ESI) parameters: capillary temperature of 300 °C, capillary voltage of -23 V, sheath gas of 45 a.u. (arbitrary unit), auxiliary gas of 10 a.u., spray voltage -4 kV, tube lens offset of -140 V.

Spectra were recorded in data-dependent scan mode. Full MS spectra were acquired with a scan range of m/z 100-1500, resolution 30,000 (FWHM at m/z 400), AGC scan target of 5 x 10^5. MS/MS spectra were acquired using the linear ion trap (LTQ), which automatically fragments the three most intense ions (intensity > 1x10^4) of the full MS scans. The trap settings are centroid mode, AGC scan target of 5 x 10^5, collision energy (CE) of 40 eV and an isolation window of 1 m/z. Activation of the dynamic exclusion function allowed MS/MS spectra to be acquired for a defined period (30 seconds) for those ions for which at least two spectra had already been acquired in 20 seconds. Xcalibur 4.0 and Chromeleon Xpress 6.80 were used for instrument control and spectra analysis. A targeted analysis was performed by searching for all the components listed in the database created by Baron *et al.*[8] on the basis of their exact mass ($[M-H]^-$), with a mass tolerance of 5 ppm. The fragmentation pattern was used to confirm the identification.

For each compound identified with an intensity ≥ 10^5, the area under the curve (AUC) was retrieved by using the Genesis algorithm of Xcalibur. The relative abundance (%) was then calculated for each fraction.

Cell Culture

Human hepatocellular carcinoma cells HepG2 were cultured in MEM (Minimum Essential Medium) supplemented with 10% (v/v) fetal bovine serum (FBS), 5% penicillin/streptomycin, 5% sodium pyruvate and 2 mM L-glutamine (Sigma Aldrich, Milan). Cells were kept regularly in a 75 cm^2 flask (SARSTEDT AG&Co, Numbrecht,

Germany) and stored in a humidified incubator (Binder, CB-150) at 37 ºC with 5% CO_2. The cell culture medium was replaced on alternate days, and cells were passaged once a week when confluency reached approximately 80%.

Fraction preparation for cell-based assay

Steatosis was induced by adding oleic acid to the MEM medium, as described in study I of this chapter. After steatosis induction for 6 hours, HepG2 were treated with the fractions to be tested (fractions C to L). Steatosis was reversed with or without the indicated fractions dissolved in DMSO. Samples of the fraction tested were prepared up to a maximum theoretical concentration of 150 mM relative to the most abundant compound in each fraction to avoid any possible toxicity due to a single compound and diluted 1:1000 in a complete medium. The final concentrations used for the assay ranged from 35 µg/mL to 180 µg/mL. The maximum final concentration of DMSO never exceeded 0.4%.

AdipoRed™ assay

See Chapter 2, study I. For phenotypic screening of isolated fractions, 1.8 x 10^4 HepG2 cells (four biological replicates for each condition tested) were plated in the 96-well plates for 24 hours in MEM complete medium. The medium was then supplemented with OA for 24 hours. Six hours after OA supplementation, fractions to be tested were added to the same medium for 18 hours. The medium was then removed, and the assay followed the protocol described in the previous study. Results were expressed as the relative percentage of lipid content setting as 100% HepG2 cells treated with OA. Statistical analysis was performed using GraphPad Prism version 8 (GraphPad Software Inc. La Jolla, CA, USA). Significance was calculated using One-way ANOVA, Adj P-value < 0.05.

Untargeted Lipidomics Analysis-LC-MS/MS

For the lipidomic experiment, 300.000 cells were seeded in a 6-well plate. The experimental setup was the same as used for the AdipoRed™ assay (three biological replicates per condition). At the end of the experiment, cells were washed twice with prewarmed PBS, and lipids were extracted by adding 400 µL of ice-cold MeOH: MTBE 50:50 v/v% containing 1 µg/mL of Splash Lipidomix (Avanti® Polar Lipids) for 1h at 4°C. Cells were then scraped and centrifuged for 10 minutes at 15.000 rpm. All solvents

contained BHT (0.1% w/v). After centrifugation, the supernatants (lipids extract) were dried and stored at -80°C until measurement.

Lipids were detected by data-dependent analysis (DDA) using LC-40D XS (Nexera Series, Shimadzu) coupled to a TripleTOF 6600 system (SCIEX). Lipids were resuspended in 50µl of Isopropanol and separated on a C18 column (Acquity premier BEH C18, 1.7x2.1x50mm) at 65°C and a flow rate of 0.55 mL/min. Using the following mobile phases: A) acetonitrile: water (6:4 v/v) with 10mM ammonium acetate and 0.1% formic acid, B) isopropanol: acetonitrile (9:1 v/v) with 10mM ammonium acetate and 0.1% formic acid. The following gradient was applied:

Time (min)	*A(%)*	*B(%)*
0	60	40
1.4	20	80
3.8	1	99
3.9	1	99
4.5	60	90

Table 2: LC conditions

MS spectra were collected over an m/z range of 140-1500 Da, operating in IDA® mode (Information Dependent Acquisition), Top15.

Source Parameters	***Value***
Ion Source Gas 1 (psi)	55
Ions source Gas 2 (psi)	65
Curtain Gas	35
Temperature (°C)	450
Stray Voltage	5500
MS Parameters	**Value**
Scan Type	TOF MS
Accumulation time (ms)	100
Declustering Potential (V)	80
Collision Energy (V)	10
Collision Energy Spread (V)	0
Range	140-1500
MS/MS Parameters	**Value**
Scan Type	TOF MS/MS
Maximum Candidate Ions	15
Intensity Threshold (counts/s)	200
Mass Tolerance (mDa)	50

Accumulation Time (ms)	50
Declustering Potential	60
CES	15
CE	35

Table 3: TOF MS and TOF MS/MS parameters

Data acquisition was performed using Analyst® TF (version 1.7.1). Raw LC-MS/MS data were processed using MS-Dial (version 5.1.230912) with a mass tolerance of 0.01 Da for MS1 and 0.025 Da for MS2. Peak detection was based on a minimum peak height amplitude of 300 and a mass slice width of 0.1 Da. Peak identification used a mass tolerance of 0.01 Da for MS1 and 0.025 Da for MS2, with an identification score cut-off of 80%. The following adducts were allowed: $[M + H]^+$, $[M + NH4]^+$ and $[M + H - H_2O]^+$. For alignment, the retention time tolerance was 0.1 min, and the MS1 tolerance was 0.025. The internal standard (Splash Lipidomix) was used to normalize the analytical signal. For lipid annotation, extracted peaks were matched with the MSDIAL-LipidDB-VS66-Public.lbm reference library. Only lipids with a reference match were included in the final dataset. Multivariate analysis was performed using MetaboAnalyst 5.0. Data were log-transformed and autoscaled before partial least squares discriminant analysis (PLS-DA). Only features found in at least 50% of samples and with CV% < 20% were included in multivariate analysis.

Results

LC-HRMS analytical profile of BLPF

The analytical profile of the total BLPF was determined by LC-HRMS operated in negative ionization mode. Compounds were identified by matching accurate mass, isotopic, and fragmentation patterns with compounds annotated in the database created by Baron *et al* [8]. Peaks found by the targeted approach were numbered progressively according to their elution order (data not shown). In total, 61 distinct compounds have been identified. Based on HRMS and MS/MS data, the major peaks could be easily assigned respectively to eriodictiol-7-O-neohexperioside (neoeriocitrin), naringenin-O-HMG (melitidine), and neohexperidin-O-HMG (brutieridine), respectively. BLPF also contains relatively large amounts of O-glycosides, C-glycosides, and HMG derivatives have been annotated for many of them. Interestingly, apigenin-7-O-rutinoside and neohesperidin-O-glucoside-O-HMG are specific for leaf polyphenolic extract[12].

Pre-fractionation and Isolation of Major Compounds

The pre-fractionation step removes the major peaks previously identified in the BLPF extract. These peaks were isolated and collected in the first purification step of our analytical workflow (Figure 2A). The removal of these major peaks was confirmed by LC-HRMS (Figure 2B).

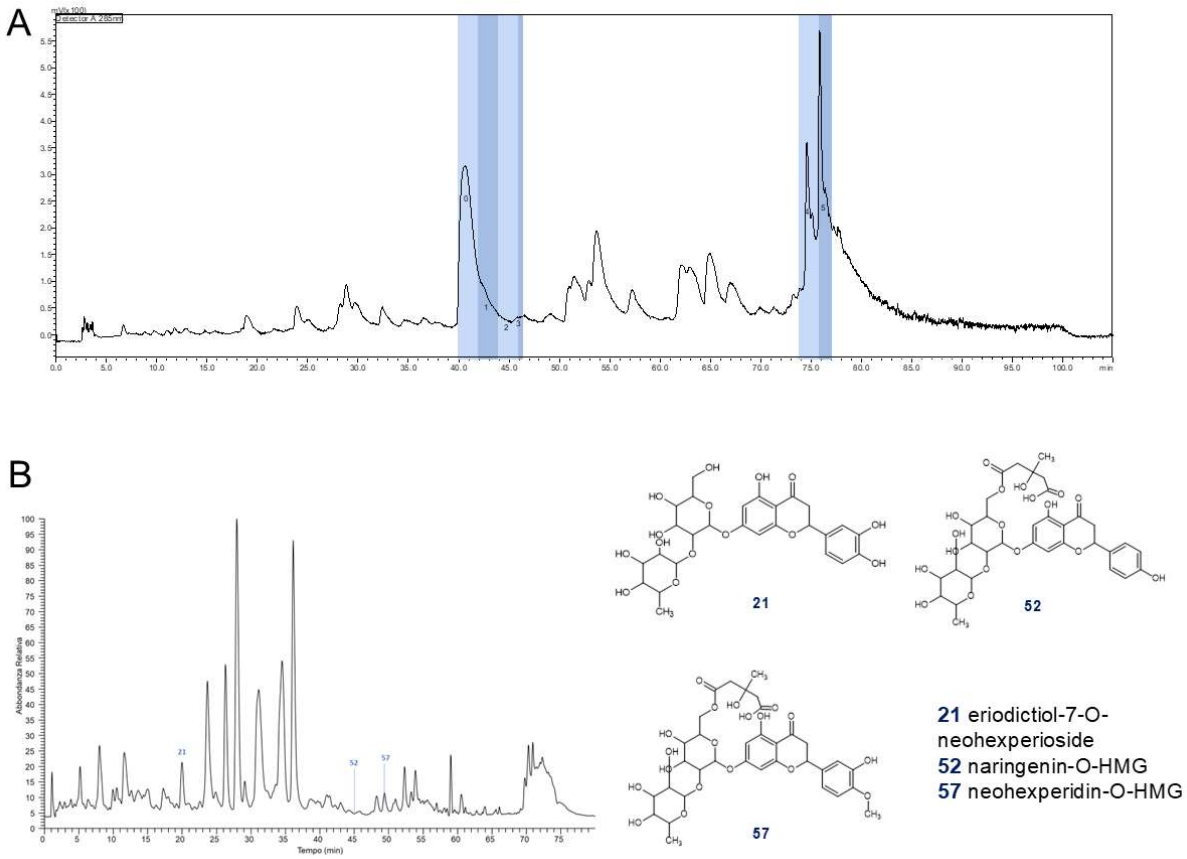

Figure 2: A) Isolation of Major Compounds. B) TIC profile of the total BLPF extract after removing eriodictiol-7-O-neohexperioside **21**, naringenin-O-HMG **52** and neohexperidin-O-HMG **57**.

BLPF bio fractionation and LC-HRMS analysis of isolated fractions

Next, a second fractionation step allowed for the separation and enrichment of the less abundant polyphenols according to their polarity. A total of 10 out of all the fractions collected by semi-preparative chromatography were selected for further analysis: 32 (Fraction A), 36 (Fraction B), 37 and 38 (Fraction C), 39 (Fraction D), 44 (Fraction E), 48 and 49 (Fraction F), 50 (Fraction G), 51 (Fraction H), 53 to 56 (Fraction I), and 61 to 63 (Fraction L) (Figure 3). As for BLPF, crude fractions obtained from the chromatographic columns were also analyzed by LC-HRMS.

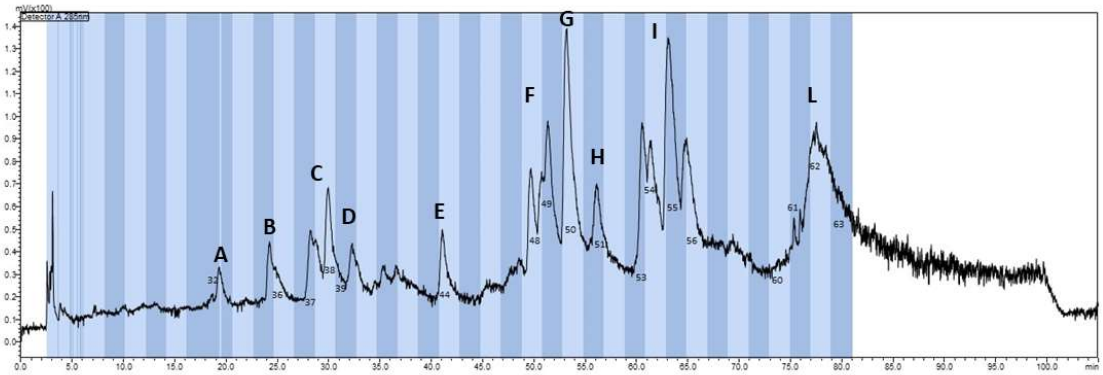

Figure 3: Fractionation chromatogram

The fractionation step reduced the chemical complexity and facilitated successive analysis to assess the biological properties of the compounds identified in our workflow. As expected, each fraction presents a distinct chemical profile, with less polar fractions enriched in glycosidic derivatives, while HMG derivatives are found in a higher percentage of the organic phase. For each compound identified in the fractions, I reported the relative abundance and the estimated concentration within the individual fraction (Table 4). Fractions A and C were discarded due to the limited amount of material recovered.

Table 4: Compounds identified in the isolated fractions of BLPF. Estimated scores and weights are reported. * To maintain the most abundant compost at a final concentration of 100 µM. Fractions A and B were discarded due to the limited amount of samples.

Fraction	Fraction weight (mg)	Compound	%Rel	Estimated weight (mg)	Molarity estimated mM	µg per single compound*	Conc mg/mL
C	1,18	2-Hydroxy-4-methoxyhydrocinnamoyl-2-O-glucoside	0,91	0,0108	4,65	1,67	182,4
		Apigenin-6,8-di-C-glucoside	7,79	0,0920	23,91	14,21	
		Chrysoeriol-6,8-di-C-glucoside	16,82	0,1985	49,11	30,67	
		Diosmetin-6,8-di-C-glucoside	34,24	0,4041	100,00	62,45	
		Eryocytorin-O-glucoside 1	7,33	0,0865	17,63	13,37	
		Eryocytorin-O-glucoside 2	27,89	0,3291	67,04	50,86	
		Naringenin 7-O-neoesperidoside-glucoside (Naringin-glucoside)	2,04	0,0241	5,02	3,73	
		P-cumaric acid	2,97	0,0350	32,98	5,41	
D	0,53	Chrysoeriol-6,8-di-C-glucoside	3,12	0,0165	5,59	4,72	151,4
		Diosmetin-6,8-di-C-glucoside	55,78	0,2956	100,00	84,47	
		Eryocytorin-O-glucoside 2	36,42	0,1930	53,75	55,15	
		Naringenin 7-O-neoesperidoside-glucoside (Naringin-glucoside)	0,85	0,0045	1,27	1,28	

		P-cumaric acid	3,83	0,0203	26,14	5,80	
E	0,28	Apigenin-6,8-di-C-glucoside	4,01	0,0112	4,53	2,69	67,1
		Apigenin-6-C-glucoside	3,43	0,0096	5,32	2,30	
		Eriodictiol 7-O-neoesperoside (Neoeriocitrin)	88,89	0,2489	100,00	59,65	
		Eriodictiol 7-O-rutinoside (Eriocitrin)	1,56	0,0044	1,76	1,05	
		Eriodictiol-7-O-glucoside	0,49	0,0014	0,72	0,33	
		Luteolin-7-O-glucoside	0,84	0,0024	1,26	0,56	
		Luteolin-C-glucoside-O-ramnoside	0,77	0,0022	0,87	0,52	
F	1,27	Bergamjuicin (melitidine-glucoside)	16,26	0,2065	20,24	20,65	127,0
		Chrysoeriol-8-C-glucoside	1,79	0,0228	4,28	2,28	
		Luteolin-7-O-neohexperidoside	53,87	0,6841	100,00	68,41	
		Naringenin 7-O-rutinoside (Narirutin)	2,02	0,0257	3,85	2,57	
		Neoeriocytorin-O-glucoside-O-HMG	26,05	0,3309	31,85	33,09	
G	0,66	Bergamjuicin (melitidine-glucoside)	3,12	0,0206	3,75	4,11	132,0
		Luteolin-7-O-neohexperidoside	24,38	0,1609	43,81	32,19	
		Naringenin 7-O-neohexperidoside (Naringin)	54,35	0,3587	100,00	71,74	
		Neoeriocytorin-O-glucoside-O-HMG	4,34	0,0287	5,14	5,73	
		Neohesperidine-glucoside-O-HMG	13,80	0,0911	16,08	18,22	
H	0,45	Bergamjuicin (melitidine-glucoside)	3,44	0,0155	4,33	4,42	128,6
		Esperetin 7-rutinoside (Hesperidin)	54,66	0,2460	100,00	70,27	
		Naringenin 7-O-neohexperidoside (Naringin)	37,35	0,1681	71,87	48,02	
		Neohesperidine-glucoside-O-HMG	4,55	0,0205	5,54	5,85	
I	2,35	Apigenin-7-O-neohexperidoside	14,12	0,3319	54,80	22,13	156,7
		Bergamjuicin (melitidine-glucoside)	0,47	0,0110	1,19	0,73	
		Chrysoeriol-7-O-glucoside	3,37	0,0791	16,33	5,27	
		Chrysoeriol-7-O-neohexperidoside	16,22	0,3812	59,83	25,41	
		Diosmetin-7-O-glucoside	3,37	0,0791	16,33	5,27	
		Diosmetin-7-O-neohexperidoside	0,42	0,0099	1,56	0,66	
		Eriocytorin-O-HMG	1,08	0,0253	3,26	1,69	
		Esperetin 7-O-neoesperidoside (Neohesperidine)	27,20	0,6393	100,00	42,62	
		Esperetin 7-rutinoside (Hesperidin)	0,88	0,0207	3,24	1,38	
		Naringenin 7-O-neohexperidoside (Naringin)	2,96	0,0695	11,43	4,63	
		Neoeriocytorin-O-HMG	29,92	0,7031	90,66	46,87	
L	1,89	255-neoesperoside-O-HMG	0,97	0,0184	1,96	1,39	143,1
		Brutieridine (Neohesperidine-O-HMG)	52,75	0,9969	100,00	75,47	
		Chrysoeriol-O-glucoside-O-HMG	3,40	0,0642	6,32	4,86	

Diosmetin-7-O-neohexperidoside-O-HMG	1,55	0,0293	2,95	2,22
Diosmetin-O-glucoside-O-HMG	6,06	0,1146	14,30	8,68
Esperetin-O-glucoside-O-HMG isomer 2	19,49	0,3684	45,83	27,89
Quercetin dimethylether C-glucoside O-HMG	7,72	0,1460	17,36	11,05
Unknown	8,05	0,1522	27,54	11,52

Bioactive fractions were screened by AdipoRed™ assay

Next, I used the AdipoRed assay to screen for lipid-lowering activity of the isolated fractions in a relatively simple but effective manner. AdipoRed is a fluorescence-based assay that allows the relative quantification of intracellular lipid droplets without laborious steps, such as cell lysis, lipid extraction, or lipid staining. In this approach, HepG2 cells were seeded in 96 wells with medium supplemented with oleic acid to promote lipid accumulation and steatosis phenotype and challenged with the different isolated fractions for 24h. The concentration tested ranged from 60 µg/mL to 180 µg/mL, calculated as described in the Materials and Methods. Cell viability of all the tested fractions on the same cell line was assessed for the same concentrations used in this assay. The results of this screening are expressed as relative percentages of lipids.

As shown in Figure 3, a significant reduction in intracellular lipid content is observed after the treatment with fractions C and F when compared with cells treated with oleic acid. Despite the similar phenotypic effects, the chemical profiles of the two fractions are different. In contrast, fractions with similar chemical profiles, such as those eluting at similar retention times, do not show the same lipid-lowering effects. This suggests that the presence and specific concentration of bioactive compounds play a crucial role in the lipid-lowering capacity.

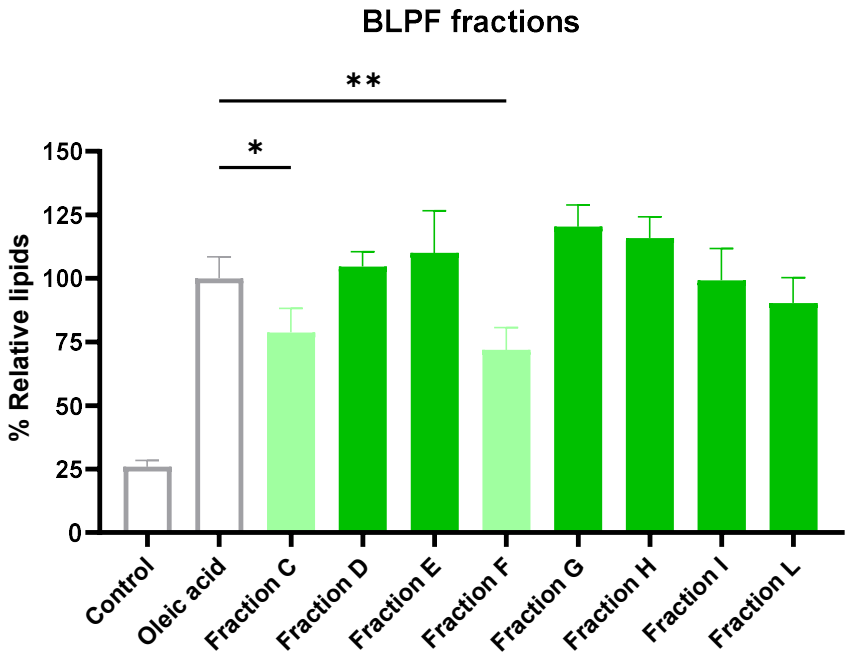

Figure 3: AdipoRed Phenotypic screening. Four biological replicates were considered for each experimental condition. * p<=0.05 and ** p<=0.01 by One-way ANOVA. Data are expressed as % relative lipid content, where 100% represents results obtained with OA-treated HepG2 cells.

The lipidomic analysis highlights lipid species responsible for the lipid-lowering effect

A QC base peak intensity (BPI) chromatogram of the lipid cellular extract in positive ESI mode is shown in Figure 4. After the initial peak picking, 465 features passed all filtering steps and were included in the final dataset for multivariate analysis. As shown in the PLS-DA score plot in Figure 5, there is a good separation of the experimental groups. Also, Fraction C and Fraction F are separated from each other and from the OA condition (steatosis condition). This likely indicates that both fractions influence the lipidomic profile and that these effects do not overlap. As expected, the main lipids driving this separation are triglycerides (TG), as indicated by the VIP score plot (Figure 5B).

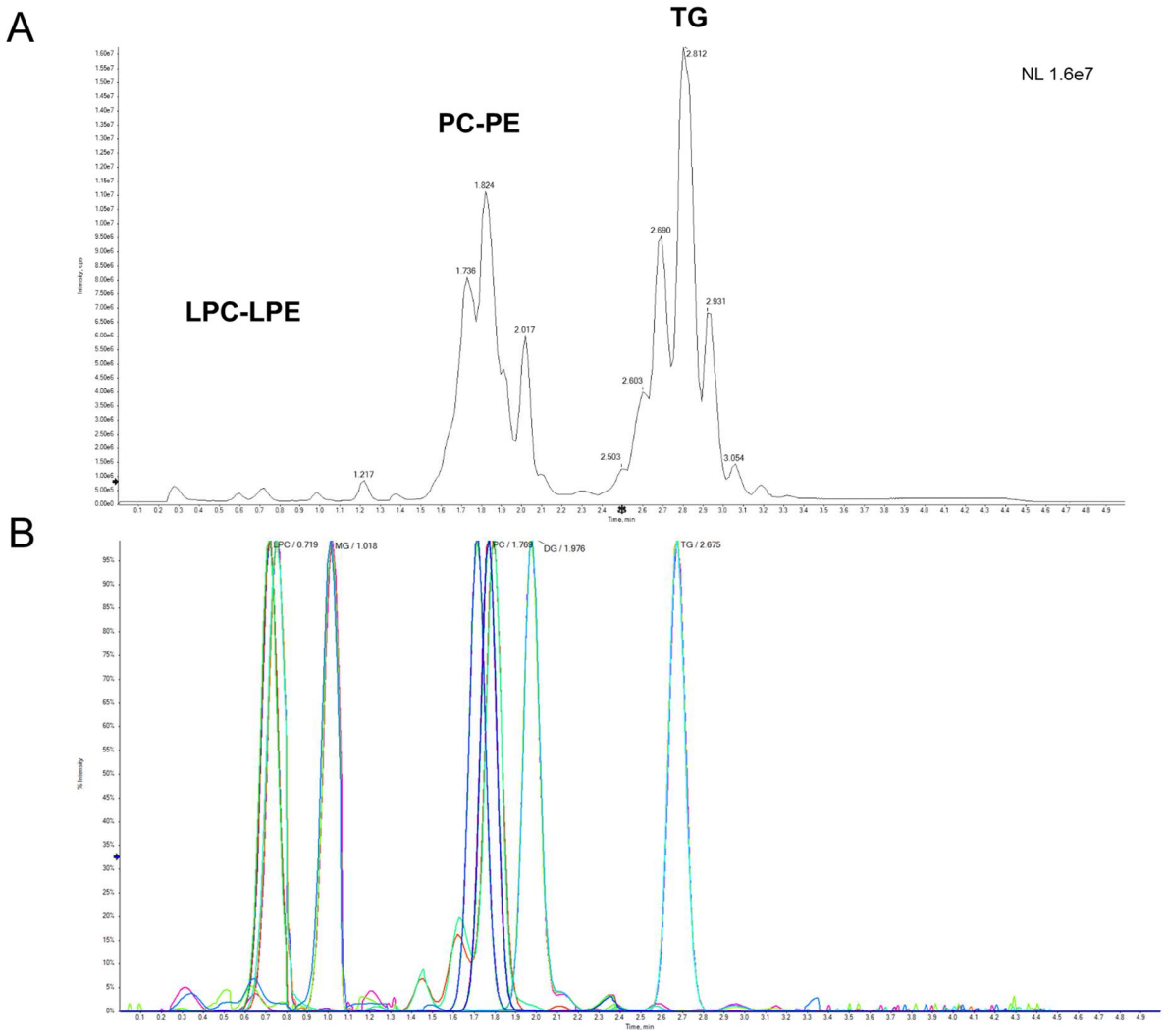

Figure 4: A) BPC in positive ionization mode of the pooled QC samples. B) Extracted ion chromatogram (XIC) obtained for the Avanti® Equisplash mix (0.1 µg/mL) from three QC samples (all overlaid). All peaks are set to 100%.

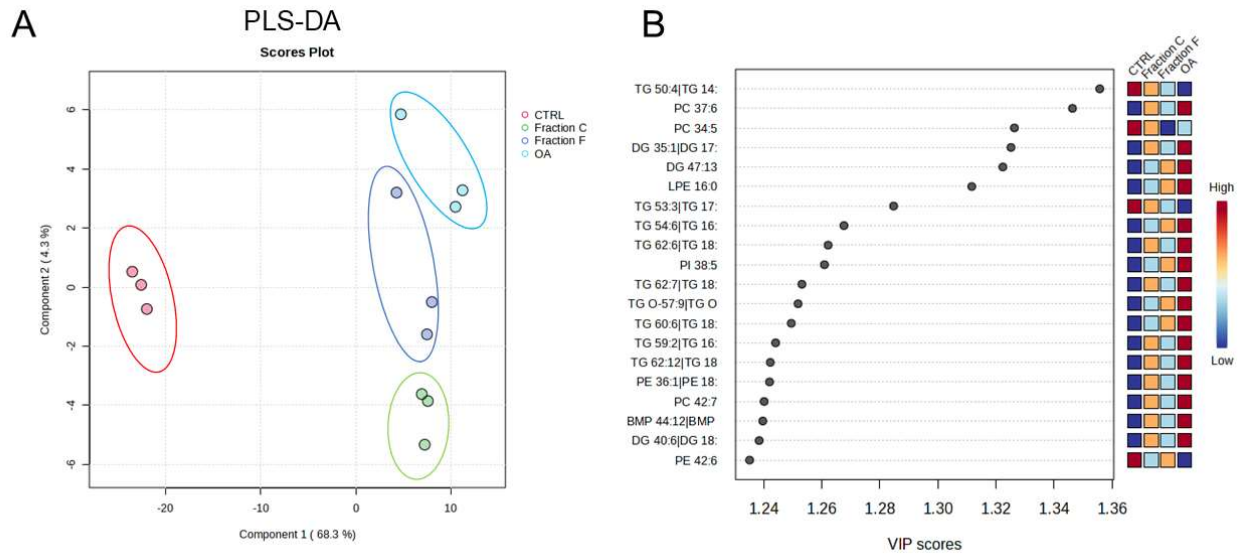

Figure 5: Multivariate statistical analysis of the filtered lipidomic data. A) PLS-DA score plot of log10-transformed LC-MS data; positive ESI mode. B) VIP score plot.

However, given the different phytochemical profiles of the two fractions, comparison allows the identification of lipid patterns that differentiate their effects. Although the interpretation of these data is still ongoing, it appears that fraction F is more effective than fraction C in reducing intracellular neutral lipid levels, an observation consistent with the phenotypic screening results. Fraction C significantly modulates sphingomyelins and ceramides profile (Figure 6). This suggests that, in addition to a targeted effect on triglycerides, some compounds in fraction C may have anti-inflammatory effects, as these lipids are known to modulate the cellular anti-inflammatory response.[13]

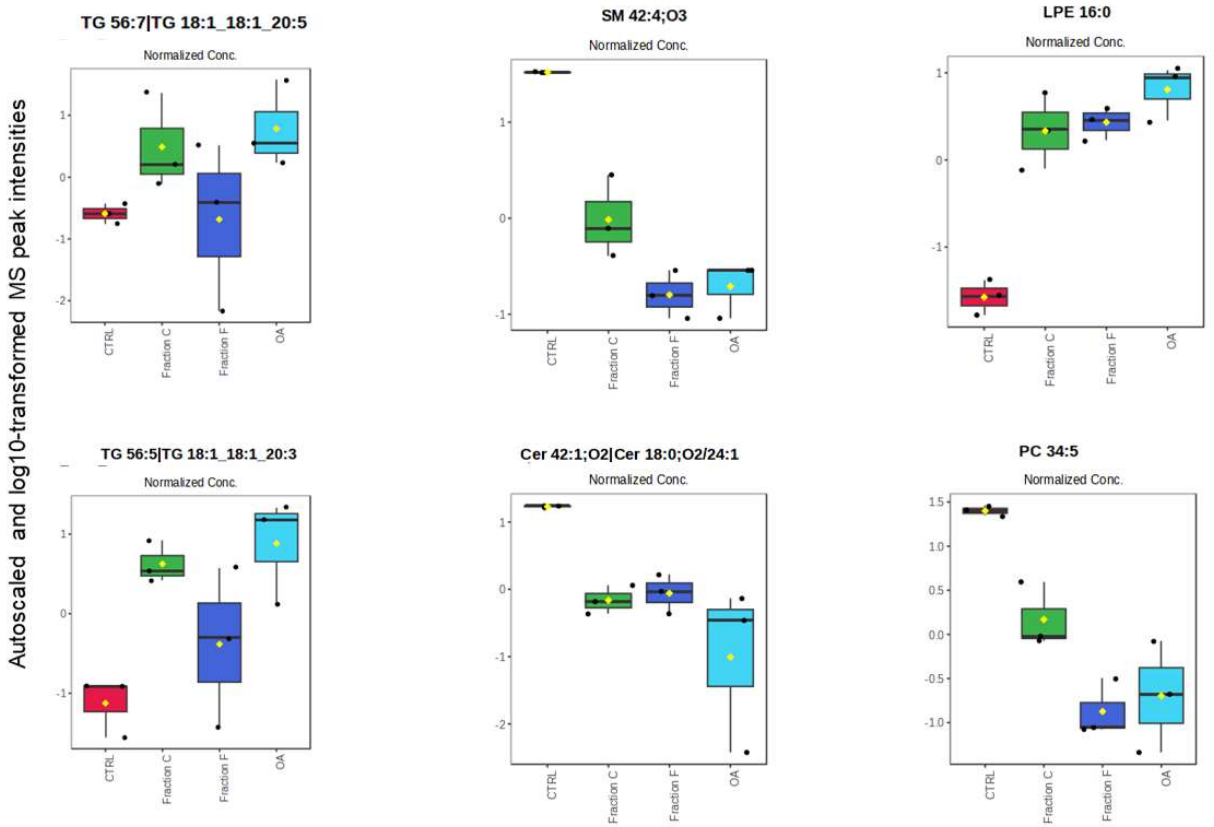

Figure 6: Boxplot of log10-transformed intensity values of extracted features in HepG2 lipid extracts, positive ESI mode.

Discussion

In this study, I aimed to identify and infer the lipid-lowering activity of bioactive compounds from bergamot leaf polyphenols by combining analytical and omics strategies. Due to its high polyphenol content, bergamot is a rich source of bioactive phytocompounds with several beneficial effects on human health and a lower spectrum

of side effects. These activities are attributed not only to polyphenols found in the bergamot fruit or juice, which are the most extensively studied, but also reasonably to the leaves, which possess a qualitative profile very similar to that of the fruit and even higher polyphenol content[11]. However, it is not known which bioactive compounds in bergamot are responsible for its hypolipidemic effect and the mechanisms underlying these effects remain fully understood. Studies suggest that most of the biological functions can be attributed to the intrinsic antioxidant properties of the polyphenolic fraction of bergamot, which can positively affect lipid metabolism [5]. Animal model studies have shown that BPF administration is associated with improved lipid-related parameters, such as increased HDL cholesterol, reduced total cholesterol, LDL cholesterol, triglycerides, decreased blood glucose, and body weight.[14]

Given the complexity of this natural matrix, a fractionation step could help with the identification of the bioactive constituents of the extract. The results demonstrate that incorporating a pre-fractionation step enables the selective removal of major peaks. Eriodictiol-7-O-neohexperioside, naringenin-O-HMG, and neohexperidin-O-HMG were obtained in pure form, and therefore, they could be potentially used as standards for other screening assays. The prefractionation step enriched the extract with less abundant compounds.

From the biofractionation of the bergamot leaf matrix, I obtained ten fractions with distinct phytochemical profiles. The AdipoRed assay screening successfully identified two fractions having significant lipid-lowering properties in HepG2. To determine which compounds were responsible for this activity, compounds found in bioactive fractions were compared with those in fractions with similar phytochemical profiles that did not show activity in the screening assay. Interestingly, Apigenin-6,8-di-C-glucoside, Chrysoeriol-6,8-di-C-glucoside, and Naringenin 7-O-neohexperidoside-glucoside were also present in other fractions different from the active one (fraction C) but at lower concentrations, thus suggesting their possible lipid-lowering roles. Moreover, the active fraction contained Eryocytorin-O-glucoside 1, absent in other fractions.

Similarly, the bioactive fraction F was compared with fractions containing the same identified compounds. In this case, the active fraction had some compounds in common with fractions G and H. Notably, Bergamjuicin (melitidine-glucoside) was present at an estimated concentration five times higher than in the inactive fractions. Moreover,

luteolin and neoeriocitrin-O-glucoside-O-HMG were the most abundant compounds in fraction F. Chrysoseriol-8-C-glucoside, and naringenin-7-O-rutinoside (narirutin) were unique to fraction F. The fact that two different fractions with diverse chemical profiles can induce the same phenotypic effect suggests that the lipid-lowering action is not due to a single compound but to the synergistic activity of phytocompounds.

Among the compounds identified in the analytical workflow, apigenin and neoeriocitrin were validated against standards (Figure 7). Apigenin showed a dose-dependent lipid-lowering activity, making it one of the possible bioactive compounds in the extract. Notably, I tested aglycones rather than the identified glucosides, which was consistent with the bioavailability data for apigenin and related flavonoids. Indeed, i*n vivo*, glucosides are deconjugated by the gut microbiota to yield aglycones and ring cleavage products that are subsequently converted to phase II metabolites[15]. Interestingly, this regulatory mechanism is altered during inflammatory processes, where conjugated metabolites can be reverted to their aglycone form through the activation of deconjugation enzymes[16].

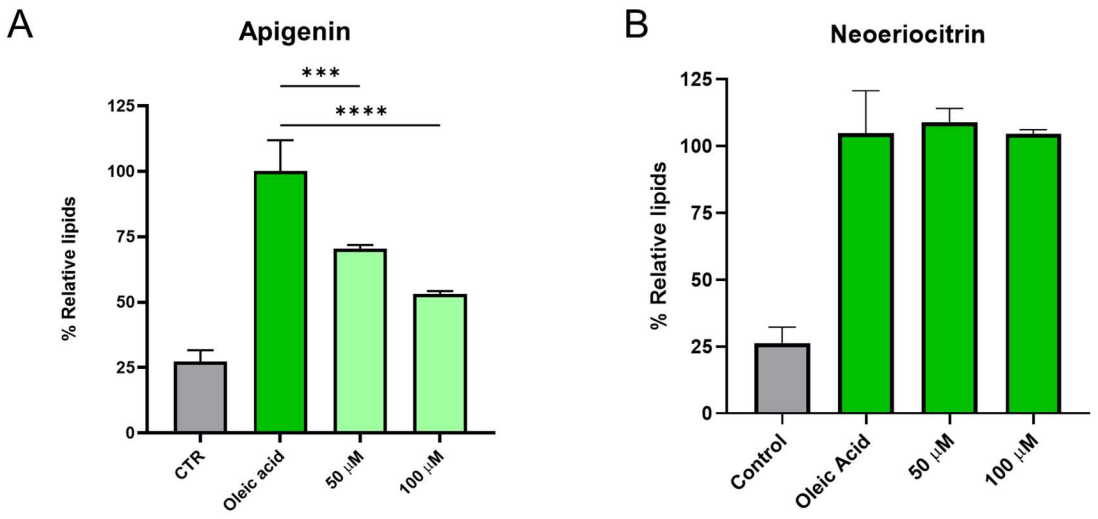

Figure 7: The lipid-lowering activity of standards by AdipoRed Assay. * p<=0.05 and ** p<=0.01 by One-way ANOVA. Data are expressed as % relative lipid content, where 100% represents results obtained with OA-treated HepG2 cells.

Besides these results, two critical aspects remain to be clarified: the mechanism of action and the molecular targets responsible for the observed phenotypic effect. These points have been partially elucidated through untargeted lipidomic analysis, which revealed that the lipid-lowering effect is associated with a remodelling of the hepatic cell lipidome,

particularly affecting triglycerides but also lipids directly involved in the regulation of anti-inflammatory response.

Overall, the proposed workflow allows screening for bioactive compounds in bergamot leaves and inferring their molecular mechanisms to make hypotheses about therapeutic targets. Additionally, our workflow offers several advantages, primarily due to the novelty of the matrix being analyzed. Combining these advanced analytical strategies with a circular economy concept to valorize industrial waste products such as bergamot leaves could reduce the impact of cultivation on waste production, minimizing disposal problems while obtaining a potential source of bioactive compounds.

Conclusion

The LC-MS/MS analysis of isolated fractions resulted in a detailed qualitative profile of the polyphenolic fraction of bergamot leaves. In total, 61 distinct compounds have been identified throughout the different fractions obtained by the pre-analytical step. The lipid-lowering activity of all the fractions was then evaluated using an AdipoRed assay. Two out of all the fractions tested in the cell-based assay showed significant lipid-lowering activity. To infer changes in the lipidome profile, I carried out an untargeted lipidomic analysis. The analysis was in accordance with findings from phenotypic screening and added a new layer of information about lipid profile changes upon the treatment with the extract. The results indicate that the analytical pipeline developed is useful for identifying bioactive compounds. The workflow involves relatively simple sample preparation and could be potentially adapted for the comprehensive study of different natural matrices.

References

(1) Stefani, M.; Rigacci, S. Beneficial Properties of Natural Phenols: Highlight on Protection against Pathological Conditions Associated with Amyloid Aggregation. *BioFactors* **2014**, *40* (5), 482–493. https://doi.org/10.1002/biof.1171.

(2) Leri, M.; Scuto, M.; Ontario, M. L.; Calabrese, V.; Calabrese, E. J.; Bucciantini, M.; Stefani, M. Healthy Effects of Plant Polyphenols: Molecular Mechanisms. *Int J Mol Sci* **2020**, *21* (4), 1250. https://doi.org/10.3390/ijms21041250.

(3) Formisano, C.; Rigano, D.; Lopatriello, A.; Sirignano, C.; Ramaschi, G.; Arnoldi, L.; Riva, A.; Sardone, N.; Taglialatela-Scafati, O. Detailed Phytochemical Characterization of Bergamot Polyphenolic Fraction (BPF) by UPLC-DAD-MS and LC-NMR. *J Agric Food Chem* **2019**, *67* (11), 3159–3167. https://doi.org/10.1021/acs.jafc.8b06591.

(4) Perna, S.; Spadaccini, D.; Botteri, L.; Girometta, C.; Riva, A.; Allegrini, P.; Petrangolini, G.; Infantino, V.; Rondanelli, M. Efficacy of Bergamot: From Anti-inflammatory and Anti-oxidative Mechanisms to Clinical Applications as Preventive Agent for Cardiovascular Morbidity, Skin Diseases, and Mood Alterations. *Food Sci Nutr* **2019***, 7* (2), 369–384. https://doi.org/10.1002/fsn3.903.

(5) Carresi, C.; Gliozzi, M.; Musolino, V.; Scicchitano, M.; Scarano, F.; Bosco, F.; Nucera, S.; Maiuolo, J.; Macrì, R.; Ruga, S.; Oppedisano, F.; Zito, M. C.; Guarnieri, L.; Mollace, R.; Tavernese, A.; Palma, E.; Bombardelli, E.; Fini, M.; Mollace, V. The Effect of Natural Antioxidants in the Development of Metabolic Syndrome: Focus on Bergamot Polyphenolic Fraction. *Nutrients* **2020**, *12* (5), 1504. https://doi.org/10.3390/nu12051504.

(6) Pekgor, S.; Duran, C.; Berberoglu, U.; Eryilmaz, M. A. The Role of Visceral Adiposity Index Levels in Predicting the Presence of Metabolic Syndrome and Insulin Resistance in Overweight and Obese Patients. *Metab Syndr Relat Disord* **2019**, *17* (5), 296–302. https://doi.org/10.1089/met.2019.0005.

(7) Impellizzeri, D.; Cordaro, M.; Campolo, M.; Gugliandolo, E.; Esposito, E.; Benedetto, F.; Cuzzocrea, S.; Navarra, M. Anti-Inflammatory and Antioxidant Effects of Flavonoid-Rich Fraction of Bergamot Juice (BJe) in a Mouse Model of Intestinal Ischemia/Reperfusion Injury. *Front Pharmacol* **2016***, 7*. https://doi.org/10.3389/fphar.2016.00203.

(8) Baron, G.; Altomare, A.; Mol, M.; Garcia, J. L.; Correa, C.; Raucci, A.; Mancinelli, L.; Mazzotta, S.; Fumagalli, L.; Trunfio, G.; Tucci, L.; Lombardo, E.; Malara, D.; Janda, E.; Mollace, V.; Carini, M.; Bombardelli, E.; Aldini, G. Analytical Profile and Antioxidant and Anti-Inflammatory Activities of the Enriched Polyphenol Fractions Isolated from Bergamot Fruit and Leave. *Antioxidants* **2021**, *10* (2), 141. https://doi.org/10.3390/antiox10020141.

(9) Lydic, T. A.; Goo, Y. Lipidomics Unveils the Complexity of the Lipidome in Metabolic Diseases. *Clin Transl Med* **2018**, *7* (1). https://doi.org/10.1186/s40169-018-0182-9.

(10) Huang, Y.; Tocmo, R.; Nauman, M. C.; Haughan, M. A.; Johnson, J. J. Defining the Cholesterol Lowering Mechanism of Bergamot (Citrus Bergamia) Extract in HepG2 and Caco-2 Cells. *Nutrients* **2021**, *13* (9), 3156. https://doi.org/10.3390/nu13093156.

(11) Baron, G.; Altomare, A.; Mol, M.; Garcia, J. L.; Correa, C.; Raucci, A.; Mancinelli, L.; Mazzotta, S.; Fumagalli, L.; Trunfio, G.; Tucci, L.; Lombardo, E.; Malara, D.; Janda, E.; Mollace, V.; Carini, M.; Bombardelli, E.; Aldini, G. Analytical Profile and Antioxidant and Anti-Inflammatory Activities of the Enriched Polyphenol Fractions Isolated from Bergamot Fruit and Leave. *Antioxidants* **2021**, *10* (2), 141. https://doi.org/10.3390/antiox10020141.

(12) Baron, G.; Altomare, A.; Mol, M.; Garcia, J. L.; Correa, C.; Raucci, A.; Mancinelli, L.; Mazzotta, S.; Fumagalli, L.; Trunfio, G.; Tucci, L.; Lombardo, E.; Malara, D.; Janda, E.; Mollace, V.; Carini, M.; Bombardelli, E.; Aldini, G. Analytical Profile and Antioxidant and Anti-Inflammatory Activities of the Enriched Polyphenol Fractions Isolated from Bergamot Fruit and Leave. *Antioxidants* **2021**, *10* (2), 141. https://doi.org/10.3390/antiox10020141.

(13) Tanase, D. M.; Gosav, E. M.; Petrov, D.; Jucan, A. E.; Lacatusu, C. M.; Floria, M.; Tarniceriu, C. C.; Costea, C. F.; Ciocoiu, M.; Rezus, C. Involvement of Ceramides in Non-Alcoholic Fatty Liver Disease (NAFLD) Atherosclerosis (ATS) Development: Mechanisms and Therapeutic Targets. *Diagnostics* **2021**, 11 (11), 2053. https://doi.org/10.3390/diagnostics11112053.

(14) Mollace, V.; Sacco, I.; Janda, E.; Malara, C.; Ventrice, D.; Colica, C.; Visalli, V.; Muscoli, S.; Ragusa, S.; Muscoli, C.; Rotiroti, D.; Romeo, F. Hypolipemic and Hypoglycaemic Activity of Bergamot Polyphenols: From Animal Models to Human Studies. *Fitoterapia* **2011**, *82* (3), 309–316. https://doi.org/10.1016/j.fitote.2010.10.014.

(15) Boronat, A.; Rodriguez-Morató, J.; Serreli, G.; Fitó, M.; Tyndale, R. F.; Deiana, M.; de la Torre, R. Contribution of Biotransformations Carried Out by the Microbiota, Drug-Metabolizing Enzymes, and Transport Proteins to the Biological Activities of Phytochemicals Found in the Diet. *Advances in Nutrition* **2021**, *12* (6), 2172–2189. https://doi.org/10.1093/advances/nmab085.

(16) Terao, J. Potential Role of Quercetin Glycosides as Anti-Atherosclerotic Food-Derived Factors for Human Health. *Antioxidants* **2023**, *12* (2), 258. https://doi.org/10.3390/antiox12020258.

CHAPTER 3:
LIPIDOME INVESTIGATION OF CARNOSINE EFFECT ON NUDE MICE SKIN TO PREVENT UVA DAMAGE

Summary

The skin lipidome plays a central role in maintaining barrier function, hydration and the protective response to external stimuli such as UV radiation. Skin exposure to UV radiation induces autophagy, chronic inflammation, and the sustained generation of reactive oxygen species (ROS), which together contribute to skin photoaging. Among the protective agents against UV-induced skin damage, carnosine, an endogenous β-alanyl-L-histidine dipeptide, has been shown to possess antioxidant properties. These properties help to mitigate photoaging and prevent changes in skin protein profile, making carnosine a promising ingredient in dermatological treatments. The aim of this work was to investigate the changes in the lipidomic profile of the skin in response to UVA exposure and the effects of topical carnosine treatment using an untargeted lipidomic approach.

Background

The skin is composed of multiple layers with distinct lipid content, each with unique and essential biological functions in maintaining skin properties and homeostasis[1]. The barrier function of the skin is largely due to the stratum corneum (SC), the outer layer of the epidermis, which is particularly enriched in barrier lipids such as long acyl chain ceramides, free fatty acids, cholesterol esters, and cholesterol sulfate. These lipids fill the extracellular spaces and form an effective barrier to the environment, thus protecting the body from external factors such as bacteria, radicals, or UV radiation. At the same time, membrane lipids found in the inner skin layers, such as glycerophospholipids, sphingomyelins, and cholesterol, have been shown to influence the skin's immune properties in both healthy and disease states and play a crucial role in metabolism, ageing, and the response to UV radiation.

The UV radiation reaching the earth's surface consists of approximately 5% UVB (290–320 nm) and 95% UVA (320–400 nm), both of which are strongly associated with human health[2]. At the molecular level, chronic UVA exposure progressively leads to extracellular matrix (ECM) disorganization, dysregulated autophagy, chronic inflammation and the production of reactive oxygen species (ROS) [3,4] causing local and systemic changes in molecular and cellular components that damage DNA, proteins, and lipids.

For instance, changes in skin lipid composition or lipid chemical properties can have severe consequences for the biological functions of the skin and are often associated with skin diseases[5]. Cholesterol, phospholipids, free fatty acids, and squalene are targets for non-enzymatic lipid oxidation that occurs through free radical mechanisms induced by UV exposure. This process produces bioactive products that contribute to skin damage. UV radiation also activates enzymes such as phospholipases, lipoxygenases, and cyclooxygenases, leading to the production of various fatty acid-derived mediators, particularly eicosanoids[6].

In response to UV-induced damage, natural antioxidants have been identified as protective agents[7]. Carnosine, an endogenous β-alanyl-L-histidine dipeptide, has demonstrated significant antioxidant and carbonyl-scavenging properties, making carnosine a compelling ingredient to consider for use in dermatology to prevent photoaging[8]. At the molecular level, carnosine inhibits elastin modification and prevents fibroblast senescence induced by 4-hydroxynonenal (HNE)[9]. Carnosine readily reacts with aldehydes such as acrolein or HNE to form non-reactive adducts that prevent protein modification and subsequent alteration of cells and tissues[10,11]. More recently, carnosine has shown promising results in preventing oxidative stress in UVA-irradiated scaffold-free human dermal spheroids[12]. In addition, proteomic analysis of UVA-irradiated nude mouse skin showed that carnosine effectively prevented proteomic changes induced by UVA exposure[3] . In this work, we aimed to understand the changes in the lipidomic profile of the skin in relation to UVA exposure and the treatment with carnosine. To study these effects, we used nude mice exposed daily to UVA radiation for six weeks and treated topically with carnosine. This study was carried out in collaboration with the group of Prof. Salvayre at the University of Toulouse (France).

Materials and Methods

Experimental treatment

Skin samples were kindly provided by Prof. Salvayre. The experimental protocol No. 12/1048/10/13 was carried out in accordance with French legislation and approved by the medical ethical committee for all studies described. Albino hairless mice Skh:hr-1 (6 weeks old) were obtained from Charles River Laboratories in Saint Germain sur l'Arbresle, France. Three animals were assigned to each condition: a control non-irradiated group, a group exposed daily (on the whole back) to UVA radiation for six

weeks (2 hours exposure per day, five days per week, resulting in a total of 600 J/cm2 at the end of the experiment), a group exposed daily to UVA and treated topically with carnosine (1% in Polyethylene Glycol - PG) after and one group exposed to UVA and treated with PG alone. After sacrifice, skin samples were taken from the backs of the mice and stored at -80°C until their use.

Sample preparation

80 mg of each skin sample was homogenized by glass bead beating (3 cycles, 60″, 350 rpm) in 300 µL of i-PrOH/H_2O (50/50 v/v), and 20 µL were taken for BCA protein assay. An aliquot corresponding to 100 µg of protein was quickly spiked with 10 µL of Splash Lipidomix (Avanti® Polar Lipids) and left in ice for 15 min. Another aliquot of each sample was transferred to a separate vial to prepare a pooled QC sample. Lipids extraction was performed using the standard MTBE protocol with MTBE/methanol/water (10:3:2.5, v/v/v) as the extraction solvent ratio. All solvents contained BHT 0.1 % w/v to prevent unwanted oxidation. Briefly, 700 µL of MTBE/MeOH (10:3) was added to each sample, vortexed for 5 s, and incubated for 1 h at 4° C in a thermomixer. The phase separation was induced by adding 140 µL of H_2O, vortexing for 5 s, and 15 mins of incubation (4° C, 210 rpm). Once centrifugated (4 °C, 15 min, 13400 x g), the upper phase was collected in a new tube. The upper phase was then dried under vacuum (Eppendorf concentrator 5301, 1 mbar). Before the LC-MS analyses, lipid extracts were dissolved in 200 µL i-PrOH/ACN (90/10, v/v, with ammonium acetate 10mM and 0,1% formic acid) and vortexed. Extraction efficiency was normalized by the addition of a mixture of deuterated internal standards before lipid extraction.

LC-MS Analysis

All samples have been analyzed using ExionLC™ AD system (SCIEX) connected to a ZenoTOF™ 7600 System (SCIEX) equipped with a Twin Spray Turbo V™ Ion Source with ESI Probe. Chromatographic separation was performed on a Kinetex® EVO C18 (Phenomenex) 100 x 2.1 mm x 1.7 µm using mobile phase A (H_2O/ACN (60/40, v/v, with ammonium acetate 10mM and 0,1% formic acid) and mobile phase B (i-PrOH/ACN (90/10, v/v, with ammonium acetate 10mM and 0,1% formic acid) at a flow rate of 400 µL/min. The column and autosampler temperatures were set at 45°C and 15°C, respectively. The sample injection volume was 5 µL. The following gradient profile was used:

Time (min)	A(%)	B(%)
0	*55*	*45*
2	*55*	*45*
12	*3*	*97*
17	*3*	*97*
17.1	*55*	*45*
20	*55*	*45*

Table 1: LC conditions

MS spectra were collected over the m/z range of 140-1500 Da, operating in IDA® mode (Information Dependent Acquisition), Top20.

Source Parameters	***Value***
Ion Source Gas 1 (psi)	55
Ions source Gas 2 (psi)	65
Curtain Gas	35
Temperature (°C)	500
Stray Voltage	4500(+)/-4500 (-)
MS Parameters	**Value**
Scan Type	TOF MS
Accumulation time (ms)	250
Declustering Potential (V)	80
Collision Energy (V)	10
Collision Energy Spread (V)	0
Range	140-1500
MS/MS Parameters	**Value**
Scan Type	TOF MS/MS
Maximum Candidate Ions	20
Intensity Threshold (counts/s)	100
Mass Tolerance (mDa)	50
Accumulation Time (ms)	50
Declustering Potential	80
CES	15
CE	35

Table 2: TOF MS and TOF MS/MS parameters

ESI positive/negative polarity with sequential injections. Three technical replicates (LC-MS/MS runs) were performed. QC samples were run at the beginning, during, and after the sequence.

Data Analysis

MS-Dial software (RIKEN, version 4.90)[13] was used to process the MS data. This included peak detection, MS2 data deconvolution, lipid identification and peak alignment across all samples. A cut-off value of 80% was used for identification. Relative quantification was based on the determination of peak intensities for each correctly identified lipid and then normalized by the intensity of the internal standard used for the corresponding lipid class. Normalized peak intensities were then exported to Excel for multivariate and univariate statistical analysis using Metaboanalyst version 5.0[14]. For volcano plot analysis, peak intensity values were first converted to a base-two logarithmic scale and then filtered for significance (Benjamini-Hochberg corrected two-sample t-test with a threshold value of 0.05 False Discovery Rate - FDR). Finally, the lipid molecules showing significant changes were identified with unique IDs corresponding to the Human Metabolome Database (HMDB) and subjected to network analysis using Ingenuity Pathways Analysis software (IPA, Qiagen). In total, only 271 out of 368 significantly altered lipids were associated with the corresponding ID and included in the pathway and network analysis.

Results and Discussion

A daily dose of UVA (20 mJ/cm^2) to the skin for six weeks induced distinct proteomic signatures[3] and triggers typical features of photoaging, associated with a significant increase in 4-HNE adduct, and elastotic material deposition[9]. Therefore, we hypothesized that a similar dose of UVA could also alter the overall lipid profile of the skin. To test this, I used skin samples from nude mice (control), nude mice exposed to UVA (UVA), and mice exposed to UVA and treated with carnosine (UVA+CAR) to investigate changes in the lipidome profile by untargeted LC-MS lipidomic analysis.

A QC BPI chromatogram of the lipid skin extract in positive ESI mode is shown in Figure 1. The untargeted lipidomic analysis supported the detection of 2405 features in the initial peak picking of the raw data, of which 937 had annotated reference spectra matched against the Lipidblast database in either positive or negative ionization mode. Subsequent filtering based on the technical repeatability of the QC samples and manual inspection allowed the identification of 683 lipid molecular species. Among them, triacylglycerols (TGs) showed the higher abundance, covering 21.8% of the identified lipidome, followed by ceramides (Cer, 15.2%), sphingomyelin (SMs, 5.3%),

phosphatidylcholines (PCs, 5.3%) and fatty acids (FAs, 5.0%). Diacylglycerols (DGs, 6.4%), cholesteryl esters (CEs, 2.2%), phosphatidylethanolamines (PEs,1.8%), lyso-phosphatidylethanolamines (LPEs), also- phosphatidylcholines (LPC) and phosphatidylinositols (PIs) complete the qualitative description of the most abundant lipid classes identified in the analysis.

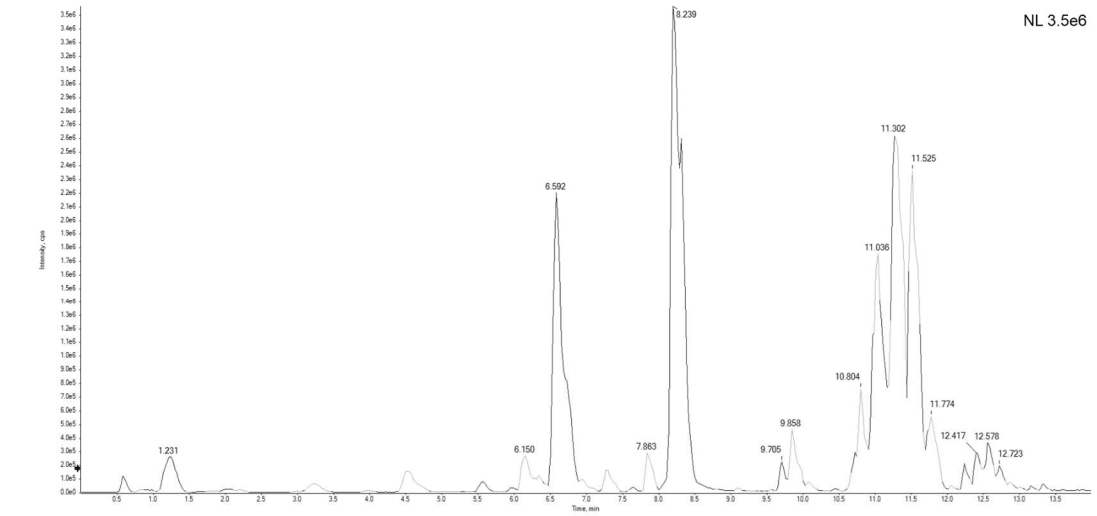

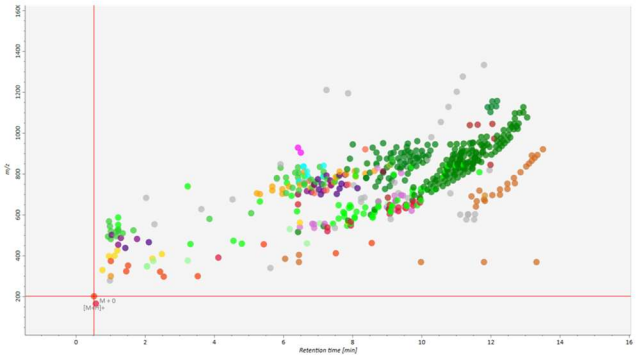

Identified features in MS-DIAL	Number of lipids 685	%	Identified features in MS-DIAL	Number of lipids	%
TG	149	21.8	PE	12	1.8
Cer	104	15.2	EtherPC	11	1.6
DG	44	6.4	LPC	11	1.6
PC	36	5.3	PI	11	1.6
SM	36	5.3	PS	11	1.6
FA	34	5	EtherPE	10	1.5
OxFA	30	4.4	MG	10	1.5
OxTG	29	4.2	NAE	8	1.2
EtherTG	25	3.6	CL	7	1
CE	15	2.2	CAR	6	0.9
HexCer	14	2	SHexCer	6	0.9
SL	13	1.9	LPE	5	0.7

Figure 1: BPC in positive ionization modes of the pooled QC samples and the respective ion map. The table on the right shows the number of lipid species putatively identified in positive and negative ion mode (CID Top20). Putative lipid annotations are reported only for reference-matched annotations.

The PCA model based on the features included in the final dataset showed a clear separation between the experimental groups. The QC cluster in the middle of the score plot indicated good analytical performance, and the biological variation was more influential than the analytical variation (Figure 2).

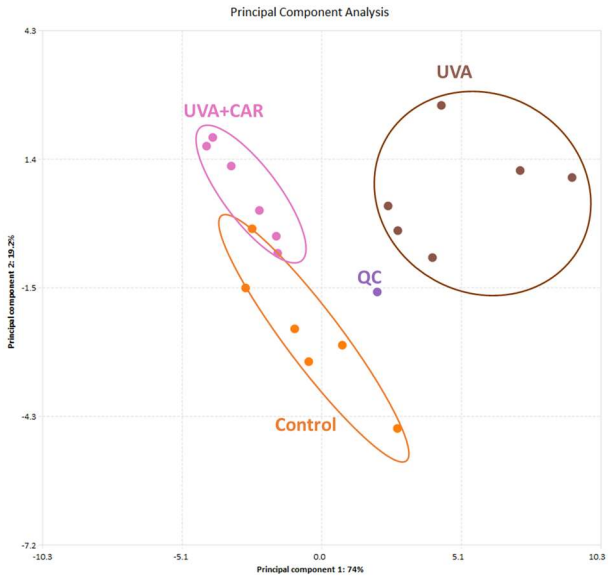

Figure 2: PCA score plot of log10-transformed LC-MS analysis via positive ESI mode Scores are coloured by experimental group.

UVA radiation modifies the lipid profile of the skin

I then compared the skin lipid profiles of UV-exposed (UVA) and control mice (control). As highlighted by the PCA analysis, UV radiation has a strong effect on the skin lipidome, as evidenced by the clear clustering and separation of groups (Figure 3). Notably, these differences are mainly driven by lipids such as Cer, TG and DG as also highlighted in the enrichment analysis (Figure 3). UV exposure induced a significant increase in sphingolipids, particularly dihydroceramides such as Cer(d42:1), Cer(d40:0), Cer(d34:1) and ultra-long chain ceramides. They are the primary catabolic product of sphingomyelin hydrolysis and are essential for maintaining cellular homeostasis. Alterations in the ceramide profile are likely to disrupt the highly organized structure of the skin's multilamellar barrier, leading to progressive fibrosis, thickening of the stratum corneum (SC)[15,16] and persistent production of inflammatory cytokines and chemokines, such as IL-1α and TNF-α[17]. Moreover, Cer directly affects the generation of ROS from mitochondria[18]. In addition to sphingolipids, UV exposure also significantly increased the levels of other lipids, including TG (52:4), TG (54:4), DG (34:3), and DG (36:3). The modelling of neutral lipids, particularly TGs, has important biological implications in the skin. Indeed, the accumulation of TGs has been linked to JNK (c-Jun N-terminal kinase) phosphorylation, which could induce cell inflammation and apoptosis[19]. Additionally, DGs act as signalling molecules and are involved in inflammatory responses[20]. Our lipidomic analysis also identified cholesterol sulfate and cholesterol esters, being

significantly increased in the skin after UVA exposure. In particular, cholesterol sulfate is known to be actively involved in the keratinocyte differentiation and desquamation process[21]. In contrast, free cholesterol has not been detected in our untargeted lipidomic analysis.

A

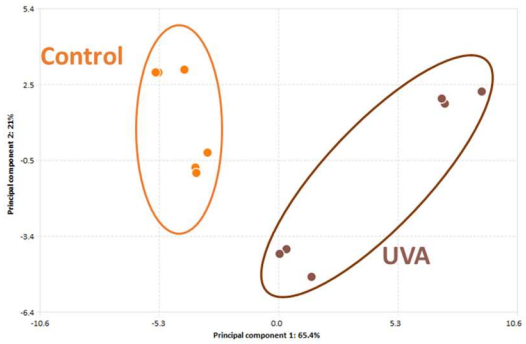

B

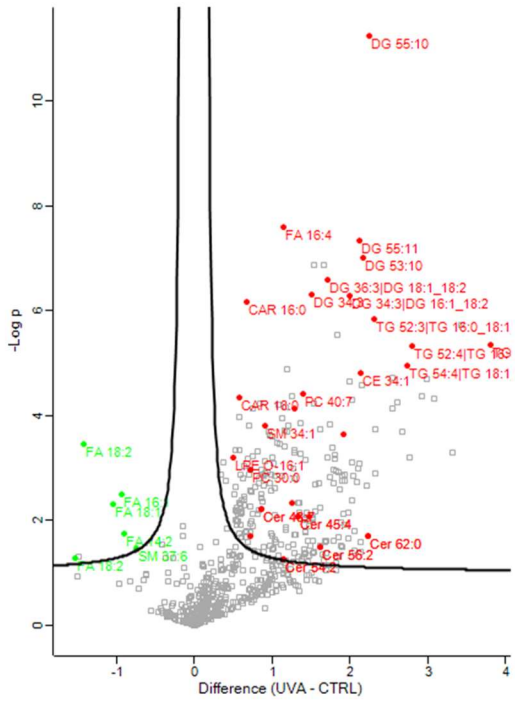

C

Term ID	Discription	Annotated	p-value	FDR q-value
	N-acylsphingosines (ceramides)			
LION:0012441	[SP0201]	104	1.10E-07	1.12E-06
LION:0000004	sphingolipids [SP]	156	3.80E-06	3.00E-05
LION:0002967	polyunsaturated fatty acid	152	4.50E-05	2.46E-04
LION:0000607	diacylglycerols [GL0201]	44	4.80E-05	2.52E-04
LION:0000622	triacylglycerols [GL0301]	171	1.00E-30	1.42E-28

Figure 3: A) PCA scores plot of log10-transformed LC-MS analysis via positive ESI mode. B) Volcano Plot of UVA vs. CTRL. In red, the features significantly increased (FC) > 1.5, adjusted p-value < 0.05. C) LION Enrichment analysis of UVA group vs control in the "ranking mode".

UVA significantly increases the levels of some polyunsaturated fatty acids (PUFAs). Increases in arachidonic acid (AA, FA 20:4) and other PUFAs as precursors of eicosanoids have been implicated in UV-induced immunosuppression and inflammatory responses[18]. AA is released from lipids containing the arachidonyl fatty acid chain (20:4) in response to cellular stimuli, often associated with the activation of phospholipase A2, the enzyme responsible for the release of the 20:4 fatty acid from the lipid. The direct involvement of AA was recently investigated in human keratinocytes (HaCaT) exposed to low (5 J/cm^2) and high (20 J/cm^2) doses of UVA[19]. A dose of 20 J/cm^2 UVA stimulated a significant amount of arachidonic acid and docosahexaenoic acid (DHA) after 24-h exposure, indicating that UVA radiations seem to accumulate PUFA and disrupt normal PUFA metabolism even after 24 h. Accumulation of PUFA can alter the skin cell membrane function by increasing fluidity and lipid peroxidation[22–24]. In fact, due to their multiple double bonds, PUFAs may be more susceptible to lipid peroxidation, increasing

the risk of oxidative stress. The resulting lipid peroxidation products could easily attack proteins, DNA and lipids, leaving the skin vulnerable to photooxidative damage.

A good indication of UVA-induced oxidative damage was provided by the work of Salvayre *et al*.[25]. Using the same experimental animal model, they showed that UVA exposure in hairless mice caused sustained lipid peroxidation and the subsequent accumulation of highly reactive carbonyl species such as 4-HNE, which forms adducts with elastin in the dermis contributing to skin elastosis and photoaging[26]. Interestingly, they also found that carnosine significantly inhibited the formation of such adducts and, thus, elastin modification. These results encouraged us to investigate whether the same beneficial effect could also be observed at the lipidome level and that this could help to better interpret the mechanism of action of carnosine.

The protecting role of carnosine on skin lipidome

To investigate the potential role of carnosine against UVA exposure on the skin lipidome, I compared UVA+CAR and UVA experimental groups. Carnosine treatment induced changes in the skin lipidome, as suggested by the clear clustering and separation of groups in the PCA score plot. Carnosine significantly reduced the DG levels, which in turn reduced the accumulation of TGs, resulting in an amelioration of ROS-induced oxidative stress[27].

Further supporting this protective effect against oxidative damage, carnosine treatment significantly reduced levels of arachidonic acid and other upregulated PUFAs. As previously discussed, PUFAs are highly susceptible to ROS attack, which can lead to lipid peroxidation. By reducing PUFA levels, carnosine could help to prevent lipid peroxidation and further oxidative damage in the skin. Carnosine also significantly decreased several ceramides, including ultra-long chain ceramides (Supplementary Figure 1). This results in improved skin plasticity, hydration, barrier function, and improved inflammatory response. In line with these results, enrichment analysis showed that terms such as ‘bilayer thickness’ and ‘plasma membrane’ were significantly enriched when I compared the UVA+CAR and UVA experimental groups.

A

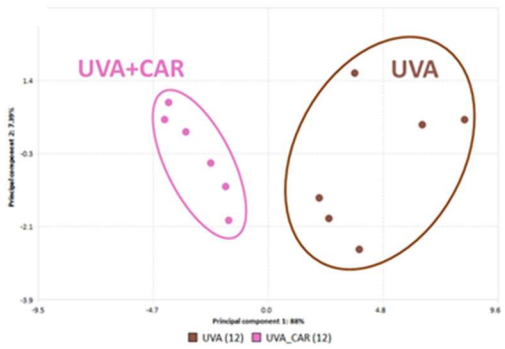

B

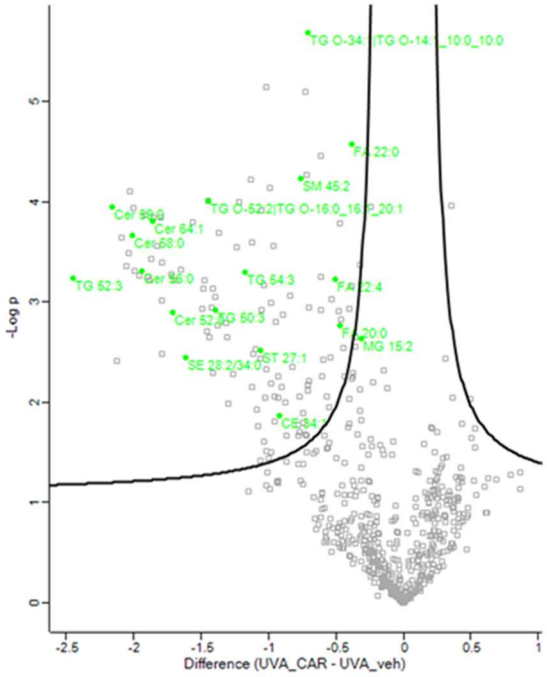

C

Term ID	Discription	Annotated	p-value	FDR q-value
LION:0080970	average bilayer thickness	22	0.00079	2.95E-03
LION:0012080	endoplasmic reticulum (ER)	196	3.00E-10	7.10E-09
LION:0012010	membrane component	213	1.30E-09	2.64E-08
LION:0000464	negative intrinsic curvature	180	8.40E-09	1.08E-07
LION:0012082	plasma membrane	154	1.30E-08	1.54E-07
LION:0002967	polyunsaturated fatty acid	152	4.50E-05	2.46E-04

Figure 4: A) PCA scores plot of log10-transformed LC-MS analysis via positive ESI mode. B) Volcano Plot of UVA+CAR vs. UVA. In green the features significantly decreased (FC) > 1.5, adjusted p-value < 0.05. C) LION Enrichment analysis of UVA+CAR group vs UVA in the "ranking mode".

Treatment with carnosine identifies specific signaling pathways underlying its mechanism of action

Based on our results, I next performed a pathway analysis on the lipids significantly modulated in the experimental groups to generate more detailed insights into the pathways affected by UVA radiation and carnosine treatment. The Ingenuity Pathway Analysis (IPA) software identified 21 connected canonical pathways that were significantly altered between the experimental groups. These included pathways associated with inflammation, apoptosis and molecular transport. In the bar graph visualizations, orange indicates a positive z-score, indicating a predicted increase in such a biological process, while blue represents a negative z-score, indicating a decrease (Figure 5).

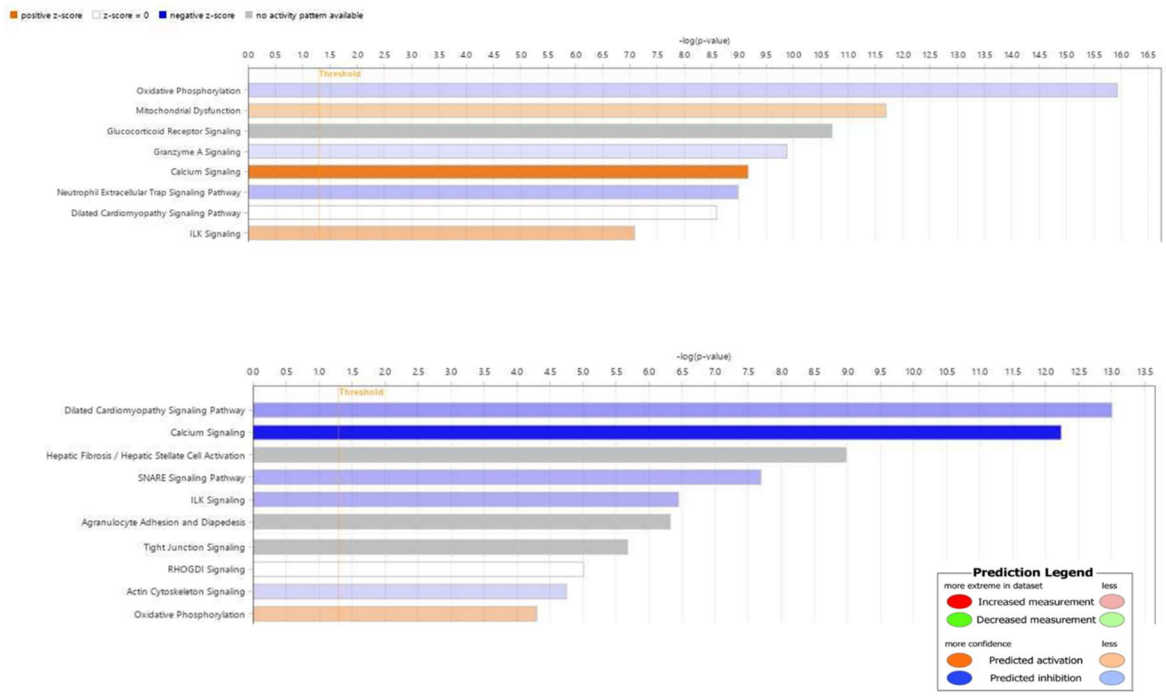

Figure 5: canonical pathways obtained comparing a) UVA vs Control and b) UVA-Car vs UVA (IPA). In orange, increased pathways (positive z-score); in blue, decreased pathways (negative z-score); in white, no change (zero as z-score); in grey, uncertain changes (NA z-score). The prediction legend is essential for understanding networks.

In particular, UVA exposure was predicted to activate Ca^{2+} signalling (p-value 1.49E-05), which plays a crucial role in skin physiology. Indeed, Ca^{2+} ions and their gradient in the epidermis control essential functions such as keratinocyte differentiation and overall skin homeostasis[28]. UVA exposure has been shown to activate a G-protein-coupled signalling pathway leading to intracellular Ca^{2+} mobilization, a process associated with cancer cell migration, invasion, and metastasis[29]. Ca^{2+} influx following UVA exposure contributes to cellular damage, skin ageing, and epidermal hyperplasia.

Conversely, carnosine treatment significantly inhibited the Ca^{2+} signalling pathway (p-value 1.49E-05), likely due to its antioxidant and anti-inflammatory properties. Interestingly, our results agreed with proteomic results obtained in the same experimental animal model[3]. Indeed, the Ca^{2+} signalling pathway was one of the functional pathways significantly activated by UVA, also at the protein level, resulting in increased oxidative stress, fibrosis, and contractile process. Key proteins involved in calcium homeostasis, such as ryanodine receptor 1 (RyR-1), were upregulated after UVA exposure. Carnosine treatment effectively restored calcium homeostasis by significantly downregulating RyR-1 and other proteins linked to this signalling pathway, such as sarcoplasmic/endoplasmic reticulum calcium ATPase (SERCA), and calcium/calmodulin-dependent protein kinase II.

Calcium signalling appears to be part of a broader molecular network related to lipid metabolism and inflammatory processes, as shown in Figure 6. One of the key lipid classes highlighted in the network is that of ceramides. UVA exposure significantly increases the levels of some ceramides, likely in response to pro-inflammatory signalling. Ceramides are the primary catabolic product of sphingomyelin hydrolysis and are essential for maintaining skin homeostasis. Alterations in the ceramide profile promoted the sustained production of inflammatory cytokines and chemokines, such as IL-1α and TNF-α [17]and are directly involved in the generation of ROS that drive skin inflammation and damage. Some forms of dihydroceramide, such as C22:0 and C24:0, induce cytotoxicity through caspase-independent mechanisms, leading to mixed cell death and increased autophagy[30].The role of dihydroceramide as an inducer of autophagy has been further supported by several studies in various cellular models[31,32]. Strongly associated with inflammation was also the c16 dihydrosphingomyelin (dhSM), which was found to be significantly increased after UVA exposure, possibly contributing to skin barrier disruption and increased expression of pro-inflammatory genes. Carnosine, on the other hand, showed antioxidant and anti-inflammatory properties that may help to counteract the negative effects of ceramides and SM in the skin (Figure 6B). Studies have shown that the topical application of carnosine can help to reduce skin inflammation, improve skin hydration, and prevent skin damage[33].

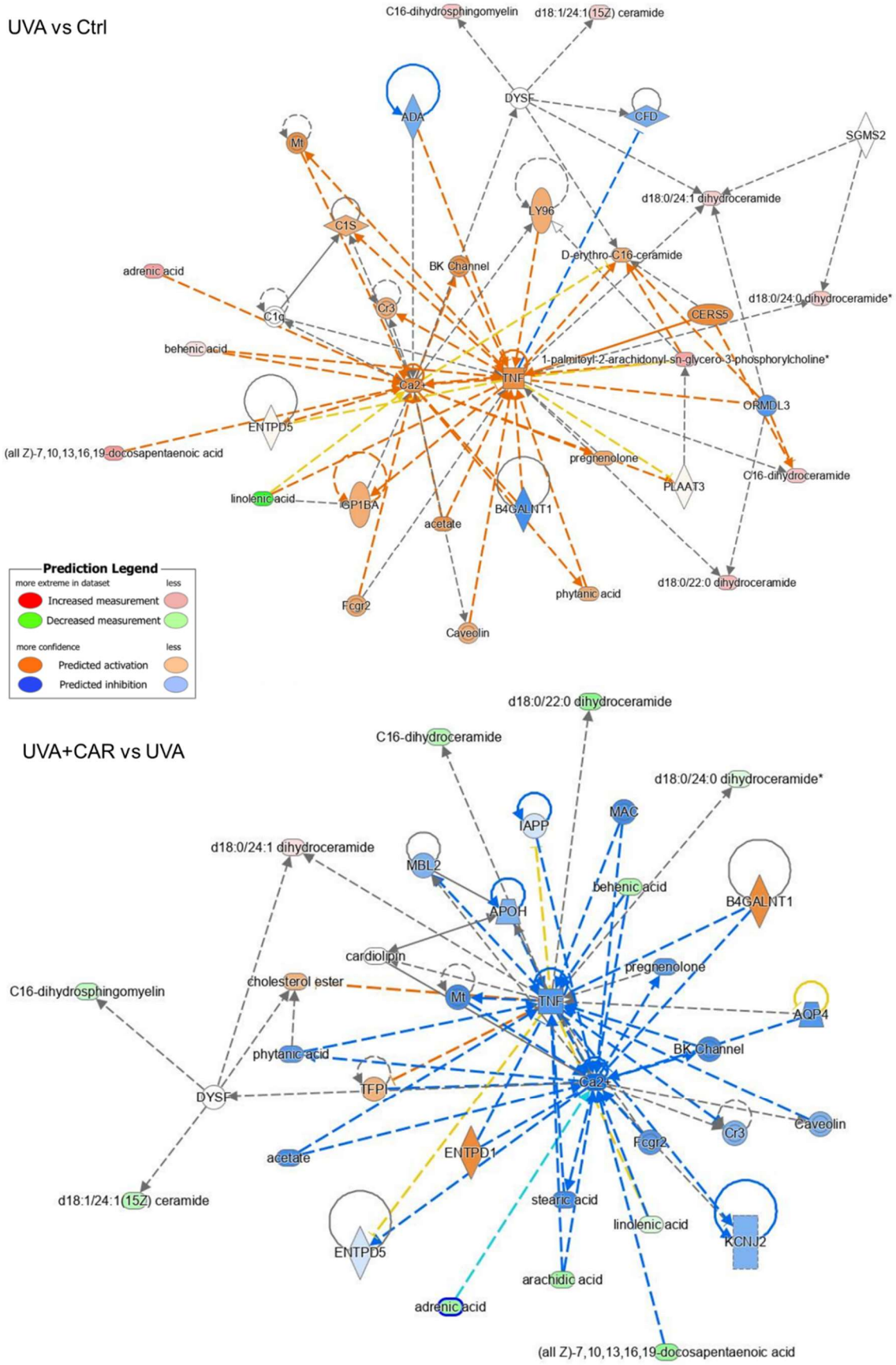

Figure 6: TNF and Ca^{2+} dysregulation after A. UV-A exposure and B. after carnosine treatment. The prediction legend (IPA) on the left is essential for understanding networks. Each network comprehends molecules from the knowledge base that were added to maximize the number of connections between the focus molecules.

Conclusions

Our untargeted lipidomic study provides a detailed and precise characterization of the changes in the skin lipidomic profile following prolonged UVA exposure and treatment with carnosine. Our findings indicate that UVA radiation induces profound changes in skin barrier composition, primarily affecting the levels of neutral triglycerides, ceramides, and fatty acids, which together play a central role in maintaining skin barrier function. These changes lead to several detrimental effects on the skin, including dermal photoaging, chronic inflammation, and increased production of ROS and TNF. To prevent UVA damage, skin treatment with carnosine effectively regulates ROS and TNF generation induced by UVA, confirming its antioxidant and anti-inflammatory properties and enhancing the skin's physiological processes essential for its barrier integrity and stability. Beyond these observations, the high sensitivity of our lipidomic approach lays the foundation for future research aimed at gaining a more comprehensive understanding of skin lipidome changes during disease and treatment, as well as evaluating the protective potential of agents that improve skin health and prevent skin disorders. Further investigation will be dedicated to a more detailed study of oxidized lipids.

Supplementary Figures

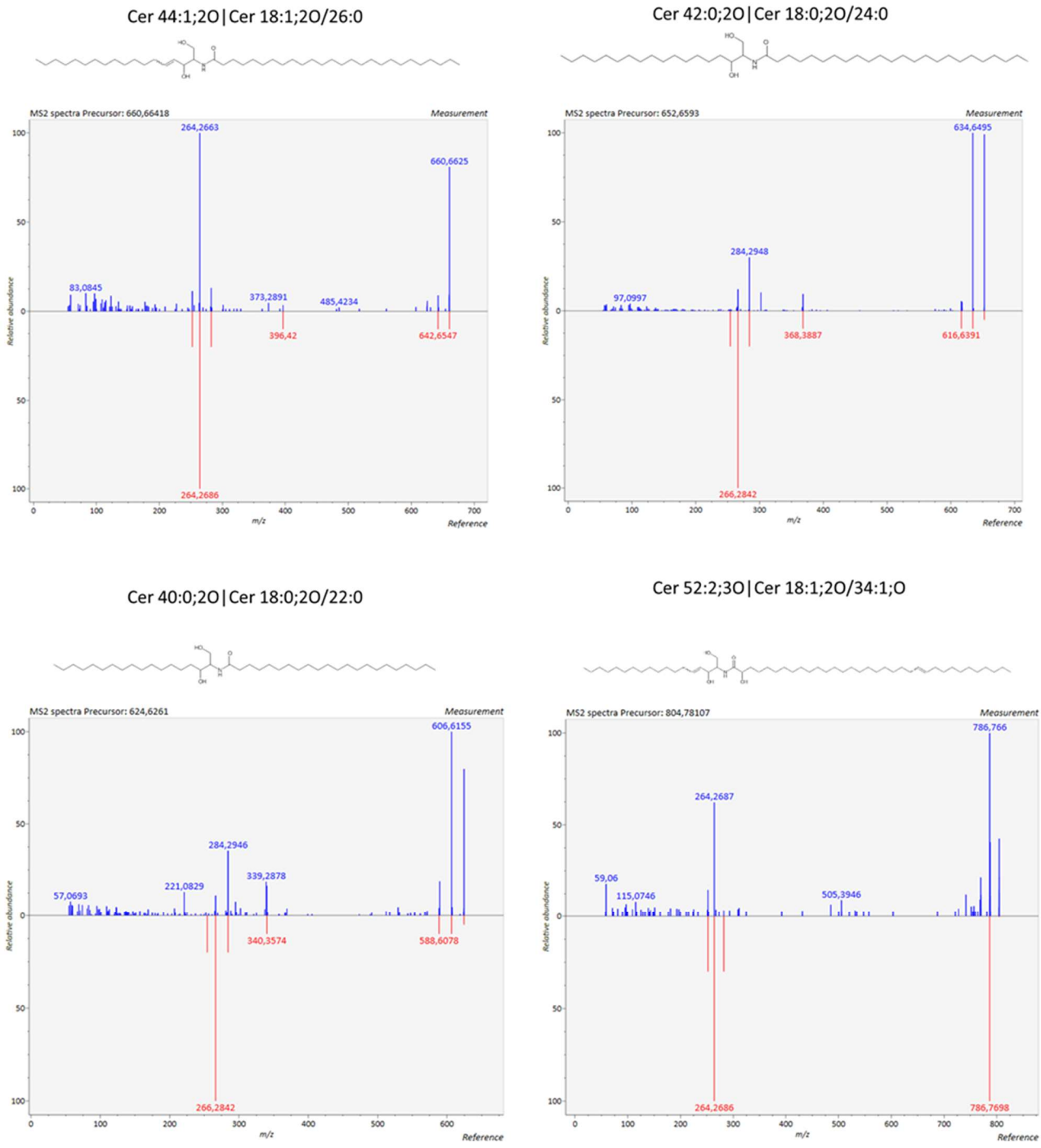

Supplementary Figure 1: MS/MS spectra of four long-chain ceramides significantly reduced by carnosine treatment. All Supplementary Tables with all the identifications, mz, RT, intensity and MS2 are available on request.

References

(1) de Szalay, S.; Wertz, P. W. Protective Barriers Provided by the Epidermis. *Int J Mol Sci* **2023**, *24* (4), 3145. https://doi.org/10.3390/ijms24043145.

(2) de Gruijl, F. R. Photocarcinogenesis: UVA vs. UVB Radiation. *Skin Pharmacol Physiol* **2002**, *15* (5), 316–320. https://doi.org/10.1159/000064535.

(3) Radrezza, S.; Carini, M.; Baron, G.; Aldini, G.; Negre-Salvayre, A.; D'Amato, A. Study of Carnosine's Effect on Nude Mice Skin to Prevent UV-A Damage. *Free Radic Biol Med* **2021**, *173*, 97–103. https://doi.org/10.1016/j.freeradbiomed.2021.07.010.

(4) Negre-Salvayre, A.; Salvayre, R. Post-Translational Modifications Evoked by Reactive Carbonyl Species in Ultraviolet-A-Exposed Skin: Implication in Fibroblast Senescence and Skin Photoaging. *Antioxidants* **2022**, *11* (11), 2281. https://doi.org/10.3390/antiox11112281.

(5) Bouwstra, J. A.; Ponec, M. The Skin Barrier in Healthy and Diseased State. Biochimica et Biophysica Acta (BBA) - *Biomembranes* **2006**, 1758 (12), 2080–2095. https://doi.org/10.1016/j.bbamem.2006.06.021.

(6) Wölfle, U.; Seelinger, G.; Bauer, G.; Meinke, M. C.; Lademann, J.; Schempp, C. M. Reactive Molecule Species and Antioxidative Mechanisms in Normal Skin and Skin Aging. *Skin Pharmacol Physiol* **2014**, *27* (6), 316–332. https://doi.org/10.1159/000360092.

(7) Gęgotek, A.; Łuczaj, W.; Skrzydlewska, E. Effects of Natural Antioxidants on Phospholipid and Ceramide Profiles of 3D-Cultured Skin Fibroblasts Exposed to UVA or UVB Radiation. *Antioxidants* **2021***, 10* (4), 578. https://doi.org/10.3390/antiox10040578.

(8) Altomare, A.; Baron, G.; Gianazza, E.; Banfi, C.; Carini, M.; Aldini, G. Lipid Peroxidation Derived Reactive Carbonyl Species in Free and Conjugated Forms as an Index of Lipid Peroxidation: Limits and Perspectives. *Redox Biol* **2021**, *42,* 101899. https://doi.org/10.1016/j.redox.2021.101899.

(9) Larroque-Cardoso, P.; Camaré, C.; Nadal-Wollbold, F.; Grazide, M.-H.; Pucelle, M.; Garoby-Salom, S.; Bogdanowicz, P.; Josse, G.; Schmitt, A.-M.; Uchida, K.; Zarkovic, K.; Salvayre, R.; Nègre-Salvayre, A. Elastin Modification by 4-Hydroxynonenal in Hairless Mice Exposed to UV-A. Role in Photoaging and Actinic Elastosis. *Journal of Investigative Dermatology* **2015**, *135* (7), 1873–1881. https://doi.org/10.1038/jid.2015.84.

(10) Aldini, G.; Facino, R. M.; Beretta, G.; Carini, M. Carnosine and Related Dipeptides as Quenchers of Reactive Carbonyl Species: From Structural Studies to Therapeutic Perspectives. *BioFactors* **2005**, *24* (1–4), 77–87. https://doi.org/10.1002/biof.5520240109.

(11) Aldini, G.; Carini, M.; Yeum, K.-J.; Vistoli, G. Novel Molecular Approaches for Improving Enzymatic and Nonenzymatic Detoxification of 4-Hydroxynonenal: Toward the Discovery of a Novel Class of Bioactive Compounds. *Free Radic Biol Med* **2014**, *69*, 145–156. https://doi.org/10.1016/j.freeradbiomed.2014.01.017.

(12) Aiello, G.; Rescigno, F.; Meloni, M.; Zoanni, B.; Aldini, G.; Carini, M.; D'Amato, A. The Effect of Carnosine on UVA-Induced Changes in Intracellular Signaling of Human Skin Fibroblast Spheroids. *Antioxidants* **2023**, *12* (2), 300. https://doi.org/10.3390/antiox12020300.

(13) Tsugawa, H.; Cajka, T.; Kind, T.; Ma, Y.; Higgins, B.; Ikeda, K.; Kanazawa, M.; VanderGheynst, J.; Fiehn, O.; Arita, M. MS-DIAL: Data-Independent MS/MS Deconvolution for Comprehensive Metabolome Analysis. *Nat Methods* **2015**, 12 (6), 523–526. https://doi.org/10.1038/nmeth.3393.

(14) Chong, J.; Soufan, O.; Li, C.; Caraus, I.; Li, S.; Bourque, G.; Wishart, D. S.; Xia, J. MetaboAnalyst 4.0: Towards More Transparent and Integrative Metabolomics Analysis. *Nucleic Acids Res* **2018**, 46 (W1), W486–W494. https://doi.org/10.1093/nar/gky310.

(15) Minton, K. Preconditioning the ECM for Fibrosis. *Nat Rev Mol Cell Biol* **2014**, 15 (12), 766–767. https://doi.org/10.1038/nrm3906.

(16) Herrera, J.; Henke, C. A.; Bitterman, P. B. Extracellular Matrix as a Driver of Progressive Fibrosis. *Journal of Clinical Investigation* **2018**, 128 (1), 45–53. https://doi.org/10.1172/JCI93557.

(17) Kanoh, H.; Ishitsuka, A.; Fujine, E.; Matsuhaba, S.; Nakamura, M.; Ito, H.; Inagaki, N.; Banno, Y.; Seishima, M. IFN- γ Reduces Epidermal Barrier Function by Affecting Fatty Acid Composition of Ceramide in a Mouse Atopic Dermatitis Model. *J Immunol Res* **2019**, 2019, 1–10. https://doi.org/10.1155/2019/3030268.

(18) Walterscheid, J. P.; Ullrich, S. E.; Nghiem, D. X. Platelet-Activating Factor, a Molecular Sensor for Cellular Damage, Activates Systemic Immune Suppression. *J Exp Med* **2002**, 195 (2), 171–179. https://doi.org/10.1084/jem.20011450.

(19) Leung, K. S.; Chan, H. F.; Leung, H. H.; Galano, J.-M.; Oger, C.; Durand, T.; Lee, J. C.-Y. Short-Time UVA Exposure to Human Keratinocytes Instigated Polyunsaturated Fatty Acid without Inducing Lipid Peroxidation. *Free Radic Res* **2017**, 51 (3), 269–280. https://doi.org/10.1080/10715762.2017.1300885.

(20) Liu刘立, L.; Yu, S.; Khan, R. S.; Homma, S.; Schulze, P. C.; Blaner, W. S.; Yin尹玉新, Y.; Goldberg, I. J. Diacylglycerol Acyl Transferase 1 Overexpression Detoxifies Cardiac Lipids in PPARγ Transgenic Mice. *J Lipid Res* **2012**, 53 (8), 1482–1492. https://doi.org/10.1194/jlr.M024208.

(21) Elias, P. M.; Williams, M. L.; Choi, E.-H.; Feingold, K. R. Role of Cholesterol Sulfate in Epidermal Structure and Function: Lessons from X-Linked Ichthyosis. *Biochimica et Biophysica Acta (BBA) - Molecular and Cell Biology of Lipids* **2014**, 1841 (3), 353–361. https://doi.org/10.1016/j.bbalip.2013.11.009.

(22) Day, C. A.; Kenworthy, A. K. Tracking Microdomain Dynamics in Cell Membranes. *Biochimica et Biophysica Acta (BBA) - Biomembranes* **2009**, 1788 (1), 245–253. https://doi.org/10.1016/j.bbamem.2008.10.024.

(23) Wiktorowska-Owczarek, A.; Berezińska, M.; Nowak, J. Z. PUFAs: Structures, Metabolism and Functions. *Advances in Clinical and Experimental Medicine* **2015**, 24 (6), 931–941. https://doi.org/10.17219/acem/31243.

(24) Hashimoto, M.; Shahdat, Md. H.; Shimada, T.; Yamasaki, H.; Fujii, Y.; Ishibashi, Y.; Shido, O. Relationship between Age-Related Increases in Rat Liver Lipid Peroxidation and Bile Canalicular Plasma Membrane Fluidity. *Exp Gerontol* **2001**, *37* (1), 89–97. https://doi.org/10.1016/S0531-5565(01)00164-4.

(25) Larroque-Cardoso, P.; Camaré, C.; Nadal-Wollbold, F.; Grazide, M.-H.; Pucelle, M.; Garoby-Salom, S.; Bogdanowicz, P.; Josse, G.; Schmitt, A.-M.; Uchida, K.; Zarkovic, K.; Salvayre, R.; Nègre-Salvayre, A. Elastin Modification by 4-Hydroxynonenal in Hairless Mice Exposed to UV-A. Role in Photoaging and Actinic Elastosis. *Journal of Investigative Dermatology* **2015**, *135* (7), 1873–1881. https://doi.org/10.1038/jid.2015.84.

(26) Guéraud, F.; Atalay, M.; Bresgen, N.; Cipak, A.; Eckl, P. M.; Huc, L.; Jouanin, I.; Siems, W.; Uchida, K. Chemistry and Biochemistry of Lipid Peroxidation Products. *Free Radic Res* **2010**, *44* (10), 1098–1124. https://doi.org/10.3109/10715762.2010.498477.

(27) Talayero, B. G.; Sacks, F. M. The Role of Triglycerides in Atherosclerosis. *Curr Cardiol Rep* **2011**, *13* (6), 544–552. https://doi.org/10.1007/s11886-011-0220-3.

(28) Katsuta, Y.; Iida, T.; Inomata, S.; Denda, M. Unsaturated Fatty Acids Induce Calcium Influx into Keratinocytes and Cause Abnormal Differentiation of Epidermis. *Journal of Investigative Dermatology* **2005**, *124* (5), 1008–1013. https://doi.org/10.1111/j.0022-202X.2005.23682.x.

(29) Predescu, D.-V.; Crețoiu, S. M.; Crețoiu, D.; Pavelescu, L. A.; Suciu, N.; Radu, B. M.; Voinea, S.-C. G Protein-Coupled Receptors (GPCRs)-Mediated Calcium Signaling in Ovarian Cancer: Focus on GPCRs Activated by Neurotransmitters and Inflammation-Associated Molecules. *Int J Mol Sci* **2019**, *20* (22), 5568. https://doi.org/10.3390/ijms20225568.

(30) Holliday Jr., M. W.; Cox, S. B.; Kang, M. H.; Maurer, B. J. C22:0- and C24:0-Dihydroceramides Confer Mixed Cytotoxicity in T-Cell Acute Lymphoblastic Leukemia Cell Lines. *PLoS One* **2013**, *8* (9), e74768. https://doi.org/10.1371/journal.pone.0074768.

(31) Signorelli, P.; Munoz-Olaya, J. M.; Gagliostro, V.; Casas, J.; Ghidoni, R.; Fabriàs, G. Dihydroceramide Intracellular Increase in Response to Resveratrol Treatment Mediates Autophagy in Gastric Cancer Cells. *Cancer Lett* **2009**, *282* (2), 238–243. https://doi.org/10.1016/j.canlet.2009.03.020.

(32) Gagliostro, V.; Casas, J.; Caretti, A.; Abad, J. L.; Tagliavacca, L.; Ghidoni, R.; Fabrias, G.; Signorelli, P. Dihydroceramide Delays Cell Cycle G1/S Transition via Activation of ER Stress and Induction of Autophagy. *Int J Biochem Cell Biol* **2012**, *44* (12), 2135–2143. https://doi.org/10.1016/j.biocel.2012.08.025.

(33) Hipkiss, A. R.; Baye, E.; de Courten, B. Carnosine and the Processes of Ageing. *Maturitas* **2016**, *93*, 28–33. https://doi.org/10.1016/j.maturitas.2016.06.002.

CHAPTER 4:
HIGH-THROUGHPUT UNTARGETED LIPIDOMIC ANALYSIS OF CARNOSINE EFFECTS ON DIET-INDUCED OBESITY

Summary

Lipidomics has been successfully applied to the study of disease, disease-related mechanisms and drug modes of action using a variety of experimental setups and model organisms. In this thesis, one area of focus has been obesity, a complex condition frequently associated with other diseases, including cardiovascular and liver disorders. The liver is commonly implicated in obesity, as prolonged caloric excess in this organ manifests as lipid deposition and dyslipidemia, which are highly correlated with the production of lipotoxic intermediates and are thought to be involved in the development of mitochondrial dysfunction, inflammation and oxidative damage in hepatocytes. Carnosine, due to its antioxidant and carbonyl scavenging properties, could help to ameliorate this pathological phenotype. However, the exact mechanism explaining the beneficial effects of carnosine on obesity remains unclear. In this study, we aimed to define the changes in lipid metabolites in rats fed with a high-fat diet to induce hyperlipidemia and to explore the efficacy and mechanism of action of carnosine in the treatment of diet-induced hyperlipidemia. This project was carried out in collaboration with ETH University during my stay abroad. The present work is divided into three main parts, each exploring different aspects of the lipidomic dataset.

1. In the first part of this study, I aimed to evaluate the applicability of high-throughput methods for a deeper analysis of the lipidome across different biological matrices and to identify specific lipidomic signatures associated with obesity in the animal model.

2. The second part of the work aimed to investigate modifications in the lipidome, particularly in the context of epilipidomics, to assess the effects of carnosine treatment on obese pathological phenotypes. This includes exploring potential oxidative modifications in the lipidome and identifying epilipidomic signatures that define the effect of carnosine.

3. The third part focused on the structural elucidation of lipid species identified in the untargeted dataset beyond their molecular level through advanced mass spectrometry approaches.

Each part of the work will be covered and discussed in the following chapters of the thesis.

Background

Many metabolic diseases, such as obesity, are associated with dysregulation of both energy and lipid homeostasis, and alterations in lipid profile have been identified as one of the main risk factors[1]. Obesity increases the risk of other comorbidities such as cardiovascular disease, type 2 diabetes and liver disorders[2]. In particular, the liver is a dynamic and metabolically active organ that plays an essential role in the detoxification and excretion of both endogenous and exogenous compounds. The liver is often involved in the pathology of obesity, which at this level can cause hepatic metabolic changes leading to the development of steatosis, resulting in non-alcoholic fatty liver disease (NAFLD) and non-alcoholic steatotic hepatitis (NASH). Lipid accumulation in liver tissue is also strongly correlated with insulin resistance and the production of lipotoxic intermediates, such as ceramides and diacylglycerols, resulting from excess triacylglycerols.[3]

Given the central role of lipids in the development and progression of this disease, the possibility of profiling up to hundreds of lipids in a single analysis in an untargeted manner represents a highly valid tool for studying the underlying mechanisms and a more accurate description of the hepatic consequences of obesity.[4]

Although this has always implied the use of long chromatographic methods to capture a wider dynamic range, the need for short methods to highlight changes and provide rapid results is becoming increasingly important in biomedical research, especially when working with large sample cohorts of clinical relevance. This is increasingly driving high-throughput methods using UHPLC-MS systems with high separation performance, increased sensitivity, and high resolution. Recently, several high-throughput methods have been proposed, allowing the accurate annotation and quantification of a large number of lipid species in different biological matrices[5].

In the present study, we applied a high-throughput 2.4-minute UHPLC-MS method to lipid profiling of plasma and liver samples of lean and diet-induced obese rats. With this method, we aimed to identify specific lipid signatures of the liver and plasma caused by obesity.

Materials and Methods

Animals and Experimental Protocol

Plasma and liver samples used in this work were kindly provided by Camila Renata Corrêa's laboratory (São Paulo State University – Unesp- Medical School, Botucatu, Brazil) and stored at -80°C. The experimental protocol was performed according to the National Institute for Health's Guide to Care and Use of Laboratory Animals, and the study project was approved by the Ethics Committee of the Use of Animals, Botucatu School of Medicine, Sao Paulo State University (Protocol number: CEUA-344/2019)[6]. Briefly, 24 male Wistar rats (±187 g) were kept in an environmentally controlled room (22 °C ± 3 °C; 12 h light-dark cycle and relative humidity of 60 ± 5 %) and randomly divided into four experimental groups. Over 17 weeks, the animals received: control diet (control, n= 6), control diet + carnosine (control + CAR, n = 6), high sugar-fat diet (HSF, n= 6), and high sugar-fat diet + carnosine (HSF + CAR, n= 6) (Table 1). The HSF groups also received water + sucrose (25%). Carnosine CAR (L-carnosine) was administered intraperitoneally (250 mg/kg) for five weeks after induction. The dose was determined based on studies in which CAR showed effective results without inducing toxicity or adverse effects in the animals[7,8]. Food and water were provided *ad libitum*. Both diets were prepared according to previous works [9] and are described in Table 1.

Components	*Control*	*HSF*
Soybean meal (g/kg)	335	340
Sorghum (g/kg)	278	80
Soy hulls (g/kg)	188	116
Dextrin (g/kg)	146	20
Sucrose (g/kg)	-	80
Fructose (g/kg)	-	180
Soybean oil (g/kg)	14	-
Lard (g/kg)	-	154
Minerals (g/kg)	25	25
Salt (g/kg)	4	8

Table 1: Diet composition and nutritional values.

Animals and biochemical characteristics

The induction of obesity in the HSF groups was verified by C.R. Correa's lab based on initial weight, weight gain and adiposity index data[10]. Additional biochemical and

hormonal markers (triglycerides, insulin, blood glucose, total cholesterol etc.) were evaluated.

Tissue extraction protocol

Lipid extraction from plasma and liver followed the same extraction protocol. Liver sectioning was performed on ice, using sterile surgical scalpels for sectioning. For tissue homogenization, 20 mg of liver tissue was added to 200 µl of MilliQ water + CH_3COONH_4 0.1% in a 2 mL microtube with approximately 20 mg of beads and homogenized using the Precellys bead beater (5800-6000 rpm, 15s, and 2 cycles). Samples were then centrifuged at 4°C for 10 min, and an aliquot of the supernatant was taken for lipid extraction. Lipids were extracted with 1mL of MMC extraction buffer methanol: MTBE: chloroform (MMC) 1.33:1:1 (v/v/v) mixture + BHT (0.1%), after 30min shaking, centrifugation at 14000 rpm and supernatant collection. Samples were dried overnight in a fume hood, reconstituted with 80 µl of IPA/MeOH 1:1, centrifuged for 10 min at 14.000 rpm at 4°C, and transferred into a glass vial. QC samples were prepared by pooling a small aliquot of all the samples. 20µl of plasma was extracted using the same protocol.

LC-MS analysis

To avoid potential bias from run order, samples were randomized. No technical replicates were used in this study. Separation was performed on an Agilent 1290 Infinity II LC system, including a binary pump manager equipped with an ACQUITY UPLC BEH C18 reversed-phase column (30mm x 2.1mm x 1.7 µm). During separation, the column temperature was maintained at 60°C and the flow rate was set at 1.2 mL/min. Lipid classes were separated by a 2.4 min gradient elution using the following mobile phases: A) acetonitrile: water (6:4 v/v) with 10mM ammonium acetate and 0.1% formic acid, B) isopropanol: acetonitrile (9:1 v/v) with 10mM ammonium acetate and 0.1% formic acid. The chromatographic gradient used for lipid analyses is shown in Table 2.

Time (min)	*A(%)*	*B(%)*
0.29	70	30
0.37	52	48
1.64	18	82
1.72	1	99
1.79	1	99
1.81	85	15
2.24	85	15

Table 2: LC conditions

After separation by UPLC, lipids were ionized by electrospray ionization, and the data were acquired in both positive and negative modes using the SCIEX ZenoTOF 7600 system with CID and operating in DDA mode. MS parameters were as follows:

Source Parameters	***Value***	***MS Parameters***	**Value**
Ion Source Gas 1 (psi)	70	*Scan Type*	TOF MS
Ions source Gas 2 (psi)	70	*Accumulation time (ms)*	75
Curtain Gas	45	*Declustering Potential (V)*	60
Temperature (°C)	700	*Collision Energy (V)*	10
Stray Voltage	5500 (+)/ 4500(-)	*Collision Energy Spread (V)*	0
		Range	70-1750
		MS/MS Parameters	**Value**
		Scan Type	TOF MS/MS
		Maximum Candidate Ions	8
		Intensity Threshold (counts/s)	100
		Mass Tolerance (mDa)	50
		Accumulation Time (ms)	15
		Declustering Potential	60
		CES	15
		CE	30

Table 3: TOF MS and TOF MS/MS parameters

Data processing and statistical analysis

All original wiff files (raw data from SCIEX) were converted to centroided mzML files (standardized format for storing MS data) using the qtof peak picker component of msconvert (ProteoWizard v 3.0.9987)[11]. The converted files were then fed into SLAW for run alignment, peak picking, and normalization to generate mgf files (Mascot Generic Format file) containing all representative MS/MS spectra acquired by DDA. Downstream analysis and annotation were performed using these mgf files. Annotation was done using our in-house annotation tool (LipidOracle; MS1 tolerance 0.01Da, MS2 0.02Da). Peaks with a %CV greater than 30% in the QC samples were detected in less than 50% of the samples belonging to the same group, and signals found in the blank samples were not included in further statistical analysis. Multivariate analysis was performed using Python. Data were log10-transformed and autoscaled. Features most influential in

PLS-DA models were taken forward for univariate analysis. Univariate statistics and plotting were all performed in GraphPad Prism[12].

Results

The experimental groups were set up for either liver or plasma samples as follows: lean rats (control group), rats fed with a high-fat and sugar diet (HSF group) and animals fed with a high-fat and sugar diet and treated with carnosine (HSF+CAR).

Untargeted LC-MS analysis of liver and plasma lipid extracts

To obtain a comprehensive profile of lipid molecular species, I performed untargeted lipidomics of liver and plasma samples on a Zeno7600 QTOF coupled to a UHPLC system using a 2.4 min gradient. The representative base peak intensity (BPI) chromatograms of lipid extracts from liver and plasma matrices are reported in Figures 1A (positive mode) and 1B (negative mode). The results are obtained by injecting 2 µl of sample in both polarities, and as expected, a higher ionization capacity is observable for the positive mode.

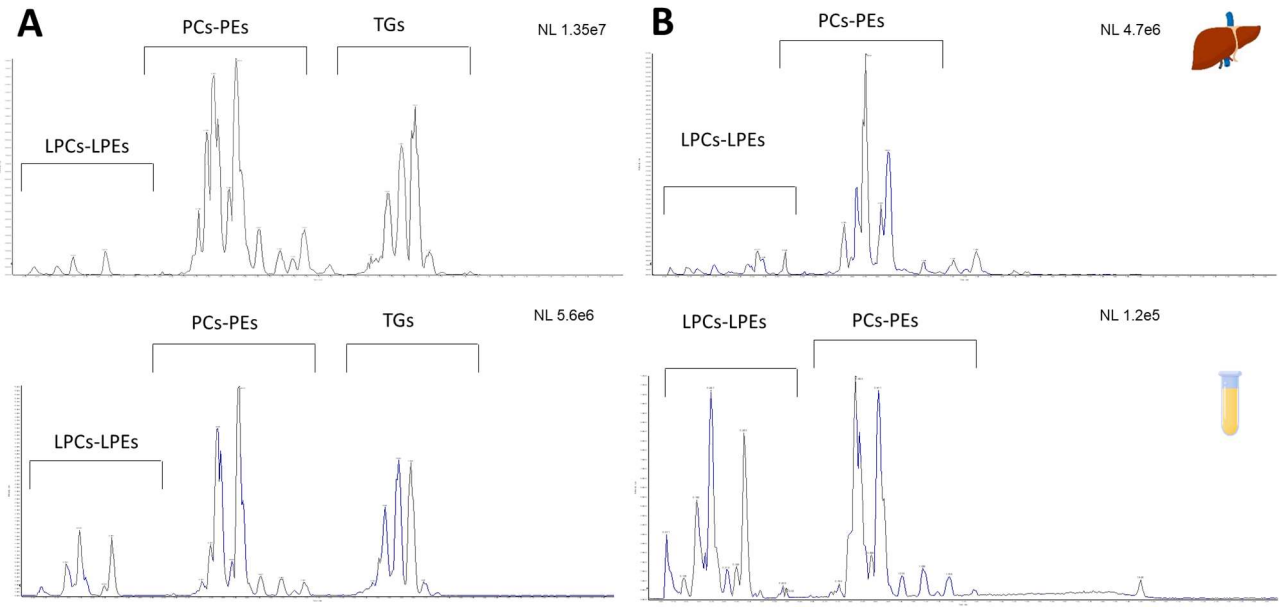

Figure 1: BPC in ESI positive (A) and ESI negative (B) ionization modes of the pooled QC samples for liver and plasma.

The 2.4-minute chromatographic run effectively separates the main lipid classes according to their polarity. The run showed high robustness and excellent repeatability. This can be appreciated by monitoring the performance of deuterated standards spiked into the samples before the analysis (Figure 2).

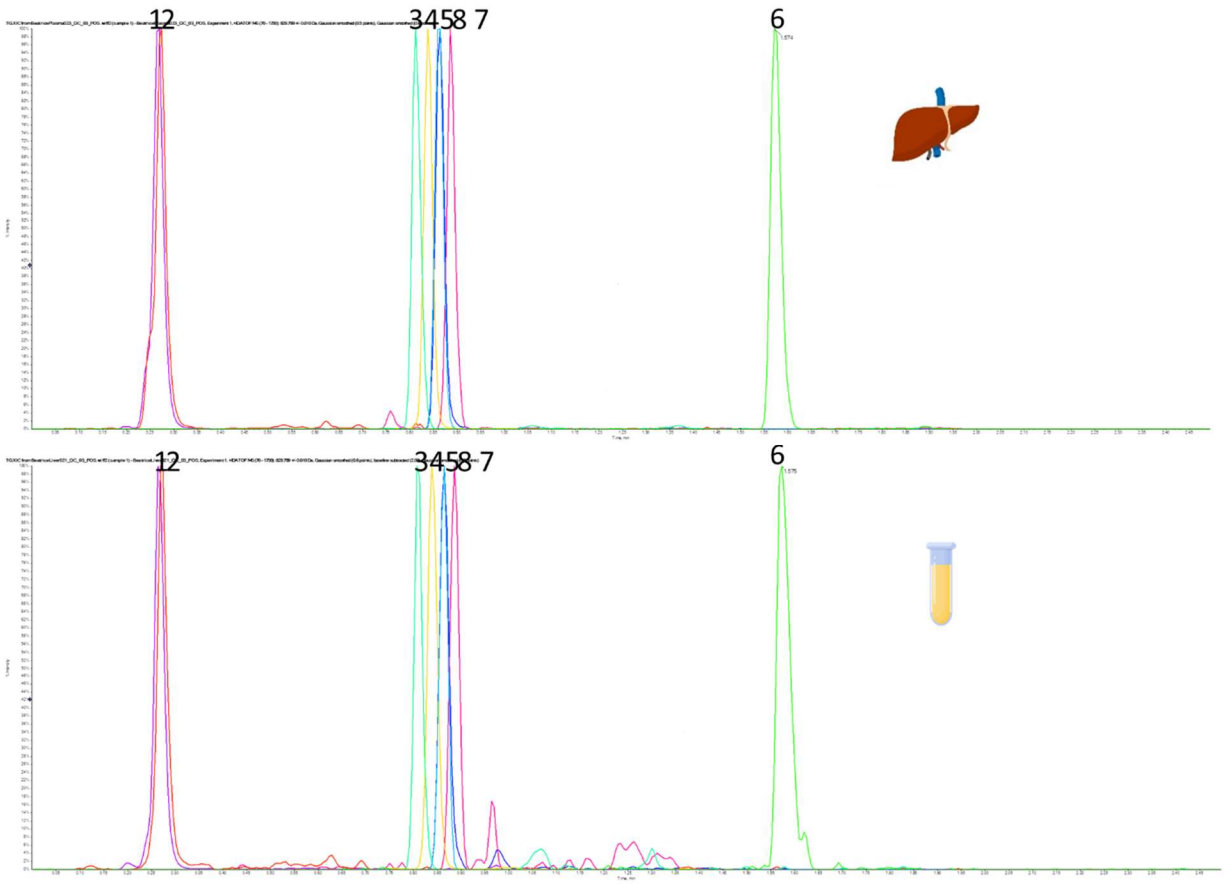

	Equisplash Mix	*rt* Liver	Plasma
1	15:0-18:1(d7) PC	0.864	0.865
2	18:1(d7) Lyso PC	0.266	0.267
3	15:0-18:1(d7) PE	0.86	0.886
4	18:1(d7) Lyso PE	0.272	0.272
5	15:0-18:1(d7) PG	0.84	0.839
6	15:0-18:1(d7)-15:0 TAG	1.575	1.574
7	d18:1-18:1(d9) SM	0.818	0.813
8	C15 Ceramide-d7	0.864	0.861

Figure 2: Extracted ion chromatogram obtained for the Avanti® Equisplash mix lipids in liver and plasma samples (0.1 µg/mL). All peaks are set to 100%.

Lipid extracts were randomly analyzed, and pooled QC samples were regularly included in the batch analysis. Of the initial features detected by peak picking of the raw chromatogram, 828 for liver and 574 for plasma samples passed all filtering steps and were included in the dataset for multivariate statistical analysis. In particular, only features with a coefficient of variance (CV) of less than 30% in pooled QC samples, found in at least 50% of the samples belonging to the same experimental group and annotated at MS2 level (tolerance 0.02 Da), were taken for further analysis (Figure 3).

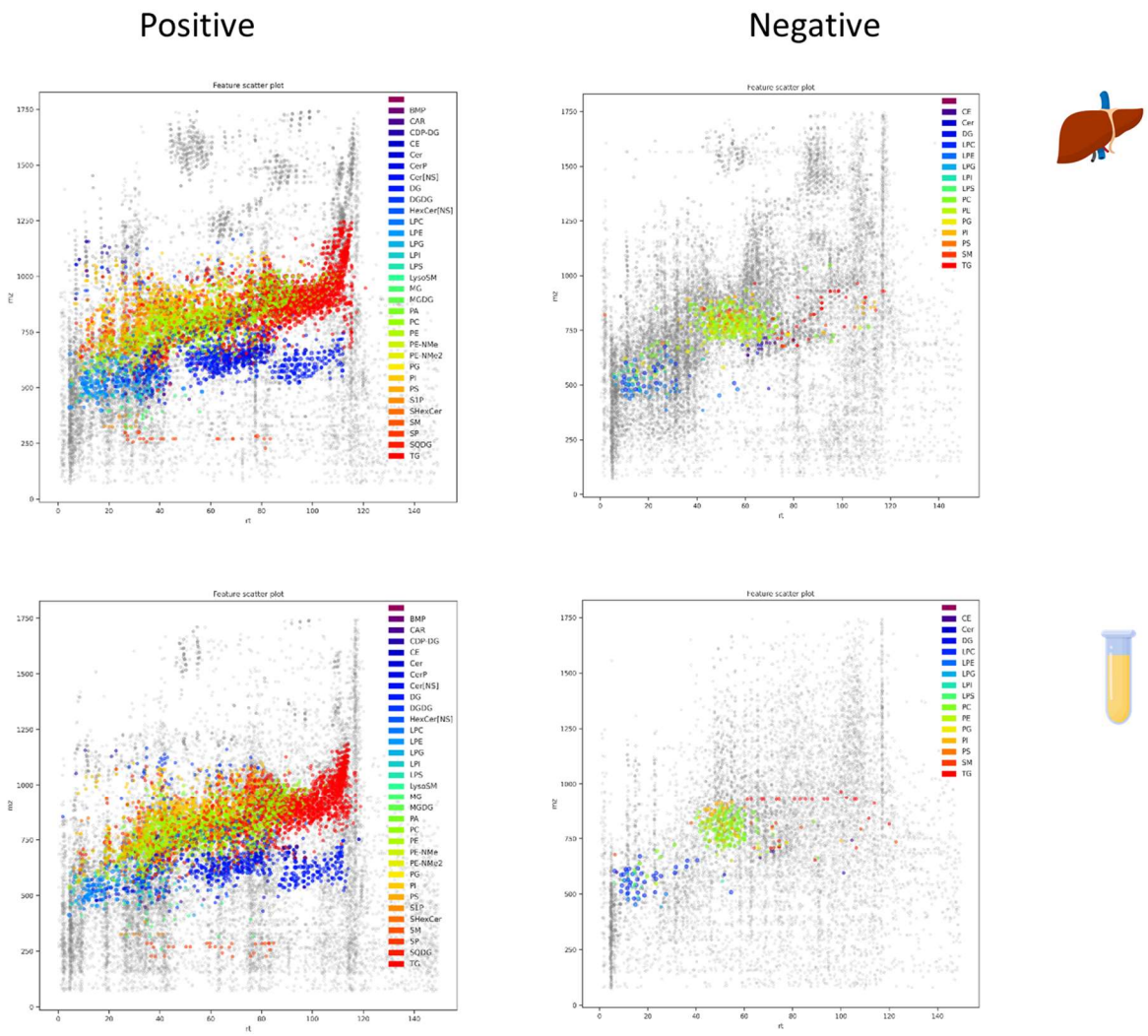

Figure 3: Ion map showing features annotated in liver and plasma samples either in positive or negative ion mode. Only MS2 annotated features were included in the final dataset and considered for further statistical analysis.

Triacylglycerols (TGs) were the most abundant in both matrices, accounting for 34 and 38% of the identified lipidome in the liver and plasma, respectively, followed by phosphatidylcholines (PCs, 24.3 and 27%), sphingomyelins (SMs, 7.3%), ceramides (Cer, 5%) and cholesteryl esters (CEs, 2%). Other annotated lipid classes are diacylglycerols (DGs), phosphatidylethanolamines (PEs), lysophosphatidylethanolamines (LPEs), lysophosphatidylcholine (LPCs) and phosphatidylinositols (PIs). Of the molecular species identified, 350 were common between the two matrices (Figure 4). It should be noted that cholesterol was not identified in either biological matrix, despite its expected abundance in high-fat diet models. This may be due to the poor ionization efficiency of cholesterol under the conditions applied in this study. As a non-polar molecule with low ionization efficiency, cholesterol often requires specific derivatization or optimized ionization methods (e.g.

chemical derivatisation, APCI) to enhance its detection. This limitation can lead to under-representation or non-detection of cholesterol in lipidomics workflows, especially when using electrospray ionisation (ESI).

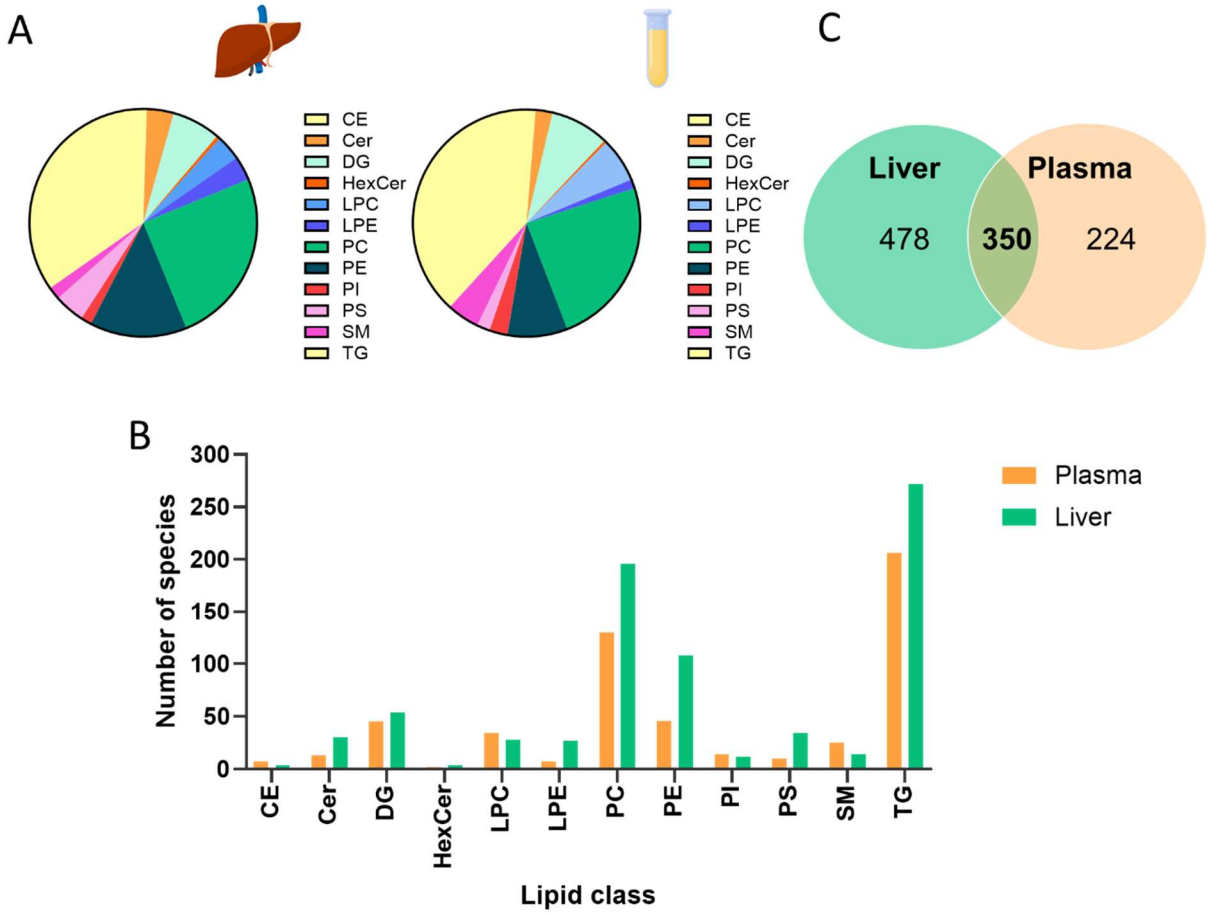

Figure 4: The number of lipid molecular species identified in liver and plasma samples.350 lipids were common between the two matrices.

Obesity impacts hepatic tissue lipidome, partly reflecting the lipid alterations observed in plasma

Next, I examined the lipid species profiles in liver tissue and plasma to identify specific signatures of obesity. PCA showed a clear distinction between lean and diet-induced obese animals by the first two components, either in plasma or liver samples. The QC cluster in the middle of the score plot indicated high technical reproducibility and that biological variation was more influential than the analytical variation. I also observed that biological replicates of the same group clustered closely together, reflecting the homogeneity of the samples (Figure 5).

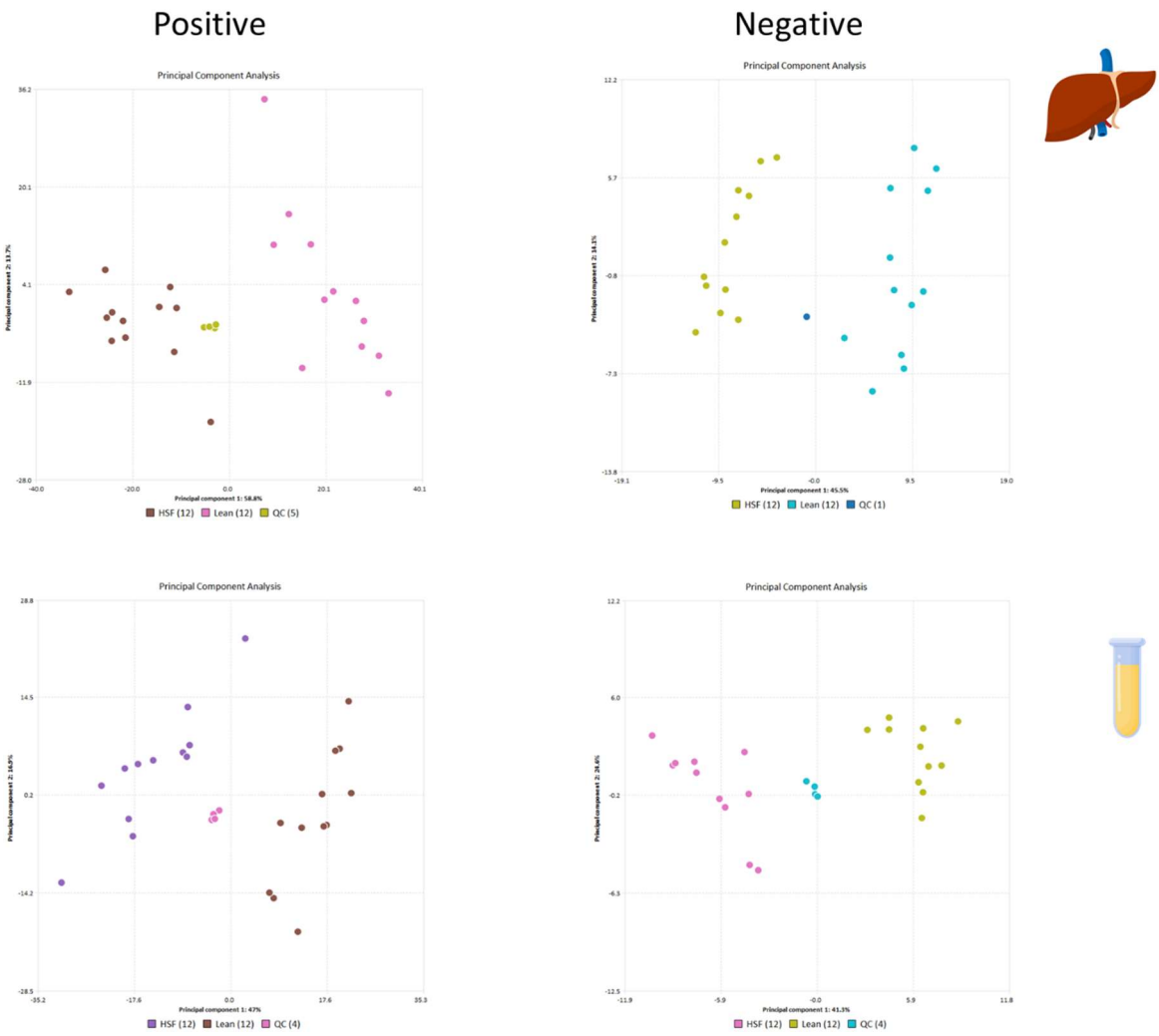

Figure 5: Multivariate statistical analysis representing the lipidomic data of liver and plasma samples. PCA score plot clearly shows differentiation between the lean and obese (HSF) animals. The pooled QCs clustered tightly, indicating high technical reproducibility.

As expected, prominent increases in neutral lipids such as TG (48:1), TG (48:2), TG (50:2), TG (52:2) and DG (32:1) were observed in the liver of the HSF group compared to the control. The increase in TG species is not consistent for all the species identified, but it mainly affects species with saturated and monounsaturated residues. Species increased in lean animals include PC (34:3), PC (38:6), PE (38:4), PI (36:4), LPC (18:1), LPC (18:1), LPC (20:4), LPC (20:5), LPE (18:1), PS (38:4), and PE (38:4). Higher liver fat content is therefore associated with TG accumulation and reduced levels of PUFA-containing phospholipids and lysophospholipids. Changes in some individual lipid species are shown in Figure 6.

In the plasma of HSF animals, I observed that TGs containing at least one PUFA residue were more abundant than controls. Notably, in contrast to what was observed in the liver, plasma levels of PC (34:1), LPE (18:1), and PE (38:4) were significantly enriched in the HSF experimental group.

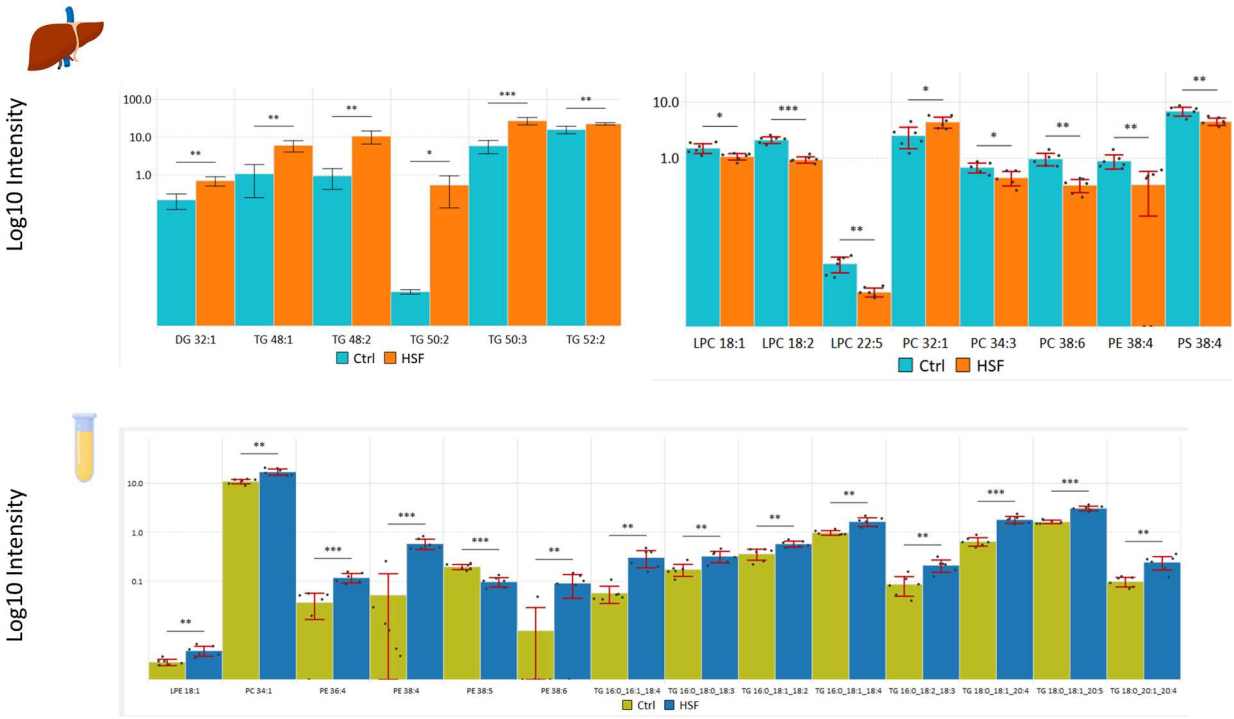

Figure 6: Box plots of log10-transformed intensity values for specific lipid species in liver and plasma lipid extracts, positive ESI mode. t-test ($p<0.05$).

Enrichment of PE (38:4) and other phospholipid species is a common feature in the plasma of obese individuals[13,14]. PE (38:4), in particular, is highly susceptible to oxidative modification due to its multiple unsaturations, making it vulnerable to attack by reactive oxygen species. Elevated levels of PE (38:4) in tissues or fluids indicate increased oxidative stress and inflammation, as this lipid plays a role in membrane integrity and cellular signalling pathways related to stress responses. In support of this, I also observed higher levels of LPC (20:4), a known marker of inflammation, LPE (16:0), LPE (18:1), and ceramides in the HSF experimental group. The accumulation of ceramides is associated with disruptions in glycosphingolipid metabolism, contributing to oxidative stress and causing cell death[15]. This overall pattern suggests systemic lipid overflow and inflammation, which are the hallmarks of obesity.

Furthermore, in both biological matrices, a clear separation was observed for ether phosphatidylethanolamine (ether-PE) and ether phosphatidylcholine (ether-PC) species, particularly plasmalogens, which were significantly reduced in the HSF group.

These findings align with previous plasma lipidomics studies in obese individuals reporting significant changes in alkylphosphatidylcholines and plasmalogens[16]. Given that ether lipids, such as plasmalogens, act as scavengers for reactive oxygen species (ROS), it is likely that the HSF phenotype induces oxidative stress at the liver level. This hypothesis is further supported by the observed increase in markers of oxidative damage, indicating that obesity may promote oxidative stress, thereby disrupting lipid metabolism and contributing to metabolic dysfunction[10].

Next, BioPAN pathway analysis allowed us to detect differences and trends regarding obesity between the two lipidomic datasets. The lipid networks at the lipid subclass level are shown in Figure 7A for the liver and Figure 7B for plasma.

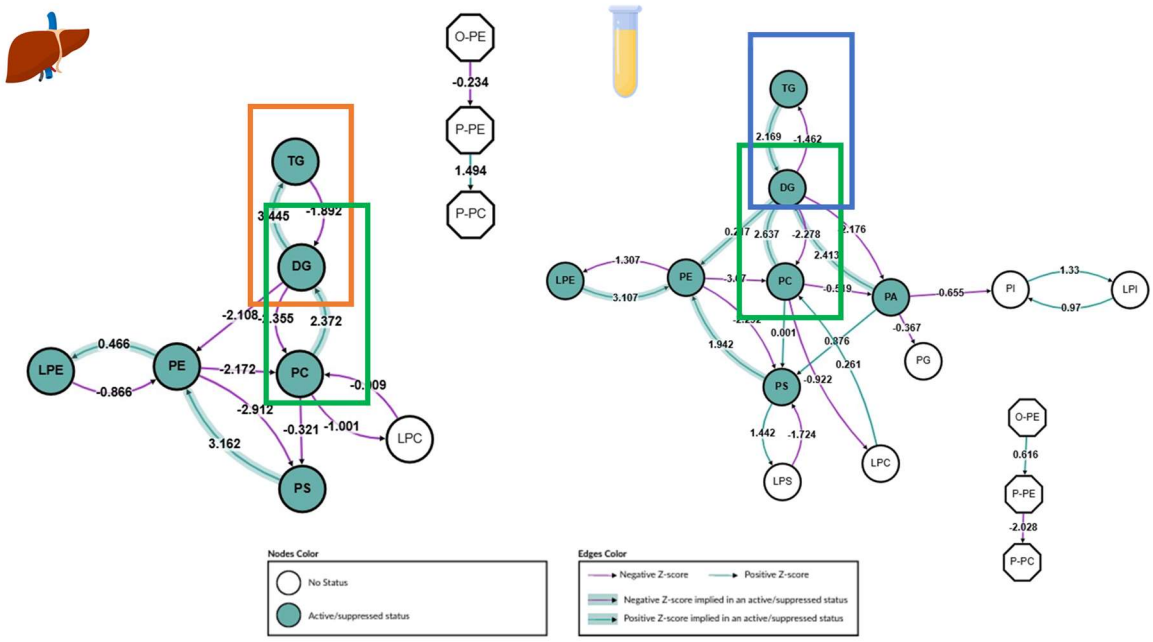

Figure 7: BioPAN lipid networks. Lipid network graphs exported from BioPAN for the liver and plasma of obese animals (HSF) compared to lean control animals. In these graphs, green nodes represent active lipids, and green shaded arrows indicate active pathways. Reactions with a positive Z-score are shown with green arrows, while those with a negative Z-score are represented by purple arrows. The pathway options include the HSF condition of interest, lean control condition, lipid type, active status, p-value of 0.05, and no paired data.

Reactions using PC lipid species as a substrate are more active in the liver and plasma of the HSF group than in the control, which aligns with the reported increase in the DG subclass as a product of this pathway (green rectangle). For triglycerides, while the overall trend is consistent across the entire TG class and between the two biological matrices reporting an increase in TG levels in the HSF group, the results of the lipid pathway analysis revealed that TG synthesis is significantly activated only in the liver (TG, Z-score = 3.445, orange rectangle). Conversely, the same pathway seems to be

shifted towards TG catabolism in the plasma samples (Z-score = -2.161, blue rectangle). These differences can likely be explained by examining the lipid molecular species responsible for these predictions. Specifically, at the plasma level, only reactions using PUFA TGs as substrates to give the respective PUFA DG products were found to be included in the node.

In addition, the pathway analysis revealed other tissue-specific variations in lipid metabolism. In particular, the reactions involving arachidonic acid-containing species (36:4 [PI, PE, PC], 38:4 [PI, PC, PE], and 38:5 [PI, PE, PC] species) were found to be activated in the plasma of the HSF groups compared to the control, but they were not modulated in the liver (Figure 8).

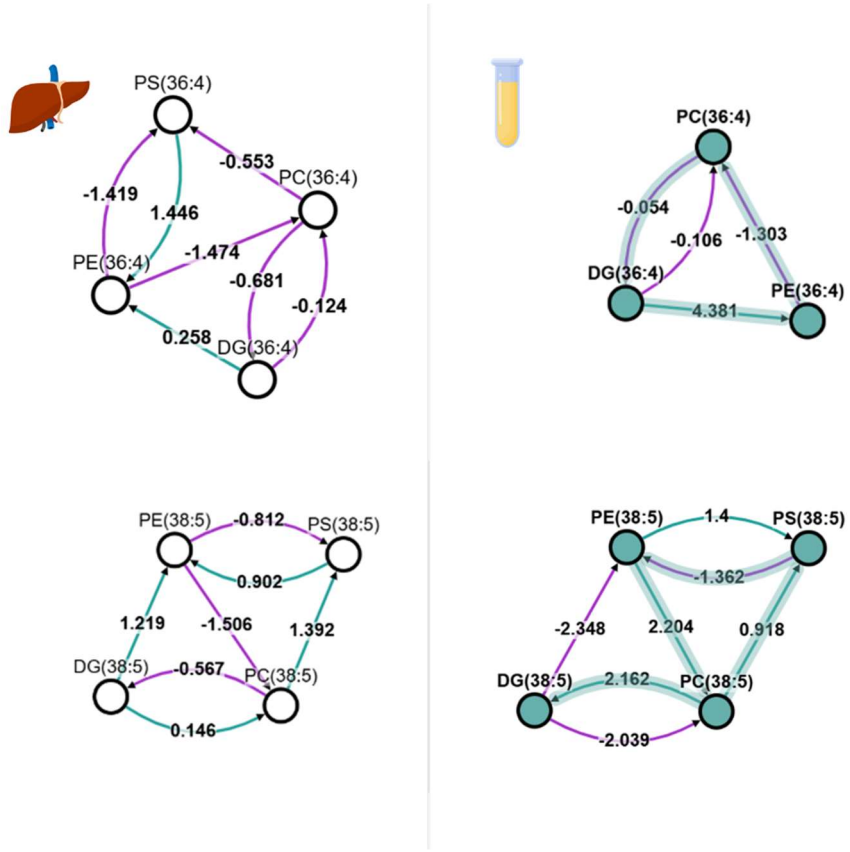

Figure 8: BioPAN lipid networks. Network graphs exported from BioPAN show lipid molecular species 36:4 and 38:4 in the liver and plasma of obese animals (HSF) compared to lean controls. In the graphs, green nodes represent active lipids, and green shaded arrows indicate active pathways. Reactions with a positive Z-score are shown with green arrows, while those with negative Z-scores are displayed with purple arrows. The pathway options include the HSF condition of interest, lean control condition, lipid type, active status, p-value of 0.05, and no paired data. The legend is reported in Figure 7.

It is well known that different tissues have specific and very specialized lipid profiles, and in our study, this was also confirmed by PCA analysis. Liver and plasma samples formed distinct clusters on the score plot, indicating clear differences in lipid patterns. The

difference in lipid composition reflects the different histological and physiological functions of the two matrices (Figure 9).

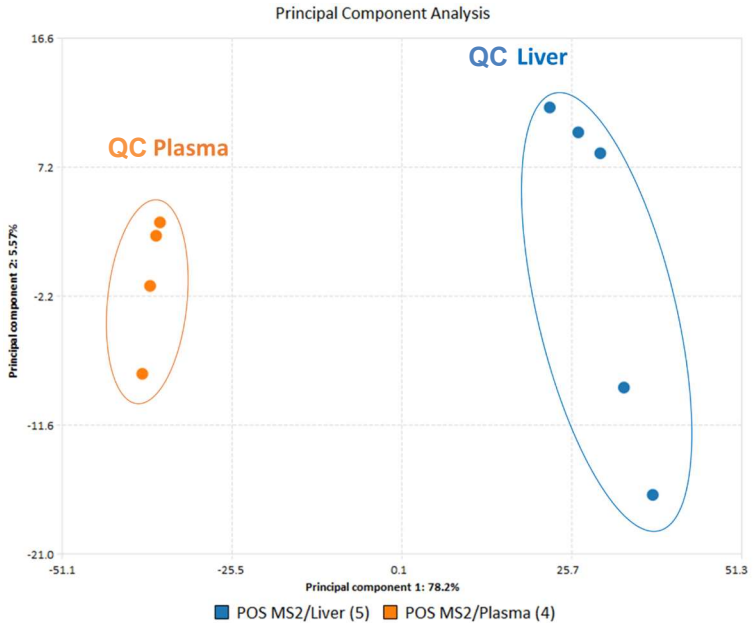

Figure 9: PCA scores plot of log10-transformed LC-MS analysis via positive ESI mode. Scores are coloured by sample type. PCs 1 and 2 explain for 74% and 19% of the variance, respectively. QC samples were normalized by group.

Indeed, the liver is a highly metabolically active organ and is rich in apolar lipids in addition to polar membrane lipids. In contrast, plasma represents a lipid-rich fluid containing large amounts of membrane lipids and lipoprotein-derived storage lipids. These differences are mainly reflected in the enrichment of neutral lipids such as TGs, DGs and SM in the liver samples and PC, LPC, Cer and also LPE in plasma. Moreover, at the level of lipid molecular species, these differences can also be highlighted by the distinct profile of fatty acids esterified to complex lipids. In general, I found that the most abundant fatty acids in liver samples are 16:0 (palmitic acid), 18:1 (oleic acid), and 18:2 (linoleic acid). In contrast, plasma contains the highest levels of PUFA arachidonic acid (20:4). These findings suggest that individual lipid species have tissue-specific distribution patterns, which could result in different changes in lipid profiles during disease progression.

Carnosine treatment identifies specific signatures on liver lipidome of obese rats

The PCA score plot showed that only a limited separation of treated and untreated animals was achieved in both experimental conditions (control or HSF) when the scores were coloured and labelled by the experimental group (Figure 10), thus indicating that

differences in lipid composition driven by carnosine are less than those observed by the phenotype.

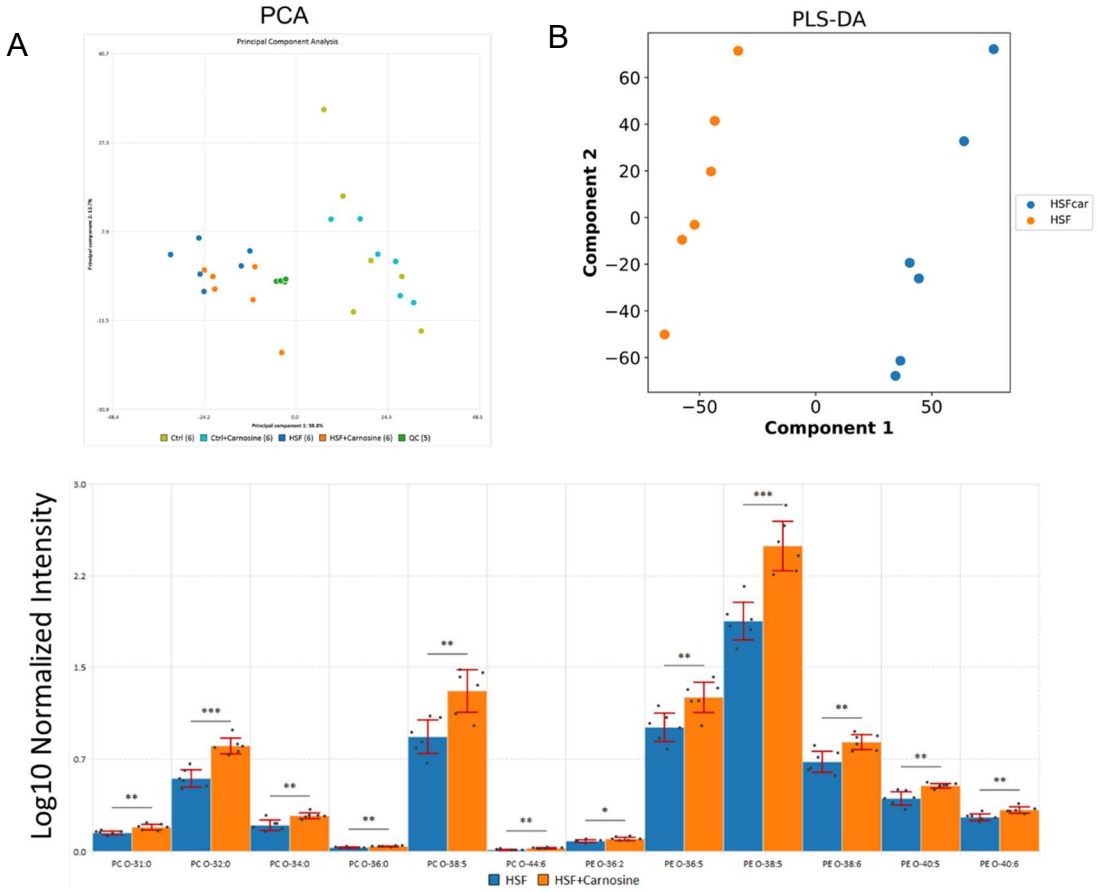

C

Term ID	Discription	p-value	FDR q-value
LION:0000095	headgroup with positive charge / zwitter-ion	1.20E-06	0.000141
LION:0001287	PE(40:6)	1.70E-06	0.000141
LION:0000193	PC(38:4)	5.00E-05	0.002075
LION:0000373	PS(38:4)	5.00E-05	0.002075
LION:0080970	average bilayer thickness	8.00E-05	0.002656
LION:0000084	ceramide phosphocholines (sphingomyelins)	0.00021	0.00581
LION:0000465	neutral intrinsic curvature	0.00038	0.0083
LION:0012086	endosome/lysosome	0.00043	0.0083
LION:0001737	average transition temperature	0.00045	0.0083
LION:0012010	membrane component	0.00078	0.012948
LION:0012082	plasma membrane	0.0016	0.024145
LION:0001740	above average transition temperature	0.00176	0.024347
LION:0000467	contains ether-bond	0.00328	0.041883

Figure 10: A) PCA score plot of log10-transformed LC-MS analysis via positive ESI mode. Scores are colored by the experimental group. Only a limited separation of treated and untreated animals was achieved in both experimental conditions (control or HSF). B) PLS-DA analysis of HSF and HSF+CAR samples showing the discrimination between the two experimental groups among component 1. ESI positive mode C) Enrichment analysis of lipid terms (LION-web), showing the top enriched terms for both HSF+CAR experimental groups.

Thus, I used the PLS-DA model to identify specific features modulated by carnosine. The PLS-DA score plots showed a clear separation between the HSF and HSF+CAR (Figure 10). On top of lipid species that can separate the HSF+CAR and HSF in the liver, I found that the best separation results could be achieved by ether-PE and PC and, in

particular, by PE (O-38:5) and PE (O-40:5), whose levels are relatively higher in the HSF+CAR experimental group compared to HSF. These results are in accordance with the role of alkyl-phosphatidylcholines and phosphatidylethanolamine plasmalogens in cellular homeostasis. To further prove that, I next conducted a LION enrichment analysis to examine the lipid terms that underlie the carnosine effect at the liver level. In accordance with the multivariate analysis, I found enrichments of terms related to membrane functions and bilayer thickness, which are affected by phospholipid composition (FDR q-value <0.05). In particular, I found that the lipids that distinguish lipidome sets are polyunsaturated phospholipids that also contain ether bonds. Since ether lipids are known to act as scavengers of radicals, I assume that oxidative stress induced by the HSF diet could be modulated by carnosine.

Discussion

Lipidomics has become an indispensable tool in biomedical research to study lipid metabolism at the lipid molecular level. In the present study, we applied comprehensive lipidome profiling to liver tissue and plasma samples to further clarify the metabolic differences between lean and diet-induced obese animals. Here, we show that the application of a 2.4-min LC-MS method for untargeted lipidome analysis provides comprehensive lipid coverage in a robust, reproducible, and rapid manner. The method benefits from high resolution and accurate MS2 level of annotation and can be applied to the screening of lipids in diverse biological matrices with excellent repeatability.

High-throughput methods in MS-based omics research are key to delivering rapid and informative results about lipidomic profiles that can be used as a tool for preclinical or clinical applications and to support drug discovery.

In support of previous studies performed at the biochemical level and carried out in the laboratory of Prof. Correa[10], our lipidomic dataset provides a detailed insight into the description of the metabolic changes observed between lean and obese rats. Multivariate statistical analysis revealed significant differences between experimental groups, particularly in triacylglycerols, phospholipids, and ether-linked derivatives. I found that the liver of lean and obese rats had distinct lipidomic patterns and that those changes were characteristic of hepatic dyslipidemia and lipotoxic fat depots[17]. Triacylglycerol accumulation in hepatocytes is a common sign of obesity and a hallmark of steatosis development. Although steatosis is considered relatively harmless and

reversible, when the liver exceeds its capacity to 'store' lipids, steatosis can induce lipotoxicity and glucotoxicity, promoting ROS generation and organelle dysfunction, making the liver more vulnerable to toxic insults. This mechanism is referred to in the literature as the 'two-hit' hypothesis[18]. Elevated hepatic DG is linked to hepatic lipotoxicity and particularly has been observed to activate inflammatory responses *in vivo*[19]. Moreover, levels of oxidative stress markers such as Malondialdehyde (MDA) and Advanced Oxidation Protein Products (AOPP) are upregulated in the liver of HSF animals, which may contribute to the metabolic dysfunction of hepatocytes[10].

Increased levels of TGs and DGs could also be explained by elevated lipogenesis, as evidenced by the high levels of species esterified to FA (16:0, 18:0, and 18:1), and in part by an increased conversion of phospholipids to DGs, as suggested by pathway analysis. Given the higher levels of DG (34:2) and lower levels of PC (34:2) and PC (36:2) in obese animals, it is possible that specific PCs are redirected to DG production due to the increased requests for DG.

Moreover, the levels of sphingolipids and glycerophospholipids differed significantly between the HSF and lean groups, and variations in their relative levels are associated with obesity[20]. In particular, I observed that several species belonging to the phospholipid class had reduced levels in the liver of obese animals. Phospholipids are an integral part of the plasma membrane and act as signalling molecules. Loss of PC may be due to sustained hydrolysis by membrane phospholipases.

Changes observed in liver lipid extracts reflect, to some extent, the changes obtained by analyzing plasma samples. Overall, plasma lipid profiling of HSF animals confirmed circulating lipid biomarkers of obesity previously observed in the mammalian plasma lipidome[21]. Total TG levels in both liver tissue and plasma were generally elevated in rodent and human models of obesity, which is also consistent with what has been reported in numerous studies highlighting the systemic lipid overload caused by obesity, which may contribute to the development of metabolic complications associated with obesity[22]. However, our study showed that liver and plasma samples have a unique lipid fingerprint at the level of the individual lipid molecules. Therefore, it is likely that the lipid patterns that are altered in the disease process are also different. This shows that although plasma is a clinically relevant sample for biomarker discovery, analysis of other tissues may also be helpful. This is particularly true for the liver, which is a dynamic and metabolically active organ and, therefore, well suited to providing information on the

metabolic state. Furthermore, the importance of analyzing the liver is that it is the key organ for the biosynthesis of lipids, so if we observe a change in the lipid composition of the blood, it is likely to be the liver that is responsible, as only the liver can change the blood lipid profile.

Another question we wanted to answer was whether we would see any differences after treatment with carnosine. Carnosine has potential preventive and therapeutic benefits for obesity[23]. For instance, carnosine can decrease the oxidation and glycation of LDL and can limit the progression of atherosclerosis in animal studies [24]. Our results also showed that carnosine supplementation has a beneficial effect on the lipidome of obese animals by reducing plasmalogens, which are important lipid species associated with redox stress.

While our analysis identified differences in lipid pathways between obese states, it remained unclear what these patterns meant for metabolite or protein levels. Indeed, intracellular lipid patterns can also be explained by examining altered levels of metabolites and proteins involved in the same pathway, which helped us to infer the actual metabolic state and whether it is an early or advanced stage of liver disease. Based on the biochemical data we have, we know that specific markers of oxidative stress and inflammation are significantly increased in the HSF groups. Obesity is highly correlated with the production of ROS and subsequent damage to the liver due to excess lipids. This damage is evident at the lipid level with increased lipid oxidation. However, the study of lipid oxidation is challenging and requires specific analytical and bioinformatic approaches.

In the next chapter, I will discuss how we have addressed this analytical and biological challenge. This will be the starting point for the next part of the study, which will examine the consequences of oxidative damage on lipids and the potential beneficial effects of the treatment with antioxidant compounds such as carnosine.

Conclusions

In the present study, we used a fast LC-MS/MS method for high-coverage lipid profiling of the liver and plasma from lean and obese rats. First, we determined the comprehensiveness and suitability of the proposed LC-MS, which revealed that it is suitable for the detailed analytical description of the lipid profile of multiple biological

matrices and allows us to investigate the extent of possible metabolic alterations in obese animals.

Supplementary Tables

Supplementary Tables are available on request.

References

(1) Lin, X.; Li, H. Obesity: Epidemiology, Pathophysiology, and Therapeutics. *Front Endocrinol* (Lausanne) **2021**, *12*. https://doi.org/10.3389/fendo.2021.706978.

(2) Rives, C.; Fougerat, A.; Ellero-Simatos, S.; Loiseau, N.; Guillou, H.; Gamet-Payrastre, L.; Wahli, W. Oxidative Stress in NAFLD: Role of Nutrients and Food Contaminants. *Biomolecules* **2020**, *10* (12), 1702. https://doi.org/10.3390/biom10121702.

(3) Lara-Castro, C.; Garvey, W. T. Intracellular Lipid Accumulation in Liver and Muscle and the Insulin Resistance Syndrome. *Endocrinol Metab Clin North Am* **2008**, *37* (4), 841–856. https://doi.org/10.1016/j.ecl.2008.09.002.

(4) Criscuolo, A.; Zeller, M.; Cook, K.; Angelidou, G.; Fedorova, M. Rational Selection of Reverse Phase Columns for High Throughput LC–MS Lipidomics. *Chem Phys Lipids* **2019**, 221, 120–127. https://doi.org/10.1016/j.chemphyslip.2019.03.006.

(5) Merciai, F.; Musella, S.; Sommella, E.; Bertamino, A.; D'Ursi, A. M.; Campiglia, P. Development and Application of a Fast Ultra-High Performance Liquid Chromatography-Trapped Ion Mobility Mass Spectrometry Method for Untargeted Lipidomics. *J Chromatogr A* **2022**, 1673, 463124. https://doi.org/10.1016/j.chroma.2022.463124.

(6) Grandini, N. A.; Costa, M. R.; Gregolin, C. S.; Siqueira, J. S.; Vieira, T. A.; Togneri Ferron, A. J.; Francisqueti-Ferron, F. V.; Romualdo, G. R.; Lúcia dos Anjos Ferreira, A.; Aldini, G.; Corrêa, C. R.; Moreto, F. Effects of Carnosine Supplementation on Markers for the Pathophysiological Development of Metabolic Dysfunction-Associated Steatotic Liver Disease in a Diet-Induced Model. *Mol Cell Endocrinol* **2024**, 582, 112138. https://doi.org/10.1016/j.mce.2023.112138.

(7) Kalaz, E. B.; Aydın, A. F.; Doğan-Ekici, I.; Çoban, J.; Doğru-Abbasoğlu, S.; Uysal, M. Protective Effects of Carnosine Alone and Together with Alpha-Tocopherol on Lipopolysaccharide (LPS) plus Ethanol-Induced Liver Injury. *Environ Toxicol Pharmacol* **2016**, *42,* 23–29. https://doi.org/10.1016/j.etap.2015.12.018.

(8) Aydın, A. F.; Bingül, İ.; Küçükgergin, C.; Doğan-Ekici, I.; Doğru Abbasoğlu, S.; Uysal, M. Carnosine Decreased Oxidation and Glycation Products in Serum and Liver of High-fat Diet and Low-dose Streptozotocin-induced Diabetic Rats. *Int J Exp Pathol* **2017***, 98* (5), 278–288. https://doi.org/10.1111/iep.12252.

(9) Francisqueti, F.; Minatel, I.; Ferron, A.; Bazan, S.; Silva, V.; Garcia, J.; De Campos, D.; Ferreira, A.; Moreto, F.; Cicogna, A.; Corrêa, C. Effect of Gamma-Oryzanol as Therapeutic Agent to Prevent Cardiorenal Metabolic Syndrome in Animals Submitted to High Sugar-Fat Diet. *Nutrients* **2017***, 9* (12), 1299. https://doi.org/10.3390/nu9121299.

(10) Grandini, N. A.; Costa, M. R.; Gregolin, C. S.; Siqueira, J. S.; Vieira, T. A.; Togneri Ferron, A. J.; Francisqueti-Ferron, F. V.; Romualdo, G. R.; Lúcia dos Anjos Ferreira, A.; Aldini, G.; Corrêa, C. R.; Moreto, F. Effects of Carnosine Supplementation on Markers for the Pathophysiological Development of Metabolic Dysfunction-Associated Steatotic Liver Disease in a Diet-Induced Model. *Mol Cell Endocrinol* **2024**, 582, 112138. https://doi.org/10.1016/j.mce.2023.112138.

(11) Chambers, M. C.; Maclean, B.; Burke, R.; Amodei, D.; Ruderman, D. L.; Neumann, S.; Gatto, L.; Fischer, B.; Pratt, B.; Egertson, J.; Hoff, K.; Kessner, D.; Tasman, N.; Shulman, N.; Frewen, B.; Baker, T. A.; Brusniak, M.-Y.; Paulse, C.; Creasy, D.; Flashner, L.; Kani, K.; Moulding, C.; Seymour, S. L.; Nuwaysir, L. M.; Lefebvre, B.; Kuhlmann, F.; Roark, J.; Rainer, P.; Detlev, S.; Hemenway, T.; Huhmer, A.; Langridge, J.; Connolly, B.; Chadick, T.; Holly, K.; Eckels, J.; Deutsch, E. W.; Moritz, R. L.; Katz, J. E.; Agus, D. B.; MacCoss, M.; Tabb, D. L.; Mallick, P. A Cross-Platform Toolkit for Mass Spectrometry and Proteomics. *Nat Biotechnol* **2012**, *30* (10), 918–920. https://doi.org/10.1038/nbt.2377.

(12) GraphPad. https://www.graphpad.com/.

(13) Pang, S.-J.; Liu, T.-T.; Pan, J.-C.; Man, Q.-Q.; Song, S.; Zhang, J. The Association between the Plasma Phospholipid Profile and Insulin Resistance: A Population-Based Cross-Section Study from the China Adult Chronic Disease and Nutrition Surveillance. *Nutrients* **2024**, *16* (8), 1205. https://doi.org/10.3390/nu16081205.

(14) Donovan, E. L.; Pettine, S. M.; Hickey, M. S.; Hamilton, K. L.; Miller, B. F. Lipidomic Analysis of Human Plasma Reveals Ether-Linked Lipids That Are Elevated in Morbidly Obese Humans Compared to Lean. *Diabetol Metab Syndr* **2013**, *5* (1), 24. https://doi.org/10.1186/1758-5996-5-24.

(15) Tanase, D. M.; Gosav, E. M.; Petrov, D.; Jucan, A. E.; Lacatusu, C. M.; Floria, M.; Tarniceriu, C. C.; Costea, C. F.; Ciocoiu, M.; Rezus, C. Involvement of Ceramides in Non-Alcoholic Fatty Liver Disease (NAFLD) Atherosclerosis (ATS) Development: Mechanisms and Therapeutic Targets. *Diagnostics* **2021**, *11* (11), 2053. https://doi.org/10.3390/diagnostics11112053.

(16) Paul, S.; Lancaster, G. I.; Meikle, P. J. Plasmalogens: A Potential Therapeutic Target for Neurodegenerative and Cardiometabolic Disease. *Prog Lipid Res* **2019***, 74*, 186–195. https://doi.org/10.1016/j.plipres.2019.04.003.

(17) Nam, M.; Choi, M.-S.; Jung, S.; Jung, Y.; Choi, J.-Y.; Ryu, D. H.; Hwang, G.-S. Lipidomic Profiling of Liver Tissue from Obesity-Prone and Obesity-Resistant Mice Fed a High Fat Diet. *Sci Rep* **2015***, 5* (1), 16984. https://doi.org/10.1038/srep16984.

(18) Mayén, A.-L.; Sabra, M.; Aglago, E. K.; Perlemuter, G.; Voican, C.; Ramos, I.; Debras, C.; Blanco, J.; Viallon, V.; Ferrari, P.; Olsen, A.; Tjønneland, A.; Langmann, F.; Dahm, C. C.; Rothwell, J.; Laouali, N.; Marques, C.; Schulze, M. B.; Katzke, V.; Kaaks, R.; Palli, D.; Macciotta, A.; Panico, S.; Tumino, R.; Agnoli, C.; Farràs, M.; Molina-Montes, E.; Amiano, P.; Chirlaque, M.-D.; Castilla, J.; Werner, M.; Bodén, S.; Heath, A. K.; Tsilidis, K.; Aune, D.; Weiderpass, E.; Freisling, H.; Gunter, M. J.; Jenab, M. Hepatic Steatosis, Metabolic Dysfunction and Risk of Mortality: Findings from a Multinational Prospective Cohort Study. *BMC Med* **2024***, 22* (1), 221. https://doi.org/10.1186/s12916-024-03366-3.

(19) Geng, Y.; Faber, K. N.; de Meijer, V. E.; Blokzijl, H.; Moshage, H. How Does Hepatic Lipid Accumulation Lead to Lipotoxicity in Non-Alcoholic Fatty Liver Disease? *Hepatol Int* **2021**, *15* (1), 21–35. https://doi.org/10.1007/s12072-020-10121-2.

(20) Hannun, Y. A.; Obeid, L. M. Sphingolipids and Their Metabolism in Physiology and Disease. *Nat Rev Mol Cell Biol* **2018**, *19* (3), 175–191. https://doi.org/10.1038/nrm.2017.107.

(21) Huang, Y.; Sulek, K.; Stinson, S. E.; Holm, L. A.; Kim, M.; Trost, K.; Hooshmand, K.; Lund, M. A. V.; Fonvig, C. E.; Juel, H. B.; Nielsen, T.; Ängquist, L.; Rossing, P.; Thiele, M.; Krag, A.; Holm, J.-C.; Legido-Quigley, C.; Hansen, T. Lipid Profiling Identifies Modifiable Signatures of Cardiometabolic Risk in Children and Adolescents with Obesity. *Nat Med* **2024**. https://doi.org/10.1038/s41591-024-03279-x.

(22) Blüher, M. Obesity: Global Epidemiology and Pathogenesis. *Nat Rev Endocrinol* **2019**, *15* (5), 288–298. https://doi.org/10.1038/s41574-019-0176-8.

(23) Baye, E.; Ukropcova, B.; Ukropec, J.; Hipkiss, A.; Aldini, G.; de Courten, B. Physiological and Therapeutic Effects of Carnosine on Cardiometabolic Risk and Disease. *Amino Acids* **2016***, 48* (5), 1131–1149. https://doi.org/10.1007/s00726-016-2208-1.

(24) Lee, Y.; Hsu, C.; Lin, M.; Liu, K.; Yin, M. Histidine and Carnosine Delay Diabetic Deterioration in Mice and Protect Human Low Density Lipoprotein against Oxidation and Glycation. *Eur J Pharmacol* **2005**, *513* (1–2), 145–150. https://doi.org/10.1016/j.ejphar.2005.02.010.

CHAPTER 5:
ADDRESSING EPILIPIDOME: STUDY OF LIPID OXIDATION IN COMPLEX BIOLOGICAL MATRICES

Summary

As a next step of the previous work, the analyses of oxidized lipids could provide a more complete understanding of the impact of oxidative damage on obesity. To this aim, we looked at the functional oxidative modification of lipids. Oxidized lipid species have been actively studied in the context of oxidative stress-related disorders, including obesity and metabolic diseases. Currently, detailed structural elucidation of lipid oxidized species, necessary to understand their biological role, is still missing as their identification in complex biological samples is challenged by the low natural abundance and the structural diversity. Thus, different analytical and computational tools are required to deal with this complexity. We introduced a lipidomics workflow based on advanced LC-MS/MS approaches for the comprehensive profiling of oxidized lipids in plasma and liver samples. The method combined a rapid 2.4-min untargeted lipidomic analysis with our newly assembled pipeline for lipid and modified lipid annotation, enabling high-throughput detection of oxidized molecular species. I applied this workflow to the lipidomic dataset of Chapter 4, comparing the control, the obese group (HSF) and the obese group after the treatment with carnosine (HSF+CAR). The proposed method provides a powerful tool for studying lipid oxidation and its implications in health and disease, and could provide a more complete understanding of the antioxidant activity and the efficacy of carnosine in ameliorating the obese phenotype.

Background

Lipids comprise a very large number of diverse molecular species with different physicochemical and structural properties. Modifications of lipids can happen both enzymatically and non-enzymatically and result in the introduction of small chemical moieties into their structure. Among these, lipid oxidative modifications occurring at the fatty acyl chains are the most actively studied[1].

Lipid oxidation occurs in many pathological conditions that are often related to oxidative stress, such as inflammatory diseases and cancer[2,3]. Moreover, obesity and its metabolic complications are closely associated with redox imbalance and the development of oxidative stress, which damages lipids, proteins, and DNA, promoting inflammation and metabolic dysfunction.

Polyunsaturated fatty acids (PUFAs) are the primary targets for oxidative modification, either in free form or esterified into complex lipids such as TGs, CEs, and PLs. Their oxidation results from enzymatic (lipoxygenases, cyclooxygenases, or cytochrome P450 systems) or non-enzymatic (free-radical peroxidation) reactions, resulting in a large number of different modifications along the acyl chain and as many oxidation products. These include hydroxy, hydroperoxy, and keto molecular species (primary oxidation), as well as truncated forms, with the subsequent formation of highly reactive electrophilic carbonylated species (secondary oxidation).[4,5]

Such chemical complexity, also rich in isomeric species, results in an extensive range of diverse lipid species involved in different complex reactions, making the detection of oxidized lipids in biological matrices a major challenge. Moreover, the lack of spectral libraries and chemically defined standards limits the large-scale and unambiguous annotation of oxidized lipids. Besides the chemical diversity, these species are characterized by low abundance, which further complicates their measurements.

To overcome these analytical limitations, oxidized species are often analysed by targeted LC-MS/MS, which, however, cannot capture the complexity of the epilipidome and prevents the discovery of new species. For more comprehensive profiling, their analysis can be performed using untargeted approaches[6]. However, due to the amount of data generated, untargeted methods require powerful annotation tools to be integrated into the lipidomic workflow. In the context of oxidized lipids, efforts have been made in this direction[7]. This is, for example, the case for LPP tiger[8], which provides useful functions for *in silico* prediction of sample-specific oxidized lipidomes and identification of lipid oxidative molecules.

In this study, I aimed to explore the diversity of lipid oxidation in complex biological matrices in a more untargeted way, thereby addressing the entire lipidome. To help with that, we introduced a pipeline for oxidized lipids annotation in LC-MS/MS workflows and applied it to the analysis of the untargeted lipidomic dataset described in Chapter 4. Indeed, a detailed structural elucidation of lipid oxidation products would support the understanding of obesity and the development of new preventive or therapeutic approaches.

Antioxidant compounds may be beneficial in managing obesity-related oxidative stress. One of these is carnosine (CAR), which, as discussed in the previous chapter, has been implicated in the regulation of oxidative and inflammatory responses, as already shown in *in vitro* and *in vivo* studies.[9]

The mechanism by which CAR acts as an antioxidant has not yet been elucidated, although some mechanistic hypotheses have been formulated. In particular, CAR is thought to act as an endogenous scavenger of reactive carbonyl species (RCS). The potential of l-carnosine as a pharmacological agent has been demonstrated in rodent models of metabolic syndrome and cardiovascular disease. [10,11]. For instance, CAR has been shown to ameliorate dyslipidaemia and liver function *in vivo*[12]. More recently, we also showed its protective effect against skin oxidative damage[13–15] and to prevent the deterioration of glucose metabolism in healthy, overweight and obese adults.[16,17]

Considering the beneficial role on lipid metabolism assigned to CAR, I aimed to study it more comprehensively and in detail to gain a better biological understanding of its mechanism of action, particularly in relation to lipid oxidation.

Materials and Methods

Sample preparation, data analysis and processing

Sample preparation and LC-MS experimental parameters are described in detail in Chapter 4 of this thesis. Lipid extraction was performed using solvents containing 0.1%BHT to avoid sample autoxidation. All original wiff files were converted to centroided mzML files using the qtof peak picker component of msconvert (ProteoWizard v 3.0.9987)[18].The converted files were then fed into SLAW[19] for data alignment and peak picking to generate mgf containing all representative MS/MS spectra acquired by DDA. Lipids annotation was performed using these mgf files.

Lipid Library Generation

To generate an internal library for the annotation of oxidized lipids, the following steps were taken: we generated a list of possible fatty acid oxidation products for either short (FA 4:0) or long (up to FA 32:0) acyl chain as the addition of one or more oxygen as keto, epoxy, hydroxylated (O), perhydroxylated (O2) derivatives and combined them with other

fatty acids, backbones, and head groups to form different oxidized lipid species. We then predicted fragmentation based on class-specific fragmentation roles in both polarities. Using this approach, possible oxidized lipid species were generated for potentially any lipid species of the following key lipid classes in one or both polarities and for multiple adducts: oxidized triglycerides (OxTG), phosphatidylcholine (OxPC), phosphatidylethanolamine (OxPE), phosphatidylglycerol (OxPG), phosphatidylinositol (OxPI), phosphatidylserine (OxPS), lysophosphatidylcholine (Ox LPC) species and lysophosphatidylethanolamine (Ox LPE).

CID annotation of Oxidized Lipids

For the annotation of modified (and unmodified) lipids, we used an in-house Python script. This tool performs rule-based annotation in both polarities by matching MS2 features against the Lipidex database or our internal CID MS/MS library, which by default included additional oxidation of side chains. In particular, for MS2 matching, the maximum number of oxygens allowed in the side chains is 3 (MS2 maxO:3), while for MS1, it is 10. For ox lipids annotation, we considered the following adducts: $[M+H]^+$,$[M+NH4]^+$,$[M+Na]^+$,$[M-H]^-$,$[M+Ac-H]^-$,$[M+HCOO]^-$. We then retrieved all feasible candidates using a mass tolerance of 0.01Da at the MS level and 0.02Da at the MS/MS level. The final list of putatively annotated lipids included only features annotated at the MS2 level with at least two fragments (ms2_matched > 2), one of which had an oxidation that matched our internal MS/MS CID library (MS2 evidence = hg; chain; oxy-chain).

Statistical Analysis

Multivariate analysis was performed in Phyton. Data were log10-transformed and autoscaled. Features most influential in the PLS-DA models were taken forward for univariate analysis. Univariate statistics and plotting (including correlation analysis) were all performed in GraphPad Prism[20].

Results

In the previous chapter, we generated an untargeted lipidomic dataset that allowed us to study the molecular patterns that define obesity. In this study, I aimed to confirm and extend our previous findings by examining changes in the profile of oxidized lipids, thereby shedding new light on the role of lipid oxidation in metabolic diseases such as

obesity and the beneficial effects of carnosine, a compound known for its antioxidant and carbonyl scavenger properties.

Generation of an automated workflow for accurate annotation of oxidized lipids

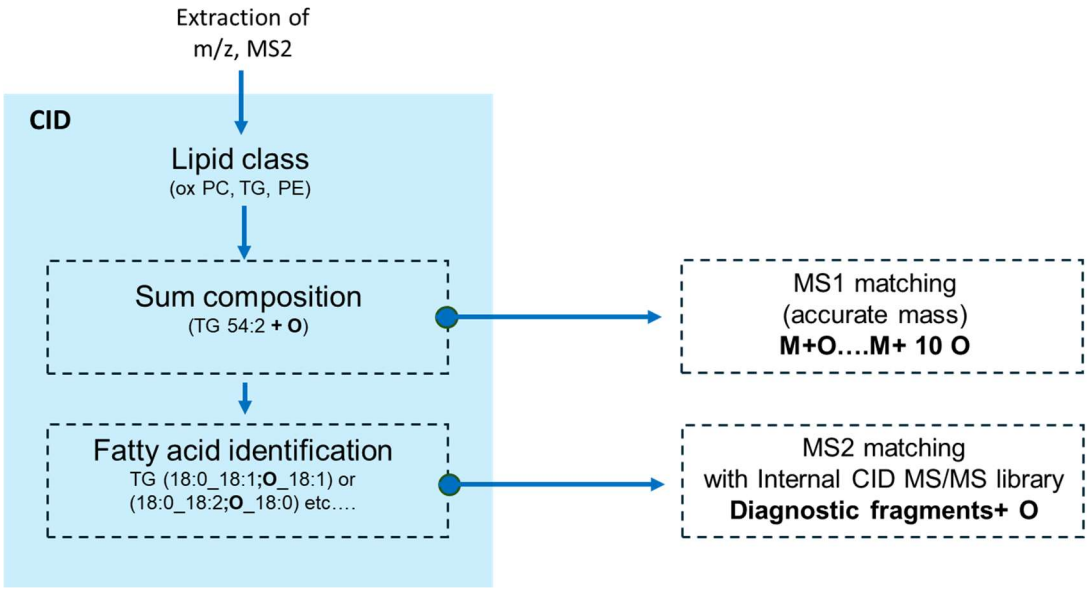

Figure 1: Hierarchical annotation workflow for CID spectra.

Figure 1 shows the full annotation workflow used in this work. The process of annotation of oxidized lipids from high-throughput DDA experiments followed the general logic of unmodified lipid identification, thus with sequential and specialized steps. MS1 and MS/MS features extracted from raw data processing are matched against either our internal or open source CID libraries to initially determine class, number of carbon atoms (sum composition), and double bonds (fatty acid identification). By default, the matching includes additional oxidation at both annotation levels. For MS1 matching (accurate mass), the search for m/z features is extended up to 10 oxygens with a tolerance of 0.01 Da. When candidate oxidized species are found based on MS1 matching, MS2 peaks are searched against our internal CID library for compatible increments of MS/MS fragment ions m/z that indicate acyl chain lengths and the presence of oxygens. Here, the maximum number of oxygens allowed in the side chains for MS2 libraries is 3, which can result from the combination of O, OH and OOH addition products. To do that, we established a set of MS/MS fragmentation rules to ensure accurate assignment of lipid class, molecular species, modification type, and the specific position of modifications in

oxidized lipids. Fragmentation rules are specific to each lipid class and have been obtained using MS/MS data from the literature and those available in other open-source libraries (Lipidblast) or those obtained experimentally (AdipoAtals).[21]

In addition, to reduce false positives, we introduced the possibility of neglecting any oxidized features not detected in the non-oxidized form. The nomenclature used to annotate oxidized lipids is consistent with the Lipidmaps ontology. The oxidized lipid structures generated can cover all the most common lipid subclasses, allowing us to increase chemical space and thus the coverage of oxidized lipids predicted in our untargeted dataset, providing a large library of potential species compared to other libraries.

Profiling of oxidized lipids in complex matrices

The annotation workflow was applied to detect epilipid signatures in complex biological matrices. To do that, I took advantage of our untargeted lipidomic dataset, already described in detail in Chapter 4.

Of features detected in the initial peak picking, I annotated 229 unique features in the liver and 88 in plasma with putative oxidation in either positive or negative ionization mode (Figure 2 and Supplementary Tables S1-3). The list of annotated lipids included only features annotated at the MS2 level with at least two fragments (ms2_matched > 2), one of which had oxidation that matched our internal MS/MS CID library (MS2 evidence = hg; chain; oxy-chain).

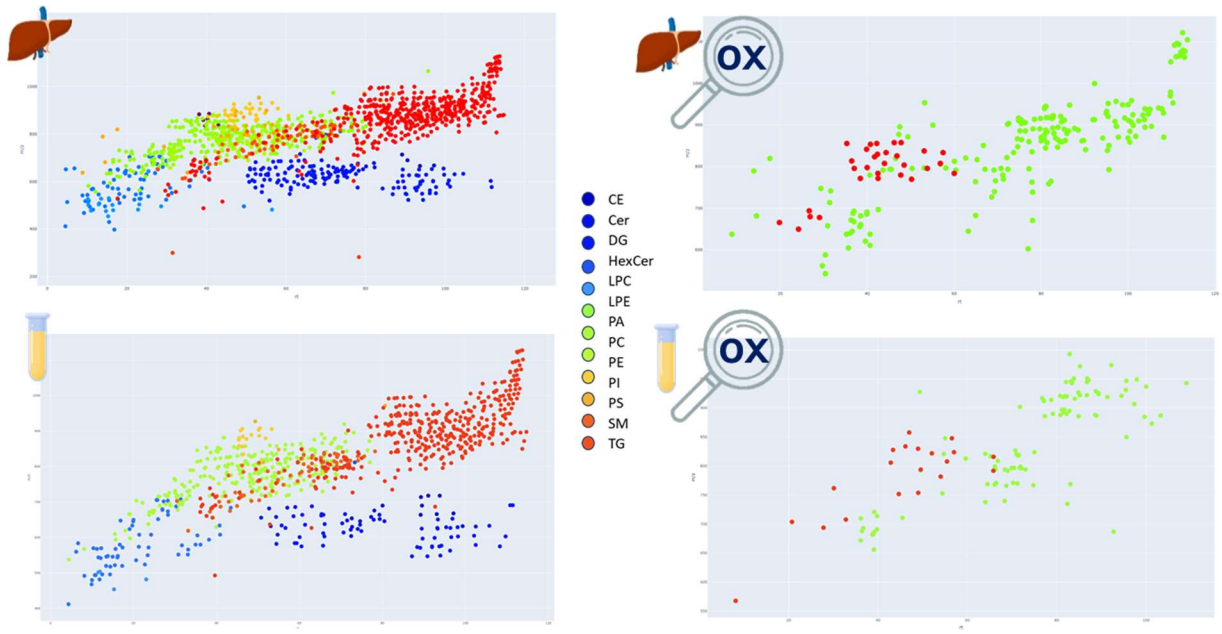

Figure 2: Annotation for LC-MS/MS analysis of unmodified (left) and putatively oxidized (right) lipids in liver and plasma lipid extracts. Positive ESI mode. annotated lipids included only features annotated at the MS2 level with at least two fragments (ms2_matched > 2), one of which had an oxidation that matched our internal MS/MS CID library (MS2 evidence = hg; chain; oxy-chain).

Of these lipids, 120 features were annotated as OxTG in liver samples, 68 as oxidized phosphatidylcholines (OxPC), 7 as oxidized phosphatidylinositols (ox PI), 22 as oxidized phosphatidylethanolamines (OxPE) and 9 etherPE (ox O-PE). In plasma samples, we annotated 62 oxTG and 18 oxPC (Figure 3). The distribution of oxidative modifications among the different oxidized lipid classes in plasma and the liver is shown in Figure 3. These derivatives were identified as epoxy-, hydroxy-, oxo- (O), hydroperoxy- (OO) products or a combination of these (OOO), and were mainly observed as $[M + NH4]^+$, $[M+H]^+$, $[M+HCOO]^-$, and $[M-H]^-$ adducts.

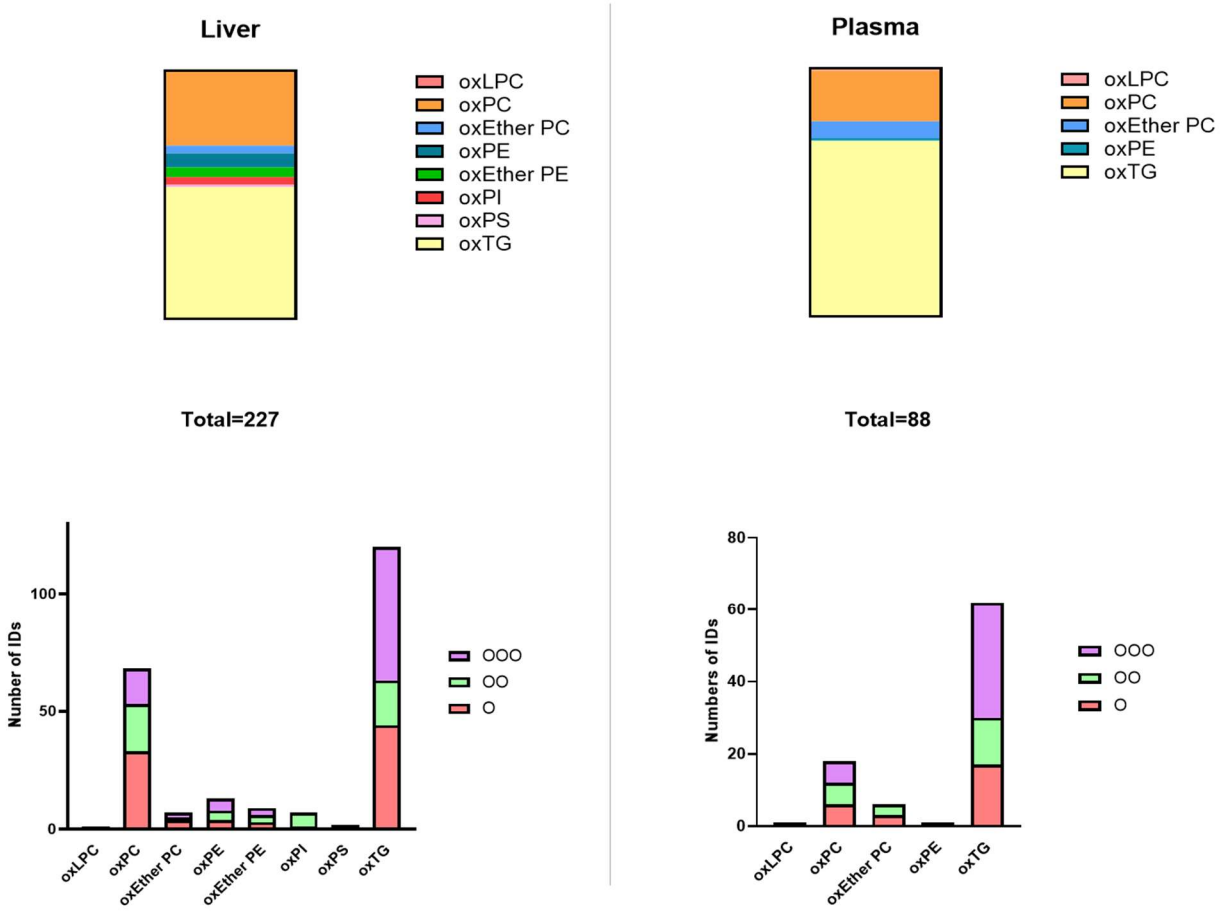

Figure 3: The distribution of oxidative modifications among the different oxidized lipid classes in plasma and liver samples. Due to the intrinsic limitations of CID fragmentation mode, it was not possible to distinguish isomers that have the same number of oxygen atoms. Specifically, this poses a challenge in differentiating between epoxy and oxo derivatives, which have been classified as (O) in the annotation process.

The initial annotation of candidate oxidized lipids was followed by manual verification of the correct assignment of diagnostic peaks according to the fragmentation rules we included in the internal MS/MS CID library. In particular, we checked the accuracy of the annotation of lipid classes, molecular species, modification type, and modification position of oxidized lipids in our dataset.

For example, Figure 4 shows the spectrum of one of the oxTGs detected in our samples. OxTG ionized in positive mode, mainly as ammoniated adducts. In this spectrum, the ammoniated parent ion can be clearly observed at m/z 890.7723. Such adduct provides informative MS/MS spectra with fragment ions indicative of the structures of the oxidized lipids. Thus, the CID spectrum of TG (16:0_18:1_18:2(+O) resulted in the formation of informative fragment ion signals, such as those corresponding to DG ions, due to the loss of each acyl group as a neutral carboxylic acid and neutral ammonia (NH3).

Moreover, other product ions can be obtained following the fragmentation of the DG fragments. For instance, acylium ions at m/z 279.22 (FA 18:2+O) and acylium ion +74 at m/z 353.2644 (18:2+O) can be observed. Using this information, the structure of oxTG can be deduced.

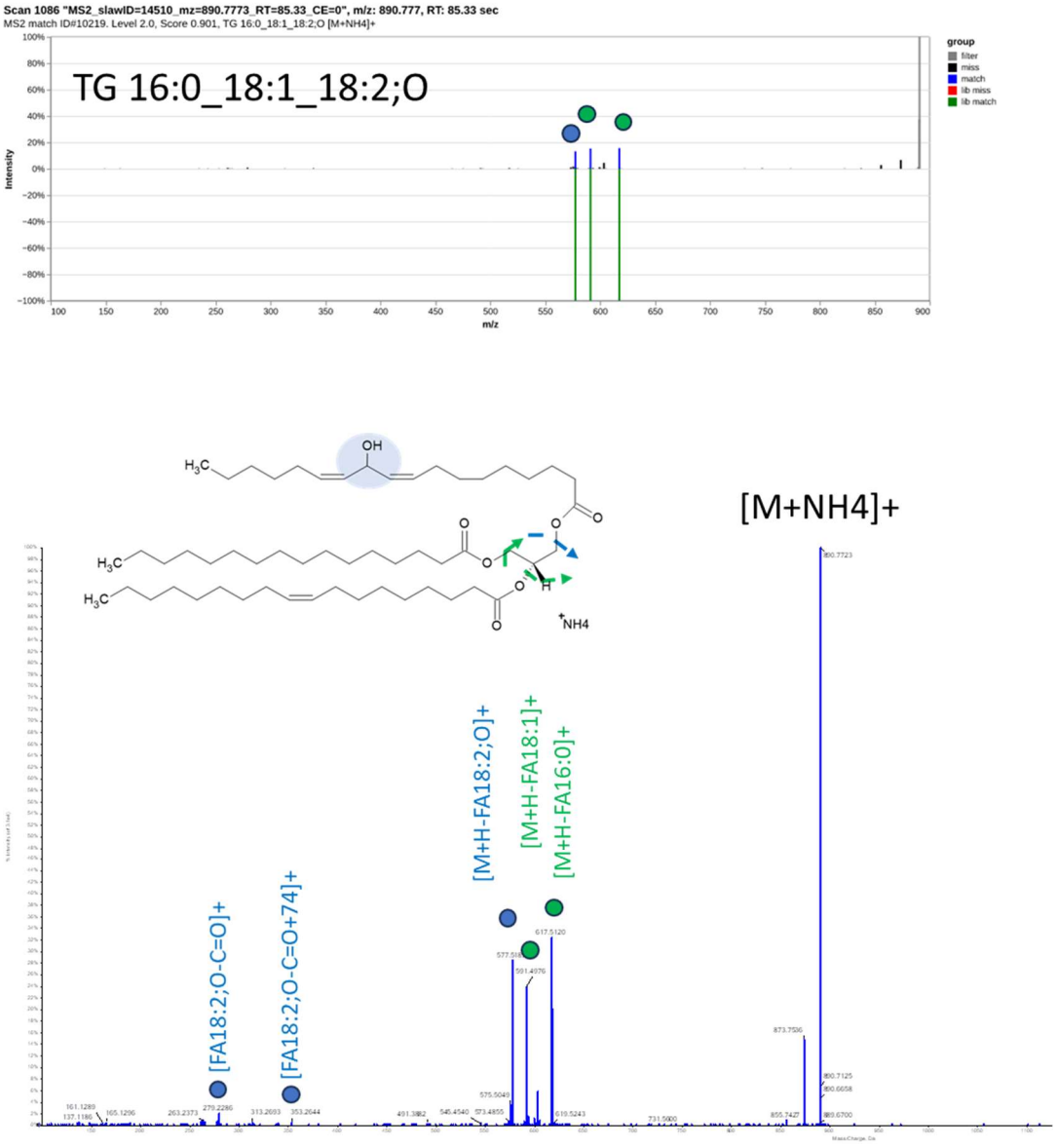

Figure 4: Evaluation of MS/MS fragmentation pattern for oxTG (16:0_18:1_18:2(+O)). Fragment ions related to DG ions allowing carrying modified FA (green) and unmodified FA (blue).

In the case of oxPC, they are preferentially ionized in negative mode as formate adducts. As shown in Figure 5, this adduct usually generates a neutral loss of 60 units (methyl formate) that can be observed from the parent ion. This adduct generates intense fragment ions that are specific to both the head groups and fatty acyl chains, including

the one with the modification. For example, CID fragmentation of the oxPC-formate adduct ion at m/z 870.585 produced diagnostic peaks related to the lipid class (head group-specific ions at m/z 184, detectable only in positive ion mode), molecular species (anions of the oxidized fatty acyl chains at m/z 319.2332 and the unmodified acyl chain at m/z 283.2281), and the type of modification (water loss indicative of a hydroxyl group at m/z 301.2175).

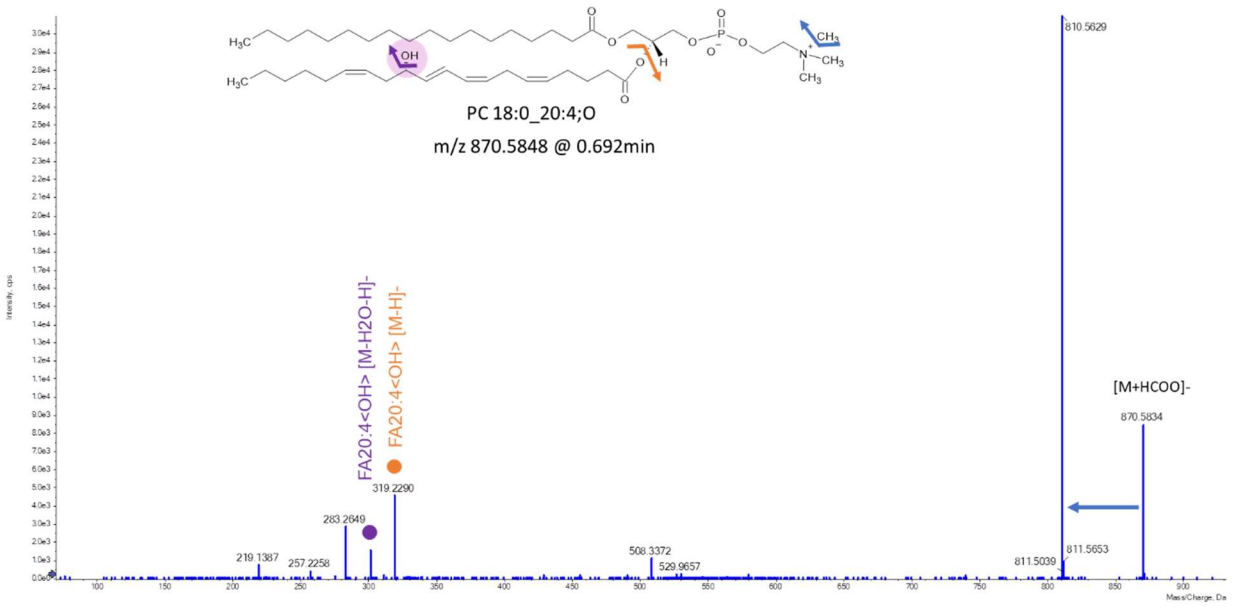

Figure 5: CID MS/MS spectra of oxPC (18:0_20:4 (+O)) with the corresponding fragment patterns. Orange and purple circles indicate fragment ions with and without oxygen modification, respectively.

Similarly to oxPC, the CID fragmentation pattern of oxPE (Figure 6) generates several diagnostic fragments that can be used for their accurate annotation. In the positive mode, one such peak is the fragment ions, including neutral losses of the headgroup (ethanolamine loss of 141 Da) in PE. However, as with oxPC, the negative ionization mode allows for a better characterization of the lipid subclass. Diagnostic peaks that can be matched may also contain information on the sn position. In particular, for PE molecular species, the most abundant fragments observed are derived from the sn-2 fatty acyl group.

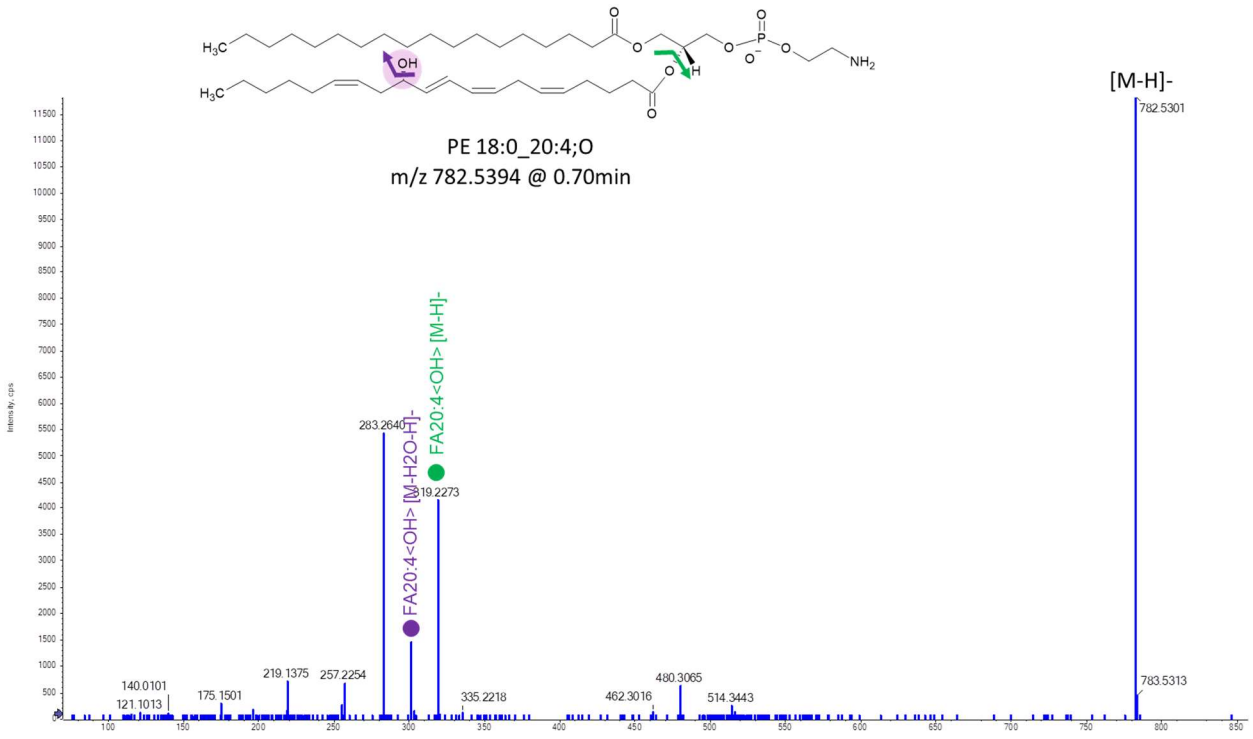

Figure 6: CID MS/MS spectra of oxPE ((18:0_20:4 (+O)) with the corresponding fragment patterns. Green and purple circles indicate fragment ions with and without oxygen modification, respectively.

The negative molecular ion from PE and PC plasmalogen and the O-alkyl PC and PE species behave identically to that of the diacyl-phospholipids except that the single abundant carboxylate anion is formed. These ether lipids can also show the loss of the sn-2 fatty acyl groups as ketene.

Of the manually confirmed lipids, I also checked that the elution time was consistent with the presence of oxidation, i.e. that the peak elutes before the corresponding unmodified lipid. Thus, I excluded oxidized lipids when the respective unoxidized species were not identified. Interestingly, for both the biological matrices, the correlation analysis between oxidized and non-oxidized lipids revealed no significant relationship between the two groups. The low correlation in Figure 7 suggests that oxidation does not occur exclusively from the most abundant or intense non-oxidized lipids, as expected. Instead, oxidation products can be formed from various lipid species independent of their abundance.

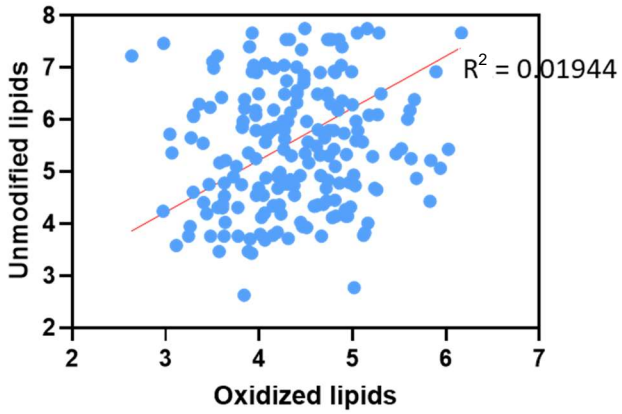

Figure 7: Correlation analysis of oxidized versus non-oxidized lipid species in biological matrices. The scatter plot showed the relationship between the intensity (log_{10} transformed) of oxidized lipids and their corresponding non-oxidized reference species. The low R^2 coefficient (Pearson correlation) indicates a lack of strong correlation between these two groups, suggesting that the formation of oxidized lipids is not necessarily linked to the abundance of non-oxidized species. The analysis showed that oxidation can occur independently of the intensity or concentration of non-oxidized substrates.

Identification of epilipidomic signatures of carnosine treatment in lean and obese animals

Next, I aimed to determine the lipid and oxilipid patterns that underlie the carnosine effect. The PLS-DA score plots showed a clear separation between the HSF and HSF+CAR groups in both positive and negative modes in each matrix. The weights of all lipids discriminating the experimental groups (HSF and HSF + CAR) were subjected to a permutation approach to generate a list of HSF and HSF+CAR-associated lipid molecular species. Using a 10% cut-off, these two lists contained 307 and 36 lipid species in plasma for the HSF and HSF+CAR groups, respectively, including oxidized lipid species. In the liver, 267 and 171 lipid species for the HSF group and HSF+CAR, respectively (Figure 8).

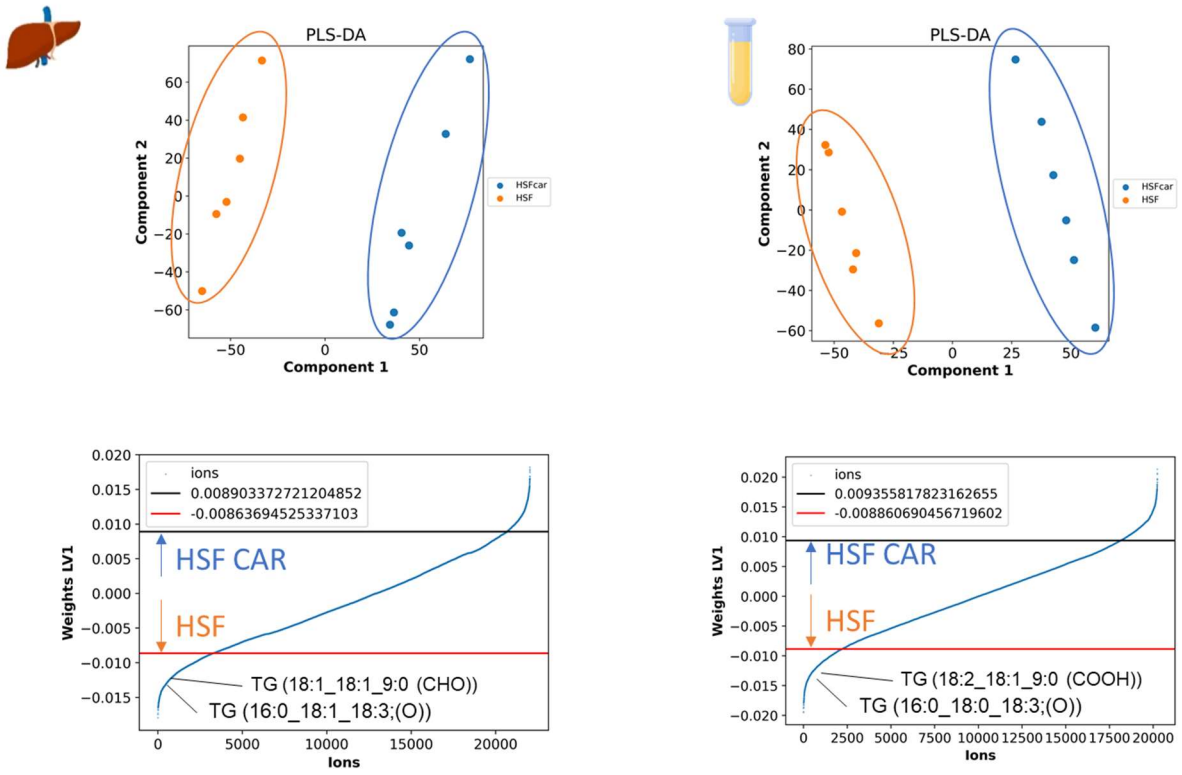

Figure 8: PLS-DA analysis of HSF and HSF+CAR samples showing the discrimination between the two experimental groups among component 1, either liver or plasma samples. Weights of the first component of the PLS-DA. The 10% and 90% percentiles associated with HSF and HSF+CAR, respectively, were determined using a permutation approach.

Most of the species significantly reduced by carnosine treatment consisted of oxidation products enriched in oxygenated 18:1, 18:2 and 18:3, 18:4 acyl chains. Among these, O mainly identified oxTG. For instance, TG (16:0_18:1_18:3(O)), TG (TG 18:2_18:2_18:2 (O)), and TG (TG 16:0_18:2_18:2 (O)) were found to be significantly reduced in either plasma or liver samples of CAR-treated obese rats. In particular, these species are reported to be elevated in TG-rich lipoproteins such as VLDL. [22,23]

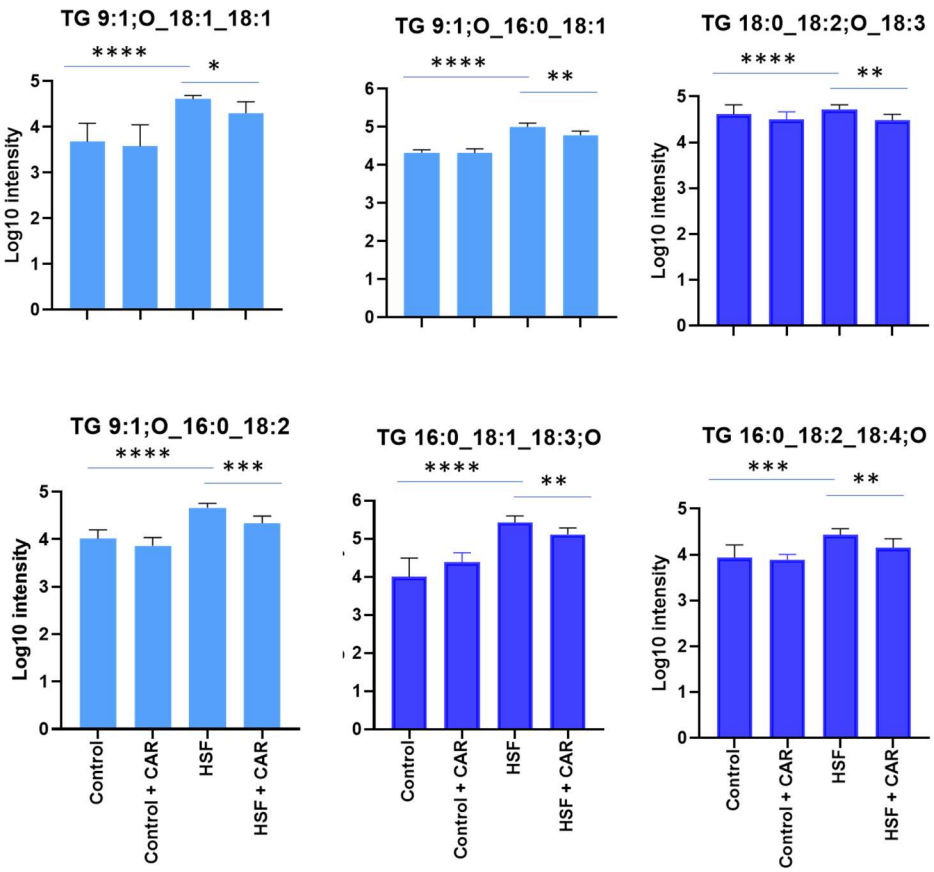

Figure 9: Box plots showing the behaviour of log10-transformed intensity values for oxidized TGs in liver lipid extracts, positive ESI mode. ANOVA ($p<0.05$). The plot differentiates between truncated and intact oxidized species, highlighted by varying tones of blue.

Looking at the oxidized triglycerides that were significantly changed in the two experimental groups, several short-chain products (aldehydes and carboxylic acid) were also observed. These were as follows: TG (18:1_18:1_9:0 (CHO)) and OxTG (16:0_18:2_9:0 (CHO)). These short-chain oxidation products are degradation products generated by prolonged PUFA peroxidation and subsequent Hock rearrangement[24]. Although we do not know which precursor lipids give rise to these truncated species, it is important to note that they are all identified with retention times lower than the potential corresponding TG. We can, therefore, infer that they are not simple products generated by in-source fragmentation but rather the result of sustained lipid peroxidation caused by ROS. Importantly, I have shown that the observed effect is specific to OxTG and does not scale with the level of the corresponding unmodified lipids (Figure 10).

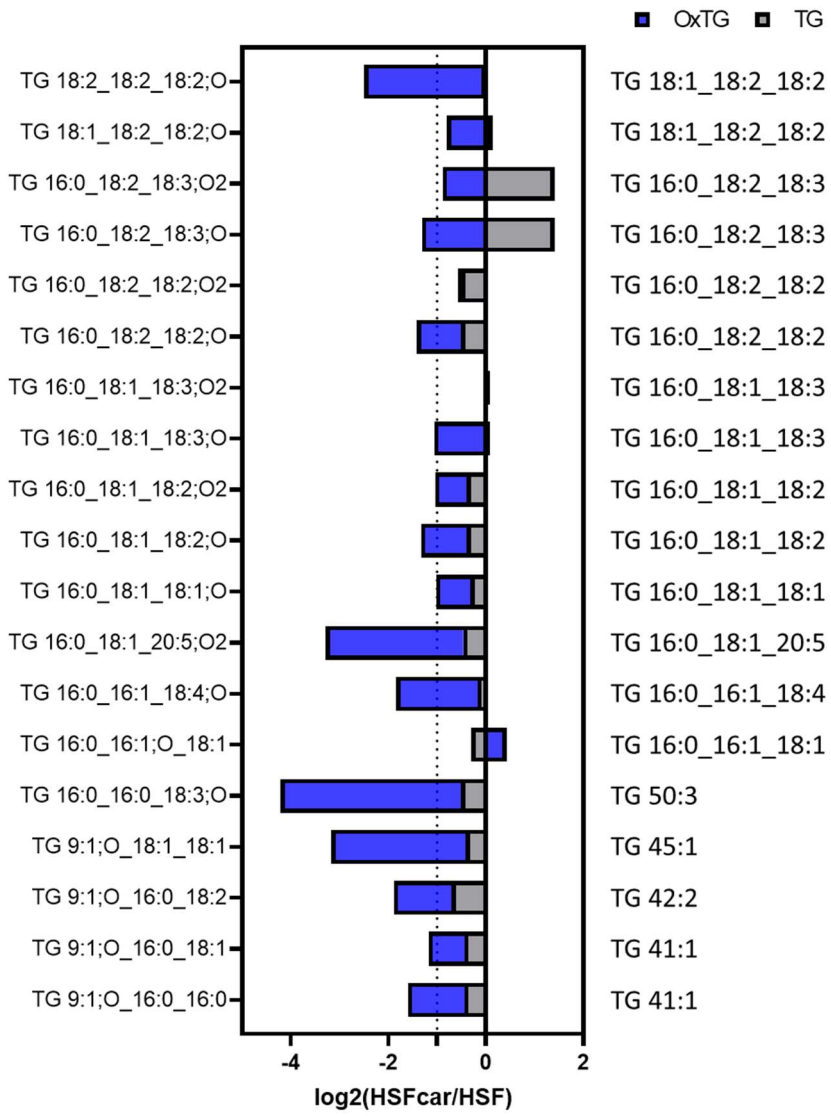

Figure 10: Log2-fold change in oxidized triglycerides (OxTGs) and corresponding unmodified TGs between the HSF+CAR and HSF groups. The data highlight the specificity of the effect of carnosine, as OxTGs show a more marked decrease compared to their non-oxidized forms, underlining the selective effect of carnosine on lipid oxidation products.

In addition to oxidized lipids and plasmalogens (described in Chapter 4), carnosine significantly reduces other lipid markers of oxidative stress. PE (38:4), LPC (20:4), and other PUFA phospholipids were previously found to be upregulated in the plasma of obese rats and subsequently reduced by the treatment with CAR.

Discussion

Automated and high-throughput annotation of oxidized lipids is challenging due to the complexity of the epilipidome, the huge number of candidate structures that far exceed

unoxidized lipids, and the lack of standard validation. Thus, advanced bioinformatic tools are required, which, however, are still few.

The aim of this work was to optimize an analytical pipeline for the discovery and characterization of oxidized lipids in complex biological matrices. To do that, I took advantage of the untargeted lipidomic dataset generated in Chapter 4 and used it here to study the epilipidomic signatures of plasma and liver from lean and obese animals while also investigating the beneficial effects of carnosine treatment.

Untargeted LC-MS/MS lipidomics can detect thousands of molecules in biological samples, but the annotation of oxidized lipids is often limited to structures present in libraries, limiting the analysis and interpretation of experimental data. Instead, our method offers a rapid approach to extracting oxidized species from complex untargeted datasets. This approach allowed us to identify putatively oxidized lipids on a minute scale, making it compatible with routine untargeted lipidomics analyses.

Overall, the workflow offers several advantages. First, it expands the analysis into a broader chemical space by introducing multiple fatty acids as substrates for oxidation and new oxidation combinations, thereby increasing the diversity of oxidized lipids that can be detected. Second, different from other analytical workflows reported in the literature, our annotation tool allows the simultaneous analysis of either unmodified or modified species, and we have demonstrated its compatibility with 2.4-min LC-MS/MS methods, thereby improving the throughput of the analysis. To our knowledge, this is one of the first studies to integrate oxidized lipid detection into a high-throughput untargeted lipidomics workflow. As discussed previously in this thesis, the future direction of omics research will increasingly rely on the use of fast LC gradients for various biomedical applications. Given the growing interest in oxidized lipids, it is important to evaluate how the analysis of those species can be incorporated into untargeted modern workflows. The method employed in this study was tailored specifically for a 2-minute LC method, which differs from more traditional approaches for assessing oxidized lipids. However, this remains a preliminary approach, and further validation is required to fully establish its utility in biomedical research. Moving forward, we plan to validate this method and further refine its application.

With this method, I successfully detected more than 200 lipids with putative oxidative modifications in liver and plasma samples. These annotations were manually checked to remove any false positives that had not been removed in the initial filtering of the untargeted dataset. Our results showed that lipid oxidation primarily occurs on the fatty acyl chains of complex lipids, such as triglycerides and phospholipids. These lipids are also among the most abundant species in the lipidome, but for both plasma and liver, I observed that oxidation does not scale with the intensity of unmodified species.

I then explored the epilipidomic signatures that define obesity and the beneficial effects of carnosine treatment. Our results showed that obese rats have distinct epilipidomic signatures, enriched in oxygenated acyl chains (18:1, 18:2, 18:3, 18:4) of TGs, and that carnosine treatment partially restored the pattern of these lipids. This effect may be attributed to the direct antioxidant action of CAR and its role as a scavenger of carbonyl species, restoring the redox balance and improving the pathological phenotype in the liver. This hypothesis is supported by the significant reduction in levels of truncated TGs, which are end products of lipid peroxidation driven by ROS, typically targeting polyunsaturated fatty acids (PUFAs), either free or esterified to complex lipids such as TGs and strongly associated with cardiometabolic disease[25]. However, it is plausible that the effect of carnosine is not limited to direct mechanisms but may also involve promoting the expression of key antioxidant enzymes through indirect mechanisms that remain to be fully elucidated.

Taken together, our method allowed the comprehensive and high-throughput profiling of oxidized complex lipids, opening up the possibility of discovering new potential biomarkers of the disease. Moreover, the annotation pipeline could be extended to other lipid modifications beyond oxidation, including modifications occurring in other parts of the lipid structure.

In addition, alternative analytical approaches can be applied for fine-grained structural elucidation of oxidized lipids. Indeed, although we have focused on CID (collision-induced dissociation) fragmentation, we aim to extend the annotation of ox lipids to other fragmentation methods to provide more detailed structural information. Given the increasing importance of redox lipidomics, this could be a crucial next step. The results of this part of the work will be discussed in the next chapter.

Conclusion

We have optimized a workflow for the annotation of oxidized lipids in untargeted lipidomic analysis. This methodology was applied to liver and plasma lipidome analysis, demonstrating its potential to address epilipidome changes in an untargeted manner and to guide future research on the role of oxidized lipids in biological systems.

Supplementary Tables

Supplementary Table 1: Complete list of oxidized lipids putatively annotated in liver samples in positive ESI mode.

mz	*Rt (sec)*	*formula*	*ion*	*species (lib_id)*	*mz*	*Rt (sec)*	*formula*	*ion*	*species (lib_id)*
650.4387	24.21	C33H64O9NP	[M+H]+	PC 25:1;O	*864.7569*	83.97	C53H98O7	[M+NH4]+	TG 50:2;O
666.4327	19.82	C33H64O10NP	[M+H]+	PC 25:1;O2	*901.7202*	87.87	C53H98O9	[M+Na]+	TG 50:2;O3
678.4698	29.04	C35H68O9NP	[M+H]+	PC 27:1;O	*879.7377*	114.49	C53H98O9	[M+H]+	TG 50:2;O3
780.5477	47.73	C40H78O11NP	[M+H]+	PC 32:1;O3	*862.7445*	80.04	C53H96O7	[M+NH4]+	TG 50:3;O
808.5765	43.98	C42H82O11NP	[M+H]+	PC 34:1;O3	*867.7026*	80.71	C53H96O7	[M+Na]+	TG 50:3;O
772.5458	42.51	C42H78O9NP	[M+H]+	PC 34:3;O	*862.745*	89.42	C53H96O7	[M+NH4]+	TG 50:3;O
804.5477	48.5	C42H78O11NP	[M+H]+	PC 34:3;O3	*894.7483*	84.18	C53H96O9	[M+NH4]+	TG 50:3;O3
784.5488	42.47	C43H78O9NP	[M+H]+	PC 35:4;O	*899.7028*	84.31	C53H96O9	[M+Na]+	TG 50:3;O3
838.61	53.11	C44H88O11NP	[M+H]+	PC 36:0;O3	*860.729*	77.23	C53H94O7	[M+NH4]+	TG 50:4;O
834.5783	44.35	C44H84O11NP	[M+H]+	PC 36:2;O3	*860.7325*	84.44	C53H94O7	[M+NH4]+	TG 50:4;O
834.5945	57.46	C44H84O11NP	[M+H]+	PC 36:2;O3	*860.7282*	84.8	C53H94O7	[M+NH4]+	TG 50:4;O
798.5623	40	C44H80O9NP	[M+H]+	PC 36:4;O	*859.7102*	100.43	C53H94O8	[M+H]+	TG 50:4;O2
814.5579	36.45	C44H80O10NP	[M+H]+	PC 36:4;O2	*875.7034*	87.05	C53H94O9	[M+H]+	TG 50:4;O3
830.5546	42.37	C44H80O11NP	[M+H]+	PC 36:4;O3	*858.7127*	81.37	C53H92O7	[M+NH4]+	TG 50:5;O
796.5476	37.03	C44H78O9NP	[M+H]+	PC 36:5;O	*919.7543*	82.8	C54H104O9	[M+Na]+	TG 51:0;O3
826.593	46.85	C46H84O9NP	[M+H]+	PC 38:4;O	*914.8097*	97.21	C54H104O9	[M+NH4]+	TG 51:0;O3
842.5886	39.87	C46H84O10NP	[M+H]+	PC 38:4;O2	*893.7341*	82.68	C54H100O9	[M+H]+	TG 51:2;O3
858.5898	46.22	C46H84O11NP	[M+H]+	PC 38:4;O3	*893.7504*	96.9	C54H100O9	[M+H]+	TG 51:2;O3
858.5943	47.81	C46H84O11NP	[M+H]+	PC 38:4;O3	*876.7633*	80.73	C54H98O7	[M+NH4]+	TG 51:3;O
856.5708	35.32	C46H82O11NP	[M+H]+	PC 38:5;O3	*891.7228*	79.71	C54H98O9	[M+H]+	TG 51:3;O3
856.567	42.21	C46H82O11NP	[M+H]+	PC 38:5;O3	*891.7374*	93.9	C54H98O9	[M+H]+	TG 51:3;O3
854.5539	40.75	C46H80O11NP	[M+H]+	PC 38:6;O3	*928.8225*	95	C55H106O9	[M+NH4]+	TG 52:0;O3
770.5665	50.22	C43H80O8NP	[M+H]+	PC O-35:4;O	*909.7825*	97.24	C55H104O9	[M+H]+	TG 52:1;O3
784.5801	60.03	C44H82O8NP	[M+H]+	PC O-36:4;O	*892.7901*	87.7	C55H102O7	[M+NH4]+	TG 52:2;O
810.5982	59.45	C46H84O8NP	[M+H]+	PC O-38:5;O	*890.7773*	85.33	C55H100O7	[M+NH4]+	TG 52:3;O
808.5803	56.82	C46H82O8NP	[M+H]+	PC O-38:6;O	*906.7719*	76.37	C55H100O8	[M+NH4]+	TG 52:3;O2

780.5396	40.61	C40H78O11NP	[M+H]+	PE 35:1;O3
796.5796	53.83	C41H82O11NP	[M+H]+	PE 36:0;O3
784.5488	42.47	C43H78O9NP	[M+H]+	PE 38:4;O
658.408	30.93	C34H60O9NP	[M+H]+	PE O-29:5;O2
714.4315	31.37	C37H64O10NP	[M+H]+	PE O-32:6;O3
712.4906	45.17	C39H70O8NP	[M+H]+	PE O-34:5;O
756.5481	54.96	C42H78O8NP	[M+H]+	PE O-37:4;O
784.5488	42.47	C43H78O9NP	[M+H]+	PE O-38:5;O2
766.5334	50.2	C43H76O8NP	[M+H]+	PE O-38:6;O
780.5537	53.25	C44H78O8NP	[M+H]+	PE O-39:6;O
926.5737	46.93	C49H84O13NP	[M+H]+	PS 43:6;O3
586.4223	24.65	C32H56O8	[M+NH4]+	TG 29:2;O2
656.5076	38.29	C37H66O8	[M+NH4]+	TG 34:2;O2
672.5033	36.29	C37H66O9	[M+NH4]+	TG 34:2;O3
671.5014	78.04	C38H70O9	[M+H]+	TG 35:1;O3
686.5174	39.92	C38H68O9	[M+NH4]+	TG 35:2;O3
682.5272	38.51	C39H68O8	[M+NH4]+	TG 36:3;O2
693.4895	37.01	C40H68O9	[M+H]+	TG 37:4;O3
691.4746	39.86	C40H66O9	[M+H]+	TG 37:5;O3
697.5892	109.65	C42H80O7	[M+H]+	TG 39:0;O
727.5637	68.66	C42H78O9	[M+H]+	TG 39:1;O3
740.6344	69.3	C44H82O7	[M+NH4]+	TG 41:1;O
770.6438	71.34	C45H84O8	[M+NH4]+	TG 42:1;O2
766.6497	69.53	C46H84O7	[M+NH4]+	TG 43:2;O
764.6374	64.93	C46H82O7	[M+NH4]+	TG 43:3;O
797.6577	86.14	C47H88O9	[M+H]+	TG 44:1;O3
780.6674	71.2	C47H86O7	[M+NH4]+	TG 44:2;O
796.6637	70.79	C47H86O8	[M+NH4]+	TG 44:2;O2
795.6253	77.22	C47H86O9	[M+H]+	TG 44:2;O3
794.651	67.09	C47H84O8	[M+NH4]+	TG 44:3;O2
812.6938	73.69	C48H90O8	[M+NH4]+	TG 45:1;O2
794.6858	72.36	C48H88O7	[M+NH4]+	TG 45:2;O
927.7343	89.91	C55H100O9	[M+Na]+	TG 52:3;O3
888.7611	81.08	C55H98O7	[M+NH4]+	TG 52:4;O
888.7608	88.54	C55H98O7	[M+NH4]+	TG 52:4;O
904.7524	72.58	C55H98O8	[M+NH4]+	TG 52:4;O2
904.7589	75.48	C55H98O8	[M+NH4]+	TG 52:4;O2
903.7383	89.45	C55H98O9	[M+H]+	TG 52:4;O3
886.7406	75.15	C55H96O7	[M+NH4]+	TG 52:5;O
886.7473	76.42	C55H96O7	[M+NH4]+	TG 52:5;O
891.7046	78.15	C55H96O7	[M+Na]+	TG 52:5;O
869.719	83.33	C55H96O7	[M+H]+	TG 52:5;O
886.7449	86.28	C55H96O7	[M+NH4]+	TG 52:5;O
902.7381	72.31	C55H96O8	[M+NH4]+	TG 52:5;O2
885.7234	100.44	C55H96O8	[M+H]+	TG 52:5;O2
901.7202	87.87	C55H96O9	[M+H]+	TG 52:5;O3
867.7026	80.71	C55H94O7	[M+H]+	TG 52:6;O
884.7282	81.42	C55H94O7	[M+NH4]+	TG 52:6;O
899.7028	84.31	C55H94O9	[M+H]+	TG 52:6;O3
910.8423	102.5	C56H108O7	[M+NH4]+	TG 53:0;O
923.796	103.92	C56H106O9	[M+H]+	TG 53:1;O3
919.7543	82.8	C56H102O9	[M+H]+	TG 53:3;O3
936.7948	92.12	C56H102O9	[M+NH4]+	TG 53:3;O3
934.7798	89.44	C56H100O9	[M+NH4]+	TG 53:4;O3
899.7401	101.2	C56H98O8	[M+H]+	TG 53:5;O2
937.8149	104.56	C57H108O9	[M+H]+	TG 54:1;O3
952.8217	95.46	C57H106O9	[M+NH4]+	TG 54:2;O3
952.8271	96.33	C57H106O9	[M+NH4]+	TG 54:2;O3
935.8004	96.83	C57H106O9	[M+H]+	TG 54:2;O3
918.8044	81.24	C57H104O7	[M+NH4]+	TG 54:3;O
918.8059	82.04	C57H104O7	[M+NH4]+	TG 54:3;O
950.8108	93.23	C57H104O9	[M+NH4]+	TG 54:3;O3
933.7804	95.12	C57H104O9	[M+H]+	TG 54:3;O3
933.7847	100.34	C57H104O9	[M+H]+	TG 54:3;O3

792.6703	69.17	C48H86O7	[M+NH4]+	TG 45:3;O
825.6913	90.32	C49H92O9	[M+H]+	TG 46:1;O3
823.6755	86.54	C49H90O9	[M+H]+	TG 46:2;O3
822.6732	72.15	C49H88O8	[M+NH4]+	TG 46:3;O2
834.6763	73.68	C50H88O8	[M+NH4]+	TG 47:4;O2
839.7418	95.27	C51H98O8	[M+H]+	TG 48:0;O2
875.7034	87.05	C51H96O9	[M+Na]+	TG 48:1;O3
836.7315	77.93	C51H94O7	[M+NH4]+	TG 48:2;O
869.7524	100	C52H100O9	[M+H]+	TG 49:0;O3
867.7381	96.73	C52H98O9	[M+H]+	TG 49:1;O3
865.7196	93.43	C52H96O9	[M+H]+	TG 49:2;O3
880.7274	85.94	C52H94O9	[M+NH4]+	TG 49:3;O3
863.7023	89.78	C52H94O9	[M+H]+	TG 49:3;O3
881.7534	93.12	C53H100O9	[M+H]+	TG 50:1;O3
881.7522	114.78	C53H100O9	[M+H]+	TG 50:1;O3
864.7569	83.97	C53H98O7	[M+NH4]+	TG 50:2;O
901.7202	87.87	C53H98O9	[M+Na]+	TG 50:2;O3
879.7377	114.49	C53H98O9	[M+H]+	TG 50:2;O3
862.7445	80.04	C53H96O7	[M+NH4]+	TG 50:3;O
867.7026	80.71	C53H96O7	[M+Na]+	TG 50:3;O
862.745	89.42	C53H96O7	[M+NH4]+	TG 50:3;O
894.7483	84.18	C53H96O9	[M+NH4]+	TG 50:3;O3
899.7028	84.31	C53H96O9	[M+Na]+	TG 50:3;O3
860.729	77.23	C53H94O7	[M+NH4]+	TG 50:4;O
860.7325	84.44	C53H94O7	[M+NH4]+	TG 50:4;O
860.7282	84.8	C53H94O7	[M+NH4]+	TG 50:4;O
916.789	79.88	C57H102O7	[M+NH4]+	TG 54:4;O
916.7882	82.53	C57H102O7	[M+NH4]+	TG 54:4;O
948.7936	86.58	C57H102O9	[M+NH4]+	TG 54:4;O3
931.7689	96.64	C57H102O9	[M+H]+	TG 54:4;O3
914.7737	78.47	C57H100O7	[M+NH4]+	TG 54:5;O
913.7582	103.79	C57H100O8	[M+H]+	TG 54:5;O2
946.7795	86.52	C57H100O9	[M+NH4]+	TG 54:5;O3
912.7596	75.5	C57H98O7	[M+NH4]+	TG 54:6;O
895.7364	83.88	C57H98O7	[M+H]+	TG 54:6;O
912.7585	85.37	C57H98O7	[M+NH4]+	TG 54:6;O
911.7433	100.15	C57H98O8	[M+H]+	TG 54:6;O2
944.7626	83.71	C57H98O9	[M+NH4]+	TG 54:6;O3
927.7343	89.91	C57H98O9	[M+H]+	TG 54:6;O3
938.8724	105.09	C58H112O7	[M+NH4]+	TG 55:0;O
917.8241	99.25	C58H108O7	[M+H]+	TG 55:2;O
913.7891	91.96	C58H104O7	[M+H]+	TG 55:4;O
940.7916	80.78	C59H102O7	[M+NH4]+	TG 56:6;O
972.792	85.19	C59H102O9	[M+NH4]+	TG 56:6;O3
955.769	93.78	C59H102O9	[M+H]+	TG 56:6;O3
970.8525	109.75	C61H108O7	[M+NH4]+	TG 58:5;O
1000.822	92.31	C61H106O9	[M+NH4]+	TG 58:6;O3
1066.949	111.8	C65H124O9	[M+NH4]+	TG 62:1;O3
1064.933	111.04	C65H122O9	[M+NH4]+	TG 62:2;O3
1094.98	111.7	C67H128O9	[M+NH4]+	TG 64:1;O3
1080.962	112.66	C69H122O7	[M+NH4]+	TG 66:6;O
1077.952	113.13	C70H124O7	[M+H]+	TG 67:6;O

Supplementary Table 2: Complete list of oxidized lipids putatively annotated in liver samples in negative ESI mode.

mz	*Rt (sec)*	*formula*	*ion*	*species (lib_id)*	*mz*	*Rt (sec)*	*formula*	*ion*	*species (lib_id)*
778.5001	37.09	C43H74O9NP	[M-H]-	PE 38:6;O	*898.5805*	54.62	C47H84O10NP	[M+HCOO]-	PC 39:5;O2
780.5169	42.55	C43H76O9NP	[M-H]-	PC 35:5;O	*898.5805*	54.62	C47H84O10NP	[M+HCOO]-	PC O-39:6;O3
780.5152	47.24	C43H76O9NP	[M-H]-	PE 38:5;O	*900.5603*	48.89	C46H82O11NP	[M+HCOO]-	PE 41:5;O3
782.5332	39.82	C43H78O9NP	[M-H]-	PC 35:4;O	*900.594*	60.06	C47H86O10NP	[M+HCOO]-	PE 42:4;O2
784.4976	41.85	C37H74O11NP	[M+HCOO]-	PE 32:0;O3	*900.594*	60.06	C47H86O10NP	[M+HCOO]-	PE O-42:5;O3
804.5095	45.83	C41H76O12NP	[M-H]-	PS 35:2;O2	*901.545*	39.12	C47H83O14P	[M-H]-	PI 38:4;O
808.5481	52.77	C45H80O9NP	[M-H]-	PC 37:5;O	*926.5745*	49.23	C48H84O11NP	[M+HCOO]-	PC 40:6;O3
810.5156	43.66	C39H76O11NP	[M+HCOO]-	PE 34:1;O3	*928.5927*	54.29	C48H86O11NP	[M+HCOO]-	PE 43:5;O3
810.5258	57.48	C44H78O10NP	[M-H]-	PE 39:5;O2	*932.674*	60.42	C54H96O9NP	[M-H]-	PC 46:6;O
812.5272	41.49	C39H78O11NP	[M+HCOO]-	PC 31:0;O3	*578.3465*	26.32	C28H54O9NP	[M-H]-	PE O-23:2;O2
814.5226	33.89	C42H76O9NP	[M+HCOO]-	PC 34:4;O	*599.3207*	17.7	C27H53O12P	[M-H]-	PG 21:0;O2
816.538	37.29	C42H78O9NP	[M+HCOO]-	PC 34:3;O	*604.3247*	6.78	C28H50O8NP	[M+HCOO]-	LPC 20:4;O
816.5403	42.58	C42H78O9NP	[M+HCOO]-	PC 34:3;O	*608.3166*	14.71	C27H50O9NP	[M+HCOO]-	PC 19:2;O
818.5487	40.06	C42H80O9NP	[M+HCOO]-	PC 34:2;O	*636.3509*	22.86	C29H54O9NP	[M+HCOO]-	PC 21:2;O
832.5338	34.43	C42H78O10NP	[M+HCOO]-	PC 34:3;O2	*638.3626*	21.53	C29H56O9NP	[M+HCOO]-	PC 21:1;O
834.5507	33.57	C42H80O10NP	[M+HCOO]-	PC 34:2;O2	*638.3626*	21.53	C29H56O9NP	[M+HCOO]-	PC O-21:2;O2
834.6266	66.67	C45H90O10NP	[M-H]-	PC 37:0;O2	*656.3792*	15.4	C29H58O10NP	[M+HCOO]-	PE 24:0;O2
839.4859	36.29	C41H77O15P	[M-H]-	PI 32:1;O2	*664.4203*	19.45	C33H64O10NP	[M-H]-	PC 25:1;O2
840.5376	37.54	C44H78O9NP	[M+HCOO]-	PC 36:5;O	*664.4202*	37.95	C33H64O10NP	[M-H]-	PC 25:1;O2
841.5011	38.52	C41H79O15P	[M-H]-	PI 32:0;O2	*676.4181*	26.74	C34H64O10NP	[M-H]-	PC 26:2;O2
842.554	37	C44H80O9NP	[M+HCOO]-	PC 36:4;O	*680.4138*	21.62	C32H62O9NP	[M+HCOO]-	PC 24:1;O
842.5495	39.84	C44H80O9NP	[M+HCOO]-	PC 36:4;O	*692.4476*	27.82	C35H68O10NP	[M-H]-	PC 27:1;O2
842.5562	41.2	C44H80O9NP	[M+HCOO]-	PC 36:4;O	*694.4296*	23.61	C33H64O9NP	[M+HCOO]-	PC 25:1;O
850.5978	23.29	C48H86O9NP	[M-H]-	PC 40:5;O	*694.4291*	42.98	C33H64O9NP	[M+HCOO]-	PC 25:1;O
858.5471	34.61	C44H80O10NP	[M+HCOO]-	PC 36:4;O2	*694.4291*	42.98	C33H64O9NP	[M+HCOO]-	PE 28:1;O
865.5032	37.64	C43H79O15P	[M-H]-	PI 34:2;O2	*708.4436*	29.95	C34H66O9NP	[M+HCOO]-	PC 26:1;O
866.5493	37.59	C46H80O9NP	[M+HCOO]-	PC 38:6;O	*713.3485*	17.87	C32H59O15P	[M-H]-	PI 23:1;O2
866.5543	39.71	C46H80O9NP	[M+HCOO]-	PC 38:6;O	*722.4624*	29.18	C35H68O9NP	[M+HCOO]-	PC 27:1;O
866.5546	37.31	C46H80O9NP	[M+HCOO]-	PC 38:6;O	*724.4417*	27.43	C34H66O10NP	[M+HCOO]-	PC 26:1;O2

866.585	49.74	C43H84O11NP	[M+HCOO]-	PC 35:1;O3
867.5167	39.48	C43H81O15P	[M-H]-	PI 34:1;O2
867.5192	40.85	C43H81O15P	[M-H]-	PI 34:1;O2
868.5652	39.44	C46H82O9NP	[M+HCOO]-	PC 38:5;O
868.5698	41.83	C46H82O9NP	[M+HCOO]-	PC 38:5;O
868.606	54.58	C48H88O10NP	[M-H]-	PC 40:4;O2
872.5393	49.62	C44H78O11NP	[M+HCOO]-	PC 36:5;O3
882.5494	34.14	C46H80O10NP	[M+HCOO]-	PC 38:6;O2
884.5644	37.99	C46H82O10NP	[M+HCOO]-	PC 38:5;O2
886.5795	39.25	C46H84O10NP	[M+HCOO]-	PC 38:4;O2

726.455	20.5	C34H68O10NP	[M+HCOO]-	PC O-26:1;O3
752.4726	33.09	C36H70O10NP	[M+HCOO]-	PC 28:1;O2
766.5148	47.29	C39H78O11NP	[M-H]-	PC 31:0;O3
766.5194	47.32	C39H78O11NP	[M-H]-	PC 31:0;O3

Supplementary Table 3: Complete list of oxidized lipids putatively annotated in plasma samples in positive and negative ESI mode.

mz	***Rt (sec)***	*formula*	***ion***	***species (lib_id)***	**mz**	***Rt (sec)***	*formula*	***ion***	***species (lib_id)***
568.3273	8.13	C26H50O10NP	[M+H]+	PC 18:1;O2	*929.743*	88.75	C55H102O9	[M+Na]+	TG 52:2;O3
694.4647	27.79	C35H68O10NP	[M+H]+	PC 27:1;O2	*890.7753*	82.21	C55H100O7	[M+NH4]+	TG 52:3;O
708.4818	32.8	C36H70O10NP	[M+H]+	PC 28:1;O2	*922.7675*	85.18	C55H100O9	[M+NH4]+	TG 52:3;O3
704.4476	20.74	C36H66O10NP	[M+H]+	PC 28:3;O2	*922.7712*	86.75	C55H100O9	[M+NH4]+	TG 52:3;O3
794.5641	49.55	C41H80O11NP	[M+H]+	PC 33:1;O3	*888.7626*	88.61	C55H98O7	[M+NH4]+	TG 52:4;O
824.6109	57	C43H86O11NP	[M+H]+	PC 35:0;O3	*888.7631*	80.81	C55H98O7	[M+NH4]+	TG 52:4;O
834.5865	46.13	C44H84O11NP	[M+H]+	PC 36:2;O3	*920.7487*	82.23	C55H98O9	[M+NH4]+	TG 52:4;O3
828.5479	43.36	C44H78O11NP	[M+H]+	PC 36:5;O3	*886.7442*	77.34	C55H96O7	[M+NH4]+	TG 52:5;O
848.6089	56.53	C45H86O11NP	[M+H]+	PC 37:2;O3	*885.7212*	99.65	C55H96O8	[M+H]+	TG 52:5;O2
858.5887	46.97	C46H84O11NP	[M+H]+	PC 38:4;O3	*902.7399*	71.76	C55H96O8	[M+NH4]+	TG 52:5;O2
782.5648	54.02	C44H80O8NP	[M+H]+	PC O-36:5;O	*945.7655*	86.78	C56H106O9	[M+Na]+	TG 53:1;O3
780.5495	50.03	C44H78O8NP	[M+H]+	PC O-36:6;O	*943.7523*	83.42	C56H104O9	[M+Na]+	TG 53:2;O3
808.5816	55.44	C46H82O8NP	[M+H]+	PC O-38:6;O	*954.8429*	99.52	C57H108O9	[M+NH4]+	TG 54:1;O3
968.7642	83.33	C56H106O9NP	[M+H]+	PC O-48:4;O2	*950.81*	93.17	C57H104O9	[M+NH4]+	TG 54:3;O3
752.5527	54.38	C39H78O10NP	[M+H]+	PE 34:0;O2	*916.7938*	84.05	C57H102O7	[M+NH4]+	TG 54:4;O
656.506	39.08	C37H66O8	[M+NH4]+	TG 34:2;O2	*948.7901*	87.12	C57H102O9	[M+NH4]+	TG 54:4;O3
672.5037	36.12	C37H66O9	[M+NH4]+	TG 34:2;O3	*948.7948*	90.67	C57H102O9	[M+NH4]+	TG 54:4;O3

688.5329	36.4	C38H70O9	[M+NH4]+	TG 35:1;O3
686.5198	39.12	C38H68O9	[M+NH4]+	TG 35:2;O3
682.5228	38.86	C39H68O8	[M+NH4]+	TG 36:3;O2
682.5242	38.74	C39H68O8	[M+NH4]+	TG 36:3;O2
712.5336	39.83	C40H70O9	[M+NH4]+	TG 37:3;O3
735.5315	82.37	C43H74O9	[M+H]+	TG 40:4;O3
740.6379	68.36	C44H82O7	[M+NH4]+	TG 41:1;O
738.6214	64.02	C44H80O7	[M+NH4]+	TG 41:2;O
770.6493	71.19	C45H84O8	[M+NH4]+	TG 42:1;O2
768.6385	66.1	C45H82O8	[M+NH4]+	TG 42:2;O2
768.6681	74.29	C46H86O7	[M+NH4]+	TG 43:1;O
766.6548	68.69	C46H84O7	[M+NH4]+	TG 43:2;O
764.6389	64.5	C46H82O7	[M+NH4]+	TG 43:3;O
796.6608	72.07	C47H86O8	[M+NH4]+	TG 44:2;O2
794.6498	66.28	C47H84O8	[M+NH4]+	TG 44:3;O2
799.6047	66.16	C47H84O8	[M+Na]+	TG 44:3;O2
794.6819	73	C48H88O7	[M+NH4]+	TG 45:2;O
794.6825	68.39	C48H88O7	[M+NH4]+	TG 45:2;O
792.6681	69.02	C48H86O7	[M+NH4]+	TG 45:3;O
771.6093	70.24	C48H82O7	[M+H]+	TG 45:5;O
769.593	64.49	C48H80O7	[M+H]+	TG 45:6;O
824.6946	75.01	C49H90O8	[M+NH4]+	TG 46:2;O2
822.6778	71.64	C49H88O8	[M+NH4]+	TG 46:3;O2
850.719	95.6	C51H92O8	[M+NH4]+	TG 48:3;O2
865.7224	93.45	C52H96O9	[M+H]+	TG 49:2;O3
908.7637	89.05	C54H98O9	[M+NH4]+	TG 51:3;O3
926.7923	89.35	C55H104O9	[M+NH4]+	TG 52:1;O3
926.8117	96.26	C55H104O9	[M+NH4]+	TG 52:1;O3
907.7687	97.35	C55H102O9	[M+H]+	TG 52:2;O3
924.7873	89.34	C55H102O9	[M+NH4]+	TG 52:2;O3
924.7959	92.95	C55H102O9	[M+NH4]+	TG 52:2;O3
914.7775	78.79	C57H100O7	[M+NH4]+	TG 54:5;O
929.743	88.75	C57H100O9	[M+H]+	TG 54:5;O3
946.7644	83.18	C57H100O9	[M+NH4]+	TG 54:5;O3
946.774	83.39	C57H100O9	[M+NH4]+	TG 54:5;O3
912.7569	77.14	C57H98O7	[M+NH4]+	TG 54:6;O
927.7227	84.86	C57H98O9	[M+H]+	TG 54:6;O3
944.7613	84.23	C57H98O9	[M+NH4]+	TG 54:6;O3
944.7626	83.37	C57H98O9	[M+NH4]+	TG 54:6;O3
943.7523	83.42	C58H102O9	[M+H]+	TG 55:5;O3
974.8072	92.22	C59H104O9	[M+NH4]+	TG 56:5;O3
972.7898	85.2	C59H102O9	[M+NH4]+	TG 56:6;O3
972.7941	88.77	C59H102O9	[M+NH4]+	TG 56:6;O3
604.324	6.32	C28H50O8NP	[M+HCOO]-	LPC 20:4;O
608.3176	14.6	C27H50O9NP	[M+HCOO]-	PC 19:2;O
694.431	23.85	C33H64O9NP	[M+HCOO]-	PC 25:1;O
722.4603	31.17	C35H68O9NP	[M+HCOO]-	PC 27:1;O
722.4603	31.17	C35H68O9NP	[M+HCOO]-	PC O-27:2;O2
750.5318	48.28	C39H78O10NP	[M-H]-	PC 31:0;O2
782.5326	*41.75*	*C43H78O9NP*	*[M-H]-*	*PC 35:4;O*
810.566	41.59	C45H82O9NP	[M-H]-	PC 37:4;O
810.566	41.59	C45H82O9NP	[M-H]-	PC O-37:5;O2
840.574	49.06	C46H84O10NP	[M-H]-	PC 38:4;O2
870.5842	41.11	C46H84O9NP	[M+HCOO]-	PC 38:4;O

References

(1) Kodali, S. T.; Kauffman, P.; Kotha, S. R.; Yenigalla, A.; Veeraraghavan, R.; Pannu, S. R.; Hund, T. J.; Satoskar, A. R.; McDaniel, J. C.; Maddipati, R. K.; Parinandi, N. L. Oxidative Lipidomics: Analysis of Oxidized Lipids and Lipid Peroxidation in Biological Systems with Relevance to Health and Disease; **2020**; pp 61–92. https://doi.org/10.1007/978-3-030-47318-1_5.

(2) Gosis, B. S.; Wada, S.; Thorsheim, C.; Li, K.; Jung, S.; Rhoades, J. H.; Yang, Y.; Brandimarto, J.; Li, L.; Uehara, K.; Jang, C.; Lanza, M.; Sanford, N. B.; Bornstein, M. R.; Jeong, S.; Titchenell, P. M.; Biddinger, S. B.; Arany, Z. Inhibition of Nonalcoholic Fatty Liver Disease in Mice by Selective Inhibition of MTORC1. *Science (1979)* **2022**, *376* (6590). https://doi.org/10.1126/science.abf8271.

(3) Watt, K. I.; Henstridge, D. C.; Ziemann, M.; Sim, C. B.; Montgomery, M. K.; Samocha-Bonet, D.; Parker, B. L.; Dodd, G. T.; Bond, S. T.; Salmi, T. M.; Lee, R. S.; Thomson, R. E.; Hagg, A.; Davey, J. R.; Qian, H.; Koopman, R.; El-Osta, A.; Greenfield, J. R.; Watt, M. J.; Febbraio, M. A.; Drew, B. G.; Cox, A. G.; Porrello, E. R.; Harvey, K. F.; Gregorevic, P. Yap Regulates Skeletal Muscle Fatty Acid Oxidation and Adiposity in Metabolic Disease. *Nat Commun* **2021**, *12* (1), 2887. https://doi.org/10.1038/s41467-021-23240-7.

(4) Sies, H.; Belousov, V. V.; Chandel, N. S.; Davies, M. J.; Jones, D. P.; Mann, G. E.; Murphy, M. P.; Yamamoto, M.; Winterbourn, C. Defining Roles of Specific Reactive Oxygen Species (ROS) in Cell Biology and Physiology. *Nat Rev Mol Cell Biol* **2022**, *23* (7), 499–515. https://doi.org/10.1038/s41580-022-00456-z.

(5) Tyurina, Y. Y.; Tyurin, V. A.; Anthonymuthu, T.; Amoscato, A. A.; Sparvero, L. J.; Nesterova, A. M.; Baynard, M. L.; Sun, W.; He, R.; Khaitovich, P.; Vladimirov, Y. A.; Gabrilovich, D. I.; Bayır, H.; Kagan, V. E. "Redox Lipidomics Technology: Looking for a Needle in a Haystack." *Chem Phys Lipids* **2019**, *221*, 93–107. https://doi.org/10.1016/j.chemphyslip.2019.03.012.

(6) Villaseñor, A.; Godzien, J.; Barker-Tejeda, T. C.; Gonzalez-Riano, C.; López-López, Á.; Dudzik, D.; Gradillas, A.; Barbas, C. Analytical Approaches for Studying Oxygenated Lipids in the Search of Potential Biomarkers by LC-MS. *TrAC Trends in Analytical Chemistry* **2021**, *143*, 116367. https://doi.org/10.1016/j.trac.2021.116367.

(7) Ni, Z.; Goracci, L.; Cruciani, G.; Fedorova, M. Computational Solutions in Redox Lipidomics – Current Strategies and Future Perspectives. *Free Radic Biol Med* **2019**, *144*, 110–123. https://doi.org/10.1016/j.freeradbiomed.2019.04.027.

(8) Ni, Z.; Angelidou, G.; Hoffmann, R.; Fedorova, M. LPPtiger Software for Lipidome-Specific Prediction and Identification of Oxidized Phospholipids from LC-MS Datasets. *Sci Rep* **2017**, *7* (1), 15138. https://doi.org/10.1038/s41598-017-15363-z.

(9) Aydın, A. F.; Bingül, İ.; Küçükgergin, C.; Doğan-Ekici, I.; Doğru Abbasoğlu, S.; Uysal, M. Carnosine Decreased Oxidation and Glycation Products in Serum and Liver of High-fat Diet and Low-dose Streptozotocin-induced Diabetic Rats. *Int J Exp Pathol* **2017**, *98* (5), 278–288. https://doi.org/10.1111/iep.12252.

(10) Feehan, J.; Hariharan, R.; Buckenham, T.; Handley, C.; Bhatnagar, A.; Baba, S. P.; de Courten, B. Carnosine as a Potential Therapeutic for the Management of Peripheral Vascular Disease. *Nutrition, Metabolism and Cardiovascular Diseases* **2022**, *32* (10), 2289–2296. https://doi.org/10.1016/j.numecd.2022.07.006.

(11) Baye, E.; Ukropcova, B.; Ukropec, J.; Hipkiss, A.; Aldini, G.; de Courten, B. Physiological and Therapeutic Effects of Carnosine on Cardiometabolic Risk and Disease. *Amino Acids* **2016**, *48* (5), 1131–1149. https://doi.org/10.1007/s00726-016-2208-1.

(12) Menon, K.; Cameron, J. D.; de Courten, M.; de Courten, B. Use of Carnosine in the Prevention of Cardiometabolic Risk Factors in Overweight and Obese Individuals: Study Protocol for a Randomised, Double-Blind Placebo-Controlled Trial. *BMJ Open* **2021**, *11* (5), e043680. https://doi.org/10.1136/bmjopen-2020-043680.

(13) Radrezza, S.; Carini, M.; Baron, G.; Aldini, G.; Negre-Salvayre, A.; D'Amato, A. Study of Carnosine's Effect on Nude Mice Skin to Prevent UV-A Damage. *Free Radic Biol Med* **2021**, *173*, 97–103. https://doi.org/10.1016/j.freeradbiomed.2021.07.010.

(14) Zoanni, B.; Aiello, G.; Negre-Salvayre, A.; Aldini, G.; Carini, M.; D'Amato, A. Lipidome Investigation of Carnosine Effect on Nude Mice Skin to Prevent UV-A Damage. *Int J Mol Sci* **2023**, *24* (12), 10009. https://doi.org/10.3390/ijms241210009.

(15) Aiello, G.; Rescigno, F.; Meloni, M.; Zoanni, B.; Aldini, G.; Carini, M.; D'Amato, A. The Effect of Carnosine on UVA-Induced Changes in Intracellular Signaling of Human Skin Fibroblast Spheroids. *Antioxidants* **2023**, *12* (2), 300. https://doi.org/10.3390/antiox12020300.

(16) de Courten, B.; Jakubova, M.; de Courten, M. P.; Kukurova, I. J.; Vallova, S.; Krumpolec, P.; Valkovic, L.; Kurdiova, T.; Garzon, D.; Barbaresi, S.; Teede, H. J.; Derave, W.; Krssak, M.; Aldini, G.; Ukropec, J.; Ukropcova, B. Effects of Carnosine Supplementation on Glucose Metabolism: Pilot Clinical Trial. *Obesity* **2016**, *24* (5), 1027–1034. https://doi.org/10.1002/oby.21434.

(17) Wang, Q.; Tripodi, N.; Valiukas, Z.; Bell, S. M.; Majid, A.; de Courten, B.; Apostolopoulos, V.; Feehan, J. The Protective Role of Carnosine against Type 2 Diabetes-induced Cognitive Impairment. *Food Sci Nutr* **2024**, *12* (6), 3819–3833. https://doi.org/10.1002/fsn3.4077.

(18) Chambers, M. C.; Maclean, B.; Burke, R.; Amodei, D.; Ruderman, D. L.; Neumann, S.; Gatto, L.; Fischer, B.; Pratt, B.; Egertson, J.; Hoff, K.; Kessner, D.; Tasman, N.; Shulman, N.; Frewen, B.; Baker, T. A.; Brusniak, M.-Y.; Paulse, C.; Creasy, D.; Flashner, L.; Kani, K.; Moulding, C.; Seymour, S. L.; Nuwaysir, L. M.; Lefebvre, B.; Kuhlmann, F.; Roark, J.; Rainer, P.; Detlev, S.; Hemenway, T.; Huhmer, A.; Langridge, J.; Connolly, B.; Chadick, T.; Holly, K.; Eckels, J.; Deutsch, E. W.; Moritz, R. L.; Katz, J. E.; Agus, D. B.; MacCoss, M.; Tabb, D. L.; Mallick, P. A Cross-Platform Toolkit for Mass Spectrometry and Proteomics. *Nat Biotechnol* **2012**, *30* (10), 918–920. https://doi.org/10.1038/nbt.2377.

(19) Delabriere, A.; Warmer, P.; Brennsteiner, V.; Zamboni, N. SLAW: A Scalable and Self-Optimizing Processing Workflow for Untargeted LC-MS. *Anal Chem* **2021**, *93* (45), 15024–15032. https://doi.org/10.1021/acs.analchem.1c02687.

(20) GraphPad. *https://www.graphpad.com/*.

(21) Lange, M.; Angelidou, G.; Ni, Z.; Criscuolo, A.; Schiller, J.; Blüher, M.; Fedorova, M. AdipoAtlas: A Reference Lipidome for Human White Adipose Tissue. *Cell Rep Med* **2021**, *2* (10), 100407. https://doi.org/10.1016/j.xcrm.2021.100407.

(22) Ito, F.; Ito, T. High-Density Lipoprotein (HDL) Triglyceride and Oxidized HDL: New Lipid Biomarkers of Lipoprotein-Related Atherosclerotic Cardiovascular Disease. *Antioxidants* **2020**, *9* (5), 362. https://doi.org/10.3390/antiox9050362.

(23) Shearer, G. C.; Newman, J. W. Lipoprotein Lipase Releases Esterified Oxylipins from Very Low-Density Lipoproteins. *Prostaglandins Leukot Essent Fatty Acids* **2008**, *79* (6), 215–222. https://doi.org/10.1016/j.plefa.2008.09.023.

(24) Do, Q.; Xu, L. How Do Different Lipid Peroxidation Mechanisms Contribute to Ferroptosis? *Cell Rep Phys Sci* **2023**, *4* (12), 101683. https://doi.org/10.1016/j.xcrp.2023.101683.

(25) de Vos, L. C.; Lefrandt, J. D.; Dullaart, R. P. F.; Zeebregts, C. J.; Smit, A. J. Advanced Glycation End Products: An Emerging Biomarker for Adverse Outcome in Patients with Peripheral Artery Disease. *Atherosclerosis* **2016**, *254*, 291–299. https://doi.org/10.1016/j.atherosclerosis.2016.10.012.

CHAPTER 6:
STRUCTURAL ELUCIDATION OF ENDOGENOUS OXIDIZED LIPIDS USING ADVANCED MS APPROACHES

Summary

Conventional fragmentation methods, such as collisional-induced dissociation (CID), struggle to accurately pinpoint the positions of oxygen and double bonds in lipid molecules. To better characterize modified lipids, alternative fragmentation techniques can be used. Among these, electron-activated dissociation (EAD) stands out, as it allows the comprehensive structural elucidation of different lipid classes by generating unique fragment ions essential for detailed lipid analysis.

In this study, oxidized lipids identified in the previous chapter were selected to generate an inclusion list to be monitored through a scheduled MRM^{HR} experiment using the EAD fragmentation mode on the ZenoTOF 7600 system to derive deeper structural information.

Background

The structural elucidation of lipid molecules has traditionally been a complex and multi-step process involving diverse characterization methods. In the MS field, Collision-induced dissociation (CID) is the most widely used fragmentation method for lipids identification and typically allows annotation of the headgroup, the lengths of acyl chains, and the number of double bonds along the acyl chains.

However, the data produced using CID preclude the information needed to resolve the structure of lipid species, leaving gaps in fully resolving lipids at an in-depth structural level, including the assignment of the double bond positions along the acyl chain and their cis/trans isoforms, the regioisomerism or the precise site of oxidation.

A more detailed understanding of lipid structures is crucial because lipids play a key role in various biological functions, and small structural differences in isomeric lipid molecules can seriously affect their functions. For example, a shift in the double bond position from $\Delta 7$ to $\Delta 9$ in a phospholipid has been proposed as a potential biomarker for breast cancer [1], and changes in the sn-1 and sn-2 positions of the acyl chain may serve as a urinary biomarker for prostate cancer[2]. Similarly, changes in the double bond positions of certain TGs have been correlated with cardiometabolic outcomes. At the same time, knowing the precise location of oxidative modifications in oxidized lipids

could help to clarify the biological function of these modified lipids, particularly in the context of metabolic diseases, including obesity.

Fully characterizing the lipidome with a single lipidomic approach is challenging, and in mass spectrometry, multiple methods are often required to achieve comprehensive lipid identification. To address these limitations, electron-activated dissociation (EAD) has emerged as a powerful alternative dissociation method for singly charged ions[3]. EAD provides unique fragmentation patterns that are not possible with CID, thus extending the level of structural information obtained within a single MS experiment.

In EAD, positively charged lipids interact with electron beams of kinetic energy, typically around 10-20 eV, which excite them by energy absorption. This excitation leads to rich fragmentations in lipid bonds, allowing for the formation of specific diagnostic fragments, including those crucial for pinpointing the location of double bonds within the acyl chain, cis/trans isomerism and the site of lipid modification in complex lipids[4,5]. Recent advances, such as the integration of EAD into the ZenoTOF 7600 system[6] on an LC timescale, have made comprehensive characterization of complex lipidomes to be more compatible with routine lipid analysis. This technique has been successfully applied to single-class and total lipid analysis[7–10].

In this study, we applied a semi-targeted data-dependent acquisition (DDA) method based on EAD fragmentation to further investigate the structural characteristics of complex oxidized lipids annotated in the plasma and liver samples. To do that, the oxidized lipids identified in Chapter 5 were used to generate an inclusion list to be monitored through a scheduled MRM^{HR} experiment on the ZenoTOF 7600 system.

Materials and Methods

LC-MS Analysis

Sample preparation is described in Chapter 4. Pooled QC samples of plasma and liver lipid extracts were resuspended in 80µl of IPA: MeOH 50:50 v/v% and 2µl were injected into the LC-MS system. Separation was performed on an Agilent 1290 Infinity II LC system, including a binary pump manager, equipped with an ACQUITY UPLC BEH C18 reversed-phase column (30 mm x 2.1 mm x 1.7 µm). During separation, the column temperature was maintained at 60°C and the flow rate was set at 1.2 mL/min. Lipid

classes were separated by a 2.4 min gradient elution using the chromatographic gradient already described in Chapter 4.

The MS analysis was done on the ZenoToF 7600 system (SCIEX) operating in high-resolution multiple reaction monitoring (MRM^{HR}) EAD mode. Samples were ionized with the TurboIonSpray and analyzed using information-dependent acquisition (IDA) top2 in positive ion mode. Data acquisition consisted of a full TOF-MS scan to collect accurate mass precursor ions and a TOF-MS/MS experiment for selective EAD fragmentation. MS parameters used for the EAD method are the following:

Source Parameters	***Value***
Ion Source Gas 1 (psi)	70
Ions source Gas 2 (psi)	70
Curtain Gas	45
Temperature (°C)	700
Stray Voltage	5500
MS Parameters	**Value**
Scan Type	TOF MS
Accumulation time (ms)	75
Declustering Potential (V)	60
Collision Energy (V)	10
Collision Energy Spread (V)	0
Range	50-1000
EAD MS Parameters	**Value**
Maximum candidate ion	2
*Inclusion list**	Inensity threshold 1000 cps
Retention time tolerance (s)	3
Accumulation time (s)	0.5
Electron Beam Current (nA)	7500
Electron Kinetic Energy (eV)	12
Time Bins to Sum	6
Reaction Time (ms)	30
Zeno trap	ON

Table 1: TOF MS and TOF MS/MS parameters

Raw Data Processing

All original wiff files were converted as centroided mzML files using the qtof peak picker component of msconvert (ProteoWizard v 3.0.9987)[11].The converted files were then fed to SLAW[12] to generate mgf files containing all representative MS/MS spectra acquired

by DDA. Downstream analysis, such as CID and EAD annotation, was performed using these .mgf files.

Results

For in-depth structural elucidation of oxidized lipids, I applied a semi-targeted EAD method on the Zeno 7600 QTOF system. For this purpose, the 124 oxidized lipids identified and manually confirmed in Chapter 5 (Supplementary Tables 1 and 2) were used to generate an RT-scheduled inclusion list for semi-targeted analysis. All the compounds were analyzed with a scheduled MRM^{HR} for optimal sensitivity. Two separate inclusion lists were created to avoid coeluting compounds that would be difficult to detect due to the limited MS scan time per ion feature.

The number of selected precursors over each RT period was controlled in terms of accumulation time, reaction time, and kinetic energy to ensure the collection of high-quality EAD spectra. These MS parameters are critical for the collection of informative EAD data in the LC-MS workflow. Indeed, from our previous works, it was found that the best conditions for generating high-quality diagnostic EAD peaks appear to be the lowest reaction time, set at 30 ms and with a high accumulation time of 500 ms[13]. Another critical factor for EAD acquisition is the appropriate kinetic energy, which can be tuned between 10 and 25 eV. For this study, it was kept constant at 12 eV for all analytes on the inclusion list. Each pooled QC sample from liver and plasma matrices was therefore run using this optimized workflow to obtain EAD spectra of isolated precursor ions of the oxidized lipid in protonated, ammoniated and sodiated forms.

As with CID in Chapter 5, the process of annotation of oxidized lipids in the EAD mode followed sequential and specialized steps based on different levels of structural information[14]. I initially determined the head group, the lengths of the acyl chains and the number of double bonds between the acyl chains to ensure that the fragments generated by EAD could provide at least the same level of structural information as that obtained by CID annotation [15.] Next, I used the EAD-specific peaks to confidently identify lipid species.

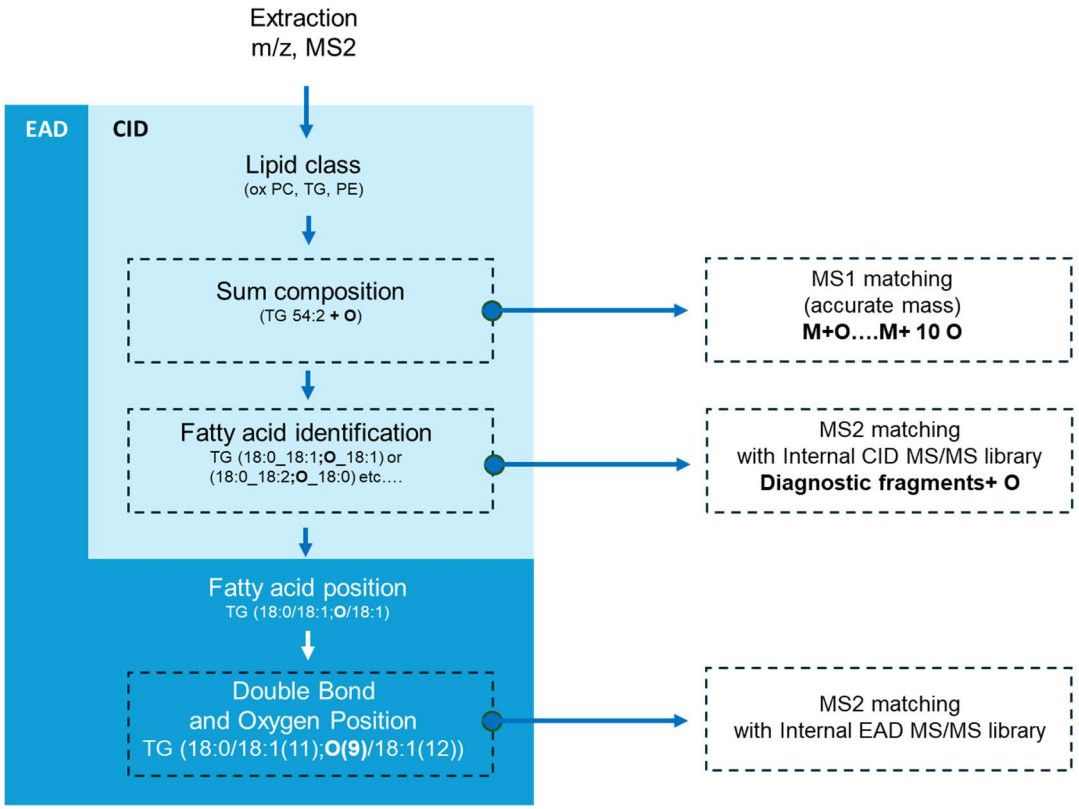

Figure 1: Hierarchical annotation workflow for EAD spectra.

Identifying lipid head groups and distinguishing regioisomers

The first step in our work was therefore to search for fragments to identify lipid classes and acyl chains. As EAD is typically performed in positive ion mode, this step focused on identifying neutral losses and acyl fragments corresponding to fatty acids.

In the case of oxidized triglycerides (oxTG), two primary types of product ions are generated. As for CID, the first type corresponds to neutral losses (NL) of acyl chains, while the second corresponds to the acylium ion and acylium ions plus 74 Da, which generates from a loss of a neutral ketene containing one of the two remaining fatty acyl chains. As shown in Figure 2, in the EAD MS/MS spectra, for ox TG (16:0_18:0_18:3 (+ O)), I observed the fragment ions m/z 615.4985, m/z 589.4830 and 576.5119, which are due to the NL of FA 16:0, FA 18:1 and FA 18:3+O, respectively. Moreover, the acylium ions for unmodified acyl chains of oxTG appear at m/z 239.2369 (16:0) and 265.2526 (18:1), while the acylium ion +74 was observed at m/z 313.2728 (16:0) and 339.2888 (18:1). These ion types are readily distinguishable in the EAD spectra, with the most abundant products found in the mass range of 300-350 Da. Interestingly, I also observed

the presence of oxidation at this level by detecting the acylium ion at m/z 277 (18:3+O) and its corresponding +74 ion.

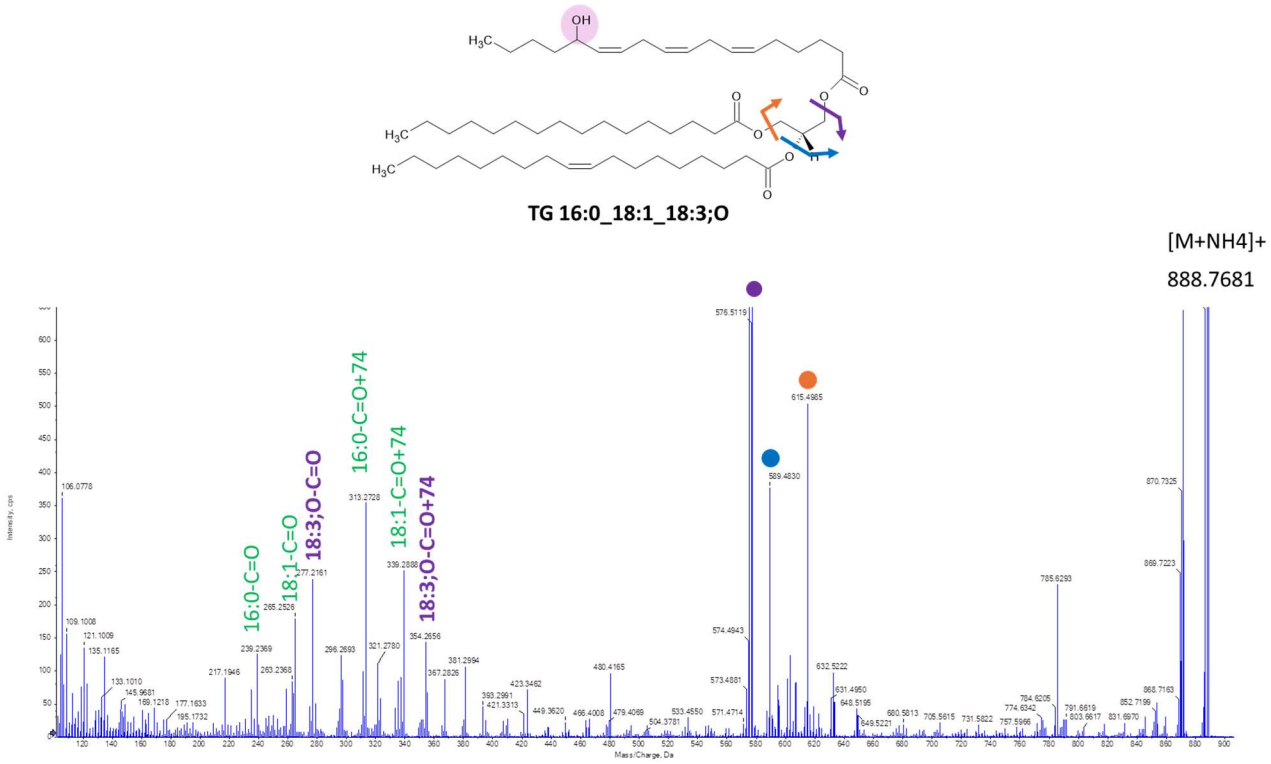

Figure 2: EAD spectra of ammoniated oxTG 16:0_18:1_18:3(+O). Two types of fragments generated can help to identify lipid class and acyl chain. The first type corresponds to neutral losses (NL) of the acyl chain from the parent ion. The second corresponds to the acylium ion and acylium ions plus 74 Da.

Similarly, in oxidized phospholipids (oxPL), signals corresponding to the acylium ion +74 at m/z 313.2732.2732 (16:0) and 341.2336.2336 (18:0) are identifiable (Figure 3 A and B, green fragments). Together with these, additional unique diagnostic fragment ions produced by EAD help to validate the headgroups and further characterize lipid species within these classes. For instance, in oxidized phosphatidylcholine (oxPC), I identified neutral losses of 59 Da and 183 Da from the precursor ion and the ion at m/z 184, all signals corresponding to the polar head of phosphatidylcholine. Moreover, for oxidized phosphatidylethanolamine (oxPE), the most abundant product ion formed by EAD is a neutral loss of 141 Da from the precursor ion.

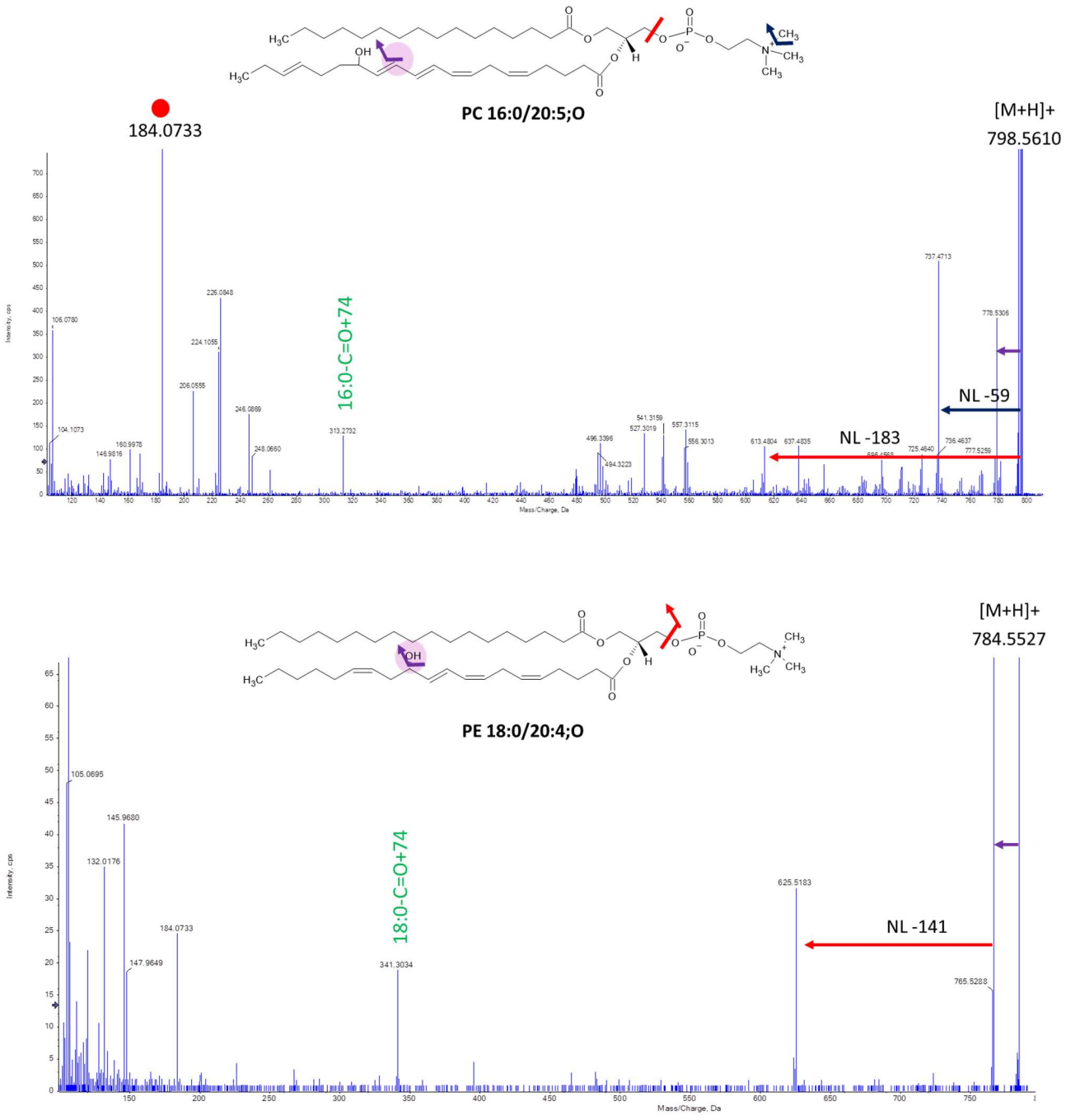

Figure 3: EAD MS/MS of oxPC and oxPE. Diagnostic fragment ions at m/z 184 (red) and neutral losses of 59 Da and 183 Da from the precursor ion identify the PC head group. Signals corresponding to the acylium ion +74 at m/z 313 (16:0) and 341 (18:0) are also identifiable. For oxPE, the most abundant product ion formed by EAD is a neutral loss of 141 Da from parent ion.

Inspection of the lower mass range signals can also reveal fragment ions that indicate sn-positions. Specifically, for oxPC the EAD spectra show two peaks of approximately equal intensity at m/z 224.1056 and 226.0838 (Figure 4). These ions correspond to the attachment points of the choline head group to the lipid backbone and are commonly recognized as C and O-type peaks. Importantly, when these fragments are detected, it is possible to determine all the sn-positions for oxidized phospholipids[16]. For example,

as shown in Figure 4, for oxPC 16:0/20:5(+O), I observed sn-1 diagnostic peaks for the acyl chain 16:0 at m/z 557.3115, 541.3159, 527.3019, confirming that the oxidized polyunsaturated fatty acids (PUFAs) 20:5(+O) occupy the sn-2 position. This position is the most reactive within the phospholipid structure and is most susceptible to ROS attack.[17]

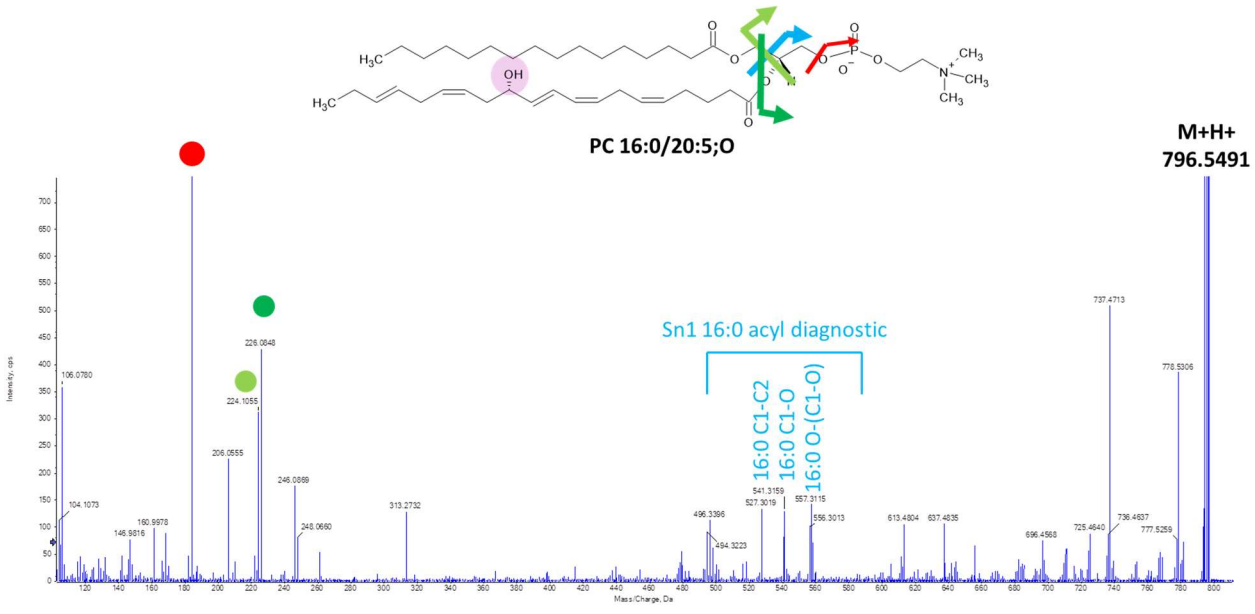

Figure 4: EAD MS/MS of oxPC. Diagnostic fragment ions of the glycerol backbone at m/z 224 and 226 (green) identify the phospholipid class. The sn-1 attachment point can be identified by examining the chain loss fragment ions in the range of 500-600 m/z (light blue).

For oxTG, the most characteristic ions corresponding to fragments indicating regioisomerism are generated within the range of 300-350 Da, as recently discussed by Baba *et al*. [18]. In particular, they highlighted that sodiated triglycerides produce the most informative fragments during fragmentation to derive information about regioisomerism. However, in our study most oxTGs were present as ammoniated species, which limited our ability to accurately verify this property for all annotated triglycerides.

Determining the Location of Double Bonds and Oxygen Positions

Next, I focused on identifying the locations of double bonds and oxygen within the acyl chains. EAD generates a rich set of fragments from the precursor ion that sequentially loses CH2 from the fatty acid backbone. These fragments typically cover the entire length of the fatty acid chains and help to confirm the position of unsaturation[7]. However,

these signals are generally less intense than other EAD fragments, and to display them clearly, the mass range corresponding to higher m/z values must be expanded.

For a saturated fatty acyl chain, such as that corresponding to 16:0 in oxPC in Figure 5, the EAD spectrum is characterized by sequential carbon losses from the precursor ion, clearly observed as fragment ions differing by CH2 (14 Da) along the acyl chain.

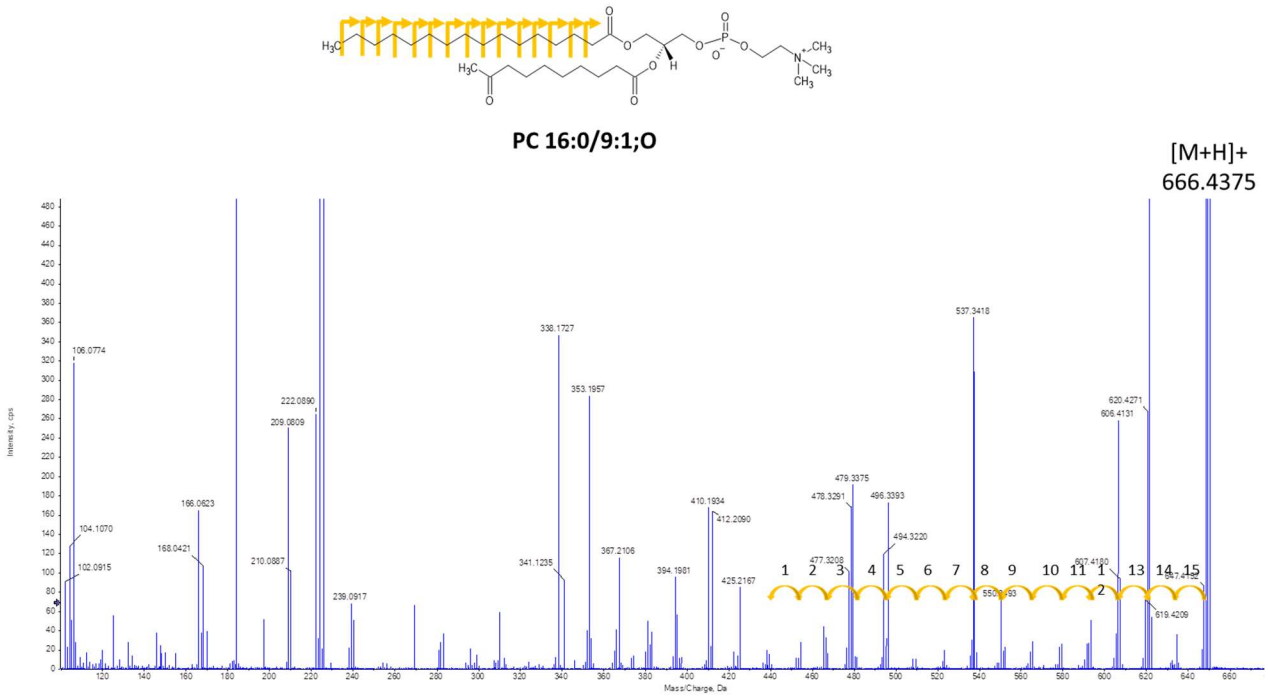

Figure 5: Determining double bond position. The EAD MS/MS spectrum for a saturated lipid is characterized by a series of sequential -CH2 carbon losses from the precursor ion. The colour coding in the spectrum indicates the origin of each fragment ion, helping to trace the breakdown of the precursor ion.

In the case of unsaturated fatty acyl chains, the expected cleavage peak is shifted by 2 Da due to a reduction of 2H (allylic cleavage) distributed between the two carbon atoms at the C=C bond. This results in two successive shorter shifts of the radical fragments in the spectrum of 12 Da instead of the usual 14 Da. As the abundance of fragments cleaved at the double bond is lower, it can sometimes be easier to determine the position of the double bond by noting the absence of a peak represented by a larger gap of 26 Da, which can appear in the spectrum as a typical V-shape[18]. However, this pattern is not always present, especially when the noise level is high or when the interference caused by fragmentation of other fatty acyl chains of the lipid is increased.

The situation becomes more complex when mapping multiple double bonds on the same acyl chain or multiple unsaturated chains within the same lipids. In these cases, manual

interpretation of the fragments becomes challenging, and reliance on automated solutions is required. However, there is a noticeable gap in the literature regarding dedicated software tools for this purpose. In response to this need, we recently showed how it is possible to do that by assigning scores to all the possible matched candidates[13]. We tested this scoring with either monounsaturated or polyunsaturated ox lipids fragmented at 12 eV, and for most of them, we obtained good preliminary results. For example, Figure 6 shows this in the case of TG (52:4(+O)). With this scoring, we successfully predicted the localization of double bonds, identifying the correct isomer for oxTG as TG (16:0/18:1(12)/18:3(5,8,13) (+O)).

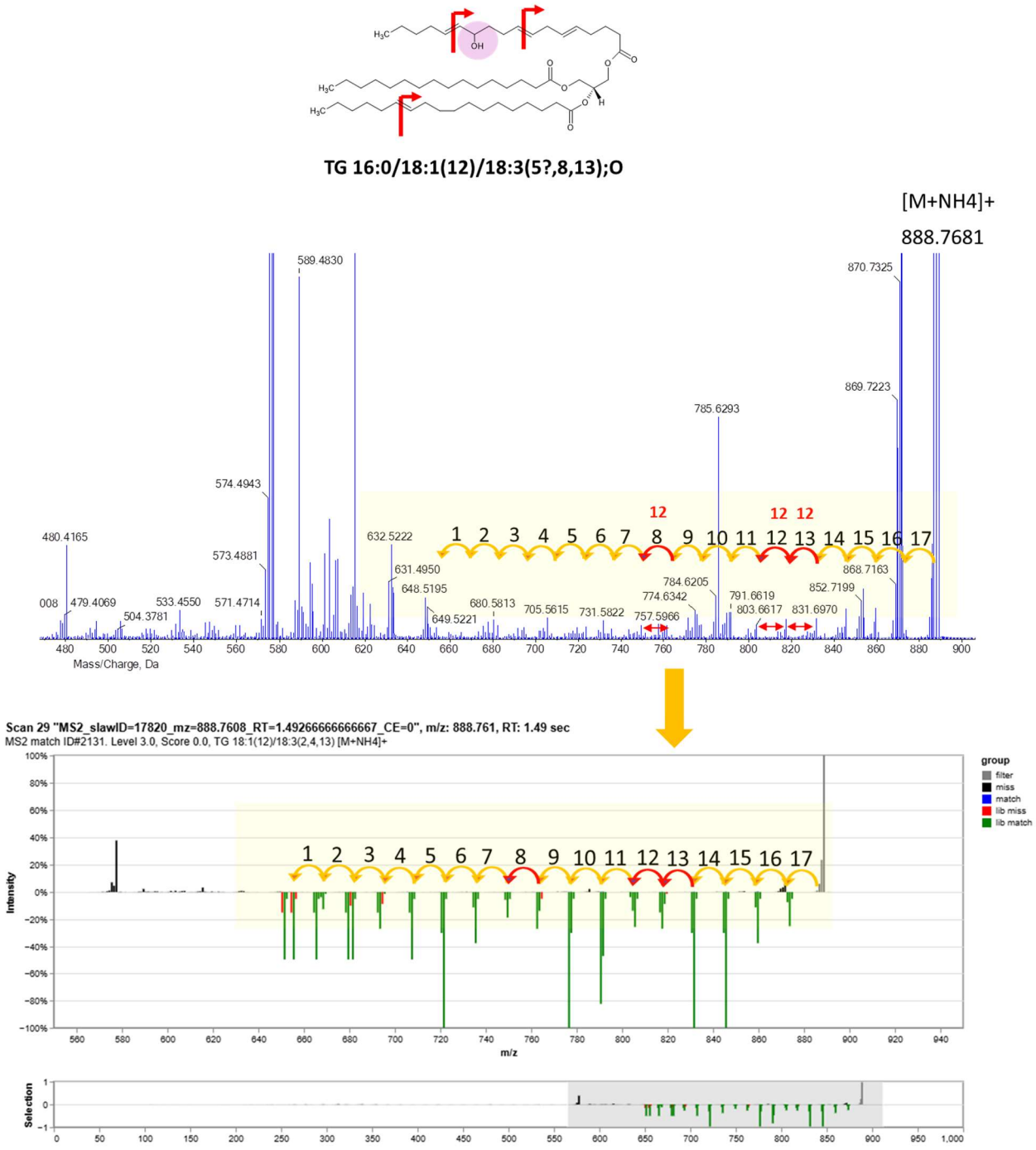

Figure 6: Determining double bond position. Putative annotation of TG (16:0/18:1(12)/18:3(5,8,13)(+O)).

We are extending the framework to simultaneously identify double bonds and oxidation sites within acyl chains. When oxygen is present on the acyl chain, the carbon atom bonded to the oxygen should show a shift of +16 Da compared to the theoretical fragmentation pattern. These fragments should also be more intense due to the stabilizing effect of oxygen on the radical.

From the manual inspection, I observed that these fragments can be easily identified for many of the monoxygenated lipids I annotated. For example, I found that for oxTG (16:0_18:8_18:1(+O)), the cleavage of the C-O bond produces two specific fragment ions (m/z 451.3784 and m/z 467.3726), both derived from the fragmentation of the ion at m/z 577.5182. These fragments confirm the presence of oxygen and allow us to localize its position within the acyl chain. In this case, the oxygen is located between C9 and C10. Following the same logic, I confirmed that it was also possible to identify fragments indicative of oxidation in oxPC.

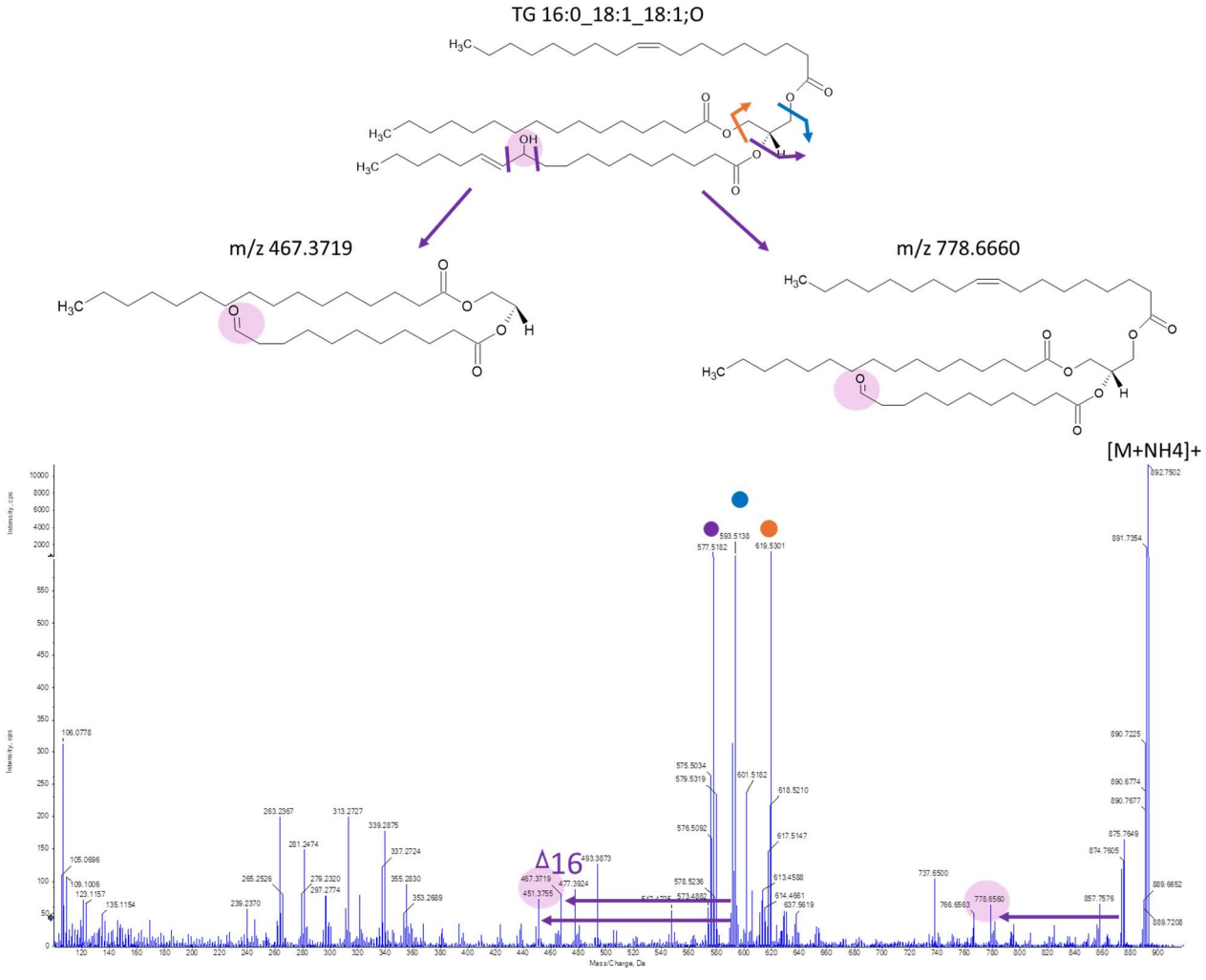

Figure 7: Determining oxygen position. For oxTG (16:0_18:8_18:1(+O)), EAD MS/MS fragmentation of the C-O bond results in two distinct fragment ions at m/z 451.3784 and m/z 467.3726, originating from the precursor ion at m/z 577.5182. The colour coding of these fragments highlights their respective origins from the precursor ion.

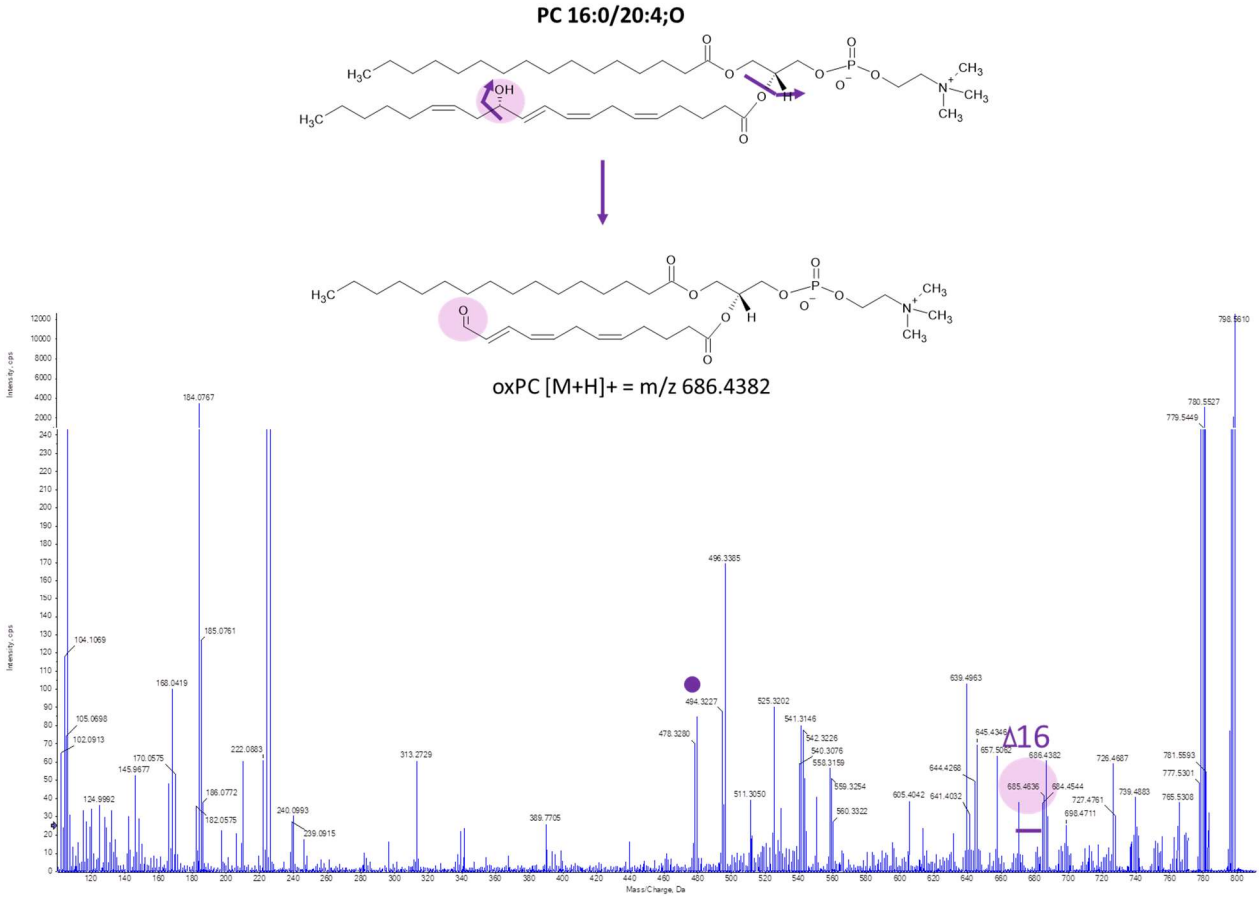

Figure 8: Determining oxygen position. For oxPC (16:0_20:4(+1O)), EAD MS/MS breakage of the C-O bond produces specific fragment ions at m/z 686.4382 from precursor ion.

Instead, for truncated lipids such as TG (9:1(+O)_16:0_18:1) and PC (16:0_9:1(+O)), I observed highly intense peaks corresponding to the loss of CHO (carbonyl – 29 Da) and COOH (carboxyl -41 Da) groups from the precursor ions, respectively, confirming the presence of oxygen as a carbonyl species (Figure 9).

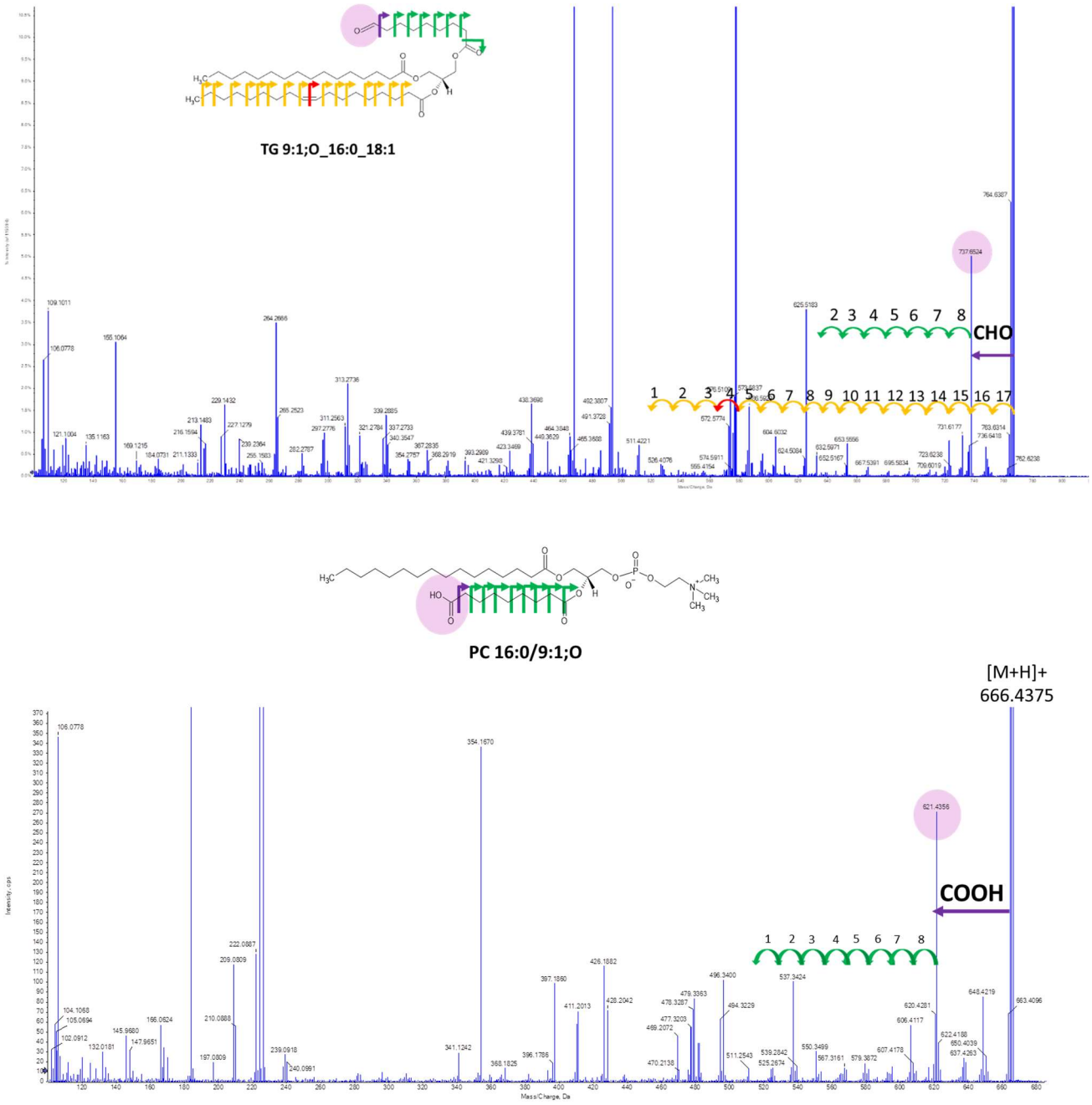

Figure 9: Determining oxygen position. EAD MS/MS fragmentation of truncated species generates losses of -29 and -41 from precursor ion.

Discussion

In this study, I used EAD fragmentation to validate previously annotated oxidized lipids and further improve their structural characterization beyond the molecular species level. To do that, each oxidized feature was monitored by a scheduled MRM experiment on the ZenoTOF 7600 system, which was applied to pooled QC samples of plasma and liver extracts.

Within a single MS experiment, EAD fragmentation produced distinct fragments that confirmed the lipid class, head group, fatty acid types, fatty acid attachment points (regioisomers), and double bond locations. In addition, EAD facilitated a more detailed understanding of oxidation modification types and sites, allowing us to precisely locate double bonds and oxidation products along the acyl chains. The optimal EAD parameters were a reaction time of 30 ms and an accumulation time of 500 ms, which produced the most diagnostic peaks. Importantly, these settings allowed us to take the advantage of EAD mode within a rapid 2.4-min LC-MS method, making it suitable for high-throughput lipidomic analysis. To our knowledge, this is the first time that EAD has been applied to the structural elucidation of oxidized lipids in complex biological matrices.

EAD is complementary to traditional fragmentation techniques when more detailed structural information is required. While the CID spectrum provided limited information for lipid species identification, EAD generated richer fragmentation patterns and improved the detection of low-abundant fragments, resulting in improved structural elucidation of the oxidized lipids.

While this approach is inherently suitable for the study of oxidized lipids with multiple unsaturated chains and, thus, presumably multiple oxidation products, the increasing complexity requires automated spectral interpretation to improve confidence in lipid identification. The ability to extract such information from real biological samples greatly enhances our understanding of the relationship between lipid structure and biological function. We believe deep structural characterization of each lipid molecule will be the next frontier in lipidomics. However, this remains a significant challenge that we are actively addressing to increase the impact of lipidomics in biomedical research. Firstly, the availability of software capable of handling this level of complexity is still limited. Even existing tools cannot fully exploit the breadth of diagnostic fragments generated by EAD. These fragments are far more abundant than those generated by other advanced fragmentation methods, such as ozonolysis or Paternò-Büchi reactions, and potentially contain a much greater depth of information. However, the extraction and interpretation of this information remain relatively underdeveloped, leaving considerable space for improvement in exploiting the potential of EAD for lipidomics.

Conclusion

The study demonstrates the potential of a fast 2.4-minute LC-MS method using a novel fragmentation technique, EAD, in ZenoTOF for the structural characterization of endogenous oxidized lipids. EAD can generate diagnostic peaks for oxidized lipid class, fatty acid composition, double bond and oxygen position on a fast LC-MS timescale.

Supplementary Tables

Supplementary Table 1: Inclusion list of oxidized lipids in the Liver matrix

mz	rt min	formula	ion	species	name
656.5076	0.638166667	C37H66O8	[M+NH4]+	TG 34:2;O2	TG 9:1;O_9:1;O_16:0
672.5033	0.604833333	C37H66O9	[M+NH4]+	TG 34:2;O3	TG 9:1;O_9:1;O2_16:0
686.5174	0.665333333	C38H68O9	[M+NH4]+	TG 35:2;O3	TG 9:1;O_10:1;O2_16:0
740.6344	1.155	C44H82O7	[M+NH4]+	TG 41:1;O	TG 9:1;O_16:0_16:0
764.6374	1.082166667	C46H82O7	[M+NH4]+	TG 43:3;O	TG 9:1;O_16:0_18:2
766.6497	1.158833333	C46H84O7	[M+NH4]+	TG 43:2;O	TG 9:1;O_16:0_18:1
770.6438	1.189	C45H84O8	[M+NH4]+	TG 42:1;O2	TG 10:1;O2_16:0_16:0
792.6703	1.152833333	C48H86O7	[M+NH4]+	TG 45:3;O	TG 9:1;O_18:1_18:1
794.651	1.118166667	C47H84O8	[M+NH4]+	TG 44:3;O2	TG 10:1;O2_16:0_18:2
822.6732	1.2025	C49H88O8	[M+NH4]+	TG 46:3;O2	TG 10:1;O2_18:1_18:1
836.7315	1.298833333	C51H94O7	[M+NH4]+	TG 48:2;O	TG 14:0_16:0_18:2;O
858.7127	1.356166667	C53H92O7	[M+NH4]+	TG 50:5;O	TG 16:0_16:1_18:4;O
860.7325	1.407333333	C53H94O7	[M+NH4]+	TG 50:4;O	TG 16:0_16:1_18:3;O
862.7445	1.334	C53H96O7	[M+NH4]+	TG 50:3;O	TG 16:0_16:1_18:2;O
864.7569	1.3995	C53H98O7	[M+NH4]+	TG 50:2;O	TG 16:0_16:1;O_18:1
867.7026	1.345166667	C55H94O7	[M+H]+	TG 52:6;O	TG 16:0_18:3_18:3;O
876.7633	1.3455	C54H98O7	[M+NH4]+	TG 51:3;O	TG 16:0_17:1_18:2;O
884.7282	1.357	C55H94O7	[M+NH4]+	TG 52:6;O	TG 16:0_18:2_18:4;O
886.7406	1.2525	C55H96O7	[M+NH4]+	TG 52:5;O	TG 16:1_18:2_18:2;O
886.7473	1.273666667	C55H96O7	[M+NH4]+	TG 52:5;O	TG 16:1;O_18:1_18:3
888.7608	1.475666667	C55H98O7	[M+NH4]+	TG 52:4;O	TG 16:0_18:1_18:3;O
890.7773	1.422166667	C55H100O7	[M+NH4]+	TG 52:3;O	TG 16:0_18:1_18:2;O
892.7901	1.461666667	C55H102O7	[M+NH4]+	TG 52:2;O	TG 16:0_18:1_18:1;O
904.7524	1.209666667	C55H98O8	[M+NH4]+	TG 52:4;O2	TG 16:0_18:2_18:2;O2
906.7719	1.272833333	C55H100O8	[M+NH4]+	TG 52:3;O2	TG 16:0_18:1_18:2;O2
912.7585	1.422833333	C57H98O7	[M+NH4]+	TG 54:6;O	TG 18:1_18:2_18:3;O
912.7596	1.258333333	C57H98O7	[M+NH4]+	TG 54:6;O	TG 18:2_18:2_18:2;O
914.7737	1.307833333	C57H100O7	[M+NH4]+	TG 54:5;O	TG 18:1_18:2_18:2;O
916.7882	1.3755	C57H102O7	[M+NH4]+	TG 54:4;O	TG 18:1_18:1_18:2;O
918.8044	1.354	C57H104O7	[M+NH4]+	TG 54:3;O	TG 18:1_18:1_18:1;O
928.8225	1.583333333	C55H106O9	[M+NH4]+	TG 52:0;O3	TG 15:0;O_18:0_19:0;O2
934.7798	1.490666667	C56H100O9	[M+NH4]+	TG 53:4;O3	TG 11:0;O2_18:2_24:2;O

936.7948	1.535333333	C56H102O9	[M+NH4]+	TG 53:3;O3	TG 16:1;O_18:2_19:0;O2
938.8724	1.7515	C58H112O7	[M+NH4]+	TG 55:0;O	TG 16:0_19:0_20:0;O
946.7795	1.442	C57H100O9	[M+NH4]+	TG 54:5;O3	TG 18:1;O_18:2_18:2;O2
650.4387	0.4035	C33H64O9NP	[M+H]+	PC 25:1;O	PC 16:0/9:1;O
666.4327	0.330333333	C33H64O10NP	[M+H]+	PC 25:1;O2	PC 16:0/9:1;O2
678.4698	0.484	C35H68O9NP	[M+H]+	PC 27:1;O	PC 18:0/9:1;O
714.4315	0.522833333	C37H64O10NP	[M+H]+	PE O-32:6;O3	PE O-10:0;O2_22:6;O
766.5334	0.836666667	C43H76O8NP	[M+H]+	PE O-38:6;O	PE O-26:5_12:1;O
772.5458	0.7085	C42H78O9NP	[M+H]+	PC 34:3;O	PC 16:0/18:3;O
784.5488	0.707833333	C43H78O9NP	[M+H]+	PE 38:4;O	PE 10:1;O_28:3
796.5476	0.617166667	C44H78O9NP	[M+H]+	PC 36:5;O	PC 16:0/20:5;O
798.5623	0.666666667	C44H80O9NP	[M+H]+	PC 36:4;O	PC 16:0/20:4;O
826.593	0.780833333	C46H84O9NP	[M+H]+	PC 38:4;O	PC 18:0/20:4;O
830.5546	0.706166667	C44H80O11NP	[M+H]+	PC 36:4;O3	PC 26:4;O/10:0;O2
854.5539	0.679166667	C46H80O11NP	[M+H]+	PC 38:6;O3	PC 28:5;O/10:1;O2

Supplementary Table 2: Inclusion list of oxidized lipids in the Plasma matrix

mz	rt min	formula	ion	species	name
568.3273	0.1355	C26H50O10NP	[M+H]+	PC 18:1;O2	PC 9:1;O/9:0;O
656.506	0.651333	C37H66O8	[M+NH4]+	TG 34:2;O2	TG 9:1;O_9:1;O_16:0
672.5037	0.602	C37H66O9	[M+NH4]+	TG 34:2;O3	TG 9:1;O_9:1;O2_16:0
682.5228	0.647667	C39H68O8	[M+NH4]+	TG 36:3;O2	TG 9:1;O_9:1;O_18:1
686.5198	0.652	C38H68O9	[M+NH4]+	TG 35:2;O3	TG 9:1;O_10:1;O2_16:0
704.4476	0.345667	C36H66O10NP	[M+H]+	PC 28:3;O2	PC 20:3/8:0;O2
738.6214	1.067	C44H80O7	[M+NH4]+	TG 41:2;O	TG 9:1;O_16:0_16:1
740.6379	1.139333	C44H82O7	[M+NH4]+	TG 41:1;O	TG 9:1;O_16:0_16:0
764.6389	1.075	C46H82O7	[M+NH4]+	TG 43:3;O	TG 9:1;O_16:0_18:2
766.6548	1.144833	C46H84O7	[M+NH4]+	TG 43:2;O	TG 9:1;O_16:0_18:1
768.6385	1.101667	C45H82O8	[M+NH4]+	TG 42:2;O2	TG 10:1;O2_16:0_16:1
768.6681	1.238167	C46H86O7	[M+NH4]+	TG 43:1;O	TG 9:1;O_16:0_18:0
770.6493	1.1865	C45H84O8	[M+NH4]+	TG 42:1;O2	TG 10:1;O2_16:0_16:0
792.6681	1.150333	C48H86O7	[M+NH4]+	TG 45:3;O	TG 9:1;O_18:1_18:1
794.6498	1.104667	C47H84O8	[M+NH4]+	TG 44:3;O2	TG 10:1;O2_16:0_18:2
794.6819	1.216667	C48H88O7	[M+NH4]+	TG 45:2;O	TG 11:1;O_16:0_18:1
794.6825	1.139833	C48H88O7	[M+NH4]+	TG 45:2;O	TG 9:1;O_18:0_18:1
796.6608	1.201167	C47H86O8	[M+NH4]+	TG 44:2;O2	TG 10:1;O2_16:0_18:1
822.6778	1.194	C49H88O8	[M+NH4]+	TG 46:3;O2	TG 10:1;O2_18:1_18:1
824.6946	1.250167	C49H90O8	[M+NH4]+	TG 46:2;O2	TG 12:1;O2_16:0_18:1
828.5479	0.722667	C44H78O11NP	[M+H]+	PC 36:5;O3	PC 14:0;O2/22:5;O
886.7442	1.289	C55H96O7	[M+NH4]+	TG 52:5;O	TG 16:0_18:2_18:3;O
888.7626	1.476833	C55H98O7	[M+NH4]+	TG 52:4;O	TG 16:0_18:1_18:3;O
888.7631	1.346833	C55H98O7	[M+NH4]+	TG 52:4;O	TG 16:0_18:2_18:2;O
890.7753	1.370167	C55H100O7	[M+NH4]+	TG 52:3;O	TG 16:0_18:1_18:2;O

902.7399	1.196	C55H96O8	[M+NH4]+	TG 52:5;O2	TG 16:0_18:2_18:3;O2
912.7569	1.285667	C57H98O7	[M+NH4]+	TG 54:6;O	TG 18:2_18:2_18:2;O
914.7775	1.313167	C57H100O7	[M+NH4]+	TG 54:5;O	TG 18:1_18:2_18:2;O
916.7938	1.400833	C57H102O7	[M+NH4]+	TG 54:4;O	TG 16:0_18:1_20:3;O
924.7873	1.489	C55H102O9	[M+NH4]+	TG 52:2;O3	TG 16:1_18:0;O_18:1;O2
944.7613	1.403833	C57H98O9	[M+NH4]+	TG 54:6;O3	TG 14:1;O2_18:2_22:3;O
946.7644	1.386333	C57H100O9	[M+NH4]+	TG 54:5;O3	TG 18:1;O_18:2_18:2;O2

References

(1) Perrotti, F.; Rosa, C.; Cicalini, I.; Sacchetta, P.; Del Boccio, P.; Genovesi, D.; Pieragostino, D. Advances in Lipidomics for Cancer Biomarkers Discovery. *Int J Mol Sci* **2016***, 17* (12), 1992. https://doi.org/10.3390/ijms17121992.

(2) Ma, X.; Chong, L.; Tian, R.; Shi, R.; Hu, T. Y.; Ouyang, Z.; Xia, Y. Identification and Quantitation of Lipid C=C Location Isomers: A Shotgun Lipidomics Approach Enabled by Photochemical Reaction. *Proceedings of the National Academy of Sciences* **2016**, *113* (10), 2573–2578. https://doi.org/10.1073/pnas.1523356113.

(3) Baba, T.; Campbell, J. L.; Le Blanc, J. C. Y.; Hager, J. W.; Thomson, B. A. Electron Capture Dissociation in a Branched Radio-Frequency Ion Trap. *Anal Chem* **2015**, *87* (1), 785–792. https://doi.org/10.1021/ac503773y.

(4) Baba, T.; Campbell, J. L.; Le Blanc, J. C. Y.; Baker, P. R. S. Structural Identification of Triacylglycerol Isomers Using Electron Impact Excitation of Ions from Organics (EIEIO). *J Lipid Res* **2016**, *57* (11), 2015–2027. https://doi.org/10.1194/jlr.M070177.

(5) Baba, T.; Campbell, J. L.; Le Blanc, J. C. Y.; Baker, P. R. S. In-Depth Sphingomyelin Characterization Using Electron Impact Excitation of Ions from Organics and Mass Spectrometry. *J Lipid Res* **2016**, *57* (5), 858–867. https://doi.org/10.1194/jlr.M067199.

(6) Campbell, J. L.; Baba, T. Near-Complete Structural Characterization of Phosphatidylcholines Using Electron Impact Excitation of Ions from Organics*. Anal Chem* **2015**, *87* (11), 5837–5845. https://doi.org/10.1021/acs.analchem.5b01460.

(7) Baba, T.; Campbell, J. L.; Le Blanc, J. C. Y.; Baker, PaulR. S.; Ikeda, K. Quantitative Structural Multiclass Lipidomics Using Differential Mobility: Electron Impact Excitation of Ions from Organics (EIEIO) Mass Spectrometry. *J Lipid Res* **2018**, *59* (5), 910–919. https://doi.org/10.1194/jlr.D083261.

(8) Baba, T.; Campbell, J. L.; Le Blanc, J. C. Y.; Baker, P. R. S. Structural Identification of Triacylglycerol Isomers Using Electron Impact Excitation of Ions from Organics (EIEIO). *J Lipid Res* **2016**, *57* (11), 2015–2027. https://doi.org/10.1194/jlr.M070177.

(9) Baba, T.; Campbell, J. L.; Le Blanc, J. C. Y.; Baker, P. R. S. In-Depth Sphingomyelin Characterization Using Electron Impact Excitation of Ions from Organics and Mass Spectrometry. *J Lipid Res* **2016**, *57* (5), 858–867. https://doi.org/10.1194/jlr.M067199.

(10) Campbell, J. L.; Baba, T. Near-Complete Structural Characterization of Phosphatidylcholines Using Electron Impact Excitation of Ions from Organics. *Anal Chem* **2015**, *87* (11), 5837–5845. https://doi.org/10.1021/acs.analchem.5b01460.

(11) Chambers, M. C.; Maclean, B.; Burke, R.; Amodei, D.; Ruderman, D. L.; Neumann, S.; Gatto, L.; Fischer, B.; Pratt, B.; Egertson, J.; Hoff, K.; Kessner, D.; Tasman, N.; Shulman, N.; Frewen, B.; Baker, T. A.; Brusniak, M.-Y.; Paulse, C.; Creasy, D.; Flashner, L.; Kani, K.; Moulding, C.; Seymour, S. L.; Nuwaysir, L. M.; Lefebvre, B.; Kuhlmann, F.; Roark, J.; Rainer, P.; Detlev, S.; Hemenway, T.; Huhmer, A.; Langridge, J.; Connolly, B.; Chadick, T.; Holly, K.; Eckels, J.; Deutsch, E. W.; Moritz, R. L.; Katz, J. E.; Agus, D. B.; MacCoss, M.; Tabb, D. L.; Mallick, P. A Cross-Platform Toolkit for Mass Spectrometry and Proteomics. *Nat Biotechnol* **2012**, *30* (10), 918–920. https://doi.org/10.1038/nbt.2377.

(12) Delabriere, A.; Warmer, P.; Brennsteiner, V.; Zamboni, N. SLAW: A Scalable and Self-Optimizing Processing Workflow for Untargeted LC-MS. *Anal Chem* **2021**, *93* (45), 15024–15032. https://doi.org/10.1021/acs.analchem.1c02687.

(13) Zamboni, N. On the benefits and role of electron-induced dissociation in lipidomics. https://metabolomics.blog/2024/04/ead-and-lipidomics/.

(14) Zhang, W.; Jian, R.; Zhao, J.; Liu, Y.; Xia, Y. Deep-Lipidotyping by Mass Spectrometry: Recent Technical Advances and Applications. *J Lipid Res* **2022**, *63* (7), 100219. https://doi.org/10.1016/j.jlr.2022.100219.

(15) Baba, T.; Campbell, J. L.; Le Blanc, J. C. Y.; Baker, PaulR. S.; Ikeda, K. Quantitative Structural Multiclass Lipidomics Using Differential Mobility: Electron Impact Excitation of Ions from Organics (EIEIO) Mass Spectrometry. *J Lipid Res* **2018**, *59* (5), 910–919. https://doi.org/10.1194/jlr.D083261.

(16) Campbell, J. L.; Baba, T. Near-Complete Structural Characterization of Phosphatidylcholines Using Electron Impact Excitation of Ions from Organics. *Anal Chem* **2015**, *87* (11), 5837–5845. https://doi.org/10.1021/acs.analchem.5b01460.

(17) Han, X. Lipidomics: Comprehensive Mass Spectrometry of Lipids; 2016.

(18) Baba, T.; Campbell, J. L.; Le Blanc, J. C. Y.; Baker, P. R. S. Structural Identification of Triacylglycerol Isomers Using Electron Impact Excitation of Ions from Organics (EIEIO). *J Lipid Res* **2016**, *57* (11), 2015–2027. https://doi.org/10.1194/jlr.M070177.

CONCLUDING REMARKS

The results presented in this thesis demonstrated the potential of MS-untargeted lipidomic approaches to address lipidome (and epilipidome) changes and to guide future research on the role of lipids in biological systems, both in physiological and pathological conditions or upon drug treatment.

For this project, I used lipidomics to address different biological and analytical questions. Our initial focus was on the application of lipidomics to phenotypic screening drug discovery in *in vitro* cellular systems. In this setup, I tested several compounds, primarily derived from natural sources, for their potential effects on fatty liver disease. The results obtained in the studies presented led us to highlight the utility of omics approaches to make hypotheses on the mechanisms of action which could help to explain the observed phenotypic effects. This was the first time in our lab that multi-omics strategies were applied to the study of natural extracts.

In the second part of the project, I have shown that fast UHPLC-MS lipidomics methods are suitable for screening lipid profiles in biological matrices of different natures in *in vivo* systems, offering wide coverage and reliable and accurate annotation of lipid molecular species. Moreover, I demonstrated that lipidomics could also support the study of oxidative modifications and that this information could be coupled with advanced MS methods for the full structural characterization of lipid molecular species.

Overall, our findings justify the extensive effort invested and highlight the importance of lipidomics in biomedical research. The comprehensive analytical description of lipidomes could help to add new layers of information about biological systems. In combination with other omics sciences, lipidomics can support the identification of new biomarkers and the discovery of new drugs. This represents the starting point for the future perspective of the project, where multiple omics (i.e. proteomics and metabolomics) can be integrated to gain more comprehensive insights into biological systems.

SCIENTIFIC CONTRIBUTIONS

Publications

- **Zoanni, B**.; Aiello, G.; Negre-Salvayre, A.; Aldini, G.; Carini, M.; D'Amato, A. Lipidome Investigation of Carnosine Effect on Nude Mice Skin to Prevent UV-A Damage. Int. J. Mol. Sci. 2023, 24, 10009. https://doi.org/10.3390/ ijms241210009

- Altomare AA, Aiello G, Garcia JL, Garrone G, **Zoanni B**, Carini M, Aldini G, D'Amato A. Protein Profiling of a Cellular Model of NAFLD by Advanced Bioanalytical Approaches. Int J Mol Sci. 2022 Aug 12;23(16):9025. doi: 10.3390/ijms23169025.

- Altomare AA, Brioschi M, Eligini S, Bonomi A, **Zoanni B**, Iezzi A, Jemos C, Porro B, D'Alessandra Y, Guarino A, Omodeo Salè E, Aldini G, Agostoni P, Banfi C. N Acetylcysteine Regenerates In Vivo Mercaptoalbumin. Antioxidants (Basel). 2022 Sep 6;11(9):1758. doi: 10.3390/antiox11091758.

- **Zoanni B**, Brioschi M, Mallia A, Gianazza E, Eligini S, Carini M, Aldini G, Banfi C. Novel insights about albumin in cardiovascular diseases: Focus on heart failure. Mass Spectrom Rev. 2023 Jul-Aug;42(4):1113-1128. doi: 10.1002/mas.21743

- Gado F, Ferrario G, Della Vedova L, **Zoanni B**, Altomare A, Carini M, Aldini G, D'Amato A, Baron G. Targeting Nrf2 and NF-κB Signaling Pathways in Cancer Prevention: The Role of Apple Phytochemicals. Molecules. 2023 Jan 31;28(3):1356. doi: 10.3390/molecules28031356.

- Aiello G, Rescigno F, Meloni M, **Zoanni B**, Aldini G, Carini M, D'Amato A. The Effect of Carnosine on UVA-Induced Changes in Intracellular Signaling of Human Skin Fibroblast Spheroids. Antioxidants (Basel). 2023 Jan 28;12(2):300. doi: 10.3390/antiox12020300.

- Altomare A, Baron G, Cambiaghi G, Ferrario G, **Zoanni B**, Della Vedova L, Fumagalli GM, D'Alessandro S, Parapini S, Vittorio S, Vistoli G, Riso P, Carini M, Delbue S, Aldini G. Screening of Mpro Protease (SARS-CoV-2) Covalent Inhibitors from an Anthocyanin Rich Blueberry Extract Using an HRMS-Based Analytical Platform. Molecules. 2024 Jun 6;29(11):2702. doi: 10.3390/molecules29112702.

Oral communications

- Zoanni B.- Application of omics studies in drug discovery and biomarker identification (SSPA Sept. 2024)

- Zoanni B. – Evaluation of carnosine effect on skin damage caused by UV-A (4th EpilipidNet meeting, July 2023)

Posters

- Zoanni B., Altomare A., Aldini G., D'Amato A., Carini M. - Optimization of NAFLD HepG2 cellular model for the evaluation of phytochemicals bioactivity from different plant extracts by quantitative proteomics studies (IMASS June.2022)

- Zoanni B., Altomare A., Aldini G., Carini M. - Quantitative proteomics study for the evaluation of Scutellaria baicalensis efficacy in the prevention of nonalcoholic fatty liver disease (NAFLD) (RDPA. Sept. 2023)

- Zoanni B., Wu V., Zamboni N., Carini M. – Hunting for lipids in complex biological matrices (PBA Sept. 2024)

Collateral activities

Attendance at Prevent It - Risk management and prevention of antibiotics resistance project Co-funded by Erasmus+. 26th November- 12th December 2022 (Chitkara,India) and Kalinga Institute of Industrial Technology (Odisha, India).